

MODIFICATION OF THE HIGH LATITUDE
IONOSPHERE BY HIGH POWER RADIO WAVES

Terence Ronald Robinson

being a dissertation submitted to the Faculty of Science,
Leicester University, in candidature for the degree
of Philosophiae Doctor.

Department of Physics,
University of Leicester.
June, 1983.

UMI Number: U341207

All rights reserved

INFORMATION TO ALL USERS

The quality of this reproduction is dependent upon the quality of the copy submitted.

In the unlikely event that the author did not send a complete manuscript and there are missing pages, these will be noted. Also, if material had to be removed, a note will indicate the deletion.



UMI U341207

Published by ProQuest LLC 2015. Copyright in the Dissertation held by the Author.
Microform Edition © ProQuest LLC.

All rights reserved. This work is protected against
unauthorized copying under Title 17, United States Code.



ProQuest LLC
789 East Eisenhower Parkway
P.O. Box 1346
Ann Arbor, MI 48106-1346



THESIS
674256

X75 0025548

For my wife Angela

and our children Adam and Rachel

Wapendwa,

Mmevumilia kwa muda mrefu kwa
sababu yangu ... ninaoamba msamaha kwa
moyo wote wangu ... sitaweza kuilipa
kamwe hii deni kubwa.

ACKNOWLEDGEMENTS

I owe a great debt of gratitude to Professor Tudor Jones, both for initially introducing me to Ionospheric Physics and for his help and encouragement throughout the period of my research. Sincere thanks too are due to the members of the Leicester Ionospheric research team each of whom has lent assistance in a variety of ways and on numerous occasions.

I would also like to thank:

Mrs. B. Abram and Mrs. E. Humphries who undertook the unenviable task of typing the manuscript,

Professor J.L.Beeby and Professor E.A. Davis for allowing me the opportunity to work in the Department of Physics at Leicester, and

the SERC for providing the wherewithall for this period of study.

Finally, I am indebted to Professor Peter Stubbe and Professor Helmut Kopka of the Max-Planck-Institut für Aeronomie, Lindau, for their cooperation during the experimental campaigns and for a number of helpful discussions, and to Professor Olav Holt of the University of Tromso for providing sites for experimental equipment.

Contents

	page
1. INTRODUCTION.	
1.1 Discovery of artificial modification of the ionosphere by radio waves.	1
1.2 Structure of the ionosphere.	2
1.3 The ionosphere as a natural plasma laboratory.	4
1.4 Aim of present investigation.	6
1.5 A note on terminology.	7
2. A REVIEW OF PREVIOUS F-REGION MODIFICATION EXPERIMENTS AND RESULTS.	
2.1 Introduction.	8
2.2 High power modification facilities.	9
2.3 Large scale plasma temperature and density modification.	12
2.4 Small scale field aligned irregularities.	14
2.5 Anomalous absorption.	16
2.6 Enhanced plasma line.	17
2.7 Artificially induced spread-F.	19
2.8 Summary.	20
3. A REVIEW OF F-REGION MODIFICATION THEORY.	
3.1 Plasma equations.	22
3.2 F-region dynamics.	25
3.3 Waves in plasmas.	29
3.4 Excitation of small scale field aligned irregularities.	41
3.5 Anomalous absorption of EM waves due to scattering from FAI.	55
3.6 Summary.	62

	page
4. THE HIGH LATITUDE EXPERIMENT IN NORTHERN SCANDINAVIA.	
4.1 The Ramfjordmoen heating facility.	64
4.2 The high power transmitters and antenna fields.	65
4.3 The diagnostic equipment.	66
4.4 Types of modification experiments.	71
4.5 Concluding remarks.	75
5. DIAGNOSTIC AMPLITUDE EFFECTS.	
5.1 Introduction.	76
5.2 High latitude anomalous absorption observations.	76
5.3 Interpretation of diagnostic absorption effects.	79
5.4 Theoretical calculation of anomalous absorption.	84
5.5 Determination of FAI scale lengths along the geomagnetic field.	94
5.6 Comparison with previous results.	97
5.7 Conclusions.	98
6. DIAGNOSTIC PHASE EFFECTS.	
6.1 Introduction.	100
6.2 Experimental results.	101
6.3 Interpretation of results.	105
6.4 Conclusions.	114
7. SELF ABSORPTION EFFECTS.	
7.1 Introduction.	115
7.2 Pump wave measurements.	116
7.3 Pump anomalous absorption and hysteresis effect.	118
7.4 A model of FAI growth and stabilization.	119

	page
7.5 Comparison of model results with observations.	145
7.6 Comparison with Grach et al.'s theory.	149
7.7 Conclusions.	150
8. F-REGION CROSS-MODULATION.	
8.1 Introduction.	152
8.2 Experimental arrangement.	153
8.3 Experimental results.	155
8.4 Carrier and sideband amplitude measurements.	157
8.5 A model of the F-region cross-modulation process.	157
8.6 Interpretation of cross-modulation data.	163
8.7 Comments and conclusions.	165
9. SUMMARY AND CONCLUSIONS.	167
APPENDICES.	
A. Differential D-Region absorption of O- and X-mode radio waves.	175
B. Approximate evaluation of integrals in chapter 7.	177
REFERENCES.	180

1. INTRODUCTION

1.1 Discovery of artificial modification of the ionosphere by radio waves

Radio wave propagation has played an extremely important role in the exploration of the earth's ionosphere. Gauss in 1839 and Kelvin in 1860 had speculated about the existence of a conducting layer in the upper atmosphere to explain certain natural geomagnetic and electrical phenomena. However the idea was not taken seriously by the scientific establishment until 1901 when Marconi succeeded in transmitting radio signals across the Atlantic. In 1902 Kennelly and Heaviside suggested that free charges in the upper atmosphere could reflect radio waves and so enable signals to propagate over the curvature of the earth's surface. However, controversy still surrounded the existence of the so called Kennelly-Heaviside layer until Appleton and Barnett (1925 a, b) and Breit and Tuve (1925, 1926) performed their definitive radio wave reflection experiments which lead to estimates of the height of the reflecting layer. The term 'ionosphere' had replaced the terms 'Kennelly-Heaviside' and 'Appleton' Layers by the end of the 1920's.

Ionospheric radio propagation developed rapidly from both a scientific and technical standpoint so that within less than ten years of the first radio wave sounding experiments, radio broadcasting on a commercial basis had become a familiar everyday occurrence. Nonlinear effects in ionospheric radio propagation were first observed soon after the Luxembourg high-power broadcasting station came into operation in 1933. Reporting in 'Nature', Tellegen (1933) wrote, "For the first time on April 10 of this year it was observed at Eindhoven, Holland, that when a radio-receiver was tuned to Beromunster (460m), the modulation of the Luxembourg station (1190m) could be heard on the background to such an intensity that during the weak passages of the programme of Beromunster the programme of Luxembourg was heard with annoying strength."

Tellegen attributed the 'Luxembourg' cross-modulation effect to the modification of the radio propagation characteristics of the ionosphere by the high power electromagnetic waves from the Luxembourg transmitter. Bailey and Martyn (1934) provided a quantitative confirmation of Tellegen's hypothesis in terms of the heating of the ionosphere by the absorption of energy from the high power radio waves.

A medium which can support wave propagation is said to be linear if (a) waves do not modify the medium and (b) different waves propagate independently. Ionospheric modification by high power radio waves and interaction between various types of ionospheric waves are therefore essentially nonlinear phenomena. Although nonlinear effects in ionospheric radio propagation have been known since the 1930s it is only recently, with the increase in power and directivity of modern radio transmitters that deliberate alteration of the properties of the ionosphere in a wide variety of circumstances has become a practical proposition.

Before commencing a detailed discussion of artificial modification phenomena it is necessary to know something of the medium to be modified, therefore, a brief outline of the ionosphere's characteristics is now presented.

1.2 Structure of the ionosphere

The solid globe of the earth is surrounded by a gaseous envelope or atmosphere, whose density, pressure and temperature vary considerably with altitude above the ground. The vertical distribution of these parameters up to 300 km is indicated in fig. 1.1. Various layers of the atmosphere are distinguished by the vertical temperature structure. The region above about 100 km where the temperature rises abruptly from 300 to over 1000K is called the thermosphere. Immediately below the thermosphere lies the mesosphere. This extends down to the stratosphere

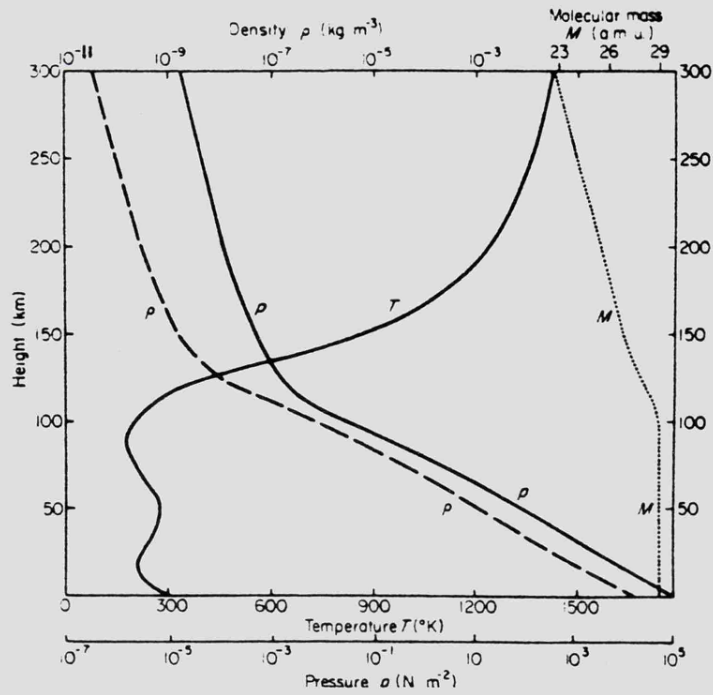


Fig. 1.1 U.S. Standard Atmosphere (Rishbeth and Garriott, 1969). Vertical distribution of pressure, p , density, ρ , temperature, T , and mean molecular mass M .

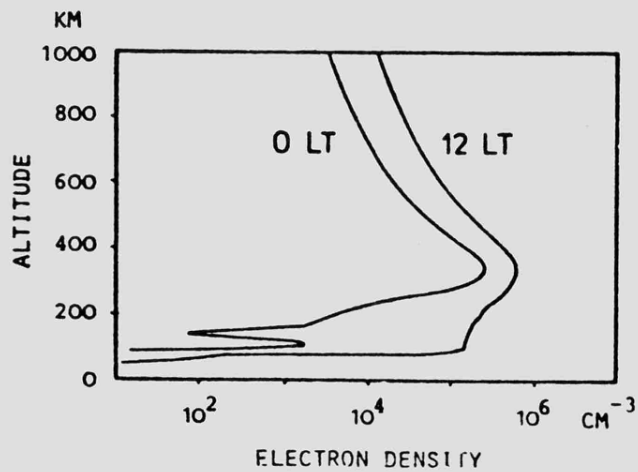


Fig. 1.2 International reference electron density profiles for local midnight (0LT) and noon (12LT) (Rawer et al., 1975).

and troposphere which occupy the bottom 30 km of the atmosphere (Rishbeth and Garriot 1969). The temperature structure of the thermosphere is dominated by the absorption of solar XUV radiation and has therefore a strong diurnal variation. In contrast to the large vertical gradient in atmospheric density and temperature, horizontal gradients are relatively weak. The atmosphere can therefore, to a good approximation, be considered homogeneous in a horizontal direction.

In addition to its heating effect solar XUV radiation produces a significant amount of ionization. The balance between photoionization and various recombination effects gives rise to an equilibrium density of free electrons and ions with a horizontal layered structure, referred to as the 'ionosphere'. Fig. 1.2 illustrates the vertical distribution of electron density in the atmosphere under both daytime and nighttime conditions.

Three layers are usually distinguished. The D-region lies between 60-90 km, the E-region between 100-150 km and the F-region lies above about 150 km. Under daytime conditions it is possible to distinguish two separate layers within the F-region, which are then referred to as the F_1 (lower) and F_2 (upper layers).

The vertical distribution of the concentration of the major chemical constituents is depicted in fig. 1.3. Below about 120 km, collisions between electrons, ions and neutrals are sufficiently frequent to equalise the electron, ion and neutral temperatures (fig. 1.4) and the vertical structure of the ionosphere in this region is dominated by photochemical processes. Above 300 km the geomagnetic field plays an increasingly important role in the structure and dynamics of the upper atmosphere, because in regions where particle collisions are few, the motion of charged particles is constrained by the influence of the magnetic field.

The earth's magnetic field is approximately dipolar. The magnetic poles are slightly displaced from the geographic poles so that the

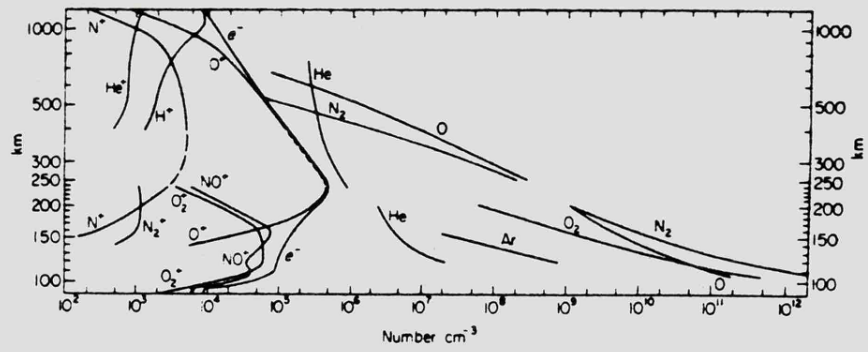


Fig. 1.3 Vertical distribution of the concentrations of the commonest chemical species in the atmosphere (Rishbeth and Garriott, 1969).

Fig. 1.4 Calculated electron (T_e), ion (T_i) and neutral (T_n) temperature profiles (from Schunk and Nagy, 1978).

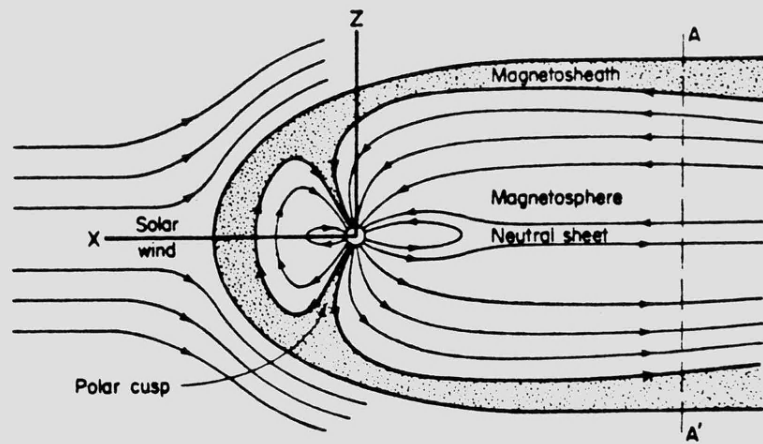
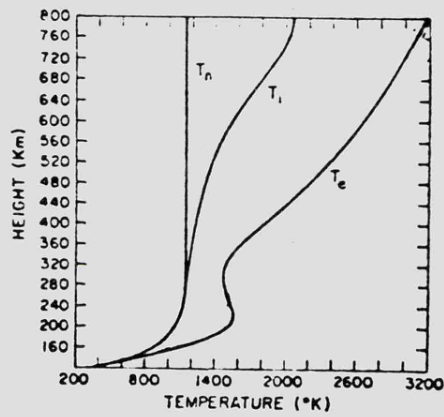


Fig. 1.5 Asymmetry of the geomagnetic field due to the effect of the Solar Wind (Ratcliffe, 1977).

location of a point on the earth's surface has, in general, different geomagnetic and geographic coordinates. Also, the angle of dip, the angle the magnetic field makes with a plane locally parallel to the earth's surface, is a function of latitude.

At high-latitudes, the geomagnetic field is nearly perpendicular to the earth's surface and field lines extend many thousands of kilometers into the interplanetary medium where they can connect into the interplanetary magnetic field (IMF). As a result, charged particles which are ejected from the sun (solar wind) are guided down the field lines into the high latitude ionosphere. The effect of the solar wind is to distort the geomagnetic field, compressing it on the sunward side and extending it on the side opposite to the sun (fig. 1.5). The interaction between the ionosphere and outer regions of the earth's aerospace environment (magnetosphere) is extremely complicated and is currently the object of intensive scientific research (see Akasofu, 1980). The regions where a strong interaction between the ionosphere and currents from the magnetosphere occur are called the auroral zones because of the well known optical phenomena which are regularly observed there. The vertical structure of the neutral atmosphere and the ionosphere in the auroral regions differs markedly from that at mid- and low- latitudes only when strong currents due to enhanced solar wind fluxes occur. Such events give rise to so called geomagnetic storms which strongly affect ground based magnetometers and radio propagation via the ionosphere.

1.3 The ionosphere as a natural plasma laboratory

The ionosphere is an example of a naturally occurring plasma. The term 'plasma' is used to describe any medium which contains enough free, charged particles for its dynamic behaviour to be significantly affected by electromagnetic forces. The ionosphere is therefore of interest both from a plasma physics as well as a geophysical point of view. Modification of the ionosphere by powerful radio waves can serve a number of scientific

and technological purposes, for example:

(i) to investigate the properties of the natural ionosphere.

Radio waves directly affect the temperature of electrons in the ionosphere in a quantifiable and repeatable manner. It is therefore possible to observe the response of the ionosphere to this imposed change, making possible the determination of rate coefficients of several important ionospheric processes such as particle diffusion and recombination.

(ii) to perform controlled plasma experiments in a natural plasma laboratory. The characteristic scale lengths of many plasma phenomena are much smaller than the scale lengths of the ionospheric plasma. Thus, plasma experiments in the ionosphere can be conducted in a very homogeneous environment compared to conventional laboratory plasmas. Unlike laboratory plasmas, the ionosphere is a long lived plasma and virtually unbound. Plasma experiments of especial interest involve the nonlinear interaction of various types of waves which can propagate in plasmas.

(iii) to produce artificial communications channels: the ionosphere has long been recognised as a medium for long distance radio communications because of its ability to reflect radio waves. It is however not a completely reliable communications channel because of its susceptibility to unpredictable variations. If the ionospheric plasma could be artificially controlled it could provide a more reliable medium for communications.

Experiments designed to explore all three of these aspects of artificial ionospheric modification began in the early seventies at a small number of sites (at mid- and low-latitudes) in the USA and the USSR, where transmitters capable of producing radio waves of sufficient power to modify the ionosphere have been constructed. Although a number of experiments designed to study D-region modification effects have been performed at these sites most interest is centred on F-region modification phenomena.

The ionosphere has been modified by techniques other than irradiation with high power radio waves. Space vehicles, for example, have been used for the release into the ionosphere of highly reactive chemicals and for the operation of charged particle accelerators (see Walker, 1979 and references therein). This thesis however is concerned only with the modifying effects of high power radio waves.

1.4 Aim of the present investigation

The ionospheric physics group of Leicester University has been invited by the Max-Planck-Institut für Aeronomie to take part in joint experiments to investigate ionospheric modification effects produced by the recently constructed high-latitude ionospheric modification facility at Ramfjordmoen, Norway.

These experiments were designed initially to confirm the existence at high-latitudes of certain artificial modification effects which had previously been observed at mid- and low-latitudes. Subsequently, building on the results obtained during the first experimental campaign studies were directed at developing techniques to measure parameters associated with the natural background and modified high latitude ionosphere. A further aim was to investigate nonlinear phenomena which were observed either for the first time or in a manner not previously reported. These two objectives correspond to items (i) and (ii) in section 1.3.

The experimental programme involved the propagation of a range of diagnostic HF radio waves through the heated region of the ionosphere. From measurements of the amplitude, phase and spectral content of the signals it was possible to deduce many of the characteristics of the modified plasma. These experiments were supplemented by measurements of the reflected heater signal and by vertical incidence ionosonde

observations.

In this dissertation the results of these investigations are presented and compared with those reported from previous modification experiments. Phenomena not previously observed are interpreted in terms of currently accepted theories. In certain cases it has been necessary to modify existing theory to account for the present observations.

1.5 A note on terminology

A high power radio transmitter employed for ionospheric modification purposes is called a 'heating facility' or often simply a 'heater' (for fairly obvious reasons). The high power radio wave itself is sometimes called a 'pump' wave because of its ability to stimulate the growth of other plasma waves in the ionosphere.

2. A REVIEW OF PREVIOUS F-REGION MODIFICATION EXPERIMENTS AND RESULTS

2.1 Introduction

Walker (1979) has recently remarked that the history of ionospheric modification by radio waves has been characterized by a failure of theory to predict phenomena before they were observed, combined with a rapid development of theory to accommodate newly observed phenomena. It is appropriate therefore to review some recent experimental observations relating to F-region modification before tackling the complicated thorny problems associated with the detailed theory of modification processes.

A great variety of plasma phenomena are excited during ionospheric modification. These include: large scale plasma temperature (Meltz et al., 1974; Mantas et al., 1981) and density (Le Levier (1970), Gurevich, 1978; see chapter 6) changes, generation of small-scale field aligned irregularities (Fialer, 1974; Minkoff et al., 1974a) induced HF anomalous absorption (Cohen and Whitehead, 1970; see chapter 5), artificial spread-F (Georges, 1970; Utlaut and Violette, 1974), artificially enhanced air glow and particle acceleration (Weinstock, 1974; Carlson et al., 1982), enhanced plasma line (Carlson et al., 1972); nonlinear radiowave reflectivity (Kopka et al., 1982; see chapter 7) and cross-modulation (Stubbe et al., 1982b; see chapter 8). A number of review papers containing details of experimental observations of modification phenomena have been published (Utlaut, 1975; Fejer, 1975; Carlson and Duncan, 1977; Fejer, 1979; Stubbe et al., 1982b; Gurevich and Migulin, 1982). Three journals have devoted entire issues to ionospheric modification, Journal of Geophysical Research (Vol. 75, Nov. 1970), Radio Science (Vol. 9, Nov. 1974), Journal of Atmospheric and Terrestrial Physics (Vol. 44, Dec. 1982).

A detailed discussion of observations relating to all of the above phenomena is beyond the scope of this review. The previous results which have the greatest bearing on the original work presented in this thesis are those concerned with (a) small scale field aligned irregularities and (b) large scale plasma density changes which occur when a high power HF radio wave illuminates the ionospheric F-region. This review is confined to these effects together with closely related phenomena such as anomalous-absorption and plasma line enhancement.

Most of the published literature refers to experiments at mid- and low-latitudes since it is only during the last 3 years that a large heating facility has become operational at high-latitudes. The modification effects are expected to differ with geomagnetic latitude because of the important role played by the geomagnetic field geometry in radio wave propagation and ionospheric plasma dynamics.

2.2 High power modification facilities

A number of high power HF radio transmitters designed specifically to modify the ionospheric F-region have been constructed in the USA (Table 2.1, from Walker, 1979) and the USSR (Table 2.2, from Gurevich and Migulin, 1982). Because the strongest interactions between radio waves and the F-region plasma occur when there is near equality between the plasma and radio frequencies, the heating facilities employ frequencies in the range 3-10 MHz.

The ability of an HF radio wave transmitter to produce observable effects in the F-region plasma depends to a great extent on the effective radiated power (ERP) it produces. ERP is defined as the product of the actual RF power, P_T , fed in to the transmitter antenna multiplied by the antenna gain, G. Then, ERP, $P_T (kW)$, G, electric field E_R and wave energy flux $F_R (Wm^{-2})$ at a range R

USA

Location	Frequency[MHz]	ERP[MW]
Arecibo	3 - 11	256
Platteville	5 - 10	200

Table 2.1 HF heating facilities in the USA (Walker, 1979).

USSR

Location	Frequency[MHz]	ERP[MW]
Moscow	4 - 5	80
Gorky	5 - 6	10
..	4 - 6	16
..	5 - 10	400
Murmansk	3.3	10

Table 2.2 HF heating facilities in the USSR (Gurevich and Migulin, 1982).

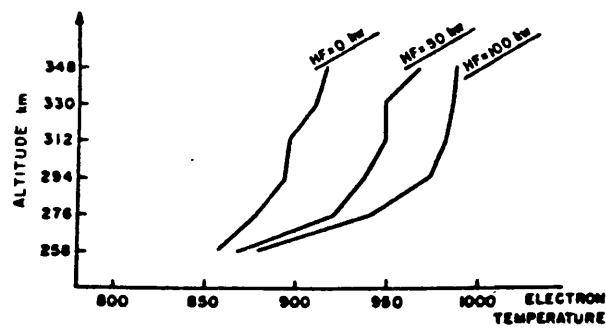


Fig. 2.1 Electron temperature profiles for zero-, half- and full-power operation of Arecibo HF facility (Gordon and Carlson, 1974).

are related by (Walker, 1979),

$$ERP = P_T \cdot G \quad 2.1a$$

$$E_R = 0.25 (ERP)^{1/2} / R = 27.5 \cdot \sqrt{FR} \quad b$$

In 2.1 a,b absorption and refraction have been neglected.

The antenna gain depends on antenna geometry. For example the Platteville transmitter (see Carroll et al., 1974) which produced the first known significant and intentional F-region modification transmits 2MW of RF power and has a nominal antenna gain of 19dB in the frequency range 2.7-25 MHz. This produces a flux of $50 \mu W m^{-2}$ at 300 km. The antennas in this case consist of crossed broad band dipoles. The Arecibo HF facility, on the other hand, employs a 1000ft. dish antenna. Although the RF power transmitted is an order of magnitude lower than that at Platteville, the HF flux at 300km is $20 \mu W m^{-2}$ (Fejer, 1979).

The high power HF transmitters constructed in the USA were originally designed to produce electromagnetic energy densities at F-region heights which are comparable with the internal energy of the ionospheric plasma. Such energy densities are characterized by an electric field, E_p , defined by Gurevich (1978) as the electric field of a radio wave required to cause temperature perturbations in the electron plasma by deviative absorption (see chapter 3 for theoretical background) which are equal in magnitude to the ambient electron temperature. E_p is the order of $1 V m^{-1}$ in the F-region.

The geomagnetic field plays a significant role in the interaction of high power radio waves with the ionospheric plasma. This is especially important in nonlinear effects involving plasma wave generation. In this case the angle between the electric field of the radio wave and the geomagnetic field, to a large extent, determines the intensity of the

generated waves (Stubbe and Kopka, 1980). The geomagnetic latitude is therefore an important consideration in the siting of high power radio transmitters for ionospheric modification. The major low- and mid-latitude facilities at Arecibo and Platteville respectively have recently been complemented by a new high-latitude installation at Ramfjordmoen near Tromso in Norway. All of the original data presented in this thesis derive from experiments employing the Ramfjordmoen facility. Two other high-latitude facilities are now in operation at Murmansk in USSR and at Fairbanks Alaska. The Murmansk facility is capable of providing only relatively low powers ($ERP=10MW$) at fixed frequency (3.3.MHz). The facility in Alaska only operates in a pulsed mode with pulse lengths of up to a few milliseconds, and is unable to generate FAI which have growth times in excess of 0.1 s (Wong et al., 1981a, Santoru et al., 1982).

The Arecibo high power facility is ideally situated to take advantage of the diagnostic capability of the 430 MHz incoherent scatter radar which in addition to the determination of the modified electron density and temperature can also detect backscatter from the parametrically excited Langmuir and ion acoustic waves. Much of the information concerning plasma modification on large spatial scales has been obtained using the Arecibo facilities (Gordon et al. (1971), Gordon and Carlson, 1974). High power incoherent scatter radar transmitters e.g. Arecibo are themselves capable of producing enough power to modify the ionosphere. However since they operate at UHF frequencies they do not interact strongly with the F-region plasma. However observations of collisional heating of the lower ionosphere with the 430 MHz Arecibo radar have been reported by Coco and Ganguly (1982).

2.3 Large scale plasma temperature and density modification

Rather few measurements have been reported of plasma density changes induced in the lower F-region by high power radio waves. Some experiments in the early seventies concentrated on the response of the electron temperature in the upper F-region (at heights exceeding 250 km). Fig. 2.1 illustrates the effect of heating by high power radio waves on the vertical electron temperature profile above Arecibo (Gordon and Carlson, 1974). A 5.1 MHz heating wave was employed and the $f_o F_2$ varied between 5.9 and 6.3 MHz during the experiment. As a result of heating at full power (transmitter power = 100kw) the mean electron temperature in the height range of 250 to 350 km increased from its background value of 900K to approximately 980K. Heating at half full power produced electron temperature enhancement slightly greater than 50% of those at full power.

Gordon and Carlson report that electron temperature enhancements were regularly seen while the heating wave was transmitted with ordinary polarization, whereas only weak effects were observed when an extraordinary polarized heating wave was employed.

Mantas et al. (1981) have recently carried out a detailed study of both the vertical structure and time response of electron temperature perturbations induced by the Arecibo heating facility. Fig. 2.2 illustrates the electron temperature profile in the height range 250 to 350 km at various times after heater switch on. Four sequences are reproduced. The induced temperature perturbations have a similar vertical structure to those reported by Gordon and Carlson (1974). The time response of electron temperature at eight different altitudes to heater switch on and switch off are reproduced in fig. 2.3. Theoretical curves fitted to each set of data points indicate rise and decay times are approximately equal in magnitude and vary between 17 and 35s in the height range 265-325 km. The shortest time constant occurred near 300 km.

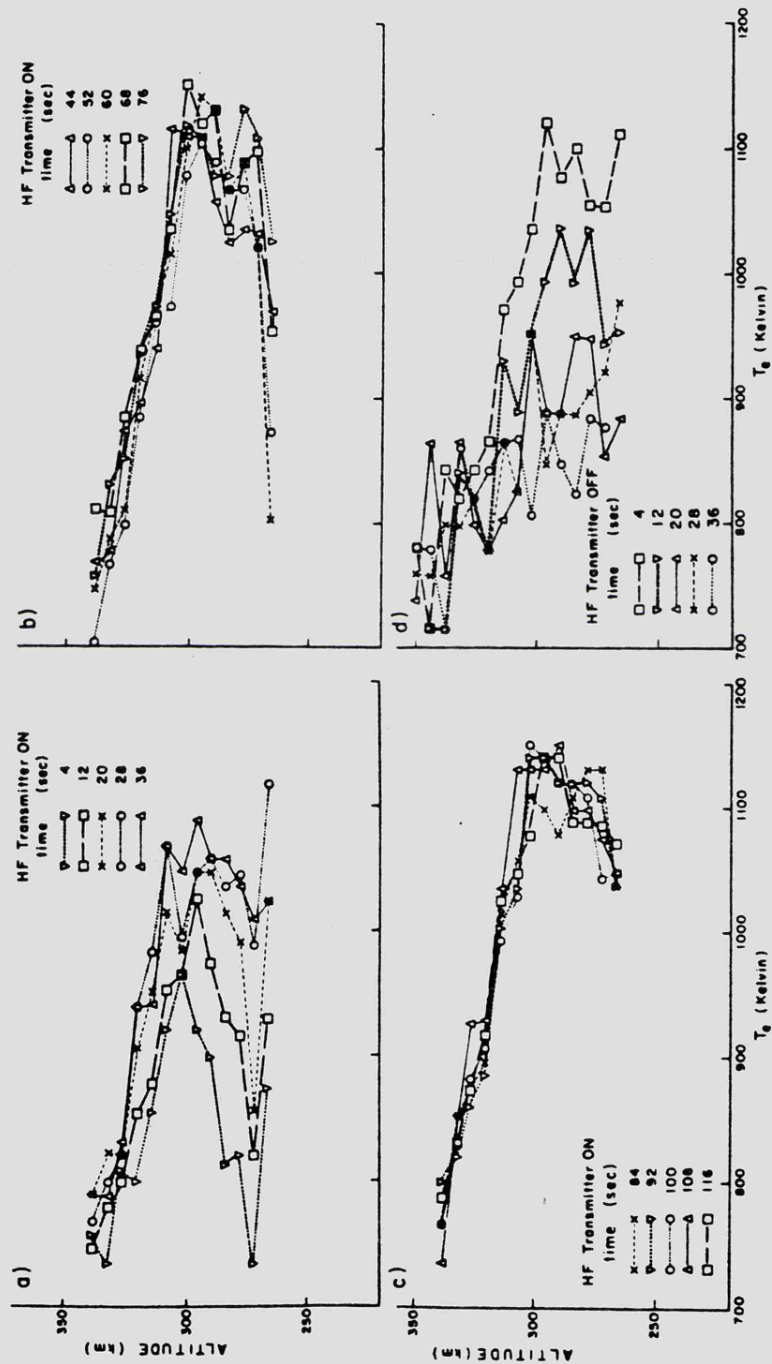


Fig. 2.2 Development of electron temperature profiles in response to 2 min-on, 2 min-off heating sequence at Arecibo. Figs. 2.2 a-c indicate temperature rise after switch-on. Fig. 2.2d indicates temperature fall after switch-off (Mantas et al., 1981).

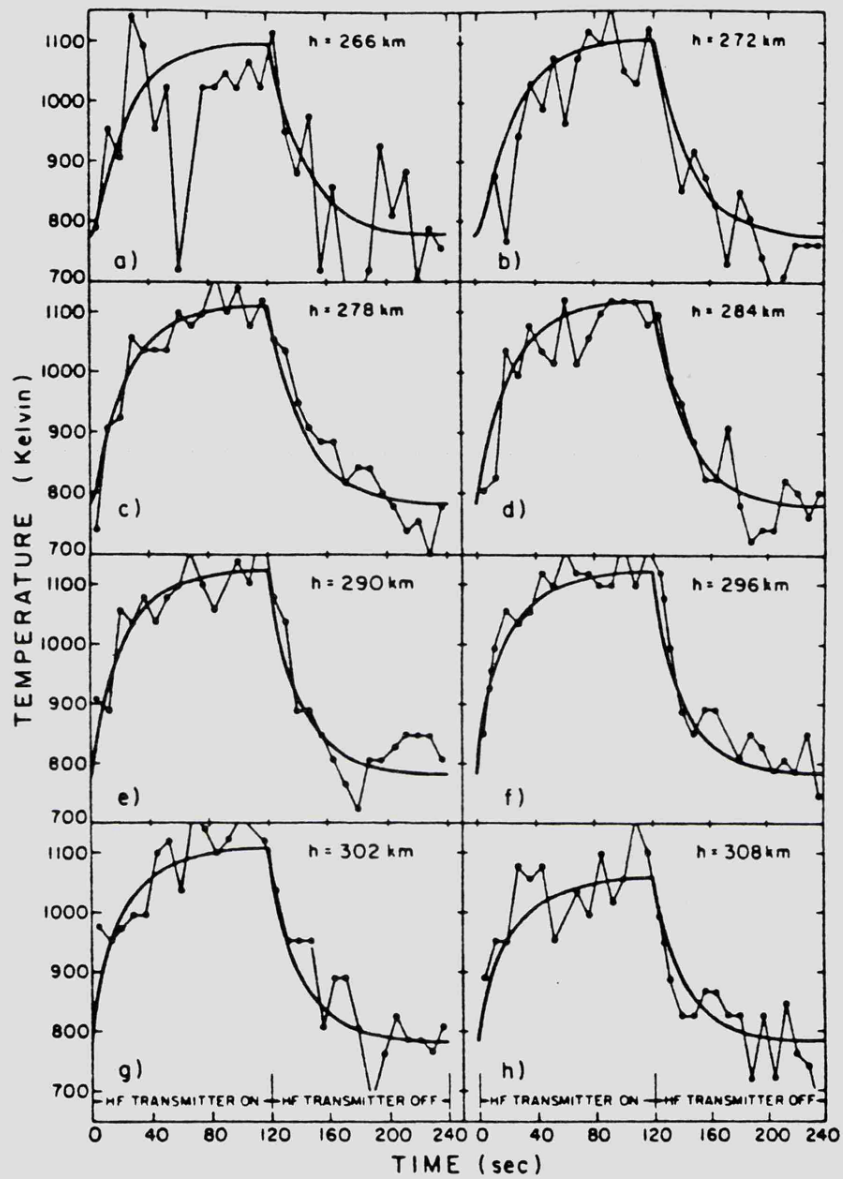
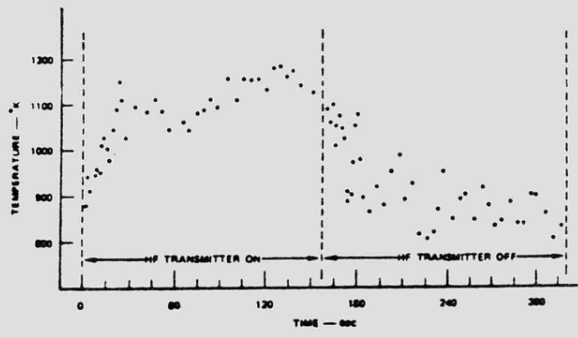


Fig. 2.3 Comparison of observed (points) and calculated (smooth curve) rise and decay of enhanced electron temperatures at several altitudes above the Arecibo heater (Mantas et al., 1981).

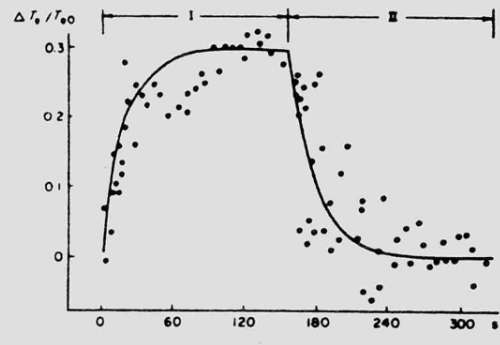
Experimental observations of electron temperature as a function of time after heating wave switch on and switch off has also been presented by Gordon and Carlson (1974). These data, which are averaged over ten on-off sequences are reproduced in Fig. 2.4. Showen and Behnke (1978), Gurevich (1978) and Mantas et al. (1981) have separately attempted to fit response curves to Gordon and Carlson's data. These theoretical best fit curves are also reproduced in fig. 2.4. The curve fitting has been carried out differently in each case. Gurevich (1978) (fig. 2.4b) assumed a single time constant and obtained a response time of 20s. Showen and Behnke claim a better fit if two time constants are assumed during the electron temperature increase after the heater is switched on (fig. 2.4 c, d). These authors associate the longer time constant with collisional heating and the shorter one with anomalous heating due to the excitation of plasma instabilities (see chapter 3). Mantas et al. (1981) argue that when spurious interference spikes due to the computer controlled transmitter turn on and turn off procedure are removed from Gordon and Carlson's data, it is not necessary to invoke two time constants during the electron temperature growth stage (fig. 2.4e).

Observations of large scale electron density perturbations due to heating by high power radio waves have not been reported in the literature in as much detail as observations of electron temperature perturbations. Meltz et al. (1974) report density decreases of about 3% of the ambient electron density after two minutes heating at Arecibo. Utlaut and Violette (1972) have inferred a 7% electron density reduction from ionograms recorded during heating experiments at Platteville. These density reductions occurred in the upper F-region (above 250 km) where they are to be expected on theoretical grounds (see chapter 3). The time constants for such changes are similar to those for the observed temperature enhancements.

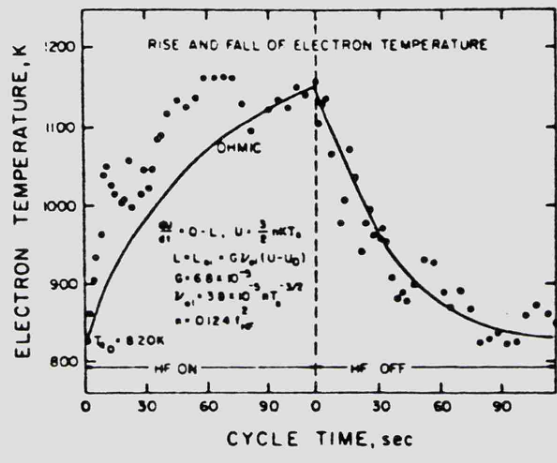
Meltz et al. (1974) point out that anomalous processes contribute slightly more than does deviative absorption of the heater wave to the plasma



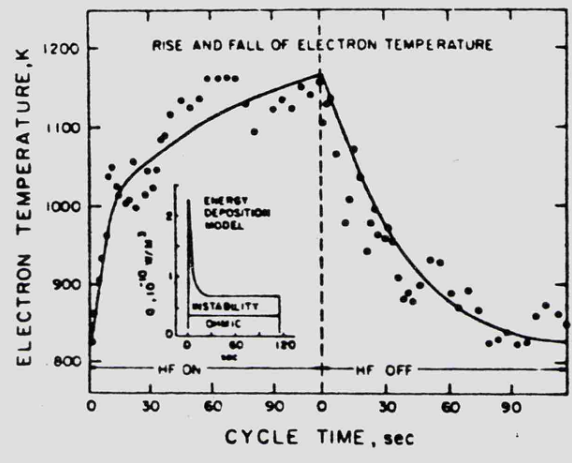
a



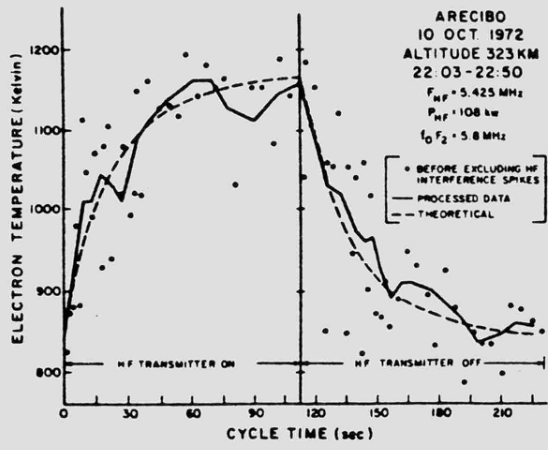
b



c



d



e

Fig. 2.4 Theoretical curve fitting to electron temperature data from Arcibo (a) (Gordon and Carlson, 1974) by (b) Gurevich (1978), (c,d) Showen and Behnke (1978) and (e) Mantas et al. (1981).

temperature and density changes observed at Platteville and Arecibo (these latter results have been confirmed by Mantas et al., 1981).

In the lower F region, the electron temperature increases when the plasma is illuminated by high power radio waves as in the case of the upper F-region (Gurevich, 1978). However, the plasma density response of the two regions is very different. In contrast to the results described above, HF doppler measurements described by Gurevich and Migulin (1982) indicate that heating in the altitude range 140 to 240 km (which includes the upper E-region and lower F-region) causes electron density enhancement. This behaviour is a consequence of the different temperature dependence of the recombination rates in the two parts of the F-region (see chapters 3 and 6).

2.4 Small Scale Field Aligned irregularities

Short scale field aligned irregularities (FAI) with scale lengths of the order of metres across the magnetic field were first detected during modification experiments at Platteville by VHF and UHF radars (Thome and Blood, 1974; Minkoff et al., 1974a; Fialer, 1974). The field aligned structure was inferred from the high aspect sensitivity returned signals from radars located at White Sands 860 km to the south of Platteville. Strong returns are obtained only when the radar beam is directed perpendicular to the geomagnetic field (see fig. 2.5).

These FAI are produced, (a) only by a high power wave of ordinary polarization and (b) only during overdense heating, i.e. when the heater wave frequency is less than the F-region maximum frequency. The received backscatter signal exhibits only a small Doppler shift which implies that the FAI are static (apart from natural plasma drifting).

The observations above, together with bistatic radar measurements reported by Carpenter (1974) and Minkoff et al. (1974b), are consistent

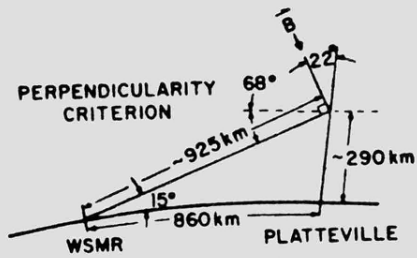


Fig. 2.5 Radar backscatter geometry for Platteville heating experiment (Minkoff et al., 1974a).

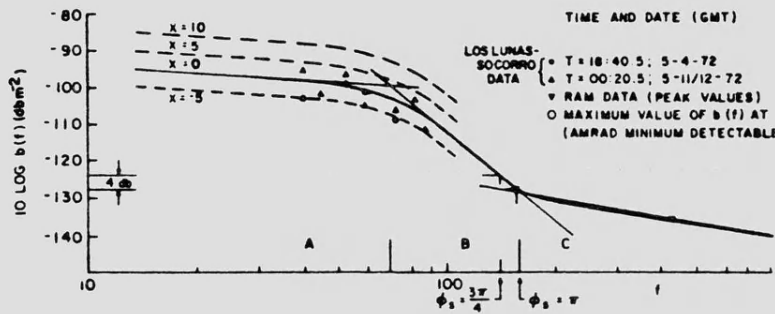


Fig. 2.6 The backscatter coefficient $b(f)$ as a function of radar frequency (f). The curves have been fitted by Minkoff (1974) to data (points) from Fialer (1974) and Minkoff et al. (1974a).

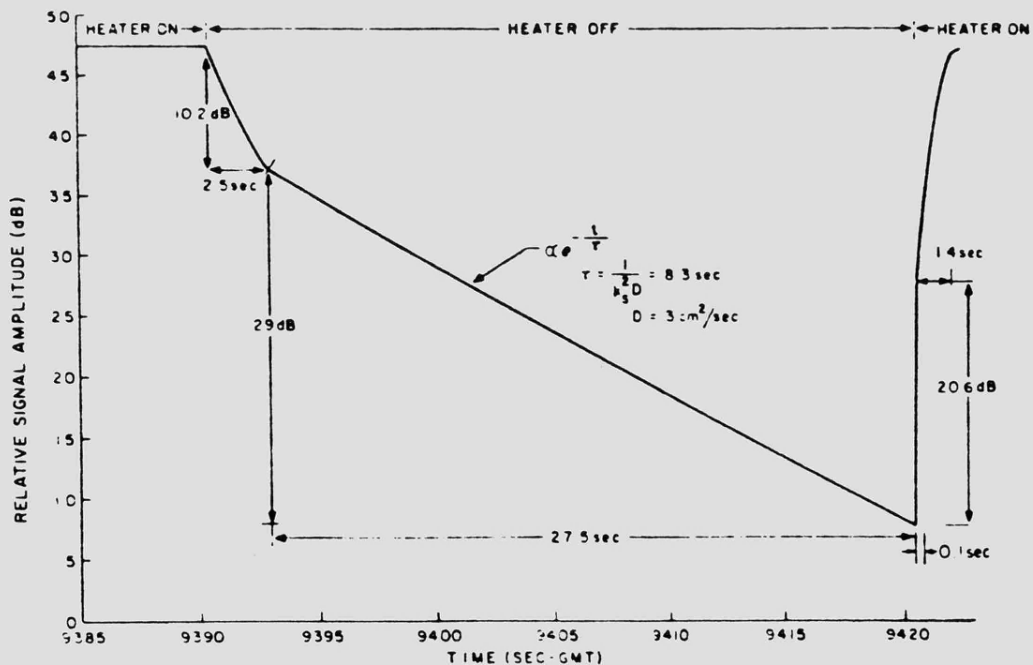


Fig. 2.7 Result of least squares fit to VHF backscatter, in response to step function heater power variation at Arecibo (Minkoff and Kreppel, 1976).

with the following model: FAI consist of plasma density inhomogeneities which are highly elongated along the magnetic field but which have cylindrical symmetry about an axis parallel to the magnetic field (Rao and Thome , 1974).

Minkoff (1974), from a compilation of the data in Fialer (1974) and Minkoff et al. (1974a) has deduced the spectral amplitude $b(f)$ of the backscatter cross section of FAI. As is well known, a backscatter radar which transmits a radio wave of frequency and wave vector receives a signal backscattered coherently from a periodic structure of wave vector $|k| = 2 |k_{\text{radar}}| = 4\pi f/c$ (Booker, 1956). Thus, by employing several radar frequencies it is possible to determine a number of spectral components of the radar cross-section of the FAI. A graph of $10 \log b(f)$ against f is illustrated in fig. 2.6. Three best fit lines have been drawn through the data points. They have the following formulae

- (a) $0 \leq f < 70 \text{ MHz} : 10 \log b(f) = -55.1 - 5.6 \log f$
- (b) $70 \leq f < 157.5 \text{ MHz} : 10 \log b(f) = 52.5 - 79.5 \log f$
- (c) $157.5 \leq f < 30000 \text{ MHz} : 10 \log b(f) = 21.6 - 18.1 \log f$

$b(f)$ exhibits a fairly sharp reduction for radar frequencies greater than 100 MHz. This indicates that FAI have minimum transverse (to the magnetic field) dimensions of the order of approximately 1 m. A precise definition of $b(f)$ and the significance of its dependence on f can be found in chapters 3 and 5.

The backscatter measurements presented by Minkoff et al. (1974a) have been further analysed by Minkoff and Kreppel (1976). These authors have determined the step response of FAI VHF backscatter amplitudes to heater on and heater off. The result of a least squares fit to their data is illustrated in fig. 2.7. Both the growth and decay stages

of FAI contain two time constants according to Minkoff and Kreppel (1976). The overall response time to heater-on is clearly much shorter than the decay time after the heater is switched off. This effect is in great contrast to the large scale plasma density and temperature changes described in the previous section for which growth and decay times were virtually identical.

2.5 Anomalous absorption

One of the earliest effects observed during the ionospheric heating experiments at Platteville was a reduction in the reflection coefficient of the heated F-region (Utlaut, 1970; Cohen and Whitehead, 1970). In experiments reported by Cohen and Whitehead (1970), a spaced diagnostic transmitter and receiver system was employed. The instrumentation consisted of multifrequency digitized ionosondes at locations 26 km east and west of the high-power transmitter. Fig. 2.8 illustrates the result of averaging ten sequential sets of received signal strengths logged at ten second intervals while the heater was being switched on and off. The time origin in fig. 2.8 coincides with heater 'on'. The mean anomalous absorption of the diagnostic signal during the one minute while the heater was on was slightly in excess of 10dB. Cohen and Whitehead point out the rapid signal amplitude decrease compared to the recovery time.

Utlaut and Violette (1974) report that anomalous absorption is visible on ionograms (taken at Platteville) from slightly below the heater frequency up to the F-region penetration frequency. For this reason the phenomenon was originally referred to as wide-band absorption. However, it must be noted that the observations at Platteville were made while the heater frequency was close to (within a few hundred kHz) the F-region critical frequency.

The ERP of the heater at Platteville during these experiments was approximately 90 MW. Similar results to those of Cohen and Whitehead were obtained at Gorkii in the USSR by Getmansev et al. (1973) with an ERP of approximately 9MW. Fig. 2.9 illustrates the response of a 5.745 MHz diagnostic as a function of time after the switch on of a 5.55 MHz heater. The F-region critical frequency was approximately 5.75 MHz. The data points in fig. 2.9 are obtained by averaging 12 consecutive heater on-off cycles. The asymmetry between the amplitude decay and recovery times apparent in Cohen and Whitehead's (1970) results (fig. 2.8) are not apparent in fig. 2.9.

A further important property of heater induced diagnostic absorption is that it only occurs when the heater is operating in the ordinary mode and that it only affects O-mode diagnostics. This observation is reminiscent of the circumstance under which small scale field aligned irregularities are excited. A number of theoretical studies have suggested a relationship between the two phenomena (e.g. Graham and Fejer, 1976) and these will be considered in detail later.

2.6 Enhanced Plasma Line

Carpenter (1974) distinguishes two types of backscatter observed with VHF and UHF radar. The first type is the aspect sensitive scatter from field aligned irregularities discussed in section 2.3. It is characterised by the backscatter frequency being almost equal to the transmitted radar frequency. For this reason it is termed centre-line scatter. The second type of scattering involves the generation and propagation of plasma waves in the ionosphere. In this case the backscatter spectrum contains two sidebands, one on either side of the transmitted radar frequency, and displaced from it by $\pm f_p$ where f_p is the heater (pump) frequency.

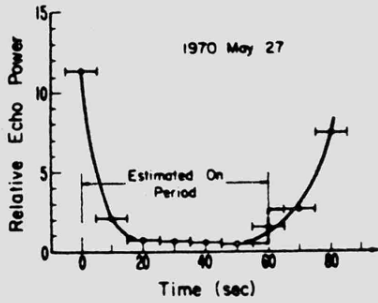


Fig. 2.8 Variation of mean diagnostic (echo) power during seven heating cycles at Platteville (Cohen and Whitehead, 1970).

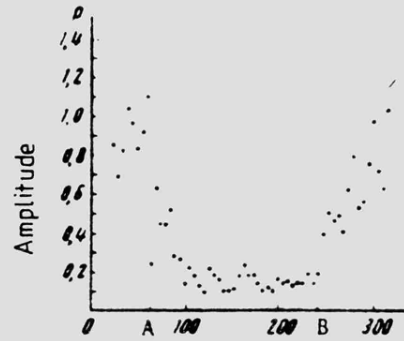


Fig. 2.9 Variation of amplitude of 5.745 MHz diagnostic during twelve heating cycles at Gorky (Getmansev et al., 1973).

Fig. 2.10 General features of the HF-induced enhancements in the UHF backscatter spectrum at Arecibo (Showen and Kim, 1978).

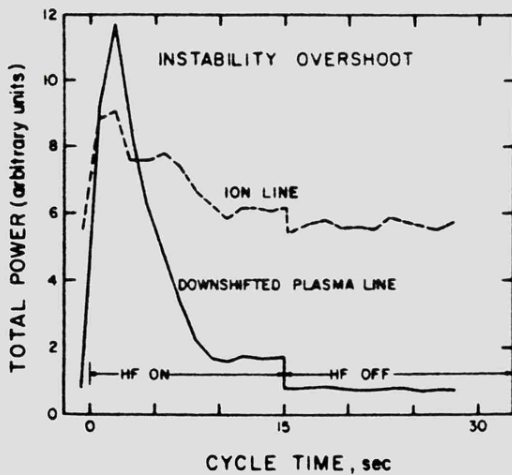
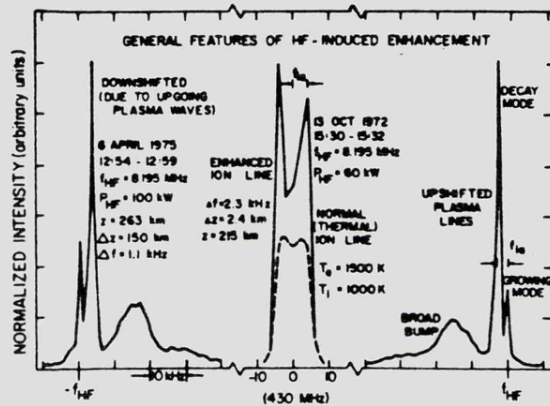


Fig. 2.11 Plasma and ion line intensities during a cyclic on-off experiment at Arecibo. The overshoot comes to a maximum 2s after heater turn-on (Showen and Kim, 1978).

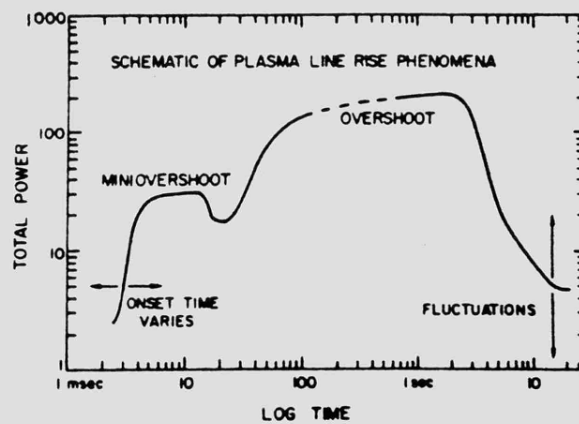


Fig. 2.12 Power in the plasma line as a function of time after heater turn-on at Arecibo (Showen and Kim, 1978).

In the absence of a modifying transmitter, Langmuir waves exist at low amplitude levels and cause weak incoherent backscatter. The backscatter is doppler shifted (up and down) by the Langmuir wave frequency which is equal to the local plasma frequency. The Doppler shift is thus a function of altitude and the up and down shifted lines are commonly called plasma lines.

When a powerful HF radio wave of ordinary polarization illuminates the F-region Langmuir waves are parametrically excited (see chapter 3) and the plasma lines are strongly enhanced. Detailed observations of the enhanced plasma line at Arecibo have been reported by Carlson et al. (1972), and Showen and Kim (1978). Fig. 2.10 is an illustration of the typical features of radar scattering spectra observed by Showen and Kim. The plasma lines(both up and down shifted) clearly exhibit two components. One is shifted from the radar frequency (430 MHz) by exactly the heater (pump) frequency. The second (usually more intense) line is shifted from the first line by a frequency equal to the local ion acoustic wave frequency. It is generated in a three wave interaction involving the modifying radio wave and excited Langmuir and ion acoustic waves (see chapter 3). The first plasma line is termed the purely growing mode and the second the decay line. It should be noted that the broad central ion line in fig. 2.10 is also enhanced by the high-power modifying wave.

The characteristics of the plasma lines which have the most important bearing on interpretation of anomalous absorption and field aligned irregularity observations are those associated with the so called 'overshoot' effect. A graph of plasma line and ion line intensities as a function of time after the switch on of the modifying wave (from Showen and Kim, 1978) is illustrated in fig. 2.11. The heater is operated in a 15 s on, 45 s off mode. It is clear from the graphs that the plasma line intensity reaches a peak after about 2s. It then falls to a moderately enhanced level (above background) but well below its peak. Showen and

Kim (1978) noted that on some occasions no overshoot was apparent. Fig. 2.12 illustrates schematically the features of the time evolution of the plasma line for a wide range of time scales between 1 ms and 10s. A mini-overshoot on a time scale of approximately 10 ms is evident. Wong et al. (1981b) have also observed rapid growth of the plasma line on similar (10 ms) time scales.

Carlson et al. (1972) determined the dependence of the intensity of the upshifted and downshifted plasma lines on the peak power of the HF modulating wave at Arecibo. Fig. 2.13 illustrates this power dependence. The intensity versus pump power curves clearly exhibit a hysteresis effect. A hysteresis effect in the nonlinear reflectivity of the pump wave itself is discussed in chapter 7.

2.7 Artificially induced spread-F

One of the most striking and reproducible phenomena observed during modification experiments at Platteville is the generation of artificial spread-F. Spread-F occurs naturally in the upper ionosphere when irregularities with scale sizes of the order of 1 km exist in the plasma. The phenomenon is readily observable in ionograms. Fig. 2.14 contains a sequence of ionograms which clearly exhibit the effects of artificially produced spread-F irregularities. According to Utlaut and Violette (1974) spread-F can be produced during X-mode heating but is mostly observed during heating with the O-mode.

Allen et al. (1974) employing an HF phased array radar have established that field aligned nature of the irregularities associated with artificial spread-F. The scale of these irregularities is intermediate between the large scale inhomogeneities described in section 2.3 and the small scale field aligned irregularities discussed in section 2.4. Artificial spread-F irregularities give rise to scintillations in signals received from stellar radio emissions (Rufenach, 1973;

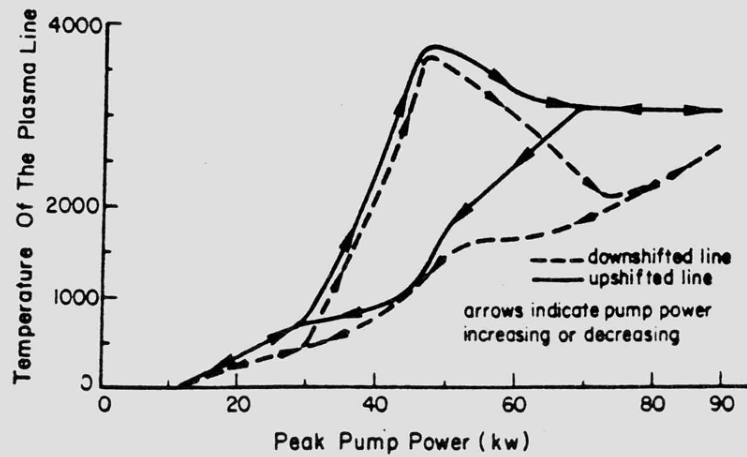


Fig. 2.13 The intensity of the plasma lines as a function of increasing and decreasing heater power at Arecibo (Carlson et al., 1972).

June 29, 1972

0100:00 GMT



0115:32 GMT



Fig. 2.14 Generation of artificial spread-F at Platteville. Ionogram (a) was taken 15 min before heater-on (b) was taken 32s after heater-on (Utlaut and Violette, 1974).

Frey and Gordon, 1982) and of satellite emissions (Bowhill, 1974; Basu et al., 1980; Livingston, 1983).

2.8 Summary

Few facilities exist for artificial modification of the ionosphere by high power radio waves. Most of the results reported in the literature were obtained at low and mid latitudes and so differ in some respects from the studies presented in this thesis. The investigations reviewed in this chapter indicate that high power radio wave modification produces an entire new range of ionospheric phenomena and a new branch of ionospheric physics has developed based on these studies.

3. A REVIEW OF F-REGION MODIFICATION THEORY

It is well known that high power electromagnetic waves heat a plasma because of collisional absorption (Ginzburg, 1970). In the ionosphere, collisional (non-deviative) absorption of EM waves dominates the D-region heating process. Prior to the heating experiments in Platteville in the early 1970s it was assumed that collisional (deviative) absorption would play a similar significant role in F-region heating (Thomson, 1970). It is now recognised however, that wave-wave interactions determine the character of F-region modification. The high power EM wave parametrically excites other wave modes and enhances plasma turbulence which in turn leads to anomalous plasma heating.

The conversion of HF electromagnetic waves into Langmuir waves for example has two major implications with regard to plasma heating. Because of their low propagation velocities relative to EM waves, the excited Langmuir waves (a) have much larger perturbation electric fields and (b) are much more efficiently absorbed (by collisions) than are the EM waves which excite them. Wong et al. (1981a) have suggested that because of (a) direct conversion of EM waves to Langmuir waves in the presence of the large scale vertical density gradient in the F-region could lead to wave trapping and the development of solitons. Result (b) suggests that anomalous absorption of EM waves is possible, which could result in more intense heating than that caused by collisional absorption of EM waves alone. The growth of small scale field aligned irregularities during heating contributes significantly to this anomalous heating process.

3.1 Plasma Equations

There are two generally recognised mathematical descriptions of plasmas: the magnetohydrodynamic theory (Landau and Lifshitz, 1960; Alfvén and Fälthammer, 1963) and the kinetic theory (Grad, 1958; Chapman and Cowling, 1970; Schunk, 1977). Whereas the kinetic theory provides a more fundamental approach, magnetohydrodynamics (MHD) has a wide range of validity and is formally and conceptually simpler. For many purposes the two approaches produce the same results, however in certain important situations only kinetic theory can be employed. For example, both theories can adequately describe the properties of electromagnetic (EM) waves in a plasma, but only kinetic theory correctly describes the characteristics of electrostatic (ES) waves.

The basic equations of plasma kinetic theory are the Boltzmann equation (Schunk, 1977),

$$\left(\frac{\partial}{\partial t} + \underline{v} \cdot \frac{\partial}{\partial \underline{x}} + \frac{e_{\alpha}}{m_{\alpha}} \underline{F} \cdot \frac{\partial}{\partial \underline{v}} \right) f_{\alpha}(\underline{x}, \underline{v}, t) = \Delta_c f_{\alpha}(\underline{x}, \underline{v}, t) \quad 3.1a$$

$$\underline{F} = \underline{E} + \underline{v} \wedge \underline{B} \quad 3.1b$$

together with Maxwell's electromagnetic equations. \underline{E} and \underline{B} are electric and magnetic fields respectively, e_{α} and m_{α} are the charge and mass of particles of species α , \underline{x} and \underline{v} are particle position and velocity, t is time and f_{α} is a distribution function from which all of the plasma properties can be derived. $\Delta_c f_{\alpha}$

is the rate of change of f_α as a result of collisions. Kinetic theory deals with plasma on a microscopic scale. Magnetohydrodynamics on the other hand is essentially a macroscopic theory based on fluid equations of mass, charge, momentum and energy continuity together with Maxwell's equations. The MHD equations can be entirely derived from kinetic theory by means of suitable approximations (Clemmow and Dougherty, 1969).

In the MHD approximation $f(\underline{X}, \underline{V}, t)$ is replaced by a number density, $N(\underline{X}, t)$ and mean velocity $\underline{u}(\underline{X}, t)$ defined by

$$N(\underline{X}, t) = \int f(\underline{X}, \underline{V}, t) d^3 \underline{V} \quad 3.2a$$

$$\underline{u}(\underline{X}, t) = \int \underline{V} f(\underline{X}, \underline{V}, t) d^3 \underline{V} \quad b$$

The MHD continuity equations are then obtained from velocity moment equations employing 3.1. The most generally applicable equations which result may be found in Braginskii (1965), Chapman and Cowling (1970), Schunk (1977) and Golant et al. (1980). The zeroth, first and second moment equations are respectively (for a Maxwellian distribution function).

$$\frac{\partial N_\alpha}{\partial t} + \underline{\nabla} \cdot (N_\alpha \underline{u}_\alpha) = \Delta N_\alpha \quad 3.3a$$

$$N_\alpha m_\alpha \frac{D \underline{u}_\alpha}{D t} + \underline{\nabla} \cdot (N_\alpha \underline{T}_\alpha) - N_\alpha e_\alpha \underline{F}_\alpha = \Delta \underline{M}_\alpha \quad b$$

$$\frac{3}{2} \frac{\partial (N_\alpha T_\alpha)}{\partial t} + \nabla \cdot \underline{q}_\alpha - N_\alpha e_\alpha \underline{E} \cdot \underline{u}_\alpha = \Delta \mathcal{E}_\alpha \quad c$$

where $\underline{F}_\alpha = \underline{E} + \underline{u}_\alpha \wedge \underline{B}$, $D/Dt \equiv \partial/\partial t + \underline{u}_\alpha \cdot \nabla$,

T_α is the temperature of the α particles, \underline{q}_α is the energy flux.

T_α and \underline{q}_α are defined by,

$$T_\alpha = \int \frac{m_\alpha}{2} \underline{v}^2 f_\alpha(\underline{x}, \underline{v}, t) d^3 \underline{v} \quad 3.3d$$

and
$$\underline{q}_\alpha = \int \frac{m_\alpha}{2} \underline{v}^2 \underline{v} f_\alpha(\underline{x}, \underline{v}, t) d^3 \underline{v} \quad e$$

Equations 3.3a-c express the conservation of (a) mass and charge, (b) momentum and (c) energy. The terms on the RHS of 3.3 a-c represent the change in these quantities due to collisions. For completeness ΔN_α includes particle production and loss due to ionization and recombination processes (i.e. inelastic collisions).

The collision terms in the momentum and energy equations can be written (Schunk, 1977)

$$\Delta \underline{M}_\alpha = \sum_\beta N_\alpha m_\alpha Z_{\alpha\beta} (\underline{u}_\beta - \underline{u}_\alpha) \quad 3.4a$$

$$\Delta \mathcal{E}_\alpha = \sum_\beta \frac{N_\alpha m_\alpha Z_{\alpha\beta}}{m_\alpha + m_\beta} [3(T_\beta - T_\alpha) + m_\beta (\underline{u}_\beta - \underline{u}_\alpha)^2] \quad b$$

where $\nu_{\alpha\beta}$ is the momentum transfer collision frequency. Various definitions of collision frequency found in the literature have been discussed by Stubbe (1968).

In terms of the three-fluid variables above, Maxwell's equations take the form

$$\epsilon_0 \nabla \cdot \underline{E} = \sum_{\alpha} N_{\alpha} e_{\alpha} \quad 3.5a$$

$$\nabla \wedge \underline{E} = - \frac{\partial \underline{B}}{\partial t} \quad , \quad \nabla \cdot \underline{B} = 0 \quad b$$

$$\nabla \wedge \underline{B} = \epsilon_0 \mu_0 \frac{\partial \underline{E}}{\partial t} + \mu_0 \sum_{\alpha} N_{\alpha} e_{\alpha} \underline{u}_{\alpha} \quad c$$

where μ_0 and ϵ_0 are respectively the free space permeability and permittivity. It is often convenient to define a charge current density \underline{J}_{α} corresponding to the mean flow velocity, \underline{u}_{α} such that

$$\underline{J}_{\alpha} = N_{\alpha} e_{\alpha} \underline{u}_{\alpha} \quad d$$

The characteristics of ionospheric plasma dynamics and wave motion can be presented in terms of the above equations.

3.2 F-region dynamics

Anisotropic plasma transport due to the presence of the geomagnetic field plays an important role in F-region dynamics. At altitudes above about 300 km where particle collisions are few, heat and particle transport along the magnetic field dominate the response of

the plasma to heating. In the lower F-region the situation is more complicated and the plasma response depends on the scale sizes of the inhomogeneities produced by heating. The plasma equations 3.3 may be readily adapted to describe the temperature and density perturbations induced in the lower F-region plasma which is illuminated by a high power radio wave with an oscillating electric field $\underline{E}_0 e^{i\omega t}$. Both large and small scale plasma inhomogeneities must be considered in the plasma heating process. Small scale plasma density changes associated with strongly field aligned structures have dimensions of a few metres across the magnetic field and several kilometres parallel to it.

Large scale changes, which are essentially isotropic in character, have dimensions across the magnetic field of the order of the beam width of the high power radio wave i.e. several kilometres.

3.2.1 Small scale plasma dynamics

The anisotropy of the small scale structures results from the greater mobility of electrons along the magnetic field than across it. The growth of small scale field aligned irregularities is dominated by plasma heat and particle transport due to temperature and density gradients. Inelastic collisions which involve charge production and recombination can be neglected. The motion of ions along the magnetic field is also negligible because the ion gyroradius is greater than the transverse dimensions of the irregularities (Das and Fejer, 1979). If the electron temperature and density perturbations are respectively T and n , then after eliminating \underline{u}_e from the plasma equation 3.3 and linearizing the energy and particle balance equations become, (Vaskov and Gurevich, 1977; Inhester et al, 1981),

$$\frac{3}{2} \frac{\partial}{\partial t} \left(\frac{T}{T_{e0}} \right) - 4.5 D_{\parallel} \frac{\partial^2}{\partial \zeta^2} \left(\frac{T}{T_{e0}} \right) + 2.7 D_{\perp} \frac{\partial^2}{\partial \xi^2} \left(\frac{T}{T_{e0}} \right) = \frac{Q}{N_0 T_{e0}} \quad 3.6a$$

and

$$\begin{aligned} \frac{\partial}{\partial t} \left(\frac{n}{N_0} \right) - \nu \left(\frac{T_{e0} + T_{i0}}{T_{e0}} \right) \left(\lambda_e^2 \frac{\partial^2}{\partial \zeta^2} + 0.5 \rho_e^2 \frac{\partial^2}{\partial \xi^2} \right) \left(\frac{n}{N_0} \right) \\ - \nu \left(1.7 \lambda_e^2 \frac{\partial^2}{\partial \zeta^2} - 0.25 \rho_e^2 \frac{\partial^2}{\partial \xi^2} \right) \left(\frac{T}{T_{e0}} \right) = 0 \end{aligned} \quad 3.6b$$

where,

$$Q = \underline{E} \cdot \underline{J}_e$$

$$D_{\parallel} = T_{e0} / (0.51 m_e \nu)$$

$$D_{\perp} = T_{e0} \nu / (m_e \Omega_e^2)$$

$$\lambda_e = (2 T_{e0} / m_e \nu^2)^{1/2}$$

$$\rho_e = (2 T_{e0} / m_e \Omega_e^2)^{1/2}$$

$$\Omega_e = eB / m_e$$

Q is the heat input per unit volume from the EM wave. ζ and ξ are respectively longitudinal and transverse coordinates. D_{\parallel} and D_{\perp} are the longitudinal and transverse electron thermal conductivities, ρ_e the electron gyroradius and λ_e the electron mean free path. The coefficients in the equations are those obtained by Braginskii (1965). In 3.6a, heat losses due to electron collisions and the effect of particle diffusion have been neglected.

3.2.2 Large scale plasma enhancements

The influence of gradients associated with large scale plasma temperature and density changes are negligible compared with collisional and recombination effects in the lower F-region (below about 250 km).

The plasma equations then reduce to (Gurevich, 1978)

$$\frac{3}{2} \frac{\partial T_e}{\partial t} = Q' - \frac{3}{2} R (T_e - T_0) \quad 3.7a$$

$$\frac{\partial N_e}{\partial t} = q_p - q_L \quad b$$

where Q' is the heat input per electron, the second term on the right hand side of 3.7a is the heat lost per electron due to background collisions (3.4b), and, q_p and q_L are respectively the particle production and loss rates. The former is mainly due to photoionization and the latter to particle recombination (Ratcliffe, 1960). In the lower F-region heating causes electron density enhancements due to a decrease in NO^+ and O_2^+ recombination rates which are decreasing functions of temperature. The consequences of this are dealt with in detail in chapter 6.

In the D-region the dominant effect is associated with the electron temperature increase due to non-deviative collisional absorption of an EM wave. Because the electron collision frequency is an increasing function of electron temperature, highpower radio waves passing through the D-region cause enhancement of the absorption coefficient (Jones, 1973; Gurevich, 1978). D-region self absorption reduces the amount of EM pump power incident in the F-region. This not only weakens direct F-region collisional heating but also reduces

the probability of exciting plasma instabilities. The D-region response to high power radio waves has recently been studied theoretically by Tomko et al. (1980) and Stubbe (1981).

3.3 Waves in plasmas

A magnetoactive plasma is capable of supporting a large variety of wave modes. Two mode types which are of particular importance in the study of ionospheric modification by high power radio waves are electromagnetic (EM) waves and electrostatic (ES) waves. In an isotropic plasma (without a magnetic field), EM waves are transverse and ES waves are longitudinal. There is no such strict distinction in a magnetoactive plasma (Ginzburg, 1970). However in the literature the distinct concepts of electromagnetic and electrostatic plasma waves are usually retained. This distinction is especially useful when applied to an inhomogeneous plasma where the transition between the two wave modes occurs in a very restricted range of altitudes (~ 10 m in the daytime F_1 region). EM and ES waves have very different characteristic propagation speeds. The EM waves have characteristic velocities comparable with the random thermal velocities of the plasma particles. For this reason the pressure term in equation 3.3b is negligible in the case of EM waves but must be included for ES waves.

The properties of plasma waves are determined by perturbation analysis of the plasma equations. The zero order terms describe the mean (background) plasma behaviour whilst first order terms describe the linear behaviour of plasma waves. Higher order terms are required when nonlinear wave-wave coupling takes place. In an inhomogeneous plasma such as the ionosphere, wave-wave coupling between different wave modes occurs only in spatially restricted regions. Outside

the coupling regions linear equations adequately describe the wave propagation characteristics.

3.3.1 Electromagnetic waves

EM waves can equally well be described by perturbation analysis of either the Boltzmann equation 3.1 or the MHD equations 3.3. Dropping the pressure term in 3.3b produces the cold plasma approximation. It effectively eliminates the ES mode from consideration. The dispersion relation of EM waves in a magneto-active plasma is derived in a number of standard texts, e.g. Ratcliffe (1959), Budden (1961), Stix (1962) Clemmow and Dougherty (1969), Ginzburg (1970) and Krall and Trivelpiece (1974). When the first order field variables are harmonic and vary as $e^{i(\omega t - \underline{k} \cdot \underline{x})}$, where ω is the angular frequency and \underline{k} the wave vector, the dispersion relation of EM waves in a collisionless plasmas can be written (Booker, 1935; Stix, 1962).

$$D(\omega, \underline{k}) = A\mu^4 - B\mu^2 + C = 0 \quad 3.8$$

where, $\mu = (c^2 k^2 / \omega^2)^{1/2}$ is the refractive index,

$$A = S \sin^2 \theta + P \cos^2 \theta$$

$$B = RL \sin^2 \theta + PS(1 + \cos^2 \theta)$$

$$C = PRL$$

$$S = \frac{1}{2} (R + L)$$

$$D = \frac{1}{2} (R - L)$$

$$R = 1 - \sum_{\alpha} (\omega_{\alpha} / \omega)^2 \left(\frac{\omega}{\omega + e_{\alpha} \Omega_{\alpha} / |e_{\alpha}|} \right)$$

$$L = 1 - \sum_{\alpha} (\omega_{\alpha} / \omega)^2 \left(\frac{\omega}{\omega - e_{\alpha} \Omega_{\alpha} / |e_{\alpha}|} \right)$$

$$P = 1 - \sum_{\alpha} (\omega_{\alpha} / \omega)^2$$

$$\omega_k^2 = N_\alpha e_\alpha^2 / m_\alpha \epsilon_0$$

$$\underline{\Omega}_\alpha = e_\alpha \underline{B} / m_\alpha$$

θ is the angle between \underline{k} and \underline{B} . Eq. 3.8 has two solutions

$$\mu^2 = (B \pm F) / 2A \quad 3.9a$$

where
$$F^2 = (RL - PS)^2 \sin^4 \theta + 4P^2 D^2 \cos^2 \theta \quad b$$

The plus and minus signs in 3.9a correspond to the ordinary (O-) and extraordinary (X-) modes.

In a right hand cartesian system (x,y,z) in which the magnetostatic field is along the z axis, the electric polarization relations can be written

$$E_y / E_x = -iD / (\mu^2 - S) \quad 3.10a$$

$$E_z / E_x = \mu^2 \cos \theta \sin \theta / (\mu^2 \sin^2 \theta - P) \quad b$$

When collisions are included, the refractive index becomes complex. If it is assumed that $m_e \ll m_i$ then the collisional form of μ is the well known Appleton-Hartree formula (Appleton, 1932),

$$\mu^2 = 1 - \frac{(\omega_e/\omega)^2}{1 - i\nu/\omega - \frac{\frac{1}{2}(\Omega_e/\omega)^2 \sin^2\theta}{1 - (\omega_e/\omega)^2 - i\nu/\omega} \pm \left(\frac{\frac{1}{4}(\Omega_e/\omega)^4 \sin^4\theta}{(1 - (\omega_e/\omega)^2 - i\nu/\omega)^2} + (\Omega_e/\omega)^2 \cos^2\theta \right)^{1/2}} \quad 3.11a$$

ν is an effective collision frequency defined by (Rishbeth and Garriott, 1969),

$$\nu = \nu_{en} + \nu_{ei} \quad 3.11b$$

where ν_{en} and ν_{ei} are respectively the electron-neutral and electron-ion collision frequencies. Equation 3.11 can be greatly simplified when the so-called quasi-longitudinal approximation is applied. Under these conditions (Gurevich, 1978)

$$\sin^2\theta \ll 2(\Omega_e/\omega) \cos\theta$$

and 3.11 reduces to

$$\mu^2 = 1 - \frac{(\omega_e/\omega)^2}{1 - i\nu/\omega \mp (\Omega_e/\omega) \cos\theta} \quad 3.12$$

3.3.2 Electrostatic Waves

Sitenko and Stepanov (1957) and Bernstein (1958) have studied in detail the properties of longitudinal plasma oscillations in the presence of a magnetic field by employing the Boltzmann equation 3.1. Bernstein assumes that the zero order distribution function, f_{e0} is Maxwellian, i.e.

$$f_{\alpha 0}(\underline{v}^2) = N_{\alpha} \left(\frac{m_{\alpha}}{2\pi T_{\alpha}} \right) \exp \left(- \frac{m_{\alpha} \underline{v}^2}{2 T_{\alpha}} \right) \quad 3.13$$

The equation for the first order distribution function $f_{\alpha 1}(\underline{x}, \underline{v}, t)$ from which the perturbation plasma field variables can be calculated is

$$\frac{\partial f_{\alpha 1}}{\partial t} + \underline{v} \cdot \frac{\partial f_{\alpha 1}}{\partial \underline{x}} - \frac{e_{\alpha}}{m_{\alpha}} (\nabla \phi_1 \cdot \frac{\partial f_{\alpha 0}}{\partial \underline{v}} + \underline{v} \wedge \underline{B}_0 \cdot \frac{\partial f_{\alpha 1}}{\partial \underline{v}}) = 0 \quad 3.14$$

where $\nabla \phi_1 = \underline{E}_1$

Two electrostatic wave modes may be distinguished. The first mode, characterized by ions being at rest, is the so called electron-acoustic (EA) wave, sometimes called a Langmuir wave or plasma wave. The second mode is characterized by ions and electrons moving in phase. It is termed the ion-acoustic (IA) mode.

(i) Electron-Acoustic (Langmuir) Waves

Eq. 3.13 is in general difficult to solve exactly even when ion motion is neglected. For a zero order distribution function which is Maxwellian, the longitudinal plasma dielectric function $\epsilon_0 D(\omega, \underline{k})$, defined by

$$\epsilon_0 D(\omega, \underline{k}) \underline{E}_1 = 0 \quad 3.15$$

can be written in terms of the Gordeyev integral I_G (Gordeyev, 1952; Clemmow and Dougherty, 1969) i.e.

$$D(\omega, \underline{k}) = 1 + \underline{k}^2 \lambda_D^2 + i\omega I_G \quad 3.16a$$

where,

$$I_G = \int_0^{\infty} \exp(-i\omega t - G(t)) dt \quad \text{b.}$$

$$G(t) = \exp\left(\frac{T_e}{m_e} \left(\frac{1}{2} k^2 t^2 + \frac{k_{\perp}^2 (1 - \cos \Omega_e t)}{\Omega_e^2}\right)\right) \quad \text{c.}$$

$$\lambda_D = (T_e/m_e)^{1/2} / \omega_e \quad \text{d.}$$

$$\text{and } \underline{k}^2 = k_{\parallel}^2 + k_{\perp}^2 \quad \text{e.}$$

λ_D is the Debye wavelength and k_{\parallel} and k_{\perp} are ES wave numbers parallel and perpendicular to the geomagnetic field.

The Gordeyev integral has an analytical form when $k_{\parallel} = 0$ (Bernstein, 1958). The dispersion relation for Langmuir waves travelling perpendicular to \underline{B}_0 is then (Clemmow and Dougherty 1969),

$$D(\omega, \underline{k}) = 1 + \underline{k}^2 \lambda_D^2 - \omega e^{-\lambda_{\Omega}^2 k^2} \sum_{n=-\infty}^{\infty} \frac{I_n(\lambda_{\Omega}^2 k^2)}{\omega - n \Omega_e} = 0 \quad 3.17$$

where $\lambda_{\Omega} = \lambda_D \omega_e / \Omega_e$ and I_n is a Bessel function with imaginary argument. Equation 3.17 has been extensively investigated by Bernstein (1958), who discovered a new plasma wave mode which is now referred to as the Bernstein mode. Bernstein waves propagate perpendicular to the magnetostatic field and have frequencies close to multiples of the electron gyrofrequency (Krall and Trivelpiece 1974).

Fejer and Calvert (1964) have derived an approximate dispersion relation which is employed in a variety of forms in the literature (Graham and Fejer, 1976; Gurevich, 1978; Inhester et al. 1981). The approximation adopted in this thesis which also includes collisional effects is

$$D(\omega, \underline{k}) = 1 - \frac{\omega_e^2}{\omega^2 - \Omega_e^2} (1 + 3\lambda_D^2 \underline{k}^2) - i\nu/\omega = 0 \quad 3.18$$

Relation 3.18 is valid when $\omega_e^2 \gg 4\Omega_e^2$.

Fejer and Calvert (1964) point out that the condition $D(\omega, 0) = 0$ for EA waves corresponds to a resonance (infinity) in the EM wave refractive index. Thus a possibility arises for mode conversion. Setting \underline{k}^2 to zero in 3.18 produces

$$\omega^2 = \omega_U^2 = \omega_e^2 + \Omega_e^2 \quad 3.19$$

ω_U is the so called 'upper-hybrid' frequency.

(ii) Ion acoustic waves

IA waves are adequately described by the warm fluid approximation (with pressure gradient included). Their dispersion relation is simply (Krall and Trivelpiece, 1974),

$$D(\omega, \underline{k}) = \omega^2 - c_i^2 \underline{k}^2 = 0$$

$$c_i^2 = (T_{e0} + T_{i0})/m_i$$

Because electron and ion motion is in phase in the IA mode the coulomb attraction between electrons and ions does not contribute to the restoring force which maintains harmonic oscillation. The IA mode oscillations are controlled by partial pressure forces and hence are non dispersive plasma sound waves.

3.3.3 Wave absorption and energy flow

Because of collisions between particles in a plasma, a proportion

of the ordered energy associated with plasma waves is transformed into random thermal energy. This leads simultaneously to wave damping and to an increase in the temperature of the plasma. Energy transfer from a wave to plasma particles occurs because collisions cause a component of the oscillating electron current density, \underline{J}_e to be in phase with the electric field, \underline{E} of the wave. The time averaged product $\overline{\underline{E} \cdot \underline{J}_e}$ is then non-zero and the wave performs a net amount of work. $\overline{\underline{E} \cdot \underline{J}_e}$ is the power per unit volume dissipated by the wave. Yeh and Liu (1972) demonstrate that in a dissipative medium, the time averaged energy density, \overline{W} and energy flux $\overline{\underline{P}}$ are related by

$$\frac{\partial \overline{W}}{\partial t} + \underline{\nabla} \cdot \overline{\underline{P}} + \overline{\underline{E} \cdot \underline{J}_e} = 0 \quad 3.20a$$

For a wave whose mean amplitude does not vary in time

$$\underline{\nabla} \cdot \overline{\underline{P}} = - \overline{\underline{E} \cdot \underline{J}_e} \equiv \frac{1}{4} (\underline{E}^* \cdot \underline{J}_e + \underline{E} \cdot \underline{J}_e^*) \quad 3.20b$$

In the case of an EM wave, $\overline{\underline{P}}$ is the time averaged Poynting vector, given by

$$\overline{\underline{P}} = \overline{\underline{E} \wedge (\underline{k} \wedge \underline{E})} / \mu_0 \omega \quad 3.20c$$

When equ. 3.20b applies, the wavenumber \underline{k} is complex. Writing $\underline{k} = \underline{k}' + i\underline{k}''$ where \underline{k}' and \underline{k}'' are real, then for a vertically propagating wave,

$$\frac{\partial |\overline{\underline{P}}|}{\partial h} = 2k'' |\overline{\underline{P}}| = \overline{\underline{E} \cdot \underline{J}_e} \quad 3.21$$

The wave decrement, k'' is determined by separating the real and imaginary parts of the complex refractive index of EM waves (3.11a). The result

is (Whitehead, 1956),

$$k'' = \frac{\nu}{2c} \cdot \frac{(\omega_e/\omega)^2 (1 + X_2 \cot^2 \theta)}{(1 + X_1 \Omega_e \cos \theta / \omega)^2 \left(1 - \frac{(\omega_e/\omega)^2}{1 + X_1 \Omega_e \cos \theta / \omega_e}\right)} \quad 3.22$$

where

$$X_1 = (1 + y^2)^{1/2} - y$$

$$X_2 = X_1 y^2 (1 + y^2)^{-1/2}$$

$$y = \frac{(\Omega_e/\omega) \sin \theta \tan \theta}{2(1 - \omega_e^2/\omega^2)}$$

In the D-region, the equation for the wave decrement, k''_D is greatly simplified for HF waves when $\omega \gg \omega_e$ (nondeviative absorption).

Then, 3.22 becomes

$$k''_D = \frac{\nu}{2c} \frac{\omega_e^2/\omega^2}{(1 + \Omega_e \cos \theta / \omega)^2} \quad 3.23$$

The wave decrement for Langmuir waves is determined in the same manner as that for EM waves but 3.18 is employed instead of 3.11a. Then

$$k''_L = (\nu/2V_e)(1 - \Omega_e^2/\omega^2) \quad 3.24$$

where V_e is the thermal electron velocity.

By comparing 3.22 with 3.24 it is clear that the absorption rate of Langmuir waves is higher than that of EM waves by a factor of the order of c/V_e . In the F-region $c/V_e \sim 10^3$ so Langmuir waves dissipate much more heat per unit volume than EM waves with the same initial amplitude.

For small wavelength Langmuir waves, Landau damping, which is

associated with wave-particle interactions is more important than collisional damping (Sanderson, 1981), however Landau damping is absent for waves travelling strictly perpendicular to the magnetic field (Clemmow and Dougherty, 1969).

The energy propagation velocity \underline{U}_E is defined in terms of the time averaged energy density and energy flux $\underline{\bar{P}}$ of the wave as

$$\underline{\bar{W}} \cdot \underline{U}_E = \underline{\bar{P}} \quad 3.25$$

Lighthill (1965) has demonstrated the equivalent of energy propagation velocity and group velocity, \underline{U}_G , for linear perturbations. \underline{U}_G is defined by

$$\underline{U}_G = \frac{\partial \omega}{\partial \underline{k}} = \frac{\partial D}{\partial \underline{k}} / \frac{\partial D}{\partial \omega} \quad 3.26$$

Group velocity is an important concept in investigating the propagation of waves in inhomogeneous media.

3.3.4 Wave propagation in weakly inhomogeneous plasma

For waves satisfying a given dispersion relation, a propagation path or ray is defined by the expression for the group velocity, (3.26). In an inhomogeneous plasma \underline{U}_G is a function of position and ray paths are in general not straight lines. The group velocity enables the time of flight between transmitter and receiver of a long radiopulse with a well defined carrier frequency to be calculated.

Efficient computer programs are available to perform these calculations for a wide variety of ionospheric models (e.g. Jones and Stephenson, 1975). Inversion of the ray tracing techniques to obtain electron density profiles from ionosonde measurements of radio wave propagation characteristics have also been developed (Jackson, 1971).

Expressions 3.9 and 3.11 for the EM wave refraction index apply strictly only to a homogeneous plasma. The ionospheric plasma density varies considerably with altitude over distances which are large compared with the wavelength of an HF radio wave. Under these circumstances the expression for refractive index, μ becomes a function of position. However, if the condition

$$|\nabla\mu| \ll |k|\mu$$

is satisfied, then μ is locally uniform. The variation in the perturbation field amplitude with distance may then be calculated by replacing $e^{i\mathbf{k}\cdot\mathbf{x}}$ with $e^{i\int\mathbf{k}\cdot d\mathbf{x}}$. This is the well-known Wentzel-Kramers-Brillouin (WKB) approximation or phase integral method (Budden 1961; Heading 1962, Weinberg, 1962).

An important property of an inhomogeneous plasma is that cut-offs and resonances, associated respectively with zeros and infinities in the value of μ , occur over extremely narrow height ranges. At cut-offs the wavelength and phase velocity become infinite while at resonances they vanish. In both cases the group velocity is zero. Physically the wave is, in general, reflected at a cut-off and absorbed at a resonance (Boyd and Sanderson, 1969). Reflection of EM waves is briefly considered here.

The reflection conditions for the ordinary and extraordinary EM wave modes can be determined by setting $\mu=0$ in 3.11a. This results in

$$\omega^2 = \omega_e^2 \quad 3.27a$$

$$\omega^2 = \omega_e(\omega_e + \Omega_e) \quad 3.27b$$

3.27a represents the O-mode reflection condition and 3.27b that of the X-mode. For vertical ionospheric propagation of a given wave frequency X-mode reflection occurs at a lower altitude than O-mode reflection. It is important to note also that the X-mode wave is reflected below the height of the upper hybrid resonance (3.19).

The study of wave propagation by phase integral and ray path calculations is generally known as the geometrical optics approximation. It is an extremely powerful mathematical technique with wide application and has received considerable theoretical attention in the literature. See for example, Landau and Lifshitz (1960), Budden (1961), Pöeverlein (1962), Ginzburg (1970) Jones (1970), Budden and Terry (1971), Bennett (1974, 1976), Suchy (1974, 1981), Smith (1975). Wave coupling processes have also been investigated by means of the WKB approximation (Heading, 1961, 1962; Budden 1961, 1972; Fuchs et al. 1981).

3.3.5 Reflection of radio waves in the ionosphere

(i) Oblique incidence

The general WKB condition for reflection from vertically stratified media is given by the disappearance of the vertical wave number. Thus for a vertically incident radio wave this is equivalent to the condition $\mu=0$ employed in section 3.3.4. When the wave is incident at an angle ψ to the plasma gradient direction then the reflection condition becomes $\mu = \sin \psi$ (Davies, 1969), and condition 3.27a is replaced by

$$\omega^2 = \omega_e^2 \sec^2 \psi$$

(ii) Amplitude swelling

As a wave approaches its reflection point its group velocity tends to zero. Eq. 3.25 indicates that under these circumstances the energy density must tend to infinity. This singularity is a consequence of the WKB approximation. The excitation of a reflected wave removes the singularity but wave amplitude enhancements do occur near reflection points. When

the presence of the reflected wave is taken into account the wave field of a radio wave below its reflection point has the form of a periodic standing wave with a slowly varying amplitude. In a linear plasma density gradient the electric field swelling factor in the largest local maximum is $1.9 \cdot (kH)^{1/6}$, where H is the plasma scale height (Budden, 1961).

(iii) Reflection from a moving ionospheric layer

The reflection point of a radio wave can be caused to move either by the bulk vertical motion of the ionosphere or by local enhancement or depletion of the electron density. In either case vertical motion of isoionic contours occurs. A variation in the position of reflection point causes the phase integral $\int \underline{k} \cdot d\underline{x}$ and the phase of a radio signal measured at the ground to alter. This provides a very sensitive method for detecting changes in the ionosphere near the reflection height of a radio wave. The time rate of change of the phase is called the Doppler shift.

3.4 Excitation of small scale field aligned irregularities

3.4.1 Nonlinear Wave-wave interaction

The generation of small scale field aligned irregularities was probably the most unexpected phenomenon observed in ionospheric modification experiments performed in the early seventies. The small scale irregularities have dimensions of a few metres across the geomagnetic field but several kilometres parallel to it. This highly elongated structure is a result of the anisotropic transport of electrons in the presence of a magnetostatic field. It is their structure which gives rise to anomalous absorption of EM waves.

All the theoretical models proposed for the generation of small scale field aligned irregularities (FAI) in the F-region by high power EM waves (see chapter 2 for previous experimental observations of FAI) involve the nonlinear interaction of high frequency plasma

waves (Stubbe et al., 1982b). Nonlinear wave-wave interactions give rise to so called parametric instabilities (Nishikawa 1968; Chen, 1974; Nayfeh and Mook, 1979). Most of the theoretical studies of wave-wave coupling reported in the literature concern three-wave interactions (see review by Fejer, 1979). Recently, Weatherall et al (1982) have suggested four-wave interactions could be important if Langmuir wave solitons develop during ionospheric heating. However, three-wave interactions are usually invoked for FAI excitation (Fejer, 1979).

In the three-wave interaction, a strong wave of angular frequency ω_0 and wave vector \underline{k}_0 causes the growth of weak waves characterized by $\omega_1, \underline{k}_1$ and $\omega_2, \underline{k}_2$. The wave parameters satisfy the matching conditions

$$\omega_0 = \omega_1 + \omega_2 \quad 3.28a$$

$$\underline{k}_0 = \underline{k}_1 + \underline{k}_2 \quad b$$

In ionospheric modification experiments ω_0 and \underline{k}_0 are associated with the high power radio wave.

3.4.2 Parametric decay instability

Initial attempts to explain the excitation of FAI emphasized the role of the so called parametric decay instability (PDI) in which $\omega_1, \underline{k}_1$ and $\omega_2, \underline{k}_2$ are associated with a Langmuir and an ion acoustic wave, respectively. The coupling mechanism between the three waves is the so called nonlinear ponderomotive force which is proportional to $\nabla \underline{E}^2$ (Landau and Lifshitz, 1960; Pitaevskii, 1961; Washimi and Karpman, 1976). In order to excite the PDI the pump electric field has to exceed E_t which is approximately

$6.7 \cdot N_o T_i \nu / \epsilon_o \omega_o$ (Stubbe and Kopka, 1980). The threshold field for typical F-region parameters is the order of 0.1 Vm^{-1} . The Ramfjordmoen heating facility is capable of exceeding this threshold (especially when amplitude swelling below the radio wave reflection height is taken into account). The growth rate, γ , of plasma waves excited by the PDI is given by

$$\gamma = \nu (E^2/E_L^2 - 1) \quad 3.29$$

γ is typically of the order 10^3 s^{-1} .

The parametric decay instability has been studied extensively in the literature (see, Silin, 1965; Perkins and Flick, 1971; Rosenbluth, 1972; Dubois and Goldman (1972); Fejer and Kuo, 1973; Perkins et al., 1974; Arnush et al., 1974; Chen and Fejer, 1975a; Kuo et al., 1983). The PDI gives rise to the enhanced upshifted and down shifted plasma lines observed with UHF incoherent backscatter radar (Carlson et al. 1972; Showen and Kim, 1978). However, because the PDI growth time is very short (10^{-3} s) compared to the observed growth time of FAI ($0.1 - 10 \text{ s}$) it is now accepted as unlikely that the PDI is directly responsible for FAI excitation. The time constants associated with FAI growth can only be explained by invoking a thermal parametric instability (TPI) in which the wave-wave coupling mechanism is thermal rather than electrostatic (ponderomotive).

Perkins (1974) retained the PDI in a model of FAI excitation by introducing multiplescattering of Langmuir waves whose interference gives rise to the required heat source. Lee and Fejer (1978) suggested that the heating that results from the random phased Langmuir waves produced by the PDI provide an energy source for FAI growth. Both mechanisms have weaknesses, however, which

make it unlikely that they alone can account for the observed phenomena (Das and Fejer, 1979).

One main disadvantage of mechanisms which rely on the saturation spectrum of the parametric decay instability to explain FAI is that there are strong indications that the parametrically excited EA waves experience an overshoot effect (Showen and Kim, 1978). The steady state amplitude of Langmuir waves reached a few seconds after pump switch on is sometimes several orders of magnitude lower than their amplitude a few milliseconds after switch-on. The drop in Langmuir wave amplitude probably coincides with FAI growth and pump extinction due to anomalous absorption. Muldrew (1978) has recently discussed the role of FAI in the generation of Langmuir waves which enhance the plasma line during heating experiments at Arecibo.

3.4.3. Linear mode conversion

Vaskov and Gurevich (1975) have suggested a mechanism entirely different from the PDI for the excitation of Langmuir waves by a high power EM pump. They propose that small scale inhomogeneities in the F-region plasma cause linear mode coupling between transverse (EM) waves and longitudinal (Langmuir) waves. Linear mode conversion was first studied in inhomogeneous plasmas with linear density gradients (Denisov, 1957; Dolgoplov, 1966; Ginzburg, 1970; Golant and Pilya, 1972; White and Chen, 1974).

Vaskov and Gurevich (1975, 1977) assume that FAI have the form of discrete aperiodic structures elongated along the geomagnetic field. They argue that collisional dissipation of Langmuir waves generated by mode conversion would enhance the FAI amplitude. The resulting instability is explosive and has an initial FAI amplitude threshold. Objections to the Vaskov and Gurevich mechanism have been raised by Dysthe et al (1983) on the grounds that the energy of

Langmuir waves generated by a single Fourier component of the FAI is distributed over a large distance perpendicular to the magnetic field and not confined to narrow transverse special regions as suggested by Vaskov and Gurevich. Vaskov (1979) has recently studied the effects of trapping of Langmuir waves in FAI.

A number of authors have recently developed Vaskov and Gurevich's original mode conversion process in a more consistent manner by employing spatially periodic FAI (Das and Fejer, 1979; Inhester et al., 1981; Dysthe et al., 1983). These theoretical developments form the basis of a unified theory of FAI growth, saturation and decay which is used to interpret the original experimental data presented in chapter 7.

Linear mode conversion can be most simply described by first order warm plasma fluid equations in the absence of a magnetic field. Then, the perturbation electric field \underline{E} is given by (Boyd and Sanderson, 1969),

$$\nabla_{\perp} \nabla_{\perp} \underline{E} + \frac{1}{c^2} \left(\frac{\partial^2}{\partial t^2} + \omega_e^2 \right) \underline{E} - \frac{V_e^2}{c^2} \nabla (\nabla \cdot \underline{E}) = 0 \quad 3.30$$

where V_e is the electron thermal velocity. \underline{E} can be split into a divergence-free component, \underline{E}_0 and a curl-free component \underline{E}_1 . \underline{E}_0 and \underline{E}_1 then correspond to the electric fields of the EM and Langmuir waves respectively, with

$$\underline{E} = \underline{E}_0 + \underline{E}_1 \quad 3.31a$$

$$\nabla \cdot \underline{E}_0 = 0 \quad b$$

$$\nabla_{\perp} \underline{E}_1 = 0 \quad c$$

On taking the curl and then the divergence of 3.30, the following two equations are obtained:

$$(\nabla_{\perp} \nabla_{\perp} + \frac{1}{c^2} (\frac{\partial^2}{\partial t^2} + \omega_e^2)) \nabla_{\perp} \underline{E}_0 = -\frac{1}{c^2} (\nabla \omega_e^2)_{\perp} \underline{E}_1 \quad 3.32a$$

$$(\frac{\partial^2}{\partial t^2} + \omega_e^2 - v_e^2 \nabla^2) \nabla \cdot \underline{E}_1 = -(\nabla \omega_e^2) \cdot \underline{E}_0 \quad b$$

It is clear from 3.32 that in the absence of plasma inhomogeneities \underline{E}_0 and \underline{E}_1 are independent i.e. mode coupling is absent.

However, when plasma density gradients are present, $\nabla \omega_e^2 \neq 0$, and EM waves are in general coupled to Langmuir waves. Equation 3.32b indicates that if an EM wave propagates such that its electric field has a component parallel to the plasma inhomogeneity gradient then a Langmuir wave will be strongly excited when,

$$D(\omega, \underline{k}) = 1 - \frac{\omega_e^2 + v_e^2 k^2}{\omega^2} = 0 \quad 3.33$$

The Langmuir wave electric field, \underline{E}_1 can be calculated from

$$\nabla \cdot \underline{E}_1 = \frac{(\nabla \omega_e^2) \cdot \underline{E}_0}{D(\omega, \underline{k})} \quad 3.34$$

$D(\omega, \underline{k})$ in 3.34 is the dispersion relation for Langmuir waves in the absence of a magnetic field. 3.34 can be easily generalized for the case of a collisional magnetoactive plasma. Then $D(\omega, \underline{k})$ in 3.18 must be substituted into 3.34.

In an inhomogeneous plasma such as exists at F-region heights, the resonant mode conversion occurs in a narrow region centred on a height where the EM wave frequency is close to the local upper hybrid frequency (3.19). Only an O-mode EM wave can undergo resonant mode conversion because its reflection point occurs at a

higher altitude than the upper-hybrid resonant point, whereas the X-mode reflection point occurs below the upper-hybrid resonance point. This result convincingly explains why FAI are only generated by O-mode heating (Graham and Fejer, 1976).

3.4.4 Thermal Parametric Instability

Thermal parametric instabilities (TPI) in homogeneous plasmas have been studied theoretically by Grach et al. (1975), Burinskaya and Volokitin (1979) and Kuo and Lee (1982). However the nature of TPI is significantly modified in inhomogeneous plasmas (Grach et al., 1977, 1979). Das and Fejer (1979) describe the TPI in the F-region in the following manner. A periodic number density of the form

$$n_2 = n_{20} e^{-ik_2 \xi} \quad 3.35$$

is assumed where ξ is a coordinate perpendicular to the magnetic field. A high power EM pump electric field has the form

$$\underline{E}_0 = \underline{E}_{00} e^{i\omega_0 t} \quad 3.36$$

It is assumed that the wavenumber of the EM wave k_0 is negligible compared to k_2 . \underline{E}_0 is assumed to be perpendicular to the magnetic field. In the presence of n_2 and \underline{E}_0 a current density \underline{J}_1 , arises, which has the form

$$\underline{J}_1(\omega_0, k_2) = (n_2(0, k_2) + n_2(0, -k_2)) \left(\frac{e^2}{im_e \omega_0} [\underline{E}_0(\omega_0, 0) - \underline{E}_0(-\omega_0, 0)] \right) \quad 3.37$$

The periodic current density \underline{J}_1 generates a periodic electric field

$$\underline{E}_1(\omega_0, k_2) \quad \text{given by}$$

$$\underline{E}_1(\omega_0, k_2) = \frac{\omega_0}{i\epsilon_0(\omega_0^2 - \omega_p^2 + i\nu\omega_0)} \underline{J}_1(\omega_0, k_2) \quad 3.38$$

This result is equivalent to equation 3.32b or 3.34. It is interesting to note that the three-wave matching relations 3.28 hold for the TPI by writing $\underline{k}_0 = 0$, $\omega_2 = 0$. Then 3.28a, b become

$$\begin{aligned} \omega_0 &= \omega_1 - 0 \\ 0 &= \underline{k}_1 - \underline{k}_2 \end{aligned}$$

A three-wave interaction in which one of the wave frequencies is zero gives rise to the purely growing form of parametric instability (Fejer and Leer, 1972). The positive feedback mechanism for growth of n_2 is provided by the interference between $\underline{E}_0(\omega_0, 0)$ and $\underline{E}_1(\omega_0, k_2)$. The total electric field energy density is approximately (Dysthe et al., 1983)

$$\begin{aligned} \nu\epsilon_0 |\underline{E}_0 + \underline{E}_1|^2 &\equiv \nu\epsilon_0 |\underline{E}_0|^2 + 2\nu\epsilon_0 |\underline{E}_0 \cdot \underline{E}_1| + \\ &+ \nu\epsilon_0 |\underline{E}_1|^2 \end{aligned} \quad 3.39$$

The three terms on the RHS of 3.39 are respectively, the collisional heating associated with the EM wave, the differential heating due to the beating of the EM and mode converted Langmuir waves and the energy density of the Langmuir wave. $|\underline{E}_0 \cdot \underline{E}_1|$ is a zero frequency term but is periodic in space with wavenumber k_2 . It therefore just matches the original FAI periodicity and can cause their enhancement. $|\underline{E}_0|^2$ and $|\underline{E}_1|^2$ have no time-independent periodicity. The latter term gives rise to the anomalous

absorption of EM waves due to scattering from FAI. This is discussed in detail in section 3.5. The $|\underline{E}_0|^2$ term is just the direct collisional heating of the EM wave.

In an inhomogeneous plasma ω_e^2 in 3.38 is a function of altitude. Assuming a linear density gradient

$$\omega_e^2 = \omega_0^2 \left(1 + \frac{h}{H} \right) \quad 3.40$$

where H is the scale height of the plasma, then

$$2\nu\epsilon_0 \overline{|\underline{E}_1 \cdot \underline{E}_0|} = \frac{2\nu E_0^* E_0 e^2 (n_2 + n_2^*)}{\omega_0^2 m_e \left(\left(\frac{h}{H} \right)^2 + \left(\frac{\nu}{\omega_0} \right)^2 \right)} \cdot \frac{h}{H} \quad 3.41$$

The total differential heat input Q_{10} to the FAI is given by

$$Q_{10} = 2\nu\epsilon_0 \int_{-\infty}^{\infty} \overline{|\underline{E}_1 \cdot \underline{E}_0|} \sec\theta dh \quad 3.42$$

where θ is the angle of inclination of the magnetic field to the vertical. If expression 3.41 is substituted into 3.42, the result is identically zero. In order to obtain a net heating effect ($Q_{10} \neq 0$), Das and Fejer (1979) had to take into account the standing wave nature of the pump below its reflection height. They assumed

$$E_0^* E_0 = \frac{E_{00}^2}{2} (1 + p \sin 2k_0 h) \quad 3.43$$

where $\rho (\leq 1)$ is the standing wave ratio. If the phase of the standing wave ratio is chosen to give a positive height gradient of the pump field intensity at the resonance point where

$\omega_0^2 = \omega_e^2$ then net heating occurs. Substituting 3.42 and 3.43 into 3.41 produces

$$Q_{10} = - \frac{2\pi\rho E_{00}^2 e^2 \nu H}{m_e \omega_0^2 \cos\theta} (n_2 + n_2^*) \int_{-\infty}^{\infty} \frac{h \sin 2k_0 h}{h^2 + \nu^2 H^2 / \omega_0^2} dh \quad 3.44a$$

$$= - \frac{2\pi\rho E_{00}^2 e^2 \nu H}{m_e \omega_0^2 \cos\theta} e^{-2\nu H/c} (n_2 + n_2^*) \quad b$$

where c is the speed of light in vacuo.

The spacially periodic heat input Q_{10} causes the electron temperature to deviate by T_2 from the mean background temperature T_{e0} . Q_{10} occurs in a very narrow altitude range $\Delta h \sim H\nu/\omega_0$. The equation for T_2 at threshold according to Das and Fejer (1979) (see section 3.2.1) may be written

$$4.5 D_{||} \frac{\partial^2 T_2}{\partial \zeta^2} - 2.7 D_{\perp} k_2^2 T_2 + \frac{Q_{10}}{N_0 T_{e0}} \delta(\zeta) = 0 \quad 3.45$$

where $\zeta = h \sec\theta$ and $\delta(\zeta)$ is the Dirac delta function.

Equation 3.46 is the stationary form of the plasma heat conduction equation 3.6a (Vaskov and Gurevich, 1977). It has a solution

$$T_2 = \frac{1}{2} Q_{10} (D_{||} \cdot D_{\perp})^{1/4} \quad 3.45b$$

Das and Fejer (1979) assume that the number density change n_2 associated with T_2 is $-N_0 T_2 / 2 T_{e0}$. This result is a consequence of a simplified form of the particle diffusion equation 3.6b and constitutes an adiabatic approximation. It is in agreement with this result to within a factor of the order of unity. The pump electric

field has then a linear threshold E_t (independent of the initial value of n_2), where

$$E_t = 2.44 T_{e0}^2 \omega_0^2 k_2^{-2} e^{-2\nu H/c} \cos\theta / \rho \nu \Omega_e e^2 H \quad 3.46$$

For typical F-region parameters the threshold field of the above TPI is of approximately the same order as that of the parametric decay instability when ρ (in 3.44) is approximately 1. It is important to note that the threshold field of the TPI is lower for smaller FAI wavenumbers.

Dysthe et al. (1983) have extended the Das and Fejer theory in two important ways:

(i) they take full account of the effect of the magnetic field on EM wave polarization and show that the net value of Q_{10} given by 3.42 is not zero when the reflected pump wave is neglected. However, the resulting FAI are sheetlike. No experimental evidence for such structures exists at present and FAI are presumed to have cylindrical symmetry about an axis parallel to the magnetic field (Minkoff, 1974; Gurevich, 1978).

(ii) they calculate the linear growth rate of the FAI by solving the exact coupled energy and diffusion equations. They employ transport equations which take account of collisions and energy transport by particle diffusion. Their results suggest that the linear growth rate of TPI is proportional to $(E_0/E_t)^4$.

The mathematical procedure adopted by these authors is outlined in detail in chapter 7 where their method is adapted to calculate the growth rate for non-linear equations which arise when secondary Langmuir wave scattering is taken into account.

3.4.5. TPI with secondary EA scattering

Inhester et al. (1981) have pointed out that the primary scattered Langmuir wave electric fields $\underline{E}_1(\omega_0, k_2)$ can scatter from the FAI plasma density $n_2(0, k_2)$ to produce secondary Langmuir wave electric fields $\underline{E}_2(\omega_0, 2k_2)$. Clearly this process can be repeated to infinite order i.e. $\underline{E}_2(\omega_0, 2k_2)$ scatters from $n_2(0, k_2)$ to produce $\underline{E}_3(\omega_0, 3k_2)$ etc. The m^{th} order Langmuir wave electric field is thus $\underline{E}_m(\omega_0, mk_2)$ where \underline{E}_m is related to \underline{E}_{m-1} by

$$\underline{E}_m = \underline{E}_{m-1} \frac{(n_2/N_0)/D_m}{1 - \frac{(n_2/N_0)^2/(D_m \cdot D_{m+1})}{1 - \frac{(n_2/N_0)^2/(D_{m+1} \cdot D_{m+2})}{1 - \dots}}}$$

3.47a

Inhester et al. (1981) define D_m as

$$D_m = 1 - \frac{\omega_e^2 + \Omega_e^2}{\omega^2} - 3\lambda_D^2 k_2^2 m^2 + \frac{\Omega_e^2}{c^2 k_2^2 m^2} - i \frac{\nu}{\omega_0}$$

3.47b

Thus, D_m differs from the dispersion function for Langmuir wave derived by Fejer and Calvert (1964) (e.g. 3.18) because of fourth term on the right hand side of 3.47b which Inhester et al. (1981) introduce to allow for smooth coupling to the EM mode.

Inhester et al. (1981) demonstrate that if $n_2/N_0 \leq \nu/\omega_0$ then the multiply scattered waves can be decoupled apart from neighbouring orders so that

$$\underline{E}_m = \underline{E}_{m-1} \cdot \left(\frac{n_2}{N_0}\right) \cdot \frac{1}{D_m}$$

3.48

The first order scattered EA wave is thus

$$\underline{E}_1 = \underline{E}_0 \left(\frac{n_2}{N_0} \right) / D(\omega_0, k_2) \quad 3.49$$

which is equivalent to Das and Fejer's (1979) result.

The beat field of \underline{E}_m with \underline{E}_{m-1} is of zero frequency and has a spatial periodicity characterized by a wave vector k_2 .

Differential heating proportional to $|\underline{E}_m \cdot \underline{E}_{m-1}|$ can thus enhance the original striations. Clearly,

$$|\underline{E}_m \cdot \underline{E}_{m-1}| \propto E_{00}^2 (n_2/N_0)^{2m-1}$$

The height integrated heating rate Q_{21} associated with the beating of primary and secondary Langmuir waves is given by

$$Q_{21} = 2\nu\epsilon_0 \int_{-\infty}^{\infty} |\underline{E}_1 \cdot \underline{E}_2| \sec\theta \, dh = -\frac{\pi\omega_0 H\epsilon_0 E_{00}^2}{\cos\theta} \left(\frac{n_2}{N_0} \right)^3 F(k_2) \quad 3.50a$$

where

$$F(k_2) = \frac{9\lambda_0^2 k_2^2 + 3\Omega_e^2/4c^2 k_2^2}{(9\lambda_0^2 k_2^2 + 3\Omega_e^2/4c^2 k_2^2)^2 + 4(\nu/\omega_0)^2} \quad b$$

The differential heating term Q_{21} in 3.50 is nonzero even without including the reflected pump wave. Q_{21} is substituted into the F-region transport equations (Vaskov and Gurevich, 1977), and the resulting pump electric field threshold is nonlinear, i.e. it depends on the initial FAI amplitude. This result has led certain authors (Inhester et al., 1981; Stubbe et al., 1982b) to propose a two stage FAI excitation process in which initial FAI amplitudes are enhanced by a linear growth mechanism such as that of Das and Fejer (1979) to a level at which the nonlinear

(FAI amplitude dependent) threshold is exceeded. FAI growth mechanisms with linear thresholds are referred to as type I instabilities and those with nonlinear thresholds, type II instabilities.

3.4.6. FAI nonlinear growth and saturation

Although FAI excitation has received much attention in the literature (see previous section for references), the nonlinear growth and saturation stages have been relatively neglected. Dysthe et al. (1983) have described the linear growth stage of type I instabilities but have ignored amplitude saturation. Several authors (Grach et al., 1979; Inhester et al., 1981; Stubbe et al., 1982a) have suggested that anomalous absorption of the pump itself may eventually limit FAI growth. Grach et al. (1979) have obtained saturation FAI amplitudes for the thermal parametric instability by taking account of pump self extinction. However, as Dysthe et al. (1983) comment, Grach et al. (1979) treat the mode conversion process in a rather complicated way which is difficult to follow. There is certainly no obvious way of applying their approach to the Das and Fejer (1979) and Inhester et al. (1981) processes. Stubbe et al. (1982a) have incorporated pump self extinction in a straightforward manner to the Das and Fejer (1979) theory. In chapter 7, their methods are applied to a unified model which incorporates both type I and type II instabilities. The saturation amplitudes are obtained as a function of pump power. The result is compared with that of Grach et al. (1979).

3.5. Anomalous absorption of EM waves due to scattering from FAI

The mode conversion mechanism by which the EM waves in the presence of FAI excite EA waves is a linear process. Thus low power EM waves passing through a region of the ionosphere where FAI have been excited by a high power EM pump will also undergo mode conversion to EA waves. This constitutes an anomalous absorption process. Ryzhov and Tamoikin (1970) and Ryzhov (1971, 1972) have demonstrated that the scattering of EM waves into Langmuir waves leads to higher anomalous absorption than the scattering of EM waves into EM waves. Low power EM waves however do not provide enough positive feedback to enhance the FAI.

A number of different methods of calculating anomalous absorption of EM waves due to scattering to Langmuir waves in the presence of plasma inhomogeneities exist in the literature. Those of Chen and Fejer (1975b), Graham and Fejer (1976) and Vaskov and Gurevich (1976) are most often encountered.

Measurements of the anomalous absorption of low power diagnostic waves passing through a volume of the F-region illuminated by high power radio waves (chapter 5) can yield information concerning the structure of FAI provided the relationship between FAI amplitudes and anomalous absorption is known.

The three calculations of anomalous absorption above differ in several important respects. Some of these differences are set out in table 3.1. Differences arise both in their initial assumptions and in the manner in which the results are presented. An especially important point of comparison between the three calculations is the method of including the presence of the geomagnetic field which affects EM waves dispersion, Langmuir wave dispersion and the mode coupling process. Chen and Fejer

Theory	Plasma Equations	Type of Calculation	Magnetic field ?		
			EM waves	EA waves	Coupling
Chen & Fejer (1975)	Kinetic	Numerical Integration	X	X	X
Graham & Fejer (1976)	Kinetic	Numerical Integration	✓	✓	X
Vaskov & Gurevich (1976)	Fluid	Analytical Expression	✓ Quasi - Longitudinal Approx.	✓	✓

Table 3.1 A comparison of anomalous absorption calculations.

(1975b) neglect the presence of the geomagnetic field completely and for this reason their calculation will be considered no further.

Graham and Fejer (1976) take account of the geomagnetic field in the dispersion of both EM and Langmuir waves. Their method of calculating mode coupling is based on the HF conductivity calculation of Dawson and Oberman (1962, 1963), which employs kinetic theory. However, the Dawson and Oberman work does not take account of the magnetic field in calculation of the source current of Langmuir waves generated by EM waves.

Vaskov and Gurevich (1976) do take the geomagnetic field into account in a consistent manner. However this is a fluid equation calculation and depends on a geometrical optics approximation for calculating wave energy fluxes. It is by no means obvious that their result should be the same as that of a kinetic theory calculation of the type Graham and Fejer employ. Finally, these two calculations are made extremely difficult to compare directly because Vaskov and Gurevich (1976) employ mean FAI plasma density amplitudes whereas Graham and Fejer employ the equivalent radar cross-sections of FAI formulated by Minkoff (1974). The Graham and Fejer theory is analysed in some detail in chapter 5 where it is modified to take full account of the effects of the geomagnetic field. The results of this new calculation are then compared with those of Vaskov and Gurevich (1976).

In order to provide a starting point for the modified calculation, the theories of Graham and Fejer and Dawson and Oberman are now briefly summarized.

3.5.1. Dawson and Oberman theory

Dawson and Oberman (1962) calculate the self consistent electric field in a magnetic field free plasma consisting of electrons and

ions in the presence of an oscillating external electric field of the form

$$\underline{E} = \underline{E}_0 e^{i\omega_0 t}$$

In the rest frame of the ions, the collisionless Boltzman equation is

$$\frac{\partial f_e}{\partial t} + \underline{v} \cdot \frac{\partial f_e}{\partial \underline{x}} - \frac{e}{m_e} (\underline{E} - \underline{\nabla} \phi) \cdot \frac{\partial f_e}{\partial \underline{v}} = 0 \quad 3.51a$$

where $\underline{\nabla}^2 \phi = \frac{e}{\epsilon_0} \left(\int f_e d^3 \underline{v} - \sum_i \delta(\underline{x} - \underline{x}_i) \right)$ b

Dawson and Oberman (1962, 1963) identify the delta function term in 3.51b specifically with ions. Here it is assumed that the ions are singly ionized. It should be pointed out however that any deviation from the zero order distribution function could be employed to replace this term. The ions are regarded as a set of fixed scatterers with position vectors \underline{x}_i . The zero order electron distribution is assumed to be Maxwellian. Then, from the first order perturbation equation derived from 3.51, Dawson and Oberman obtain the oscillating part of the perturbation potential $\phi_{\underline{k}}(\omega)$ associated with the \underline{k} Fourier component of the spatial ion distribution. They find

$$\phi_{\underline{k}}(\omega) = - \frac{2e}{\pi \epsilon_0 k^2} \underline{k} \cdot \underline{\epsilon} \left\{ \sum_i e^{-i\underline{k} \cdot \underline{x}_i} \right\} \frac{e^{i\omega t}}{D(\omega, \underline{k})} \quad 3.52a$$

where $\underline{\epsilon}$ is the electron displacement under the influence of \underline{E} , given by

$$\underline{\epsilon} = -e \underline{E}_0 / m_e \omega_0^2 \quad b$$

and $D(\omega, \underline{k})$ is the plasma dielectric function given by

$$D(\omega, \underline{k}) = 1 + \omega_e^2 \int_0^\infty dt t \exp(-it\omega - \frac{1}{2} \underline{k}^2 V_e t^2) \quad 3.52c$$

Clearly when $D(\omega, \underline{k})$ in 3.52c is set to zero the Langmuir wave dispersion relation in a magnetic field free plasma is obtained.

V_e is the electron thermal velocity. From 3.52 Dawson and Oberman (1963) obtain the average electric field experienced by the ions \underline{F}_{ie} due to the electrons. They find

$$\underline{F}_{ie} = \underline{\epsilon}_{ie} \cdot \underline{E}_0 e^{i\omega t} \quad 3.53a$$

where,

$$\underline{\epsilon}_{ie} = \frac{e^2}{(2\pi)^3 \epsilon_0 m_e N_0 \omega_0} \int d^3 \underline{k} \left(\frac{1}{D(\omega, \underline{k})} - \frac{1}{D(\omega_0, \underline{k})} \right) \cdot \left(\sum_{j,l} e^{i\underline{k} \cdot (\underline{x}_l - \underline{x}_j)} \right) \underline{k} \underline{k} \quad b$$

$\underline{\epsilon}_{ie}$ is related to the HF conductivity $\underline{\sigma}_{HF}$ of the plasma by

$$\underline{\sigma}_{HF} = (\omega_e / \omega_0)^2 \underline{\epsilon}_{ie} \quad c$$

$\underline{\sigma}_{HF}$ strongly depends on ion correlations through the factor $\sum_{j,l} \exp(i\underline{k} \cdot (\underline{x}_l - \underline{x}_j))$ in 3.53b. Graham and Fejer (1976) take up the theory at this point.

3.5.2 The Graham and Fejer theory of anomalous absorption

GF assume a vertically propagating EM wave with an electric field vector \underline{E} and a wave vector \underline{k}_0 in the x, z plane. The z axis is taken parallel to a magnetostatic field. The vertical power flux P of the EM wave is then equal to the time averaged Poynting vector (eq. 3.20c). P can be written in terms of the

electric field components as

$$P = \frac{\mu_r \epsilon_0}{2} \left(\frac{c}{\mu_0} \right)^{1/2} \left\{ |E_y|^2 + |E_z|^2 \sin^2 \theta + |E_x|^2 \cos^2 \theta - 2 |E_x| |E_z| \sin \theta \cos \theta \right\} \quad 3.54$$

The power lost per unit height dP/dh due to scattering from FAI is proportional to P in a linear process i.e.

$$\frac{dP}{dh} = -a(h) \cdot P \quad 3.55$$

Height integration of 3.55 results in

$$P = P_0 \exp \left\{ -2 \int a(h) dh \right\} \equiv P_0 e^{-\Gamma} \quad 3.56$$

The factor of 2 appears because of the inclusion of a reflected wave. Γ is the anomalous absorption in Neper's.

GF deal with the FAI amplitudes in terms of Minkoff's (1974) backscatter cross-section formulae. The FAI are assumed to be cylindrically symmetrical about an axis parallel to the geomagnetic field. The mean perturbation plasma density associated with FAI, $\langle |n^2| \rangle^{1/2}$ is related to the measured backscatter cross section $b(k)$ by (Minkoff, 1974),

$$\langle |n^2| \rangle = \frac{32\pi \epsilon_0 m_e^2 c^4}{e^4} \int_0^\infty k b(k) dk \quad 3.57$$

GF write Dawson and Oberman's formula for the force per unit volume acting on the ions as (GF equ.28)

$$\begin{aligned} \underline{F}_{ie} = & \left[\frac{e^3}{4\epsilon_0 m_e \omega_0^2} (2\pi)^4 V T_L \right] \int \frac{k}{k^2} \cdot n^2(k, \omega) \left\{ \sin \omega_0 t \left\{ \left[(D_r/|D|^2)_{\omega+\omega_0} + \right. \right. \right. \\ & \left. \left. \left. + (D_r/|D|^2)_{\omega-\omega_0} \right] k_x E_x + \left[(D_i/|D|^2)_{\omega+\omega_0} - (D_i/|D|^2)_{\omega-\omega_0} \right] k_y E_y \right\} \right. \\ & \left. + \cos \omega_0 t \left\{ \left[-(D_i/|D|^2)_{\omega+\omega_0} + (D_i/|D|^2)_{\omega-\omega_0} \right] k_x E_x + \right. \right. \end{aligned}$$

$$\begin{aligned}
& + [(D_r/|D|^2)_{\omega+\omega_0} + (D_r/|D|^2)_{\omega-\omega_0}] k_y E_y - 2 \sin \omega_0 t \{ (D_r/|D|^2)_\omega k_x E_x \} \\
& - 2 \cos \omega_0 t \{ (D_r/|D|^2)_\omega k_y E_y \} \] d^3 k d\omega
\end{aligned} \tag{3.58a}$$

where D_r and D_i are the real and imaginary parts of the plasma dielectric functions in 3.52c, and V and T_L are volume and duration of the fluctuations \mathcal{N} , whose Fourier spectrum is $\mathcal{N}(\underline{k}, \omega)$. GF attribute Dawson and Oberman's (1963) correlation factor $\sum_{j,i} \exp(\underline{k} \cdot (\underline{x}_i - \underline{x}_j))$ (equ. 3.48b) to the electron FAI structure. By taking account of the cylindrical symmetry of \mathcal{N} about the direction of the magnetic field implied by 3.57, 3.58 reduces to (equ. 29 in GF)

$$\begin{aligned}
\underline{F}_{ie} = & (e^3/\epsilon_0 m_e \omega_0^2) (c^4/\omega_0^4) N_0^2 \cdot 2\pi \int dk k b(k) \cdot \{ \sin \omega_0 t (D_r/|D|^2)_\omega - \\
& - \cos \omega_0 t (D_i/|D|^2)_\omega - \sin \omega_0 t (D_r/|D|^2)_0 \} E_x \hat{i} + \{ \sin \omega_0 t (D_i/|D|^2)_\omega \\
& + \cos \omega_0 t (D_r/|D|^2)_\omega - \cos \omega_0 t (D_r/|D|^2)_0 \} E_y \hat{j} \] ,
\end{aligned} \tag{3.59b}$$

where \hat{i} and \hat{j} are unit vectors along the x and y axes respectively.

Because of the force \underline{F}_{ie} on the ions, the power lost from the wave per unit volume is

$$\frac{dP}{dh} = \text{Re} (\underline{J}_{ie} \cdot \underline{E}^*) \tag{3.59a}$$

where

$$\underline{J}_{ie} = \frac{e \underline{F}_{ie}}{i m_e \omega_0} \tag{b}$$

Substituting 3.58 into 3.59 produces

$$\frac{dP}{dh} = \left(- \frac{\pi \epsilon_0 c^4}{\omega_0^3} \right) \cdot I \cdot (E_x^2 + E_y^2) \tag{3.60a}$$

$$\text{where } I = \int dk k b(k) \cdot (D_i/|D|^2)_\omega \tag{b}$$

GF employ the following approximation for $D(\omega, k)$

$$D(\omega, k) = 1 - \omega_e^2 ((\omega^2 - \Omega_e^2)^{-1} - 3k^2(T_e/m)/\omega^4) - i\nu/\omega \quad 3.61$$

3.61 approximates to a delta function centred on

$$k = k_\omega \simeq [(\omega^2 - \omega_e^2 - \Omega_e^2)/(3T_e/me)]^{1/2} \quad 3.62$$

Thus, approximately

$$D(\omega, k) = (\partial D_r / \partial k)(k - k_\omega) - i\nu/\omega \quad 3.63a$$

and

$$\int D_i / |D|^2 dk = -\pi / (\partial D_r / \partial k) = -\pi / 6\lambda_D^2 k \quad b$$

where λ_D is the Debye wavelength.

Substituting 3.63b into 3.60 produces finally

$$\frac{dP}{dh} = \frac{\pi^2 \epsilon_0 c^4 b(k)}{6\omega^3 \lambda_D^2} (E_x^2 + E_y^2) \quad 3.64$$

GF then proceed to calculate the anomalous absorption numerically, employing, 3.64, 3.54, 3.56 and 3.57 together with the refractive index and polarization relations for an EM wave 3.9 and 3.10 and the empirical spectrum $b(k)$ obtained by Minkoff (1974). A graph of $b(f_{\text{radar}})$, with $f_{\text{radar}} = ck/4\pi$ is reproduced in fig. 2.6 in the previous chapter.

3.5.3 The Vaskov and Gurevich anomalous absorption calculation

Vaskov and Gurevich's calculation of anomalous absorption of EM waves due to scattering from FAI is given in detail in Vaskov and Gurevich (1976) and Gurevich (1978). Their starting point is the fluid equations for momentum and charge continuity of electrons from which they derive a polarization charge density $\rho(\omega)$ generated by the oscillating electric field of the EM wave. $\rho(\omega)$ provides an oscillating dipole source for Langmuir waves. Vaskov and Gurevich employ geometrical optics in the calculation of scattered Langmuir wave amplitude. They also employ the quasi-longitudinal approximation for the refractive index of EM waves; see section 3.3.1 (eq. 3.12). Their final result for Γ is analytic in form. They have

$$\Gamma = \frac{\frac{\langle |n|^2 \rangle}{N_0^2} (1-u)^2 \pi \omega u^{-1/4} \left(\frac{1-\sqrt{u}}{1+\sqrt{u}} \right)}{c \left| \frac{dV}{dh} \right|_{h=h_1}} \quad 3.65$$

where $u = (\Omega_e/\omega)^2$, $v = (\omega_e/\omega)^2$ and h_1 is the height at which the EM wave frequency is equal to the local upper-hybrid frequency.

3.6 Summary

The basic equations of plasma dynamics which are applicable to the ionospheric F-region, together with the properties of transverse (electromagnetic) and longitudinal (electrostatic) wave motions that the plasma can support have been considered. The generation mechanisms of small scale field aligned irregularities which arise when the F-region is illuminated by powerful radio waves have been

presented. Of the proposed generation mechanisms attention has been focussed on the so called thermal parametric instabilities. The small scale inhomogeneities cause anomalous absorption of EM waves due to mode conversion into Langmuir waves. The enhanced (anomalous) absorption of the high power EM wave itself gives rise to intense plasma heating which causes large scale plasma temperature enhancements. In the lower F-region this gives rise to large scale plasma density enhancements. Only the O-mode wave can generate field aligned irregularities and undergo anomalous absorption. In contrast heating on large spatial scales due to deviative (collisional) absorption of EM waves can occur during both O- and X-mode heating.

Self-focussing instabilities which give rise to medium scale field aligned depletions in the upper F-region (Fejer, 1979) have not been considered here. They are generally supposed to be responsible for heater induced spread-F (Cragin et al., 1977). Self-focussing instabilities have been studied theoretically by Perkins and Valeo (1974), Cragin and Fejer (1974) and Vaskov and Gurevich (1976a, 1977a). Spread-F produced in heating experiments in Northern Scandanavia has yet to receive serious attention (see chapters 4 and 9).

CHAPTER 4. THE HIGH LATITUDE EXPERIMENT IN NORTHERN SCANDANAVIA

During the last five years the Ionospheric Physics Group at Leicester University has carried out an extensive series of experimental studies of the auroral ionosphere in the vicinity of Tromso, Norway. These experiments have been carried out in collaboration with the University of Tromso and the Max-Planck-Institute für Aeronomie, Lindau. The initial experiments were concerned with studies of naturally occurring ionospheric disturbances. However during the last three years the major effort has been directed towards observations of artificial disturbances produced by the high power facility at Ramfjordmoen near Tromso.

4.1 The Ramfjordmoen heating facility

The construction of a high power HF modification facility undertaken jointly with the Max-Planck-Institut für Aeronomie, Lindau and the University of Tromso, at Ramfjordmoen (Norway) was completed in 1980. Ramfjordmoen is a high latitude site (69.6°N) and the decision to build a new modification facility there was motivated by a number of factors. Firstly, there is clearly a need for a high power modification facility of comparable power to those at mid- and low-latitudes in order to examine the latitudinal dependence of modification phenomena. Particularly strong wave interaction effects are expected at high latitudes because of the large dip angle of the geomagnetic field. Secondly, the medium to be modified, the high latitude auroral ionosphere, is quite different from that at mid- and low-latitudes. The presence of horizontal and field aligned currents, precipitating particles, naturally occurring plasma instabilities and plasma density gradients on a wide variety of scales creates experimental conditions for ionospheric modification which are certain to lead to new modification effects (Stubbe et al.,

1982b). Thirdly, the Ramfjordmoen site has the special advantage of unique accumulation of excellent diagnostic facilities. In particular, it is the site of the new European Incoherent Scatter Radar (EISCAT).

Geomagnetic parameters appropriate to the Ramfjordmoen site are listed in table 4.1.

4.2 The High Power Transmitters and Antenna Fields

The high power facility at Ramfjordmoen consists of twelve transmitters each capable of generating a power of up to 125 kW continuously in a frequency range 2.5-8 MHz. The power from the transmitters can be fed into any one of three antenna arrays depending on the transmitted frequency required. The frequency range of each antenna array is 2.5-4, 3.85-5.65 and 5.5-8 MHz. In order to reduce the likelihood of the high power transmitter adversely affecting public radio communication systems in the vicinity of Tromso, the Norwegian government has restricted transmitted frequencies available for modification experiments to bands a few kHz wide centred on the frequencies,

2.759, 3.324, 3.515, 4.040, 4.544, 4.9128, 5.423, 6.770, 6.960, 7.100 and 7.953 MHz.

Each of the antenna arrays consists of six rows of six crossed full wavelength horizontal dipoles. Each row of crossed dipoles is driven by two transmitters; one for each dipole orientation. This enables circularly polarized (O- or X-) radiation to be transmitted. The orientation of the dipoles is either east-west or north-south. The rows are east-west orientated so the beam may be tilted in the north-south meridian plane by introducing relative phase shifts between the transmitters.

The antenna gain is 24 dB ($\bar{+}$ 1dB) depending on frequency. The corresponding beam width (3dB contour) is 14.5° . The maximum ERP is thus (eq. 2.1a) 360 MW. The highest power so far employed (up to Oct. 1982) is 290 MW corresponding to a power of 100 kW from each transmitter.

The transmitters are capable of being operated continuously or in a modulated mode including on-off keying. The facility was designed mainly for CW operation so that if the transmitter output is modulated into pulses the peak pulse power cannot exceed the CW power. The minimum pulse length available is $20 \mu\text{s}$ but there is no limitation on the duty cycle. Modulation frequencies between 0 and 50 kHz are thus obtainable although modulation frequencies between 15 and 200 Hz are not used because of possible mains supply filter resonance. Since September 1981 computer control of the high power facility has been possible with regard to transmitter power setting, carrier frequency, polarization, modulation frequency, modulation depth and pulse duty cycle. Preprogramming of the control computer enables complicated heater sequences to be generated which would be otherwise impossible by manual control. (See for example the power stepping sequences described in chapter 7).

Because of strong radiation coupling between the antennas in each array the initial switch-on of the heater requires careful iterative tuning of the transmitters. This procedure takes approximately 3 minutes. After the initial switch-on, heater-off is not a complete switch-off (i.e. not a zero transmitted power situation). It corresponds to the lowest possible applied synthesizer voltage which produces an ERP 37.5dB below the power during heater-on.

4.3 The Diagnostic Equipment

The experimental data presented and discussed in chapters 5, 6

Ramfjordmoen, Norway

Geomagnetic Latitude	Geomagnetic Longitude	Dip Angle I	Gyrofrequency (MHz)
67.1° N	19.2° E	78°	1.4

Table 4.1 Geomagnetic data for Ramfjordmoen, Norway.

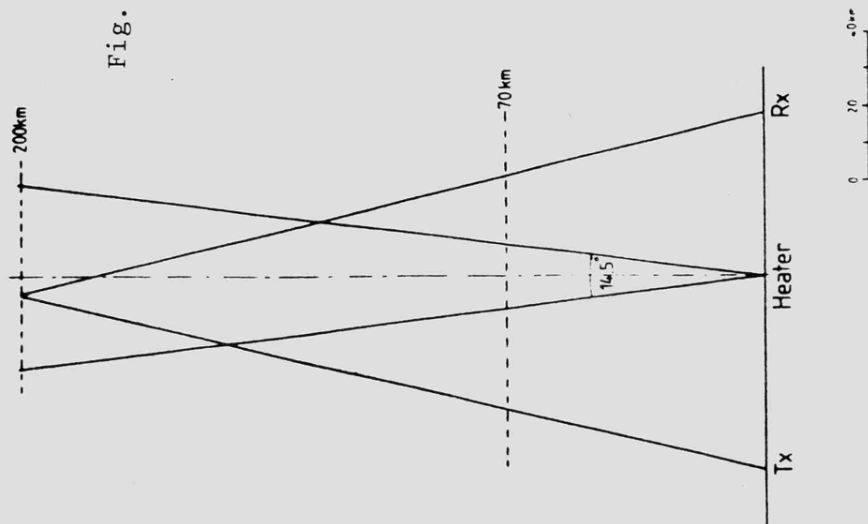


Fig. 4.1 Vertical section heater beam and diagnostic ray path, in the plane of the magnetic meridian.

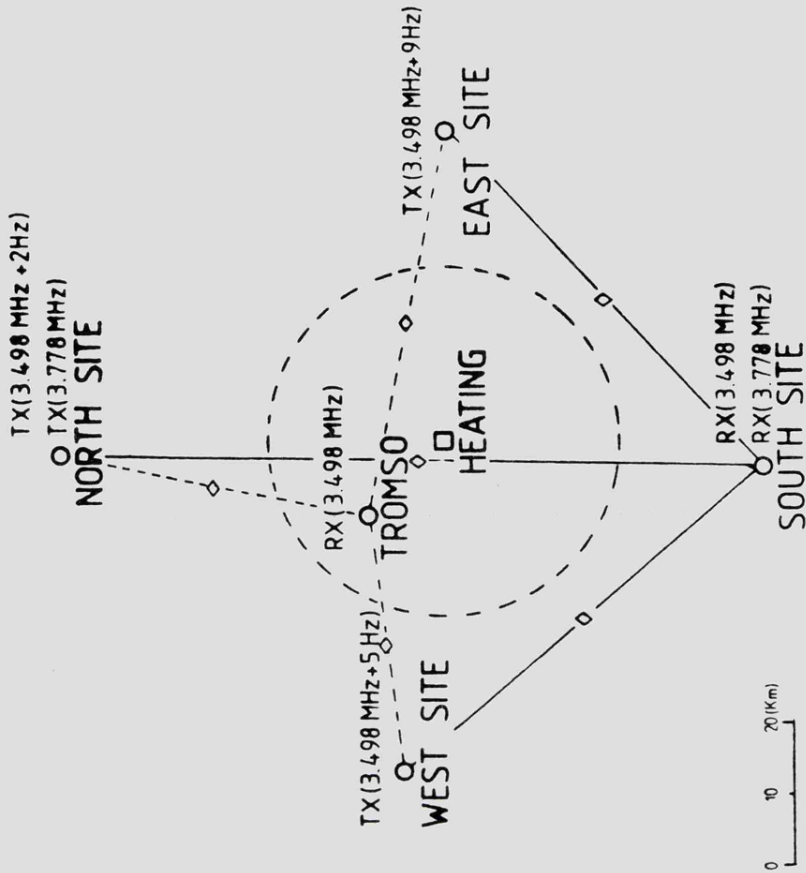


Fig. 4.2 Plan of the positions of the diagnostic transmitters and receivers relative to the heating facility at Ramfjordmoen during the October 1980 campaign.

and 8 of this thesis derive from low-power ($\sim 30\text{W}$) HF diagnostic radio signals which propagate through that volume of the F-region illuminated by high power radio waves from the Ramfjordmoen facility. In certain experiments the reflected high power wave itself was employed as a diagnostic (see chapter 7). The experiments were all conducted during 2 to 3 week campaigns in October, 1980; September, 1981 and October, 1982.

The purpose of the low-power HF diagnostic waves is to investigate the effects of heating on the F-region plasma.

In view of the results obtained during heating experiments at Platteville and Arecibo (see chapter 2), a number of modification phenomena could be expected to cause observable effects on low power diagnostics passing through the heated volume. Small scale field aligned irregularity generation causes absorption of radio waves. Plasma density changes on large spatial scales alters the refractive index for radio waves. These two effects influence respectively the amplitude and phase of diagnostic radio waves. Thus diagnostic amplitude and phase measurements should yield valuable information regarding the generation of plasma density irregularities during heating.

A spaced transmitter-receiver system was therefore employed so that the diagnostic ray path between the transmitter and receiver (via the ionosphere) would avoid the heated D-region.

Fig. 4.1 is a scale drawing of a vertical section (approximately in the meridian plane) through the heater beam (3dB contour) and the north-south diagnostic ray path reflected from a height of 200 km. The ray reflection points are assumed to be the mid-path points. This approximation is valid when the radio frequencies involved are more than a few MHz below the critical F-region frequency (see chapter 5). Fig. 4.1 clearly demonstrates that the diagnostic ray path avoids that part of the D-region (~ 70 km altitude) illuminated by the heater beam.

Fig. 4.2 illustrates the position of the transmitter and receiver sites relative to the Ramfjordmoen heating facility for the experimental campaign in October 1980. In fig. 4.2 the main diagnostic path is that of the 3.778 MHz signal between a transmitter at a site 53 km north and a receiver 44 km south of the heater. The ionospheric reflection point of this path, assumed to be approximately at the mid-path point is within 5 km of the centre of the heater beam. The 3dB contour of the heater beam at 200 km is indicated by the circle centred on the heater. A more realistic 3dB contour together with diagnostic reflection points are calculated by ray tracing through F-region electron density profiles determined from ionograms during actual experiments, are presented in chapter 5 (fig. 5.5).

Also illustrated in fig. 4.1 are the positions of 3.498 MHz transmitters, one at the north site and one at each of two sites to the east and west of the heater, employed in a spaced Doppler system with receivers at Tromso (16km north-west of Ramfjordmoen) and another at the south site. During subsequent campaigns in Sept. 1981 and Oct. 1982 two further transmitters were installed at the north site with two corresponding receivers at the south site so that the centre of the heater beam could be probed by diagnostics on 3 different frequencies simultaneously.

All of the diagnostic radio transmitters mentioned above operate at CW. In addition to these, a vertical incidence ionosonde was available at the south site. The main purpose of this instrument was to provide information concerning the state of the background (unmodified) ionosphere during the experiments. The ionosonde was also used to search for heater generated spread-F.

All real time data logging is carried out at the south site (fig. 4.2). Communication between the south site and the heater control room at Ramfjordmoen is possible via a VHF radio link. Communication with the north (transmitter) site for the purpose of requesting

alterations of the diagnostic transmitter frequencies is possible over an HF link. To facilitate rapid transmitter frequency changes the dipole antennas at the north site are in the form of metal tapes whose length can be easily changed by their being wound onto (or off) spools.

The transmitting receiver and data capture system employed for the phase and amplitude measurements is illustrated schematically in Fig. 4.3. A highly stable frequency synthesizer drives a transmitter with the fundamental transmit frequency, f_o . A similar synthesizer provides the VFO ($f_o - 100\text{KHz}$) for the receiver. A 100 KHz signal from the receiver synthesizer is mixed with the IF ($\approx 100\text{KHz}$) output of the receiver in a phase comparator. The voltage output of the comparator is proportional to the phase of the resulting mixed signal. Since only the receiver IF frequency changes due to the varying phase path of the propagating radio wave the phase comparator output voltage then provides a measure of the radio wave phase. The phase comparator output is displayed on a chart recorder. An example of phase variation reversal induced in a diagnostic signal during a period when the heater was switched on and off is reproduced in fig. 4.4.

The IF output of the receiver is also fed into an amplitude detector. The output of the amplitude detector is connected to a separate chart recorder. An example of the diagnostic amplitude data recorded during heater switch on and switch-off is reproduced in fig. 4.5. When three diagnostic radio waves are employed for phase and amplitude measurements at 3 different frequencies simultaneously, then system in fig. 4.3 is triplicated.

Each diagnostic receiver is capable of operation with a number of bandwidth settings. Bandwidths of 100, 300, 1200, 6000 and 13000 Hz are available. The receivers were generally operated on their lowest (100Hz) bandwidth setting.

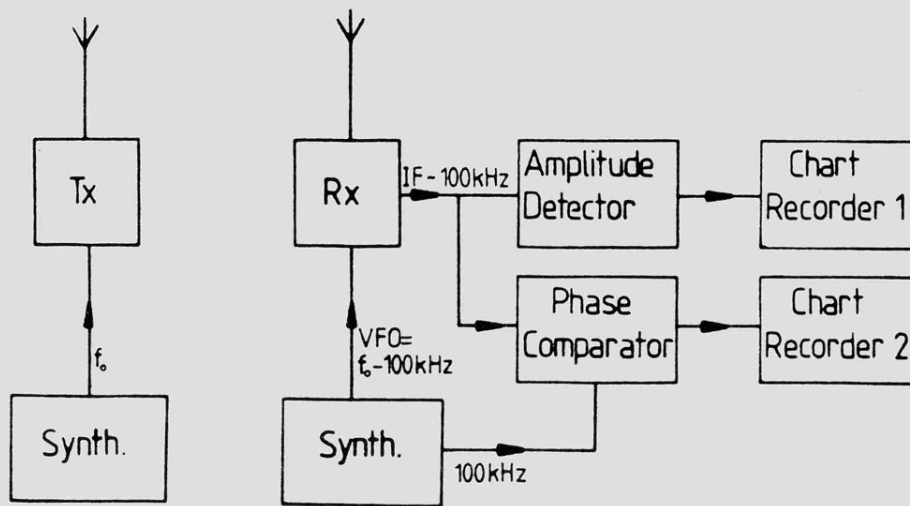


Fig. 4.3 Schematic diagram of the equipment for recording diagnostic amplitude and phase.

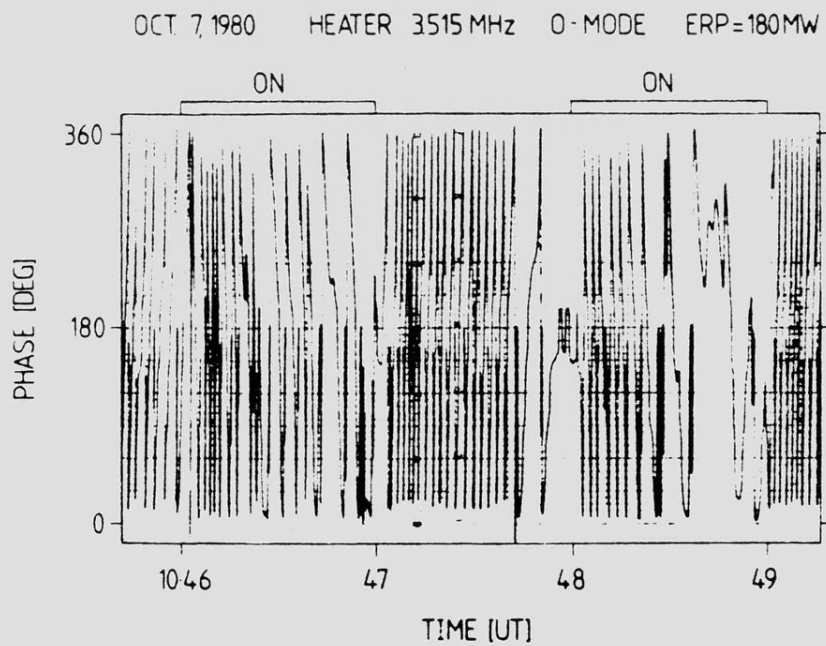


Fig. 4.4 An example of phase data from a 3.778 MHz diagnostic signal during heating at Ramfjordmoen.

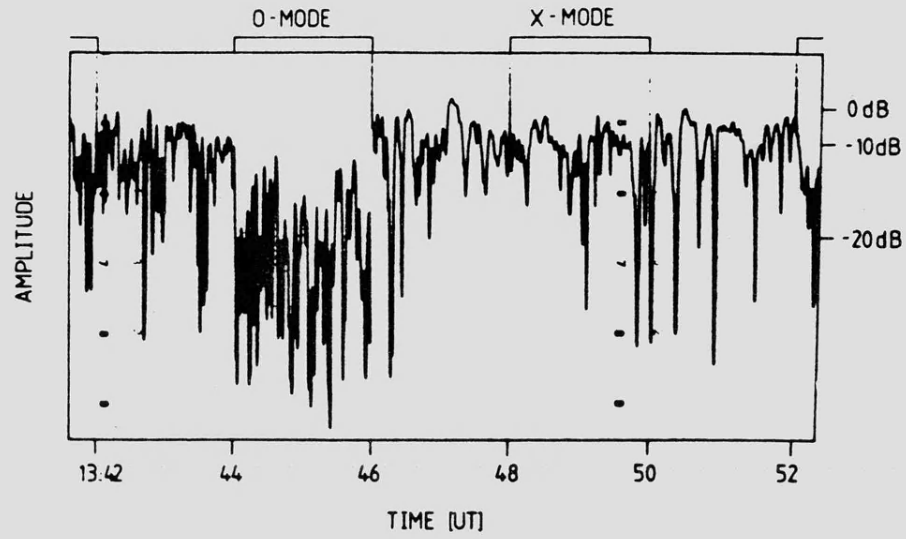


Fig. 4.5 An example of amplitude data from a 3.778 MHz diagnostic signal during heating at Ramfjordmoen.

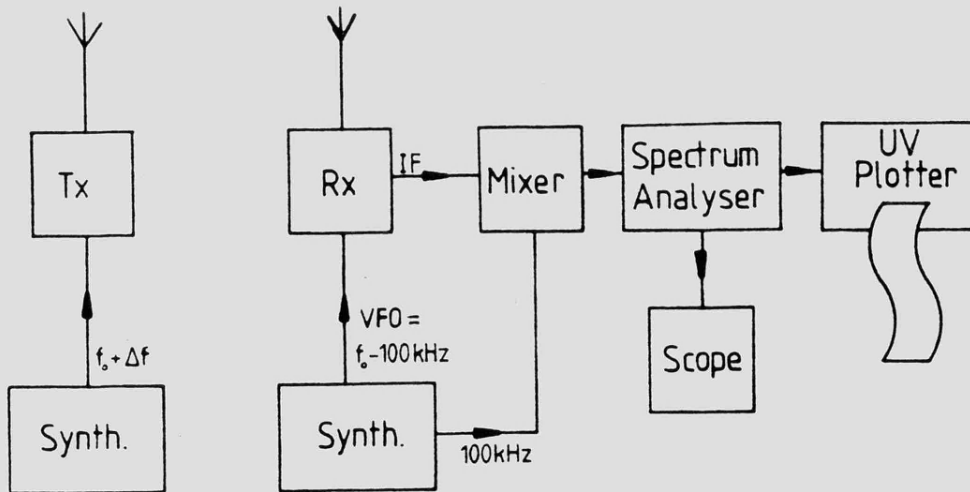


Fig. 4.6 Schematic diagram of the equipment for recording real-time spectra of HF diagnostic signals.

In order to obtain spectral information from the HF diagnostic signals a second type of receiver system, illustrated in fig. 4.6 is employed (the transmitter system is identical to that in fig. 4.3). A VFO signal of frequency $f_0 - 100\text{kHz} - \Delta f$ is supplied to the receiver from a synthesizer. f_0 is the transmitted frequency and Δf an offset which is determined by the spectral width of interest. A reference signal of 100 kHz and the receiver IF signal are combined in a mixer whose output is then fed into a Ubiquitous audio spectrum analyser. The output of the spectrum analyser is displayed on an oscilloscope and hard copies of the spectrum can be made with a UV plotter.

The diagnostic detection system just described can be employed in the detection of heater induced cross-modulation sidebands (see chapter 8) or as a conventional Doppler sounder (Davies et al., 1962). In circumstances where several spaced transmitters but a single carrier frequency are employed, as in the 3-transmitter system in fig. 4.7, then a small offset frequency is added to each transmitted frequency so that the signals can be distinguished at the receiver after spectral analysis.

For the campaigns in Sept. 1981 and Oct. 1982 a Doppler transmitter was installed at Kiruna, Sweden and its signal received at the South site. Kiruna is some 200 km South of Ramfjord and the Kiruna-south site path provides a reflection point approximately 120 km south of the heated volume. The purpose of this diagnostic was to detect heater generated gravity waves (see section 4.4.3).

During the 1980 campaign the south diagnostic station was located near Storsteinnes (69.20°N, 19.12°E). For subsequent campaigns the South diagnostic station moved to a location near Seljelvnes (69.25°N, 19.20°E) which is approximately 8 km from the original Storsteinnes site. The difference in the radio ray paths from the north site to these two south sites is minimal. The lengths of the two paths are almost

identical and their azimuths differ by approximately 4.5° .

Throughout the 1981 and 1982 campaigns the reflected heater signal itself was monitored at the south site by a receiver system identical to that in fig. 4.3.

4.4 Types of modification experiments

Ionospheric modification experiments performed with the Ramfjordmoen high power facility together with the diagnostics described in section 4.3 may be classified as follows:

(a) Measurements of diagnostic wave amplitude and phase changes induced by F-region heating.

(b) Measurements of diagnostic wave Doppler shifts induced (directly) by heating.

(c) Measurements of diagnostic modulation depth and sideband frequency during modulated heating (cross-modulation).

(d) Measurements of ionospherically reflected pump signal amplitudes as a function of transmitted power.

(e) Search for artificial spread-F with an ionosonde and CW diagnostic spectral analysis.

(f) Search for acoustic gravity waves generated by periodic heating. Experiments of the type (a), (c) and (d) have yielded important new information with regard to modification of the high latitude ionosphere and have been employed extensively in the heating campaigns since 1980. These experiments are described and their results discussed in detail in chapters 5, 6, 7 and 8. Experiments of types (b), (e) and (f) were not developed to the same extent and are briefly dealt with in the following three subsections.

4.4.1 Diagnostic Doppler Shifts Induced by the heater

Fig. 4.7 illustrates an example of three station Doppler data

recorded at the South site (near Storsteinnes) in Oct. 1980 (see fig. 4.2 for plan of transmitter and received sites). The three transmitters at the North, West and East sites operated on a single frequency of 3.498 MHz but with small offsets to separate the signals (in the spectrum analyser) of 2, 5 and 8.9 Hz respectively. The heater was operating at 3.515 MHz in ordinary polarization. The Doppler response to heater on and heater off is almost identical for all three signals. In fig. 4.7 a sharp positive Doppler shift and slow decay to zero shift may be observed as the heater switches on for a period of 1 minute at full power (160 MW in this case). As the heater is switched off a sharp negative shift is apparent followed by a slow decay to zero (while the heater remains off for 1 minute). The rapid change in diagnostic frequency at heater on and heater off is approximately 2 Hz in amplitude. There is a slight time lag in the diagnostic response because of the time constant of the spectrum analyser (~ 5 s).

One interesting difference between the three traces in fig. 4.7 is evident. The trace corresponding to the north site transmitter is completely absent shortly after heater switch on whereas the west and east site signals although reduced in strength are still visible on the UV record. The reduction in the trace visibility is due to the anomalous absorption of diagnostic radio waves passing through the heated F-region (see section 3.5 and chapter 5). From fig. 4.2 it is evident that the north-south diagnostic reflection point is close to the centre of the heater beam whereas the west to south and east to south path reflection points are just outside the 3dB point contour of the heater beam. It is therefore probable that the north-south diagnostic suffers stronger anomalous absorption due to the action of the heater wave than do the other two diagnostic paths.

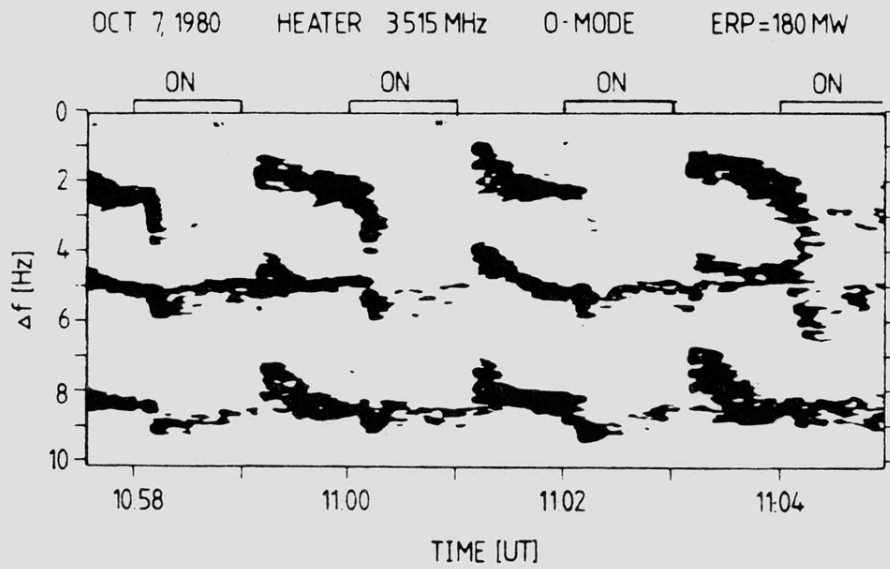


Fig. 4.7 An example of the Doppler shifts induced in three HF signals during heating at Ramfjordmoen.

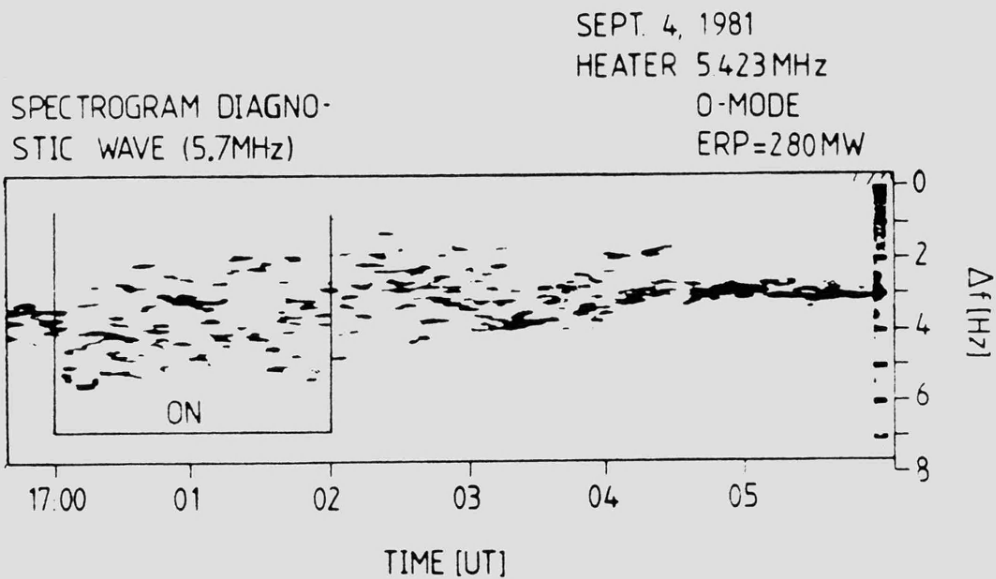


Fig. 4.8 Heater induced spread in diagnostic spectrum during heating at Ramfjordmoen.

The observed Doppler shifts represent a phase path change induced by a lowering of the diagnostic reflection heights during heater "on" periods. This is in complete agreement with the phase changes observed in the 3.778 MHz diagnostic (see section 6.1).

4.4.2 A search of artificial spread-F

Utlaut and Violette (1974) refer to heater induced spread-F a phenomenon which was most consistently and easily produced during modification experiments at Platteville (see section 2.7), as indicated by vertical incidence ionograms (fig. 2.14). All attempts to reproduce these results with the Ramfjordmoen heater have proved negative. Many vertical ionograms have been taken at the south site and at Ramfjordmoen but none has exhibited the characteristics of artificially induced spread-F.

Of the large number of Doppler measurements recorded during F-region heating only on a few occasions have signs of diagnostic signal spreading (rather than the shifting described in the previous subsection) consistent with artificially induced spread-F been apparent. An example of one such positive effect is illustrated in fig. 4.8. It is evident that within seconds of turning on the heater (5.423 MHz, O-mode ERP = 280 MW) at 1700 UT on 4 Sept. 1981, the spectralwidth of a diagnostic signal (5.701 MHz) was broadened from approximately 1 Hz to 4 Hz. The diagnostic signal spectrum remained broad during the 2 minutes that the heater remained on. The broadening persisted for approximately 3 minutes after the heater was turned off.

Any differences in the manner in which medium scale irregularities, which give rise to artificial spread F, are excited at mid- and high-latitude should shed light on the theories which are invoked to explain this phenomenon (see Fejer, 1979; Stubbe and Kopka, 1980).

4.4.3 Artificial generation of acoustic-gravity waves

Grigory'ev (1975) has proposed that F-region heating of the electron plasma can result in significant neutral heating with a time constant of the order of 10^2 s. It is feasible therefore that periodic heating with an on-off frequency lower than the local Brunt-Vaisala frequency of the neutral atmosphere could generate so called acoustic-gravity waves (Yeh and Liu, 1974; Gossard and Hooke, 1975). The oscillation period corresponding to the Brunt-Vaisala frequency in the thermosphere is approximately 14 minutes.

During the heating campaign of Sept. 1981 an attempt was made to generate neutral acoustic-gravity waves in the F-region above Ramfjordmoen by employing periods of O-mode heating at 5.432 MHz in sequences of 10 min-on, 10 min-off, thus imposing a 20-min neutral temperature oscillation on the region of the thermosphere illuminated by the heater.

Acoustic-gravity waves from natural sources are commonly observed at F-region heights by radio methods as travelling ionosphere disturbances (TID). TID are most easily detected by simple Doppler sounding systems such as that described in section 4.3 (see Georges, 1970). Hines (1960) was first to suggest the connection between acoustic-gravity waves and TID and there is now overwhelming observational evidence to support Hines' theory (Beer, 1974).

It is anticipated therefore that heater generated acoustic-gravity waves propagating away from the source region should give rise to a TID. The Kiruna Doppler transmitter described in section 4.3 was employed in an attempt to detect such a TID which results from the heater-generated acoustic gravity wave. Although oscillations characteristic of acoustic-gravity waves were observed on the Kiruna Doppler, none were correlated with periodic heating, even allowing for acoustic-gravity wave propagation time from the source to the detection region.

4.5 Concluding remarks

The high power heating facility and HF diagnostics described in this chapter have been employed in a series of three campaigns to investigate systematically the effect of high power radio waves on propagation characteristics of the ionospheric F-region. A number of tentative experimental results have been presented in section 4.4 of the present chapter. In the following chapters other results are presented and discussed in detail in the light of previous modification experiments at mid- and low-latitudes and current theories of ionospheric modification processes.

5. DIAGNOSTIC AMPLITUDE EFFECTS

5.1. Introduction

The relationship between small scale field aligned irregularities (FAI), generated by a high power EM pump wave and anomalous absorption of a low power diagnostic signal passing through the heated volume is now well established (Stubbe et al, 1982b). This chapter presents a theory of anomalous absorption which takes full account of the effect of the geomagnetic field. From this analysis a new technique is developed for deducing certain features of FAI structure from measurements of anomalous absorption at a high-latitude site.

Anomalous absorption effects were first observed at a high-latitude site during heating experiments employing the Ramfjord heating facility in October 1980. Details of these first observations and their interpretation in terms of the generation of FAI during heating have already been published in Stubbe et al. (1982a) and Jones et al. (1982). These early experiments have recently been further developed to include 3 diagnostic signals which can simultaneously determine anomalous absorption at 3 different F-region heights. The results of these experiments are presented and interpreted in terms of the new theoretical analysis. Among the new results are the first determination of FAI scale lengths parallel to the geomagnetic field.

5.2. High latitude anomalous absorption observations

The following experiments were performed on a number of days during October 1980, September 1981 and October 1982. The data presented are representative of experiments during which positive heating effects were observed. Positive effects were invariably seen at geomagnetically quiet times between mid-morning and late afternoon when the F-region critical frequency (deduced from ionograms) was well

above (approximately 3 MHz) the pump and diagnostic frequencies. These ionospheric conditions result in the following HF propagation characteristics

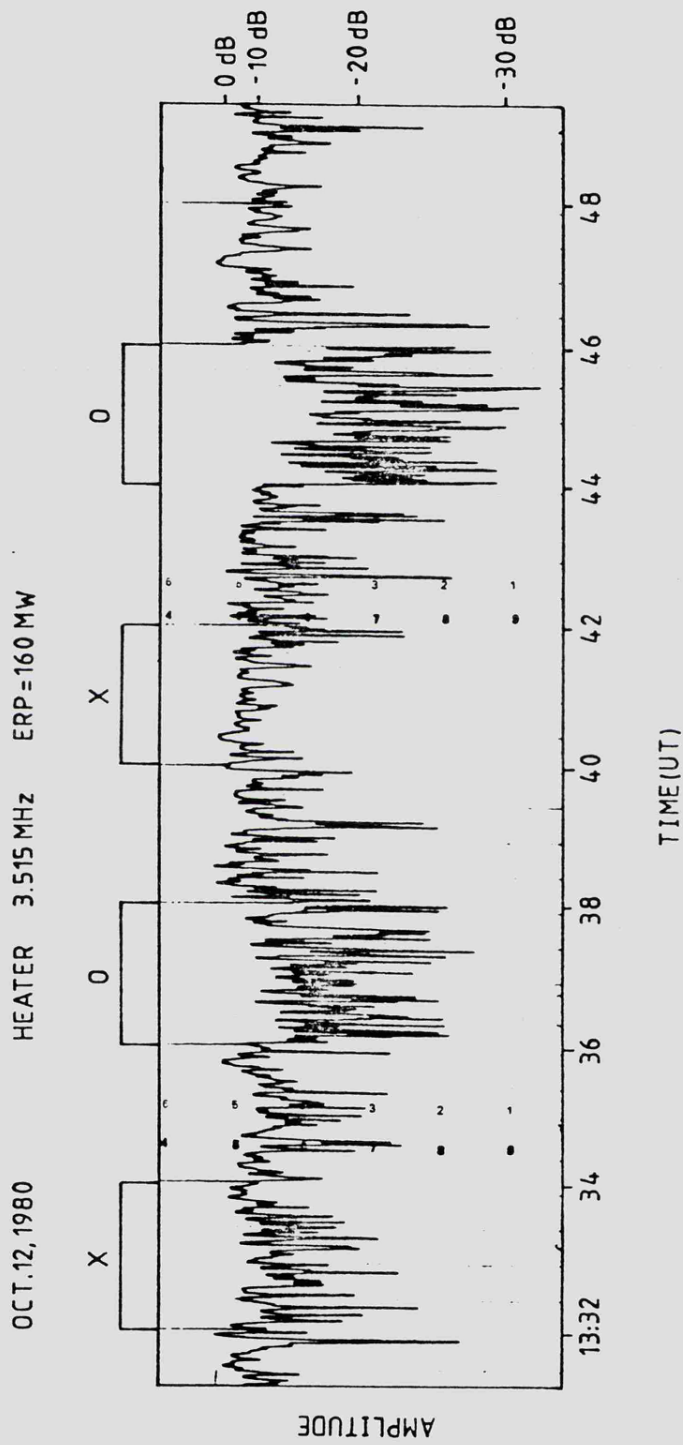
- (a) The horizontal separation of the O- and X-mode reflection points is minimized (less than 5km).
- (b) The altitude separation of the reflection heights of the pump and diagnostic waves is also minimized (less than 20km).
- (c) The presence of a daytime D-region ensured that the absorption of the X-mode greatly exceeded that of the O-mode for the frequencies employed.

Experiments were also performed during times when the ionosphere was disturbed, when the pump and diagnostic frequencies were close to $f_o F_2$ and after dusk. For these conditions no heating effects could be detected. This was either because the effects were very weak or natural amplitude fading was in excess of heater induced amplitude changes.

5.2.1 O- and X-mode heating effects

In the first series of experiments a high power pump was operated in a sequence of cycles of 2 min-on and 2 min-off at full power. Consecutive "on" cycles were alternately of ordinary then extraordinary polarization. Typical examples of diagnostic amplitude recorded during these heating sequences are illustrated in fig. 5.1a-c (b-c include three diagnostic and the pump skywave). From these data it is evident that O-mode heating causes a considerable diagnostic amplitude reduction (occasionally in excess of 10dB), whereas X-mode heating has a negligible effect (less than 1 dB change).

The results obtained when three diagnostic signals were monitored simultaneously are particularly significant (fig. 5.1 b-c). The range of diagnostic frequencies employed ensures sensitivity to absorption effects over the full height range of the heated region. The rapid



a.

Fig. 5.1a Amplitude of 3.778 MHz diagnostic signal vs. time, Oct. 12, 1980, 1332-1348 UT, during 0- and X-mode heating.

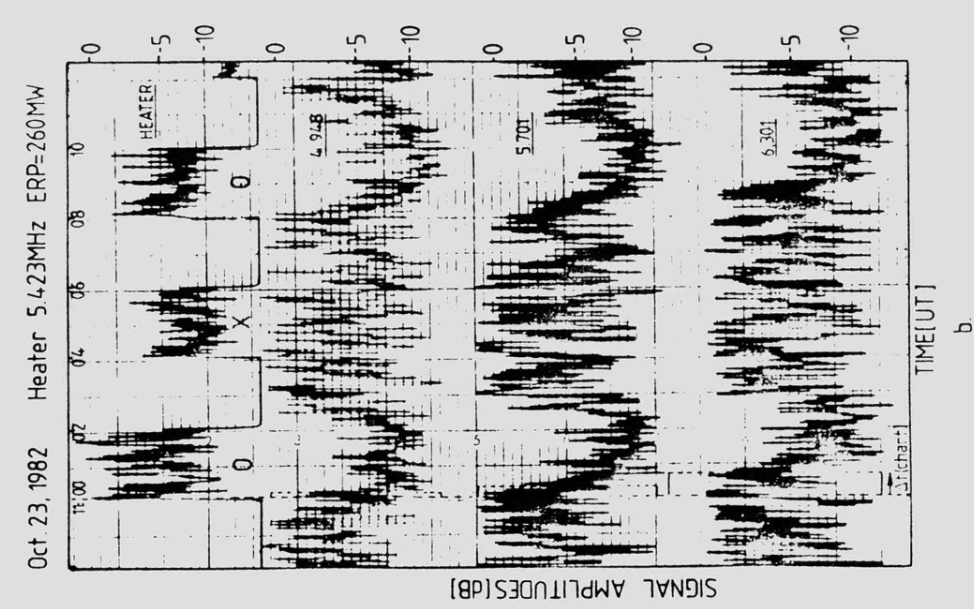
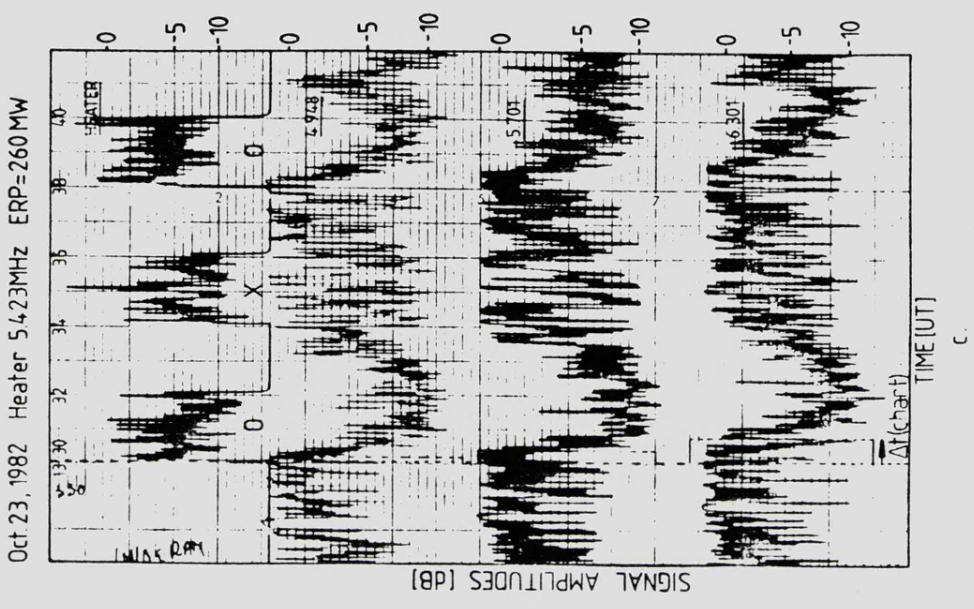


Fig. 5.1b,c. Amplitude of 4.948, 5.701 and 6.301 MHz diagnostic signals vs. time Oct. 23, 1982, (b) 1100-1110 UT, (c) 1330-1340 UT, during 0- and X-mode heating.

response to pump switch-on and switch-off (in O-mode) is also significant. It is at least as fast as the response time of the amplitude recorder (0.5s) in the example in fig. 5.1a. Also in this example, a marked increase in the fading rate of the diagnostic amplitude is observed after switch on of the O-mode pump.

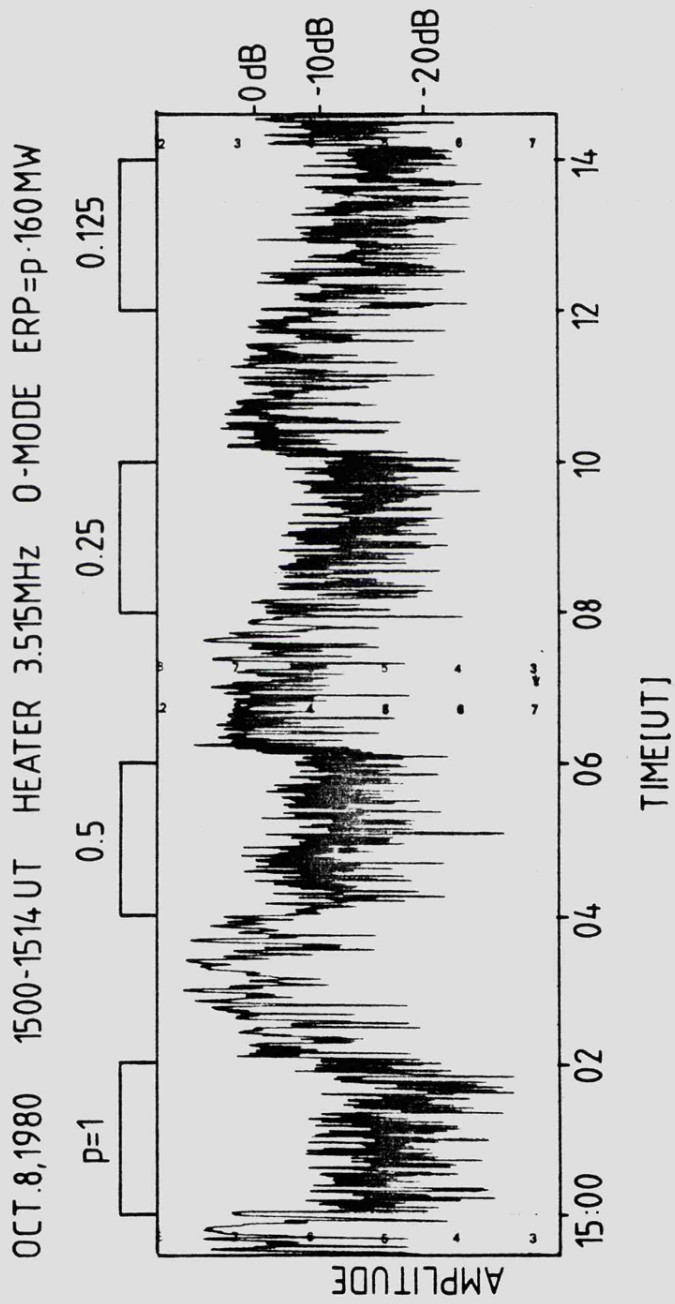
5.2.2 Effects of changing ERP

Experiments to study the effect on diagnostic amplitudes of changing the effective radiated power (ERP) during O-mode heating were performed on 8/10/80, 12/10/80 and 23/10/82. Some typical examples of these observations are illustrated in Fig. 5.2a-f (e and f have three diagnostic signals and the reflected pump signal). The heating sequence consisted of heater 'on' periods (separated by off periods) with $ERP = p \times \text{full power}$, where $p=1$ in the first 'on' period followed by decreasing fractions 0.5, 0.25, 0.125 (8, 12/10/80) or 0.35, 0.1 (23/10/82) in successive 'on' cycles.

As might be expected, in most of the data examined the absorption of the diagnostic during heating decreased with decreasing ERP. However, the data in fig. 5.2b represent a striking example of ERP changes having little effect on diagnostic absorption. It should be noted that for the cases where the absorption is dependent on ERP the diagnostic amplitude has a fast fading rate. This observation is consistent with the theory which indicates that amplitude fading plays an important role in the generation mechanism of FAI (see section 7.4.10; Stubbe et al 1982a).

5.2.3 Dependence of diagnostic absorption on diagnostic frequency

On 8th September 1981 the signal strengths of diagnostics operating at 4.948, 5.701 and 6.506 MHz were monitored in order to determine the diagnostic absorption induced while operating the pump at full power (260 MW effective radiated power), 5.423 MHz O-mode in a sequence



a.

Fig. 5.2a Amplitude of 3.778 MHz diagnostic signal vs. time, Oct. 8, 1980, 1500-1514 UT during 0-mode heating with changing ERP.

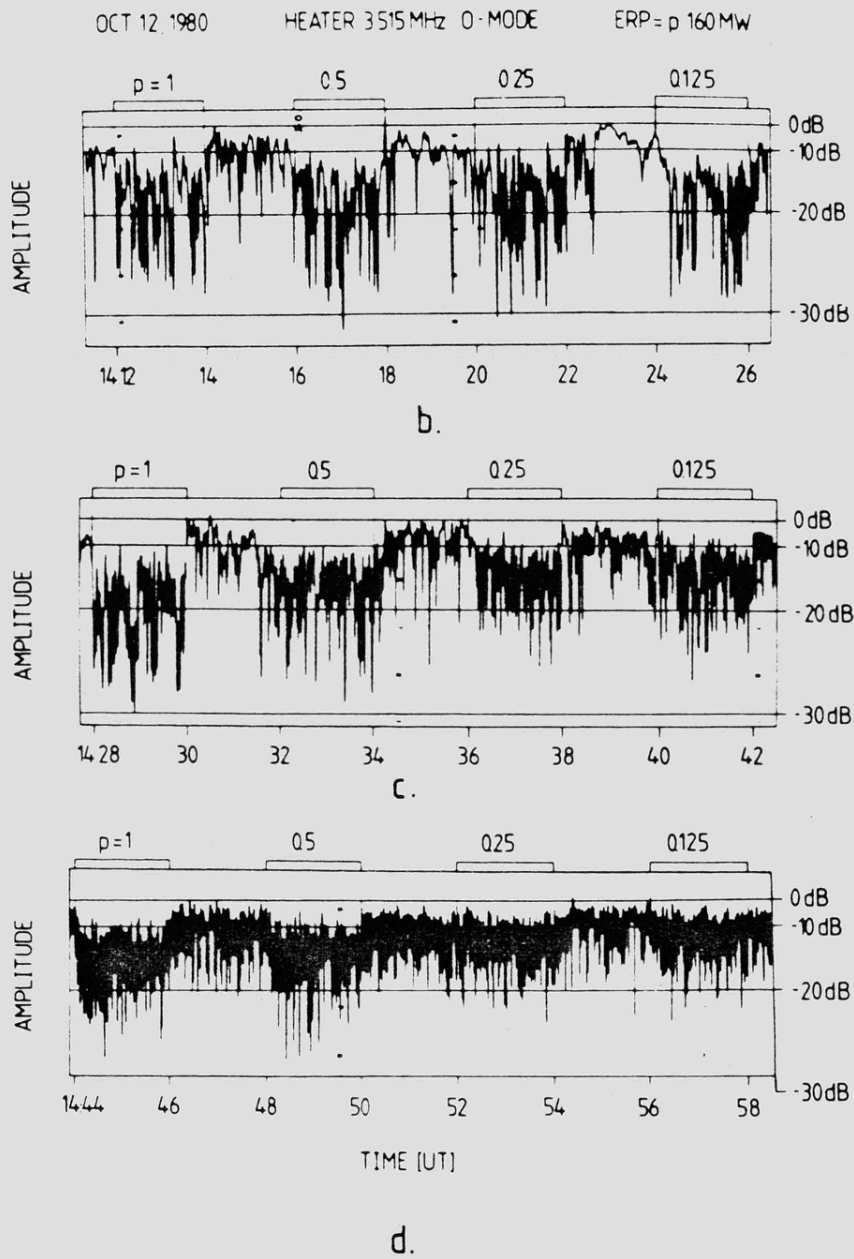
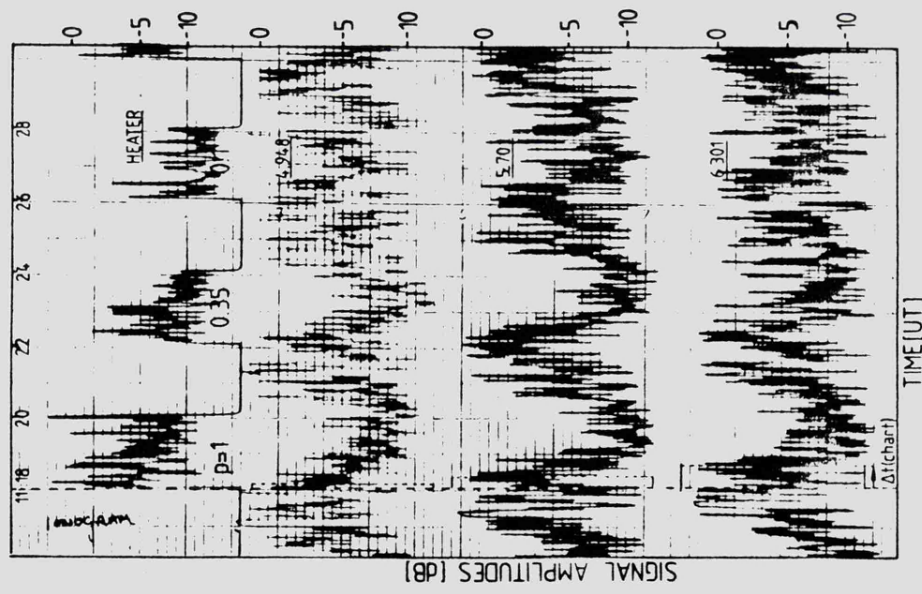


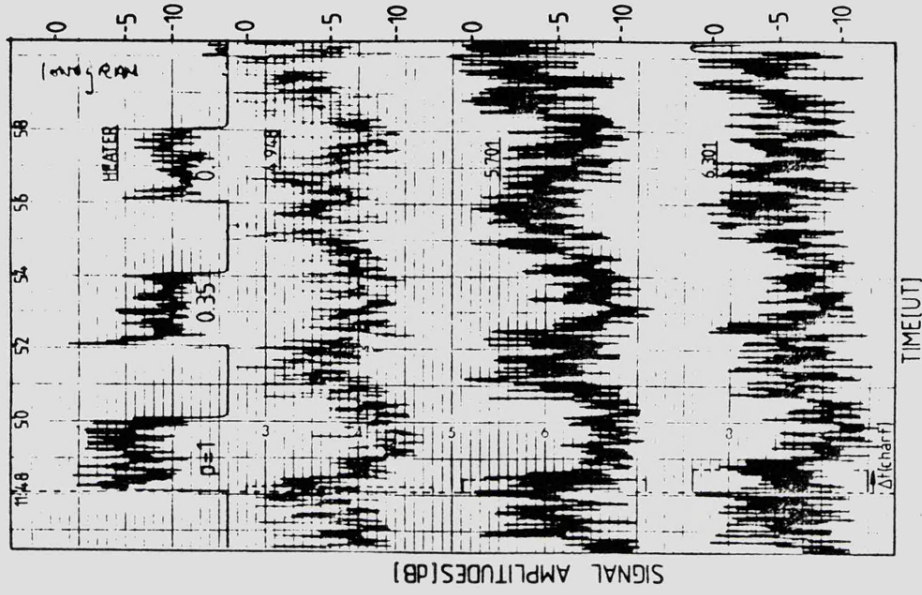
Fig. 5.2 b-d As 5.2a but on Oct. 1412-1458 UT.

Oct. 23, 1982 Heater 5.423MHz ERP=p.260MW



e.

Oct. 23, 1982 Heater 5.423MHz ERP=p.260MW



f.

Fig. 5.2 e, f Amplitude of 4.948, 5.701 and 6.301 MHz diagnostic signals vs. time, Oct. 23, 1982 (e) 1118-1128 UT, (f) 1148-1158 UT, during 0-mode heating with changing ERP.

3-min on, 3-min off cycles.

Due to a calibration problem it was only possible to obtain reliable absorption measurements for all three diagnostics during two on-off cycles. Reliable simultaneous absorption measurements of the 5.701 and 6.506 MHz diagnostics were obtained over 10 on-off cycles. The mean values of absorption for the two diagnostic frequencies obtained from the 2 on-off cycles are well within one standard deviation of the means obtained from the 10 cycles.

It is assumed therefore that the two cycle mean is a reliable measure of absorption. The absorption values of all three diagnostics are presented in table 5.1a.

A similar experiment was performed on 23 October 1982 with diagnostics of 4.948, 5.701, 6.301 MHz and heater parameters identical to those above. A sequence of 2 min-on, 2 min-off cycles was employed. The mean values of diagnostic absorption for 21 cycles are listed in table 5.1b. These data are to be described in greater detail in section 5.5 where they are employed to deduce the structure of FAI which give rise to anomalous absorption.

5.3 Interpretation of diagnostic absorption effects

It is convenient to define the absorption induced in a diagnostic during heating as follows. The diagnostic signal level measured by a receiver when no heating is taking place is S_{OFF} dB above a nominal voltage. When the high-power pump is operating, a signal level S_{ON} dB above the same nominal level is observed. The induced absorption, A_d is then

$$A_d = S_{OFF} - S_{ON} \quad 5.1$$

8-9-81

a.

Diagnostic Frequency [MHz]	4.948	5.701	6.506
Mean Diagnostic Absorption [dB]	$7.3 \pm 0.4^*$	12.7 ± 1.6	4.9 ± 1.0

23-10-82

b.

Diagnostic Frequency [MHz]	4.948	5.701	6.301
Mean Diagnostic Absorption [dB]	5.9 ± 1.6	7.3 ± 1.6	5.2 ± 1.6

Table 5.1 a,b Mean values of diagnostic absorption obtained during experiments on (a) Sept. 8, 1981 (10 cycle averages except* which is a 2 cycle average), and (b) Oct. 23, 1982 (21 cycle average). The heater operated at 260 MW, 0-mode in each case.

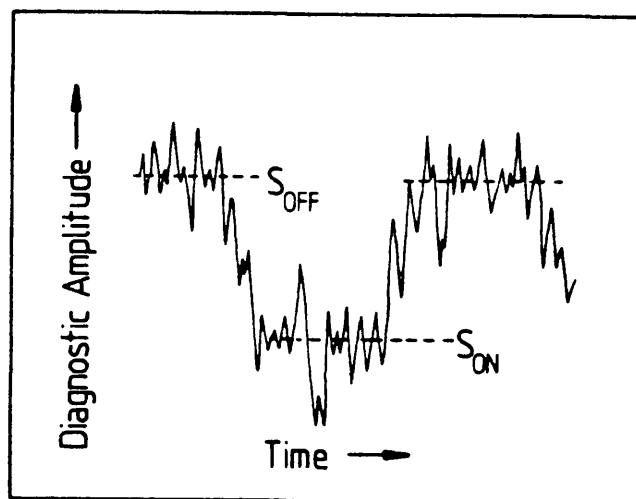


Fig. 5.3 Schematic diagram illustrating method of evaluating the diagnostic signal levels during heater on and off periods.

The situation is complicated somewhat by the finite time constant of the transition between S_{OFF} and S_{ON} . Usually this time is a small fraction of the heater on time or heater off time. Thus after the short transition time the diagnostic signal becomes quasi-stationary. In this case these quasi-stationary levels are used to estimate S_{OFF} and S_{ON} (see fig. 5.3).

The voltage level V_{OFF} corresponding to S_{OFF} can be written in terms of the transmitted diagnostic power P_{TD} Watts as

$$V_{OFF}^2 = K \cdot P_{TD} \cdot e^G \cdot e^{\Gamma_D + \Gamma_F} \quad 5.2$$

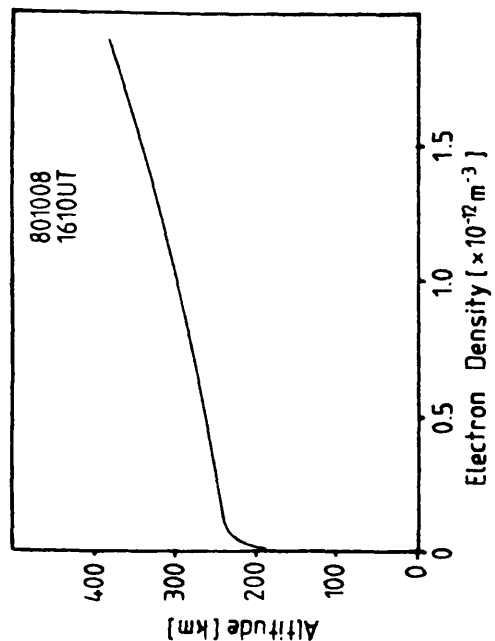
where K is a scaling factor, e^G is a geometrical factor which takes antenna gain, beam spreading and refraction effects into account and Γ_D and Γ_F are absorption coefficients of HF waves due respectively to D-region (non-deviative) and F-region absorption. Γ_F can be separated into two parts Γ_{FC} , collisional (deviative) absorption and Γ_{FA} anomalous absorption. If heating increases G , Γ_D and Γ_F by ΔG , $\Delta \Gamma_D$ and $\Delta \Gamma_F$ respectively then

$$A_d = S_{OFF} - S_{ON} = (\Delta G + \Delta \Gamma_D + \Delta \Gamma_F) \cdot 10 \log e \quad 5.3$$

The experiments described in the previous section were designed to test the relative importance of ΔG , $\Delta \Gamma_D$ and $\Delta \Gamma_F$.

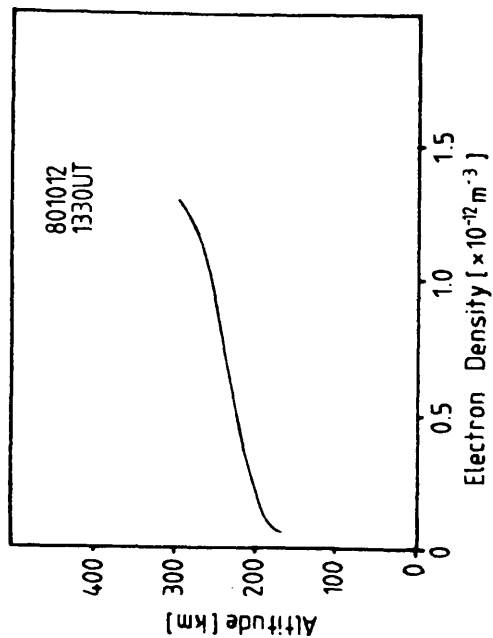
Electron density profiles have been determined from ionograms by means of a standard reduction program (Jackson, 1971).

The profiles deduced for times before or after the heating sequences in figs. 5.1,2 are reproduced in fig. 5.4. From these profiles the following parameters are derived:



Radio Wave	Heater O-mode	Diagnostic
Frequency (MHz)	3.515	3.778
Reflection Height, h_p (km)	1930	197.4
Scale Height H (km)	79.6	79.6

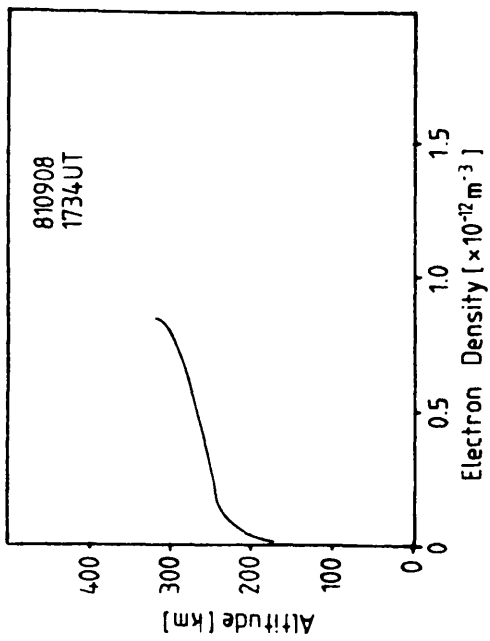
a.



Radio Wave	Heater O-mode	Heater X-mode	Diagnostic
Frequency (MHz)	3.515	3.515	3.778
Reflection Height, h_p (km)	193.3	178.5	195.0
Scale Height H (km)	56.3	20.2	53.2

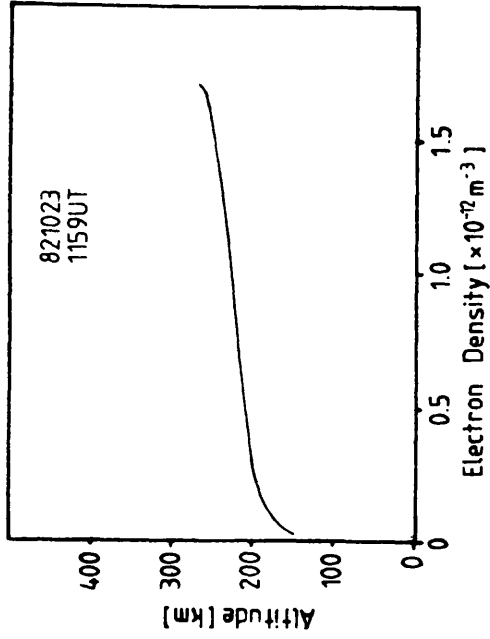
b.

Fig. 5.4 a, b Electron density profiles deduced from ionograms taken during heater off periods. The tables below each profile contain the values of the reflection height, h and local plasma scale height, H for each radio wave involved.



Radio Wave	Heater O-mode	Diagnostic 1	Diagnostic 2	Diagnostic 3
Frequency [MHz]	5.423	4.948	5.701	6.506
Reflection Height, h_p [km]	265.0	259.2	268.3	279.4
Scale Height H [km]	41.0	41.0	41.0	41.0

c.



Radio Wave	Heater O-mode	Heater X-mode	Diagnostic 1	Diagnostic 2	Diagnostic 3
Frequency [MHz]	5.423	5.423	4.948	5.701	6.301
Reflection Height, h_p [km]	205.1	199.3	201.9	206.6	210.0
Scale Height H [km]	20.8	27.8	24.6	20.8	18.4

d.

Fig. 5.4 c,d As fig. 5.4 a,b

(a) the reflection heights h_R , of the pump and diagnostic waves (by ray-tracing calculations using the Standard Jones 3-D programme, Jones and Stephenson, 1975), and

(b) the ionospheric scale height, H at each reflection height. The scale height is defined with respect to a reference frequency (for reasons which will become apparent in section 5.4) which is chosen (arbitrarily) to be 6MHz. H is then defined for a given radio wave frequency, f_o (MHz) as

$$H(f_o) = 36 \cdot \left. \frac{\Delta h}{\Delta f^2} \right|_{f=f_o} \quad 5.4$$

where h is the altitude in km and f the plasma frequency in MHz.

H and h_R are tabulated with their respective electron density profiles in fig. 5.4. The ray tracing calculation confirmed conclusions (a) and (b) of the previous section. Fig. 5.5 illustrates the positions of the reflection points of the diagnostics within the O- and X-mode pump 3dB contours on 23 Oct 1982.

A simple D-region model appropriate for quiet daytime equinox conditions shows that conclusion (c) (of the previous section) is valid (see appendix A). The values of $\Gamma_{DX} - \Gamma_{D0}$, the amount (in dB) by which X-mode absorption exceeds O-mode absorption in the D-region are approximately 56 dB at 3.78MHz and 9 dB at 6.5MHz. If diagnostic absorption A_d induced by the heater does not exceed $\Gamma_{DX} - \Gamma_{D0}$ it is reasonable to assume that A_d is caused only by absorption of the diagnostic O-mode.

5.3.1 Significance of O- and X-mode heating results

There are three possible mechanisms which cause the amplitude of a diagnostic wave to be strongly affected by the action of a high

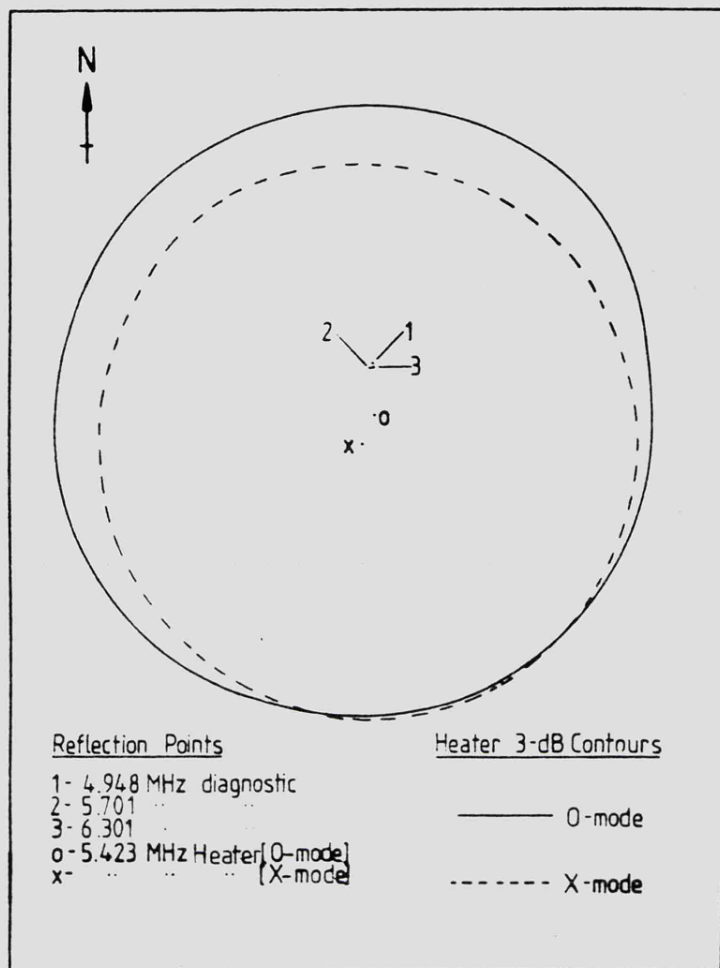


Fig. 5.5 The positions of the reflection points of the 4.948, 5.701 and 6.301 MHz diagnostics with respect to the 3dB contour and reflection points of the vertically projected 0- and X-mode heater waves. These positions (and contours) have been deduced by ray tracing through the electron density profile depicted in Fig. 5.4b (Oct. 23, 1982).

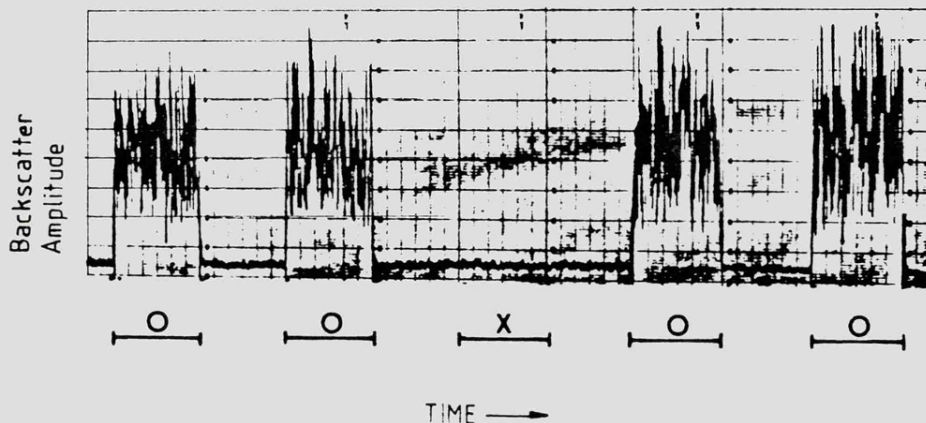


Fig. 5.6 Backscatter amplitude vs. time during 0- and X-mode heating at 5.423 MHz (from Hedberg et al., 1982).

power pump (see chapter 3),

- (a) enhanced D-region absorption (Δf_D),
- (b) F-region defocussing due to large scale plasma density change (ΔG)
- (c) F-region scattering of EM waves into Langmuir, waves from small scale FAI i.e. 'anomalous absorption' (Δf_{FA})

The data presented in section 5.2 strongly suggests that the diagnostic absorption during O-mode heating is due to mechanism (c), for the following reasons.

(i) The spaced transmitter-receiver diagnostic system was designed to avoid as far as possible the effects of D-region heating (see chapter 4). A crucial test of the absence (or otherwise) of D-region absorption effects on diagnostic amplitudes is provided by a comparison of O- and X-mode heating. A powerful wave of either polarization is capable of causing strong increase in D-region absorptivity (Gurevich, 1978; Fejer, 1979). The negative effect produced by X-mode heating provides conclusive evidence that the heater induced diagnostic absorption reported in section 5.2 is not due to D-region effects. Mechanism (a) can therefore be ruled out.

(ii) The second mechanism (b) could involve either collisional or anomalous absorption. However defocussing can be eliminated on the grounds that it requires large scale plasma density changes. In the lower F-region (200-250 km altitude), the time constant of large scale plasma density changes is greater than 30s (see chapter 6). The time constant for diagnostic amplitude changes is smaller than this (see chapter 8), as is evident from fig. 5.1a. In this case the growth and decay times of the diagnostic amplitude are smaller than the amplitude fading time. The lower limit on the measured amplitude changes when the pump is switched on or off is the response time of

the pen recorder. For the data in fig. 5.1a the amplitude response time to heater on and off must be less than 5s.

(iii) O-mode heating has a strong effect on diagnostic amplitudes over a diagnostic frequency range of approximately 1.5 MHz. This is an important feature of the so called 'wide-band absorption' which has previously been observed during midlatitude heating (Fejer, 1979).

Direct evidence that the X-mode pump does not produce FAI has been obtained from HF backscatter observations of Hedberg et al. (1982) during heating experiments employing the high power facility at Ramfjordmoen. These authors report strong induced backscatter amplitudes during F-region heating only while an O-mode pump was operating (fig. 5.6). The conditions under which their observations were performed were similar to those for the diagnostic absorption measurements described in section 5.2.

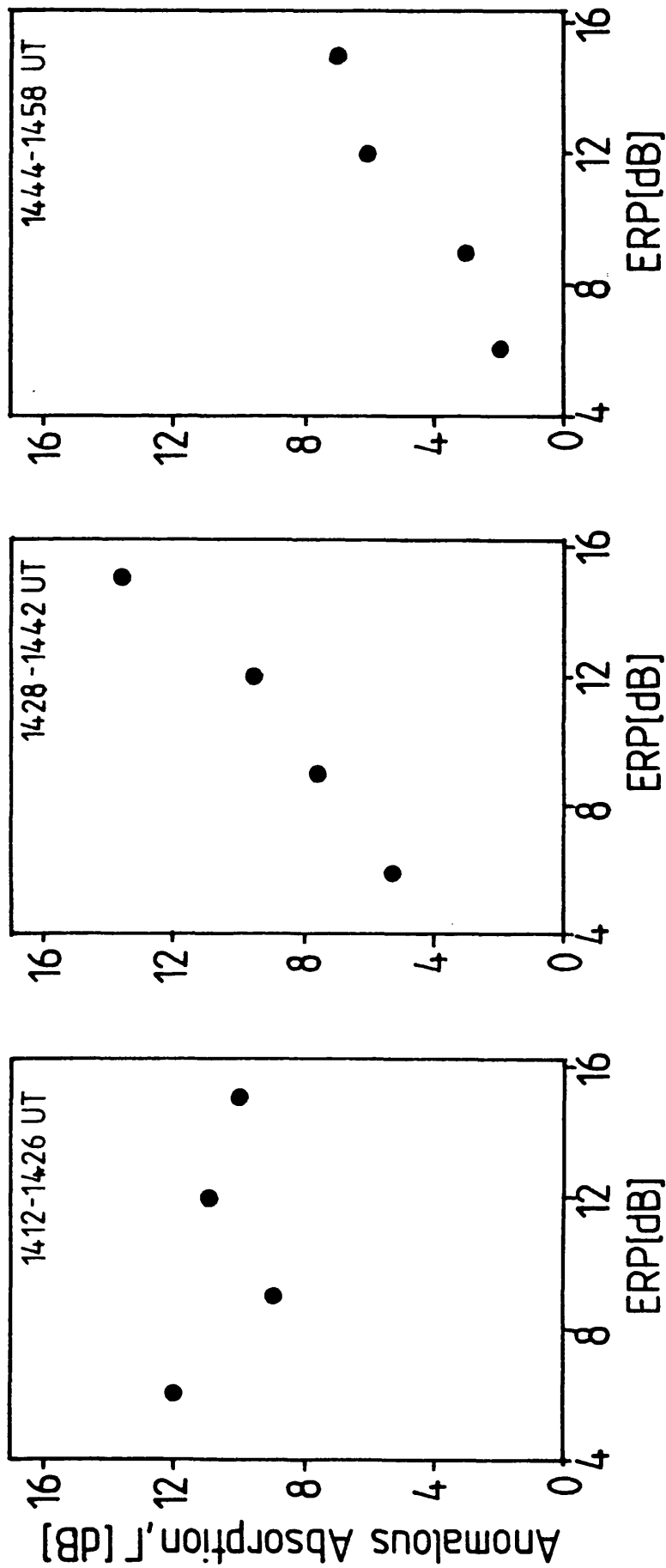
In view of the evidence presented, diagnostic absorption induced by the O-mode pump is regarded as being equivalent to anomalous absorption, Γ , associated with the generation of FAI.

5.3.2 Correlation between anomalous absorption and pump ERP

Graphs of anomalous absorption Γ against ERP are drawn in fig. 5.7 a-c from the data in Fig. 5.2b-d. In fig. 5.7d,e similar graphs for data from 8/10/80 are reproduced. There is no correlation between Γ and ERP in graphs 5.7a, d and e, although there does appear to be a positive correlation in 5.7 b and c.

Similar results from 23/10/82 in which 3 diagnostics were simultaneously employed are reproduced in fig. 5.8 a-c. Here the data points are averages over 5 heater power change sequences. In figs. 5.8 a-c some degree of correlation between Γ and ERP can be observed. It has already been noted (see section 5.2.2) that the

OCTOBER 12, 1980 0 dB(ERP) = 5 MW



a. b. c.

Fig. 5.7 a-c Graphs of the 3.778 MHz diagnostic anomalous absorption, Γ , vs. heater (3.515 MHz) ERP for three consecutive sequences of changing ERP, Oct. 12, 1980 1412-1458. Each data point represents one period of heating.

OCTOBER 8, 1980

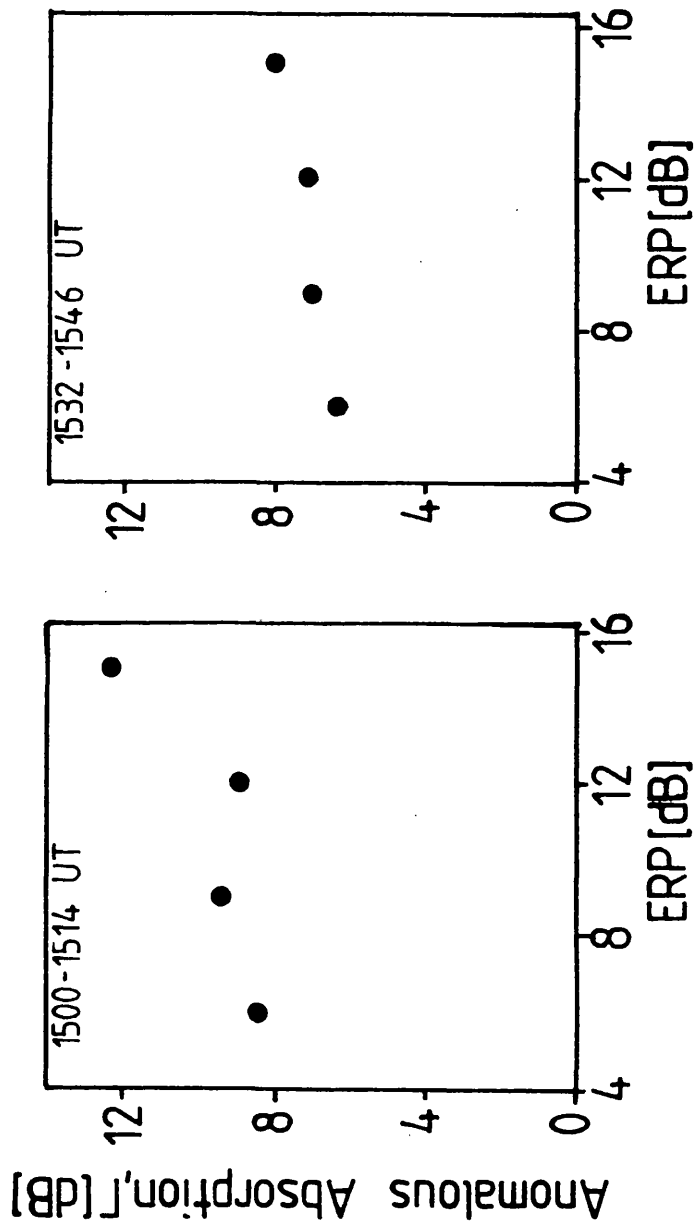
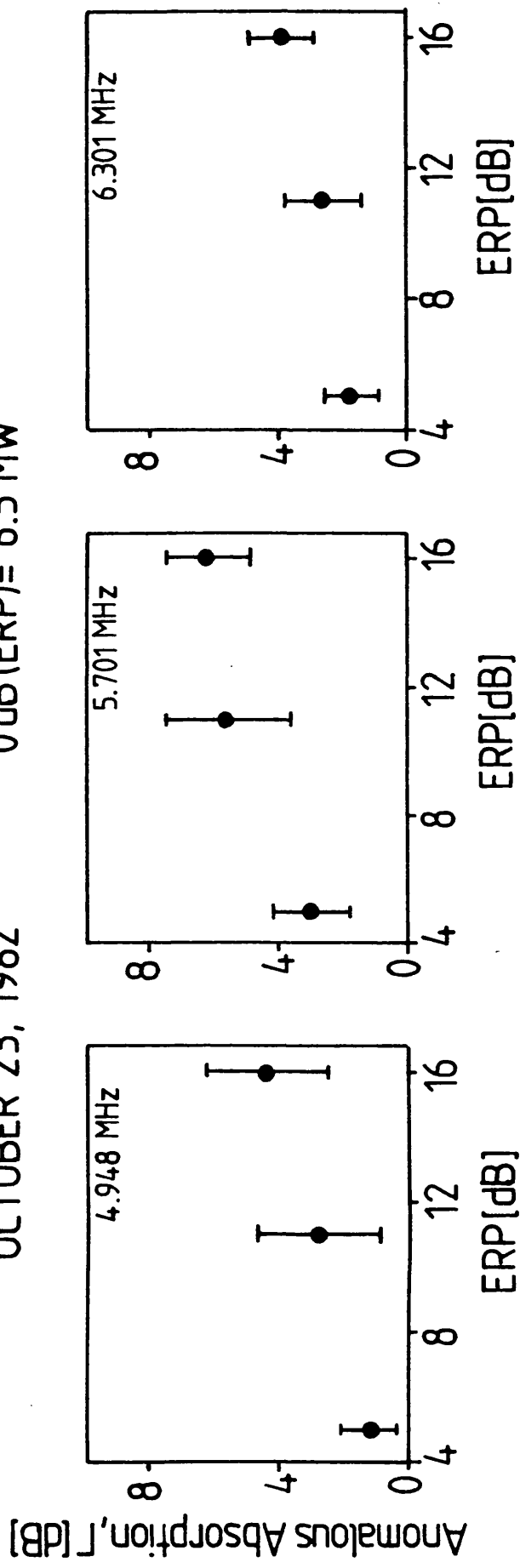


Fig. 5.7 d,e
d. Graphs of the 3.778 MHz diagnostic anomalous absorption, Γ vs heater (3.515 MHz) ERP for two sequences of changing ERP, Oct. 8, 1980 (a) 1500-1514 UT and (b) 1532-1546 UT. Each data point represents one period of heating.
e.

OCTOBER 23, 1982 0 dB(ERP)= 6.5 MW



a. b. c.

Fig. 5.8 a-c Graphs of the mean values (5 sequences) of anomalous absorption, Γ , of the (a) 4.948, (b) 5.701 and (c) 6.301 MHz diagnostic signal vs heater (5.423 MHz) ERP, Oct. 23, 1982.

diagnostic amplitude records all exhibited fast fading when is dependent on ERP. Stubbe et al. (1982a) have interpreted this observation in terms of the FAI generation theory of Das and Fejer (1979), who propose that the pump generates FAI at its upper hybrid resonance point. When fading is fast FAI amplitudes do not have time to saturate because the generation region moves within the plasma. The FAI amplitudes are then strongly power dependent. When the fading rate is low the resonance point remains long enough at one height in the plasma for FAI to saturate. This saturation amplitude is largely independent of ERP as long as ERP exceeds a certain threshold. The topic of FAI growth and saturation is discussed in detail in chapter 7.

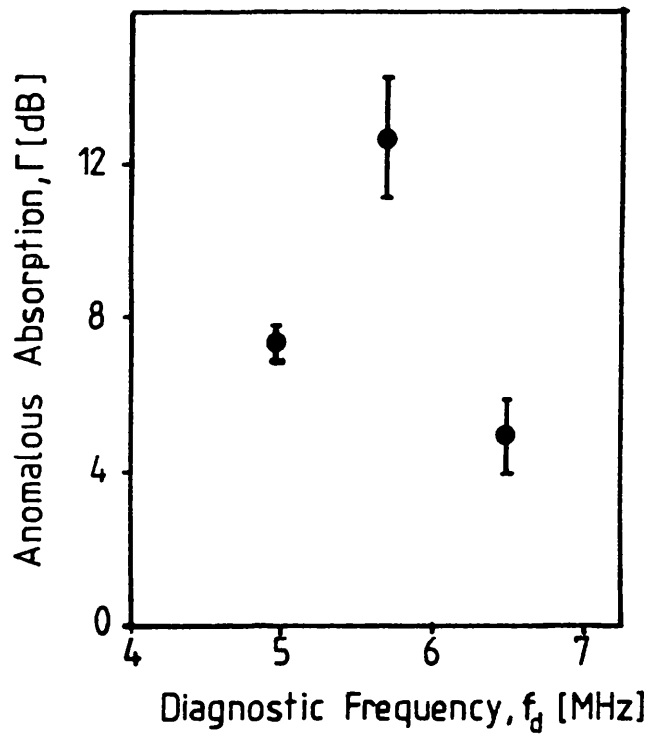
5.3.3. Anomalous absorption as a function of diagnostic frequency

Graphs of anomalous absorption Γ against diagnostic frequency f_d , from tables 5.1a, b are reproduced in fig. 5.9a, b. A dependence of Γ on f_d is apparent in both cases. In order to interpret these results it is necessary to know how Γ depends explicitly on f_d and also on parameters associated with the FAI and the background ionosphere. A detailed theoretical discussion of this relationship is therefore required.

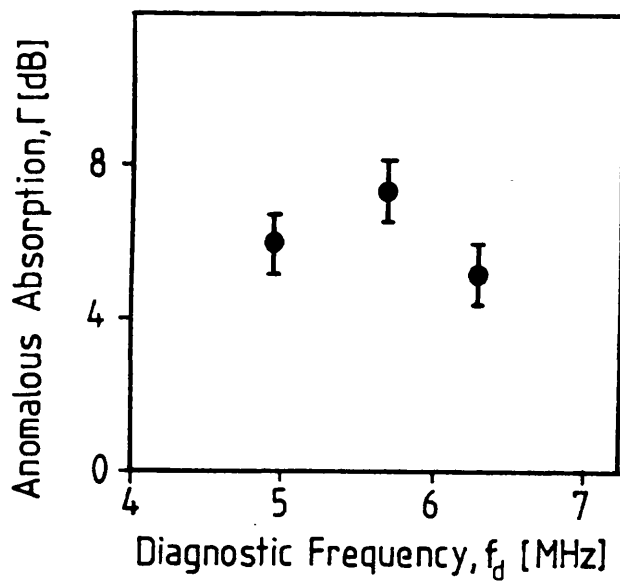
5.4 Theoretical calculation of anomalous absorption

Two theories of anomalous absorption are extensively referred to in the literature. For reasons set out in chapter 3 the theories, those of Graham and Fejer (1976) (hereafter referred to as GF) and Vaskov and Gurevich (1976) are difficult to compare directly.

Graham and Fejer take into account the effect of a magnetic field on the dispersion relation of both EM and Langmuir waves but not its effect on the motion of electrons in the calculation of



a.



b.

Fig. 5.9 a,b Graphs of mean anomalous absorption against diagnostic frequency (a) Sept. 8, 1981 (b) Oct. 23, 1982.

HF conductivity. It is proposed therefore to recalculate the anomalous absorption coefficient of an EM wave due to scattering from FAI into Langmuir waves following GF but to modify the HF conductivity calculation to take account of the effects of an external magnetic field. The results of this new calculation are then compared with GF and the results of Vaskov & Gurvich (1976).

A summary of the Graham and Fejer theory, together with the calculation of the high frequency plasma conductivity by Dawson and Oberman (1962, 1963) on which GF is based, can be found in chapter 3.

5.4.1 Modification of theory in GF

It is assumed that the scale length of FAIs perpendicular to the magnetic field is small compared with both their parallel scale length and the wavelength of an EM diagnostic wave. The theory of Dawson and Oberman (1963) (hereafter referred to as DO) then applies. These authors, proceeding from the Vlasov equations for a plasma, calculate the high frequency microscopic electric field, $\underline{E}_{ie}(\omega)$, which arises because of the difference in response of the lighter electrons and heavier ions to an external HF electric field, $\underline{E} = \underline{E}_0 e^{i\omega_0 t}$. They find that, to first order, \underline{E}_{ie} is proportional to $\underline{\epsilon}(\omega_0)$ the electron displacement. In DO $\underline{\epsilon}$ is defined as

$$\underline{\epsilon}(\omega_0) = -e \underline{E}(\omega_0) / m_e \omega_0^2 \quad 5.5$$

where, e and m_e are the electronic charge and mass respectively. However, when an external magnetic field is present, $\underline{\epsilon}$ must be replaced by $\underline{\epsilon}'$ where,

$$\underline{\epsilon}' = -\frac{e}{m_e \omega_0^2} \left(\frac{\underline{E}(\omega_0) + i\sqrt{u} \underline{E}(\omega_0) \wedge \underline{b}}{1 - u} \right) = -\frac{e}{m_e \omega_0^2} \cdot \underline{E}'(\omega_0) \quad 5.6$$

and $u \equiv \Omega_e^2/\omega_o^2$, Ω_e is the electron gyrofrequency and \underline{b} is a unit vector in the direction of the geomagnetic field.

Graham and Fejer take up the Dawson and Oberman theory at this point and write the microscopic electric force \underline{F}_{ie} in the plasma in terms of the power spectrum $|n_{\underline{k}}(\underline{k}, \omega)|^2$ of the FAI, where \underline{k} and ω are respectively the wave vector and frequency of the FAI spectrum. To take account of the magnetic field \underline{E}' is substituted for \underline{E} and equations (28) in GF (see equations 3.53 and 3.58) becomes

$$\underline{F}_{ie}(\omega_o) = \frac{e^3}{m_e \omega_o^2 \epsilon_o (2\pi)^3 V} \int \frac{\underline{k}}{k^2} \underline{k} \cdot \underline{E}' \left(\frac{1}{D(\underline{o}, \underline{k})} - \frac{1}{D(\omega_o, \underline{k})} \right) |n_{\underline{k}}|^2 d^3 \underline{k} \quad 5.7$$

where $D(\omega_o, \underline{k})$ is the plasma dielectric constant. The general form of $D(\omega, \underline{k})$ for a magnetoactive plasma is complicated. It has the form (Clemmow and Dougherty, 1969; chapter 3, equ. 3.16a-e),

$$D(\omega, \underline{k}) = 1 + \underline{k}^2 \lambda_D^2 + i\omega \int_0^\infty \exp(-i\omega t - [\frac{T_e}{m_e} (\frac{1}{2} \underline{k}^2 t^2 + \frac{k_\perp^2 (1 - \cos \Omega_e t)}{\Omega_e^2})]) dt \quad 5.8a$$

It reduces to (Fejer and Calvert, 1964)

$$D(\omega, \underline{k}) = 1 - \frac{\omega_e^2}{\omega^2 - \Omega_e^2} (1 + 3 \lambda_D^2 \underline{k}^2) - i\nu/\omega, \quad 5.8b$$

when $\omega \gg 2\Omega_e$ and \underline{k} is perpendicular to the magnetic field and where λ_D is the Debye wavelength, ν is the electron collision frequency and ω_e the plasma frequency.

Equation 5.7 above differs from (28) in GF in that \underline{E}' is substituted for \underline{E} , furthermore, it has been assumed that the FAI amplitudes do not depend on time. No such time dependence appears

in the calculations of Minkoff (1974) and it also disappears from the analysis in GF.

Following GF, $\underline{F}_{ie}(\omega_0)$ can now be written in terms of Minkoff's radar scattering theory, but instead of (29) in GF (equ.3.586), becomes

$$\underline{F}_{ie} = \frac{4\pi m_e \epsilon_0}{e\omega_0^2} \int dk k b(k) \underline{E}'_{\perp} \left(\frac{1}{D(0, \underline{k})} - \frac{1}{D(\omega_0, \underline{k})} \right) \quad 5.9$$

where $b(k)$ is the radar scattering cross-section of the FAI, and \underline{E}'_{\perp} is the component of \underline{E}' perpendicular to \underline{b} .

The current density \underline{J}_{ie} generated by \underline{F}_{ie} can be derived from 5.9 and instead of equ.3.59a

$$\underline{J}_{ie} = \frac{e}{im_e \omega_0} \left(\frac{\underline{F}_{ie} + i\sqrt{\mu} \underline{F}_{ie} \wedge \underline{b}}{1 - \mu} \right) \quad 5.10$$

It is possible to derive the mean power per unit volume, Q_{11} lost by the EM waves due to scattering from the FAI using 5.9 and 5.10 as follows

$$Q_{11} = \underline{\nabla} \cdot \underline{P} = \frac{1}{4} (\underline{E}^* \cdot \underline{J}_{ie} + \underline{E} \cdot \underline{J}_{ie}^*) \quad 5.11$$

where \underline{P} is the Poynting flux of the EM wave. If the flux is vertical then,

$$\underline{\nabla} \cdot \underline{P} = \frac{dP}{dh} = - \frac{2\pi \epsilon_0 c^4}{\omega_0^3} \cdot I \cdot |\underline{E}_{\perp}|^2 \left(\frac{(1+\mu) - (4\sqrt{\mu} |\alpha|)(1+|\alpha|^2)^{-1}}{(1-\mu)^2} \right) \quad 5.12$$

where $\alpha = E_y/E_x$, $|\underline{E}_\perp|^2 = E_x^2 + E_y^2$, h

is the altitude and I is given by

$$I = \int dk k b(k) |D(\omega_0) - D^*(\omega_0)| / 2 D(\omega_0) \cdot D^*(\omega_0) \quad 5.13$$

The fact that $D(0) - D^*(0) \equiv 0$ (from Eq. 5.8a) has been used in deriving 5.13. The cartesian axes, x , y and z are identical to those defined in GF.

Using the dispersion relation 5.8, 5.12 becomes

$$\left| \frac{dP}{dh} \right| = \frac{\pi^2 \epsilon_0 c^4 b(k_{\omega_0})}{3 \omega_0 \lambda_D^2} \cdot |\underline{E}_\perp|^2 \cdot \left(\frac{(1+u) - (4\sqrt{u}|\alpha|)(1+|\alpha|^2)^{-1}}{(1-u)^2} \right) \quad 5.14$$

where k_{ω_0} is the root of $D(\omega, k) = 0$. GD point out that this result (5.14) is independent of ν . Remembering that the absorption region is traversed twice by a reflected 0-mode wave, the absorption coefficient, Γ is

$$\Gamma = \int 2 \left| \frac{dP}{dh} \right| P^{-1} dh \quad 5.15$$

Using equation 3.20c for P in terms of \underline{E} , Γ can be written,

$$\Gamma = \int \frac{4\pi^2 c^3 b(k_{\omega_0}) (1+|\alpha|^2) \{ [(1+u) - (4\sqrt{u}|\alpha|)(1+|\alpha|^2)^{-1}] (1-u)^{-2} \}}{3 \omega_0^3 \lambda_D^2 \mu (|\alpha|^2 + |\beta|^2 \sin^2 \theta + \cos^2 \theta - 2|\beta| \sin \theta \cos \theta)} dh \quad 5.16$$

where μ is the EM wave refractive index (equ. 3.9), θ is the angle between the EM wave vector and \underline{b} , and $\beta = (E_z/E_x)$. The

explicit frequency dependence of the expression for Γ , 5.16, differs from that in GF by the factor inside $\{ \}$

5.4.2 Numerical evaluation of Γ

The method for evaluating Γ numerically is described in detail in GF and is briefly outlined below.

The variables α, β, λ_D and μ in 5.16 which are functions of h can be evaluated from a known electron density profile. $b(k_{\omega_0})$ which is given by Minkoff (1974) as a function of radar frequency (see fig. 2.6), can be determined as a function of h as follows. From the dispersion relation 5.8 k_{ω_0} can be found as a function of h through its dependence on ω_e and λ_D . The FAI with wave number k_{ω_0} coherently scatters radar wave numbers, $k_{\text{radar}} = k_{\omega_0}/2$.

Thus $b(k_{\omega_0}(h))$ can be determined from the corresponding radar frequency, $f_{\text{radar}} = c k_{\omega_0}/4\pi$.

Following the method of GF, the frequency dependence of Γ is determined assuming a linear electron density profile. This parameter has been evaluated both with and without the factor inside $\{ \}$ included in 5.16 for the frequency range of interest, i.e. 4 to 7 MHz. The results are reproduced in fig. 5.10. Values of scale height = 41 km, gyrofrequency = 1.4MHz and $\theta = 12^\circ$ (corresponding to the Ramfjord site) have been assumed in the calculation. It is clear from fig. 5.10 that the inclusion of the factor in $\{ \}$ has two effects. Firstly, the average value of Γ is reduced by about 50% and secondly, the ω dependence of Γ becomes extremely weak. In the absence of the factor $\{ \}$, Γ is a decreasing function of increasing ω as pointed out in GF. The very weak dependence of Γ on ω predicted by the present calculation has a significant bearing on the interpretation of the experiment outlined

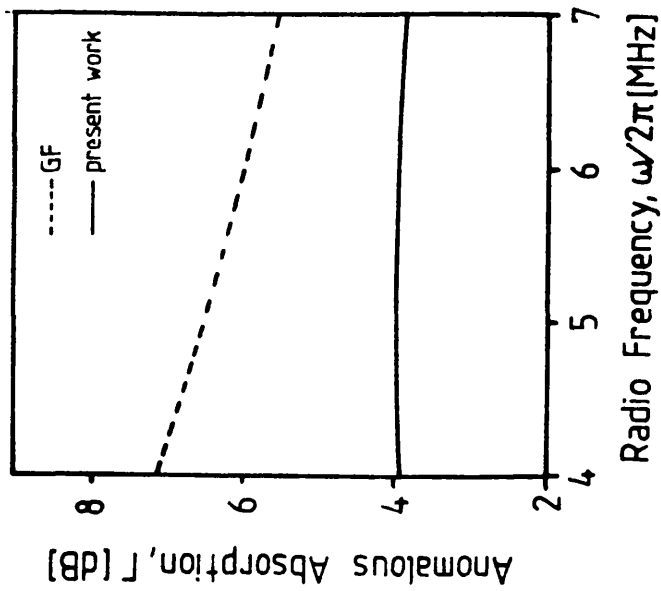


Fig. 5.10 A comparison of theoretical calculations of radio frequency. The dashed line is obtained from Graham and Fejers' (1976) theory (see section 3.5) and the solid line from equation 5.16.

Frequency $\omega/2\pi$ [MHz]	Anomalous Absorption Γ [dB]	
	Numerical Integration of eq. 5.16	Analytical Expression 5.17
4	3.93	3.90
5	4.02	3.99
6	3.90	3.94
7	3.84	3.82

Table 5.2 Values of anomalous absorption as a function of frequency determined from the numerical integration of equation 5.16 and the analytical expression 5.17.

Frequency $\omega/2\pi$ [MHz]	Anomalous Absorption Γ [dB]	
	Analytical Expression 5.17	Quasi-Longitudinal Approx. 5.20
4	3.90	4.23
5	3.99	4.42
6	3.94	4.46
7	3.82	4.42

Table 5.3 Values of anomalous absorption as a function of frequency determined from the analytical expression 5.17 and the quasi-longitudinal approximation, 5.20.

in 5.2.3 and will be considered in greater detail in section 5.5.

The numerical integration of 5.16 can be developed into an analytical expression for Γ which then allows a direct comparison of the theory in GF with the anomalous absorption theory of Vaskov and Gurevich (1976).

5.4.3 An analytical expression for Γ

An approximate analytical expression for Γ can be obtained from 5.16 as follows.

The only significant contribution to the integral in 5.16 occurs near an altitude, h_1 , where the diagnostic frequency is close to the local upper-hybrid frequency, so $b(h)$ can be treated as a delta function of the form $b_0 \delta(h-h_1)$. Expression 5.16 then reduces to

$$\Gamma = R(h_1) \int k_{\omega_0} b(k_{\omega_0}) dk_{\omega_0} \quad 5.17$$

where

$$R(h_1) = \left| \frac{8\pi^2 \omega_e^2 c^3 (1+|\alpha|^2) \{ [(1-u) - 4\sqrt{u} |\alpha| (1+|\alpha|^2)^{-1}] (1-u)^{-2} \}}{\omega_0^3 (d\omega_e^2/dh) \mu (|\alpha|^2 + |\beta|^2 \sin^2 \theta + \cos^2 \theta - 2|\beta| \sin \theta \cos \theta)} \right|_{h=h_1} \quad 5.18$$

In 5.17 the integral has been transformed from one over h to one over k_{ω_0} by employing 5.8. The integral in 5.17 above can be evaluated in terms of the mean square amplitude $\langle |n|^2 \rangle$ of the FAI by means of equation 3.57 (Minkoff 1974), reproduced here

$$\langle |n|^2 \rangle = \frac{32\pi \epsilon_0 m e^2 c^4}{e^4} \int_0^\infty k b(k) dk \quad 3.57$$

Γ then reduces to

$$\Gamma = \sigma \langle |n|^2 \rangle \quad 5.19a$$

where

$$\sigma = R(h_1) \cdot (e^4 / 8\pi\epsilon_0^2 m_e^2 c^4) \quad b$$

$R(h_1)$ contains parameters such as ω_e^2 , $d\omega_e^2/dh$, μ , α and β calculated at h_1 . At this height ω_e^2 is equal to $\omega_0^2(1-u)$. $R(h_1)$ is determined by substituting this value of ω_e^2 in the appropriate expressions for μ, α, β etc. Expression 5.18 indicates that Γ is proportional to $H(h_1) = \omega_e^2 / (d\omega_e^2/dh)$, the scale height determined at the resonance height, h_1 . Clearly, if $\langle |n|^2 \rangle$ were a function of h , its value at $h=h_1$ would be substituted into 5.17. As a check on the above expression 5.19 Γ has been calculated under the same conditions using 5.16 and 5.19. These values are reproduced in table 5.2 and it is clear that the two calculations are in excellent agreement.

5.4.4 Quasi-longitudinal approximation

Expression 5.18 can be further simplified for the case when the geomagnetic field is close to the vertical and the EM wave is then quasi-longitudinal (Ginzburg, 1970 and eq. 3.12). In this case,

$\theta = 0$ and 5.19 becomes

$$\Gamma = \frac{\pi\omega_0(1-u)^2(1-\sqrt{u})}{c u^{1/4} (dV_1/dh)(1+\sqrt{u})} \delta^2 \quad 5.20$$

where

$$V_1 = \omega_e^2 / \omega_0^2 \Big|_{h=h_1}, \quad \delta^2 = \langle |n|^2 \rangle / N_1^2$$

and N_1 is the plasma density at h_1 .

Expression 5.20 above is identical to expression (30) of Vaskov and Gurevich (1976) (see also Gurevich, 1978 and eq. 3.62). In table 5.3 the values of Γ , calculated using 5.20 are compared with those obtained from the full analytical expression 5.19 with $\theta = 12^\circ$. The quasi-longitudinal approximation overestimates the value of Γ by about 10% over the frequency range of interest.

The diagnostic waves in the Ramfjord experiment propagate at about 8° to the vertical. The approximation of vertical propagation employed in the theoretical calculation of Γ introduces an error at least as great as that due to the quasi-longitudinal approximation. Equation 5.20 is probably quite adequate for evaluation of Γ at high latitude sites such as Ramfjord.

When evaluating Γ from 5.20 for different diagnostic frequencies it must be remembered that δ^2 is implicitly a function of ω_0 because of the dependence of h_1 on ω_0 . Since it is usually the absolute mean square perturbation amplitudes, $\langle |n|^2 \rangle$, that are of interest it is convenient to define a mean square amplitude, δ_0^2 relative to a reference plasma density, N_0 , such that

$$\delta_0^2 = \langle |n|^2 \rangle / N_0^2 \quad 5.21$$

Then, if $\langle |n|^2 \rangle$ is independent of altitude, so is δ_0^2 .

The explicit frequency dependence of Γ can be determined from 5.20. For a given plasma scale height and mean square FAI amplitude, Γ is proportional to $F(X)$ where

$$F(X) = \left(\frac{X-1}{X+1} \right) X^{-1/2}$$

$$X = \omega_0 / \Omega_e = u^{-1/4}$$

Fig. 5.11 is a graph of $F(X)$ against X illustrating the weak dependence of $F(X)$ on X in the range $X = 3$ to 5 . There is also a broad maximum at $X = (2 + \sqrt{5})$ i.e. at $\omega_o = 2\pi \cdot 5.9$ MHz with $\Omega_e = 2\pi \cdot 1.4$ MHz.

5.4.5. Geomagnetic latitude dependence

From equation 5.20 the dependence of Γ on the angle of inclination of the geomagnetic field to the vertical has been calculated. This dependence for a diagnostic of 6 MHz (corresponding to $N_o = 4.5 \cdot 10^{11} \text{ m}^{-3}$) with $H=41\text{km}$ and $\delta_o = 0.015$ is reproduced in Fig. 5.12. A strong decrease of Γ with increasing θ is evident. This result justifies the need to perform heating experiments at high latitude (where θ is small). For convenience the points corresponding to the values of θ at Ramfjordmoen (R, $\theta = 12^\circ$), Platteville (P, $\theta = 22^\circ$) and Arecibo (A, $\theta = 45^\circ$) are indicated on the graph.

5.4.6. Experimental determination of Γ

The definition of Γ in expression 5.15 is equivalent to writing

$$\underline{E}_r^2 = \underline{E}_i^2 e^{-\Gamma} \quad 5.22$$

where \underline{E}_i and \underline{E}_r are respectively the incident and reflected electric field strengths of a radio wave passing twice through an absorbing region containing FAI below the wave reflection point. The units of Γ in 5.22 are Nepers. Clearly \underline{E}_i^2 and \underline{E}_r^2 cannot be determined absolutely. However, the signal strength of an ionospherically reflected wave measured in volts at a receiver during heater off V_{OFF} (when $\Gamma = 0$) is clearly proportional to $|\underline{E}_i|$. Similarly the signal strength V_{ON} measured during heater on is proportional to $|\underline{E}_r|$.

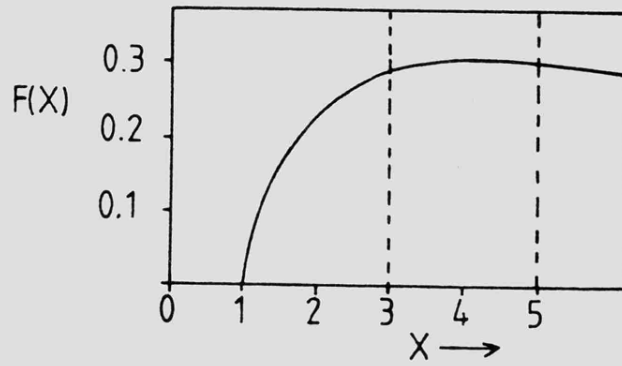


Fig. 5.11 Graph of $F(x)$ vs. $x = \omega/\Omega e$ to illustrate the frequency dependence of Γ ($\propto F(x)$).

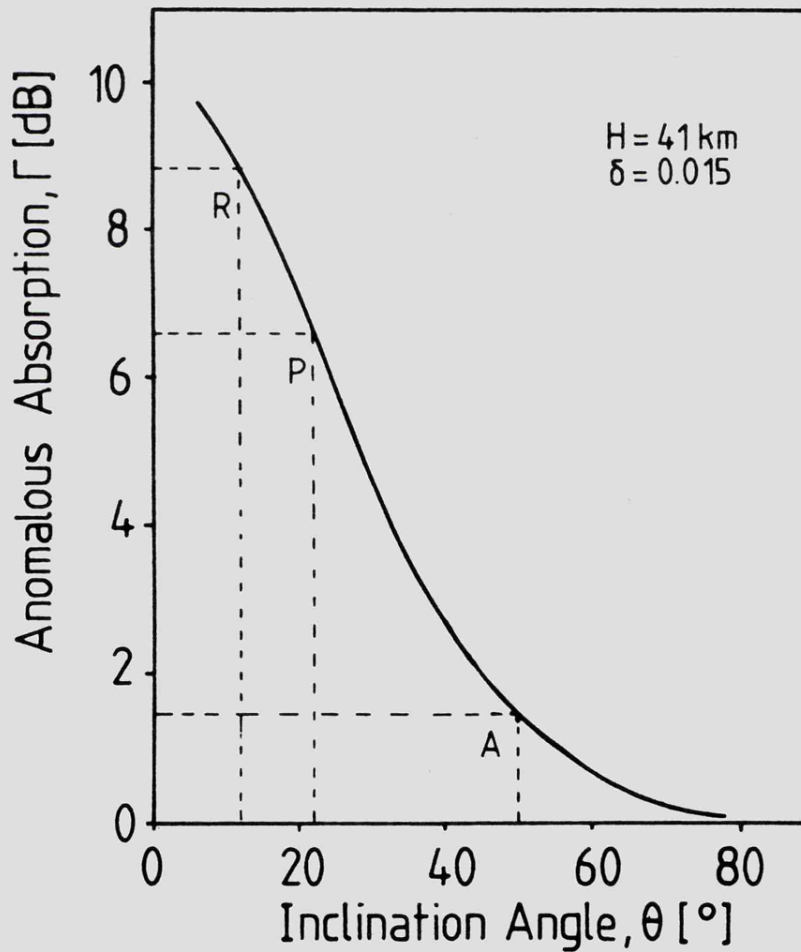


Fig. 5.12 Graph of Anomalous absorption vs. angle of inclination of the geomagnetic field to the vertical. Points corresponding to the inclination angles of Ramfjordmoen (R), Platteville (P) and Arecibo (A) are indicated.

Thus,

$$V_{OFF}^2 = K \cdot |\underline{E}_i|^2$$

$$V_{ON}^2 = K \cdot |\underline{E}_r|^2$$

where K is a constant. Therefore, 5.22 becomes

$$\ln \frac{V_{OFF}^2}{V_{ON}^2} = \Gamma$$

Expressed in dB, Γ is then entirely equivalent to the anomalous absorption defined in Section 5.3.

5.5 Determination of FAI scale lengths along the geomagnetic field

Mean values of the anomalous absorption levels of the 4.948, 5.701 and 6.506 MHz diagnostic waves from the experiment on 8/9/81, are plotted as a function of diagnostic frequency in fig. 5.9a. These data are reproduced in fig. 5.13 together with theoretical curves of Γ (dB) calculated from equation 5.17 for different values of δ_0 .

The electron density profile (fig. 5.4c) indicates that the scale height, $H(h)$ (normalized to 6 MHz) was constant (41 km) across the whole range of diagnostic frequencies. Thus, $H(h_1) = 41\text{km}$, and $\theta = 12^\circ$ were used in eq. 5.19 to calculate Γ in each case. From fig. 5.13 it is evident that experimental values of Γ are frequency dependent and the maximum value is observed for the diagnostic closest to the pump frequency. This implies that the striation amplitude (δ_0) decreases with distance from the pump resonance height (both above and below). δ_0 varies from about 2% near the pump resonance height. This value is about twice that deduced by Minkoff (1974)

from radar backscatter data during heating experiments at Plattville (see comments at the end of this section).

In a linear electron density profile, the resonance height is at a distance , $\Omega_e^2 \cdot (dh/d\omega_e^2)$ below the reflection height for each radio wave. This distance is independent of diagnostic frequency and is approximately equal to $H/20$. The distance Δh between the diagnostic and pump resonance heights is then just the difference between respective reflection heights. Values of Δh for the three diagnostics derived from the electron density profile in fig. 5.4c are listed in table 5.4.

In fig. 5.14 a graph of Γ against $|\Delta h|$ has been drawn with a logarithmic scale for the ordinate. According to the theory presented in section 5.4, Γ is virtually independent of diagnostic frequency and since the plasma density scale height is constant over the whole diagnostic frequency range, the variation in is attributable to the change in $\langle |n|^2 \rangle$ as a function of $|\Delta h|$.

From the graph in fig. 5.14 the scale length parallel to the magnetic field, $L_{||}$ of the FAI can be deduced. It is assumed that the maximum value of δ_0 occurs at the pump resonance height h_0 and that the FAI are symmetrical about a plane perpendicular to the field through an axial point at h_0 . It is also assumed that Γ is proportional to $\langle |n|^2 \rangle$ where

$$\langle |n|^2 \rangle = n_0^2 \exp(-2|\Delta h|/L_{||} \cos\theta)$$

where θ is the angle between the magnetic field and the vertical direction (see fig. 5.15). A least squares straight line is fitted to the data in fig. 5.14 and from its gradient $L_{||}$ is determined to be 27.2 km.

8-9-81

Diagnostic Frequency [MHz]	4.948	5.701	6.506
Δh [km]	5.8	32	14.3

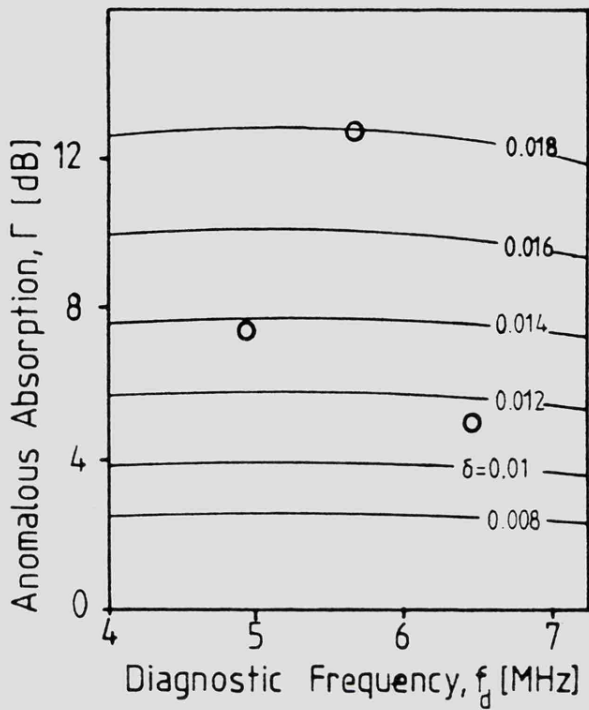


Table 5.4 Separation distance (Δh) between the reflection heights of the 0-mode heater (5.423MHz) and 4.948, 5.701 and 6.506 MHz diagnostic determined by ray tracing through the electron density profile in Fig. 5.4c (Sept. 8, 1981).

Fig. 5.13 Diagnostic absorption data from fig. 5.9a plotted together with theoretical Γ vs frequency contours.

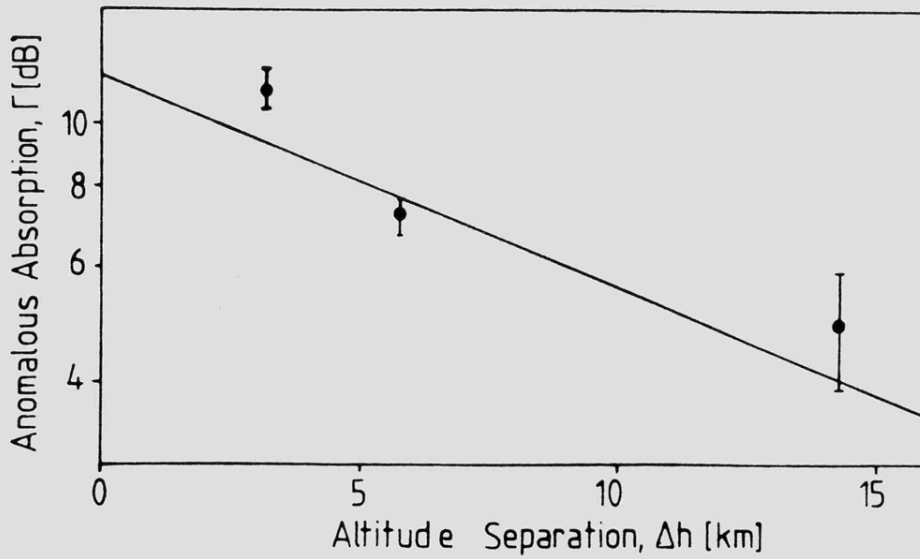


Fig. 5.14 A graph of measured diagnostic absorption vs reflection height separation, Δh , for data from Sept. 8, 1981.

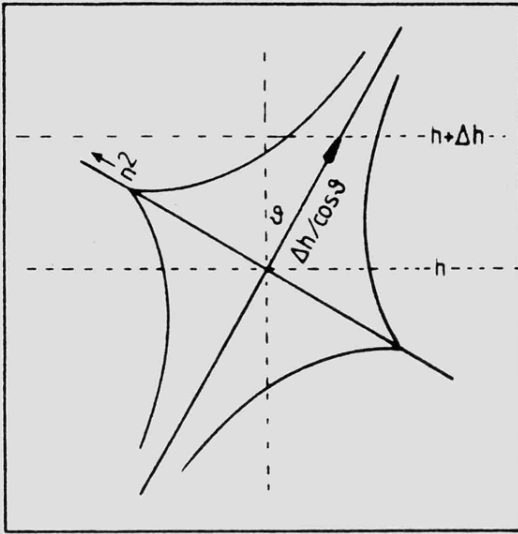


Fig. 5.15 Field aligned irregularity density model. The irregularity density squared is an exponential function of the distance along a field line from a heater reflection point.

Table 5.5 Separation distance (Δh) between the reflection heights of the 0-mode heater (5.423 MHz) and 4.948, 5.701 and 6.301 MHz diagnostics determined by ray tracing through the electron density profile in fig. 5.4 d (Oct. 29, 1982).

23-10-82

Diagnostic Frequency [MHz]	4.948	5.701	6.301
Δh (km)	2.5	1.5	5.0

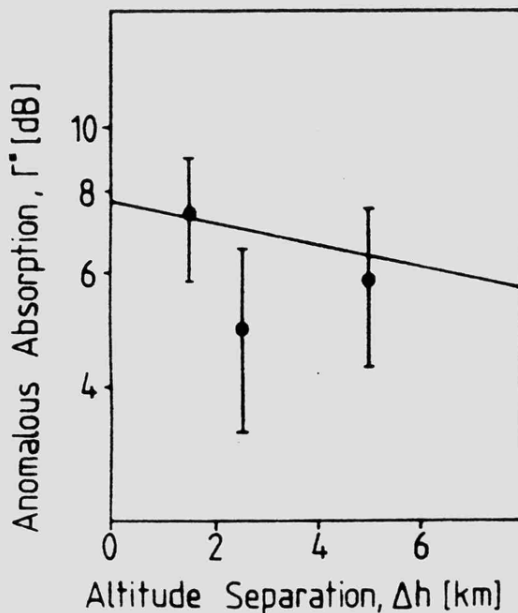


Fig. 5.16 A graph of normalized diagnostic absorption, Γ^* vs reflection height separation, Δh , for data from Oct. 1982.

A similar calculation was performed for the amplitude data from October 23, 1982. Here the results are complicated by the variation in scale height $H(h_1)$ at each diagnostic resonance height corresponding to each diagnostic frequency f_d (see fig. 5.4d). The theory presented in section 5.4 predicts that Γ is proportional to $H(h_1)$. The measured values of Γ must be normalized to Γ^* where

$$\Gamma^* = \Gamma H_{f_d} / H_{5.701}$$

The normalizing scale height of $H_{5.701}$ of the 5.701 MHz diagnostic has been chosen arbitrarily.

Furthermore the separation of the reflection heights of the pump and diagnostic waves (given in Fig. 5.4d) are not the same as the separation of their respective resonance heights, $|\Delta h|$ because of the variation of H with diagnostic frequency. It is assumed that the separation of reflection height and resonance height at each frequency is small compared to H and so can be calculated from

$$h_r - h_1 = H \Omega_e^2 / (2\pi \cdot 6)^2 \approx 5.4 \cdot 10^{-2} H$$

where h_r and h_1 are respectively the reflection height and resonance height of the diagnostic. Table 5.5 contains a value of Δh deduced in this way for each diagnostic. In fig. 5.16 a graph of Γ^* against Δh is drawn. The scale length $L_{||}$ deduced from this graph is 52.4 km.

The amplitude of the FAI near the pump resonance height deduced from the data on 23/10/82 is about 2% of the background plasma density. This is identical to that obtained on 8/9/81. The generally lower values of Γ on the 23/10/82 compared to 8/9/81 are due to the smaller plasma scale heights (H) and not to any difference

in δ_0 .

5.6 Comparison with previous results

The values of FAI amplitudes determined by the technique described in the previous section agree well with those obtained by previous workers (Minkoff 1974; Gurevich 1978). However, as far as is known, the present work constitutes the first determination of FAI scale lengths from anomalous absorption measurements.

Hedberg et al (1982) have observed HF backscatter at 3 MHz and 7 MHz during heating experiments at Ramfjord when a 5.423 MHz pump was operating. By employing raytracing techniques to determine the backscattering regions these authors deduced that the FAI generated by the pump with amplitudes significantly above the ambient background exist at distances up to 100 km below the pump resonance height and 60 km above it. These "scale lengths" cannot be compared directly with those obtained in section 5.5, for the following reason: Anomalous absorption measurements enable $\langle |n|^2 \rangle$, the mean square irregularity amplitude averaged over the wave number spectrum, to be determined in a very narrow altitude range (~ 10 m) near the upper hybrid resonance level. A backscatter radar is sensitive to only one value of k (equal to $2 k_{\text{radar}}$) but the backscatter cross sections are averages over a relatively large volume of plasma in the vicinity of the backscatter radar reflection region illuminated by the beam.

HF radar backscatter cross-sections could be obtained over a number of different k values if several radar frequencies are employed. However, because of F-region refraction each radar frequency would backscatter from a different altitude. Since each spectral component of n has a different scale length (see chapter 3) only a single spectral component amplitude n_k can be obtained at a single height.

VHF radars do not suffer from the refraction problem and so could be used to study the height dependence of N_k . However, VHF radars are only sensitive to the high wavenumber spectral components of FAI and at high latitudes have difficulty in meeting the requirement that the radar beam be perpendicular to the magnetic field. It is clear that anomalous absorption measurements can provide good height resolution but poor spectral resolution of FAI amplitudes. The opposite is true for radar backscatter. There is obviously a good case for simultaneous backscatter and anomalous absorption observation of FAI.

Such combined observations have in fact already been carried out at Ramfjord employing the present HF diagnostic system together with backscatter radars sited at Kiruna (3 MHz and 7 MHz) operated by Uppsala University and Oulu (14 MHz) operated by the University of Toulon. The value of $L_{||}$ obtained above is clearly an average over the wavenumber spectrum of the FAI. Data from a coordinated experiment enable estimates of the relative spectral amplitudes of FAI to be applied to the measured values of $\langle |n|^2 \rangle$.

5.7 Conclusions

It has been demonstrated that calculations of the HF conductivity of the ionosphere require the influence of the earth's magnetic field to be included. Thus, the kinetic theory of Dawson and Oberman (1963) has been extended to take account of this effect. The anomalous absorption coefficient, Γ , of a diagnostic wave, due to scattering by FAI generated during heating, has been determined from this modified theory following the procedure of Graham and Fejer (1976). The exact expression for Γ requires numerical integration over altitude across the resonant interaction region. The region turns out to be extremely narrow and this allows an analytical expression for Γ to be obtained. Further simplification of the expression results from an assumption of

quasi-longitudinal propagation of the pump wave. In this form the results are found to be identical to those obtained by Vaskov and Gurevich (1976) from plasma fluid theory.

It is possible to interpret diagnostic absorption induced during F-region heating by a high power radio wave as anomalous absorption when the diagnostic wave avoids the heated D-region. Measurements of anomalous absorption performed in this manner on two separate days at Ramfjord, indicate that Γ varies with diagnostic frequency. This behaviour suggests that the FAI amplitude decreases with distance from the pump resonance height. The scale length of the mean-square amplitude of the irregularities along the magnetic field, determined from anomalous absorption data, has a value typically of a few tens of kilometres. The amplitudes of the striations relative to the background plasma, deduced with the aid of the theory are about 2% near the pump resonance height. This value is approximately twice that deduced by Minkoff (1974) from radar backscatter observations during heating experiments at Platteville.

6. DIAGNOSTIC PHASE EFFECTS

6.1. Introduction

In the previous chapter the effects on the amplitude of a low power diagnostic wave of small-scale field aligned irregularities generated by a heater was discussed. The small scale irregularities cause mode conversion of EM waves into Langmuir waves, which have much small group velocities than EM waves. Consequently they are much more effectively absorbed by collisional damping than EM waves, in the vicinity of the upper hybrid resonance. However, EM waves are strongly absorbed near their reflection point (deviative absorption) and so the collisional damping of EM waves and Langmuir waves gives rise to strong plasma heating.

Differential heating which causes FAI to grow is spatially periodic, however, both deviative and anomalous absorption are not associated with any spatial periodicity and so tend to cause bulk (large scale) plasma density and temperature changes throughout the heated volume. Thus diagnostic waves passing through the heated region experience a phase path change as a result of a refractive index modification associated with the induced large scale plasma density inhomogeneities. A study of the phase changes of the diagnostic signal thus provides important information regarding large scale plasma density perturbations. Of particular interest is the relative contribution of deviative and anomalous absorption of heater wave energy to the production of these large scale effects.

Results obtained from experiments at Arecibo and Platteville (see chapter 2) indicate that, at low and mid-latitudes, the contribution of anomalous absorption to ionospheric heating is comparable with and somewhat exceeds that of deviative absorption

(Meltz et al., 1974; Mantas et al., 1981). Since certain plasma instabilities are more effective at high latitudes (Stubbe and Kopka, 1980) anomalous absorption might be expected to make a larger contribution to heating in the auroral ionosphere. If a latitude dependence of the relative contribution of anomalous absorption to the total heating can be established, it should aid our understanding of the physical processes involved.

6.2. Experimental Results

6.2.1. Single diagnostic data

The location of the diagnostic transmitter and receiver with respect to the heater for experiments in which the diagnostic phase response was investigated is identical to that described in chapter 5 (see also chapter 4) for diagnostic amplitude measurements. The experiments, which were carried out on 8th, 12th and 13th October 1980, employed a 3.515 MHz heating wave having an effective radiated power of 160 MW (Full power) and a 3.778 MHz low power diagnostic. Heating sequences consisted of cycles of 2 min on, 2 min off on 8th and 12th October, but 7.5 min on, 7.5 min off on 13th October.

The immediate aim of the experiments was to

- (a) determine the phase change time constants,
- (b) investigate the effects of changing ERP of the heater,
- (c) compare the effectiveness of O- and X-mode heating.

Phase changes induced in the diagnostic signal provided an estimate of plasma density changes, while the difference in diagnostic amplitude when the heater was on and off indicated the level of heater-created anomalous absorption. Variations in the level of the natural background absorption were obtained by comparing the diagnostic signal level

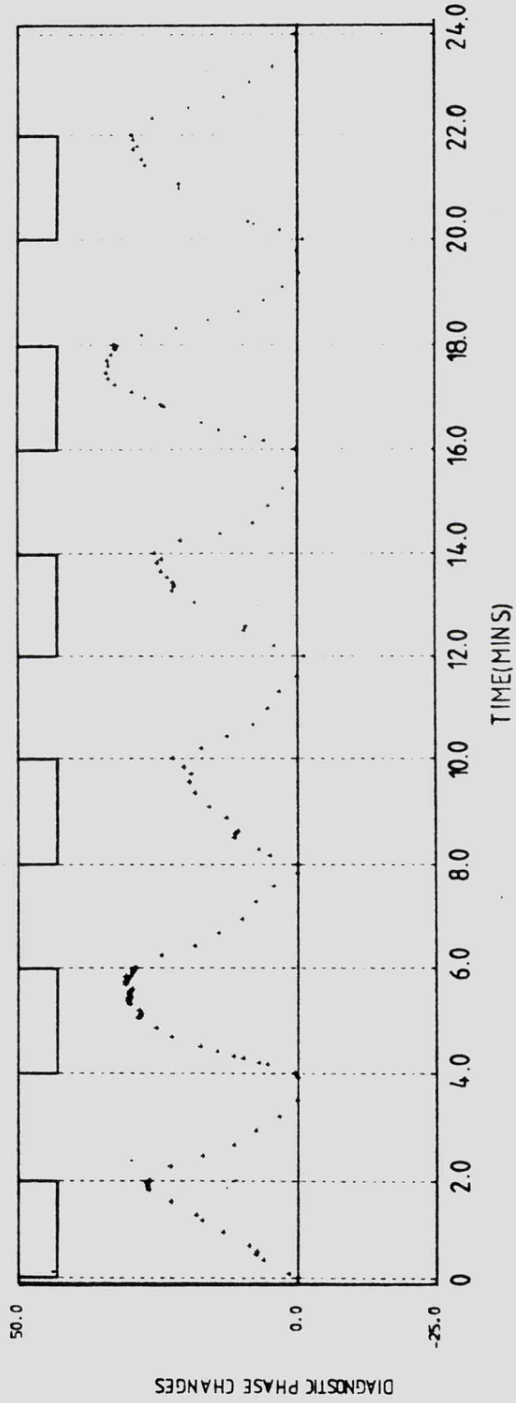
during successive heater 'off' periods. The fading rate of the diagnostic signals provides a qualitative indication of the variability of the background ionosphere. The influence of ionospheric variability in establishing the field aligned irregularities which cause anomalous absorption has been discussed by Stubbe et al., (1982a).

From the diagnostic phase measurements the phase change was plotted as a function of time as in figures 6.1 a-g. It should be noted that a phase advance in the diagnostic wave relative to the phase of a standard oscillator corresponds to a decrease in the phase path of the diagnostic wave because of plasma density increases. The data in Fig. 6.1 a,b consists of on-off heating cycles in which the pump was operated at full power (160 MW) with Ordinary polarization in each 'on' period. In the on-off cycles reproduced in figure 6.1 c-f, the 'on' periods of each cycle corresponds to O-mode heating with successive reductions in ERP, i.e. $ERP = 160 \text{ MW} \times p$, $p = 1, 0.5, 0.25, 0.125$. In sequences 6.1 c-e the phase changes exhibit no strong dependence on pump ERP. However, a strong ERP dependence is apparent in cycle 6.1f.

The effects observed during alternate X- and O-mode heating in which an ERP of 160 MW was used in each 'on' period are reproduced in figure 6.1g. The background trends in phase have been removed to some extent by setting the phase to zero at the instant of each heater switch-on. A linear change in background phase is then assumed to occur between successive switch-on times and this is subtracted from the measured phase values.

The overall characteristics of the diagnostic phase change response ($\Delta\varphi$, in units of 2π) are well defined. During each heater 'on' period, the diagnostic phase path decreases indicating

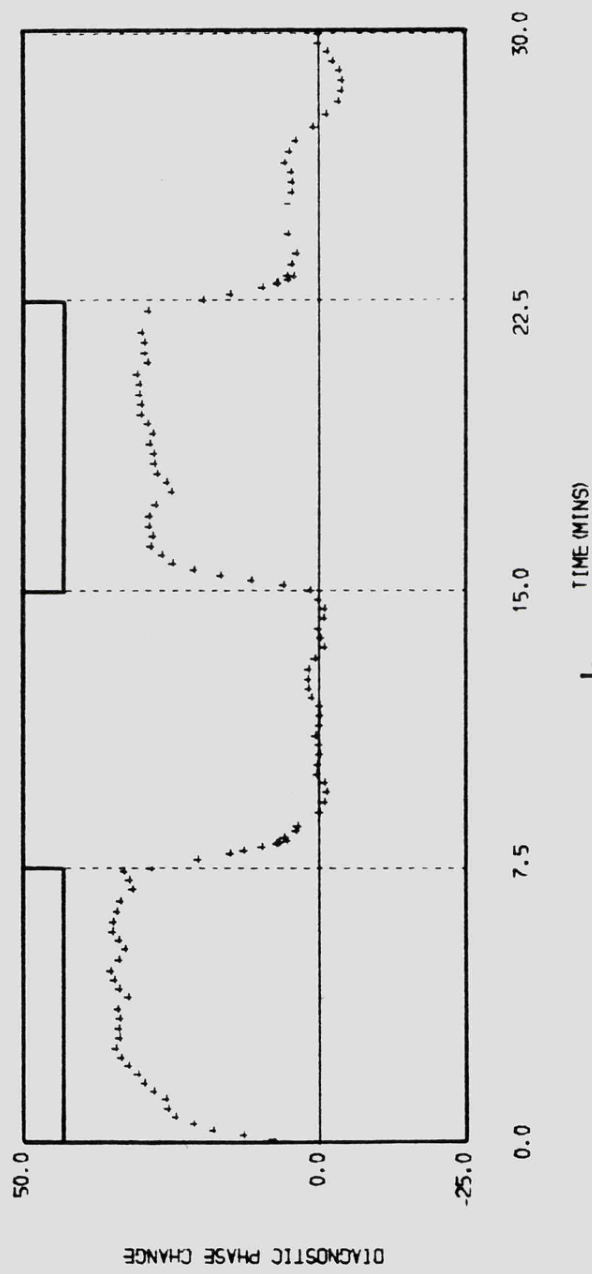
OCT. 8, 1980 1308-1332 UT HEATER 3.515MHZ 0-MODE ERP=160MW



a.

Fig. 6.1a Phase changes of 3.778 MHz diagnostic signal during periods of heater on at full power (ERP = 160 MW) and heater off, Oct. 8, 1980. The bars indicate heater on periods.

OCT. 13, 1980 1113 -1143 UT HEATER 3.515MHZ 0-MODE ERP=160MW



b.

Fig. 6.1b As 6.1a but on Oct. 13, 1980, 1113-1143 UT.

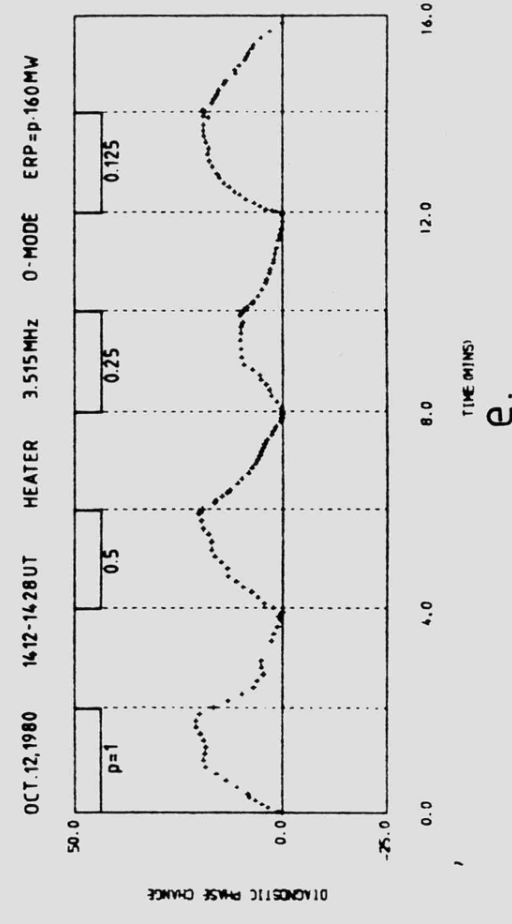
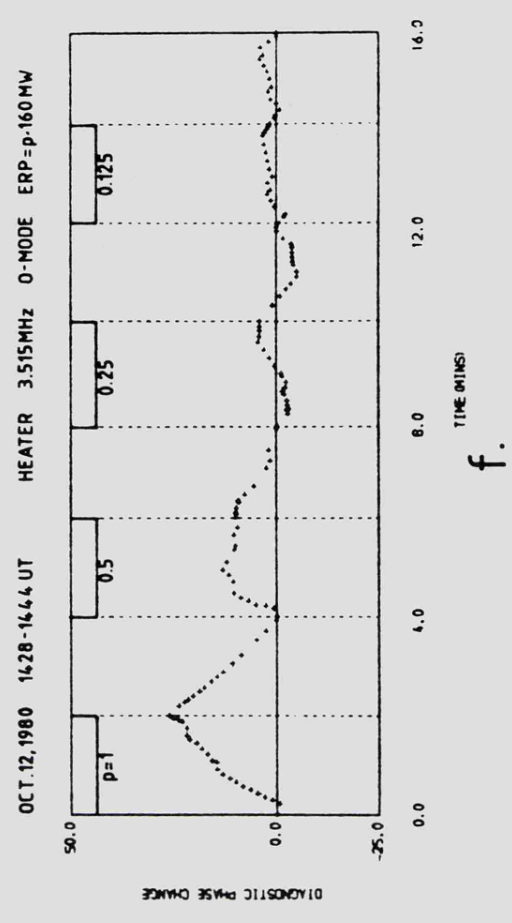
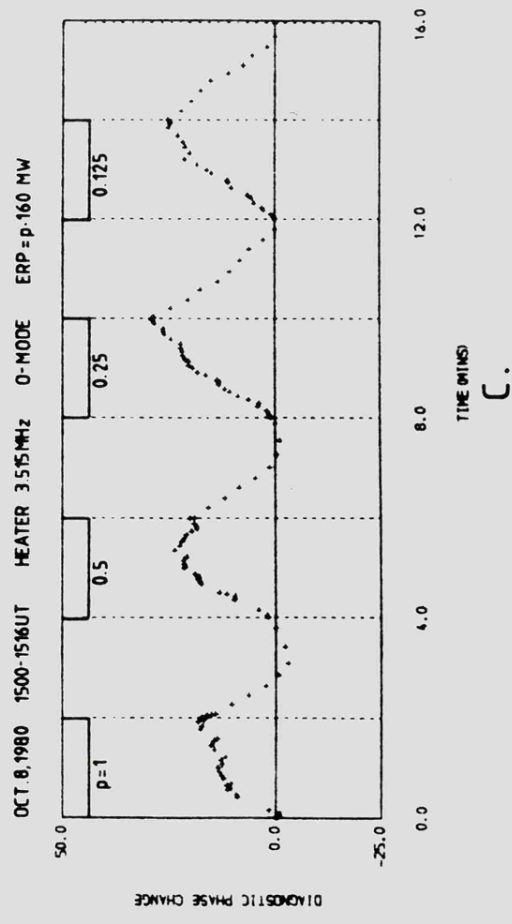
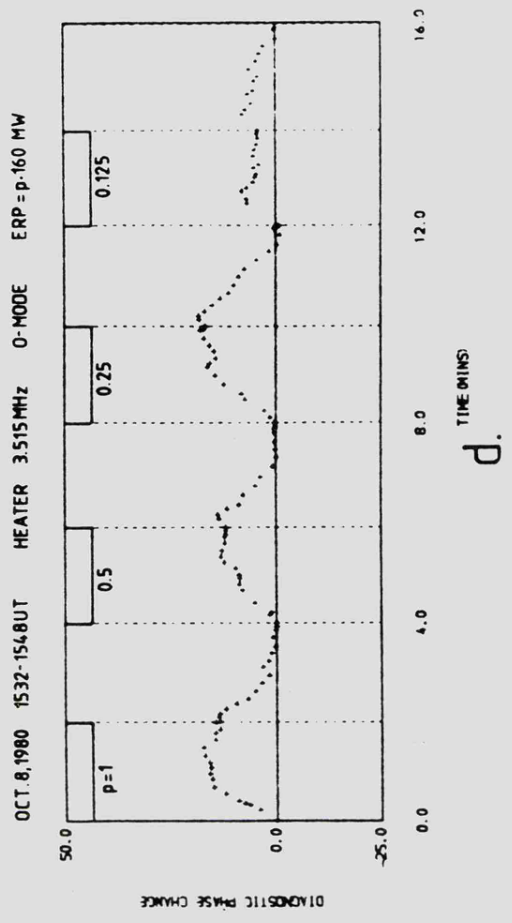


Fig. 6.1 c-f Phase changes of 3.778 MHz diagnostic signal during periods of changing heater ERP (c,d) Oct. 8, 1980 (e,f) Oct. 12, 1980.

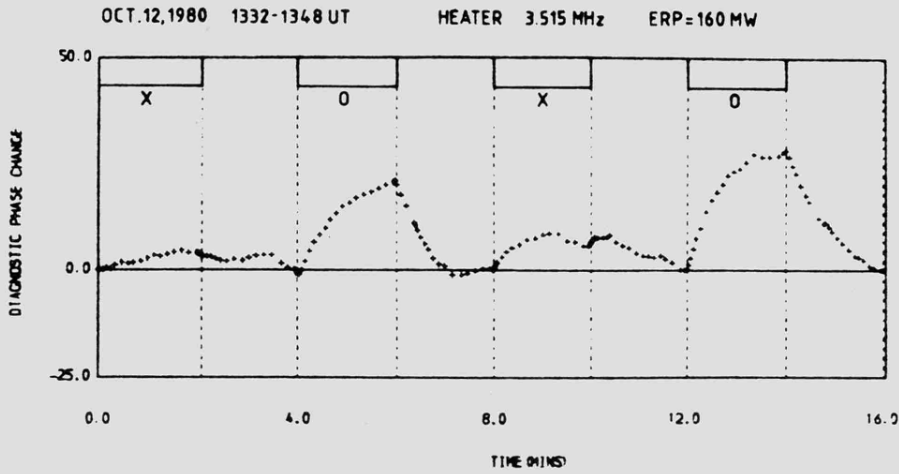
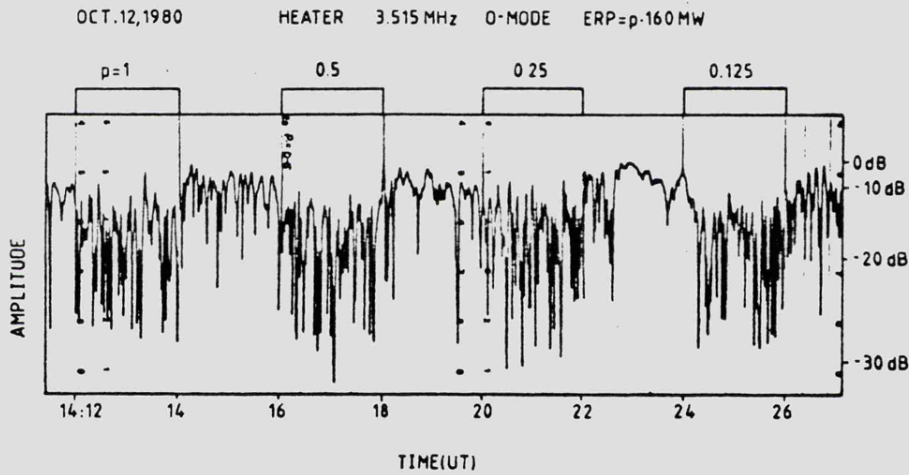
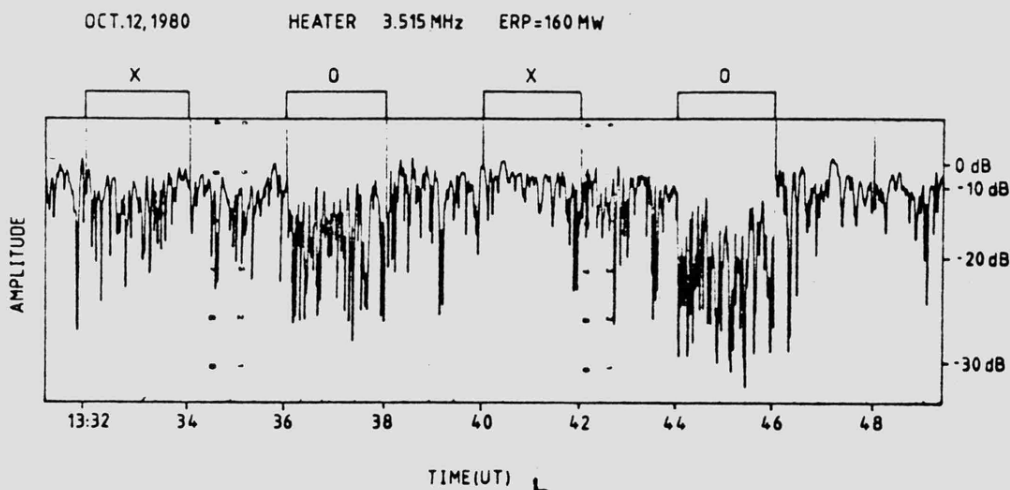


Fig. 6.1g Phase changes of 3.778 MHz diagnostic signal during periods of 0- and X-mode heating, Oct. 12, 1980.



a.



b.

Fig. 6.2 a,b Examples of amplitude changes of the 3.778 MHz diagnostic: (a) occurred during periods of changing ERP at the same time as phase changes in fig. 6.1c; (b) occurred during periods of 0- and X-mode heating at the same time as phase changes in fig. 6.1g.

an increase in plasma density along the path. During heater 'off' periods the phase path increases indicating a plasma density decrease. In the lower F-region, these plasma density changes correspond to the expected electron temperature enhancement during heating which are discussed in greater detail in the following section.

The time evolution of the phase response has roughly the form

$$\Delta\varphi_0(1 - e^{-t/\tau_1}) \text{ during 'on' periods and } \Delta\varphi_0 e^{-t/\tau_2}$$

during 'off' periods, where $\Delta\varphi_0$ is constant over each period, t

is time and τ_1 and τ_2 are characteristic rise and decay times

respectively. This phase change time dependence is shown

particularly well by the data in fig. 6.1b. The heater 'on'

and heater 'off' periods were each 7.5 min in this case, allowing

times for the phase changes to reach their equilibrium levels.

Numerical fitting of the data to the exponential curves produced

a range of values of τ_1 and τ_2 . The mean value of τ_1 was

(38.0 \pm 9.1)s and of τ_2 , (37.3 \pm 9.3)s. There is no clear

dependence of τ_1 or τ_2 on ERP or on whether the heater was in X-

or O-mode, even though the effect of X-mode heating was much smaller

than for O-mode heating. Both τ_1 and τ_2 appear to be independent

of $\Delta\varphi_0$.

For comparison, typical time variation of the diagnostic signal amplitude during heating cycles are reproduced in figure 6.2a, b. Figure 6.2a represents a cycle in which ERP was reduced in successive periods of heating and figure 6.2b represents a cycle of alternate X- and O-mode heating. A detailed analysis of these diagnostic amplitude data in terms of anomalous absorption is presented in chapter 5. With regard to the present phase change study, the amplitude data provides an indication of the overall amount of

power transferred from the heater wave to the ionospheric plasma. The diagnostic wave suffers attenuation, typically between 10 and 15 db, due to anomalous absorption during O-mode heating. However, there is no detectable attenuation of the diagnostic wave during X-mode heating.

Reduced ionogram data presented in chapter 5 indicate that the heater reflection level was about 200 km \pm 10 km and that the diagnostic reflection height was always a few kilometers above that of the heater.

6.2.2 Three frequency diagnostic data

During heating campaigns conducted in September 1981 and October 1982 amplitude (see chapter 5) and phase changes induced by the heating simultaneously on three diagnostics were investigated. Reduced phase data from the experiment on 8th September 1981 for diagnostics with frequencies of 4.948, 5.701 and 6.506 MHz are illustrated in fig. 6.3 a-c. The pump was operated at 5.423 in ordinary polarization. In the sequence of 3 min-on, 3 min-off heating cycles, the effective radiated power (ERP) was equal to p. 260 MW in each cycle where p = 1 in cycle one, then 0.35 in cycle two and 0.1 in cycle three. The phase changes exhibit a dependence on pump ERP similar to the single diagnostic data in fig. 6.1f. This pump power dependence was observed in all three diagnostic data sets during the 1981 and 1982 campaigns.

Data from an experiment on 23rd October 1982 for diagnostics of 4.948, 5.701 and 6.301 MHz is illustrated in fig. 6.4 a-c. The pump was operated at 5.423 MHz with ordinary, then extra-ordinary

Sept. 8, 1981 1618-1636 UT Heater 5.423MHz 0-mode ERP=p · 260MW

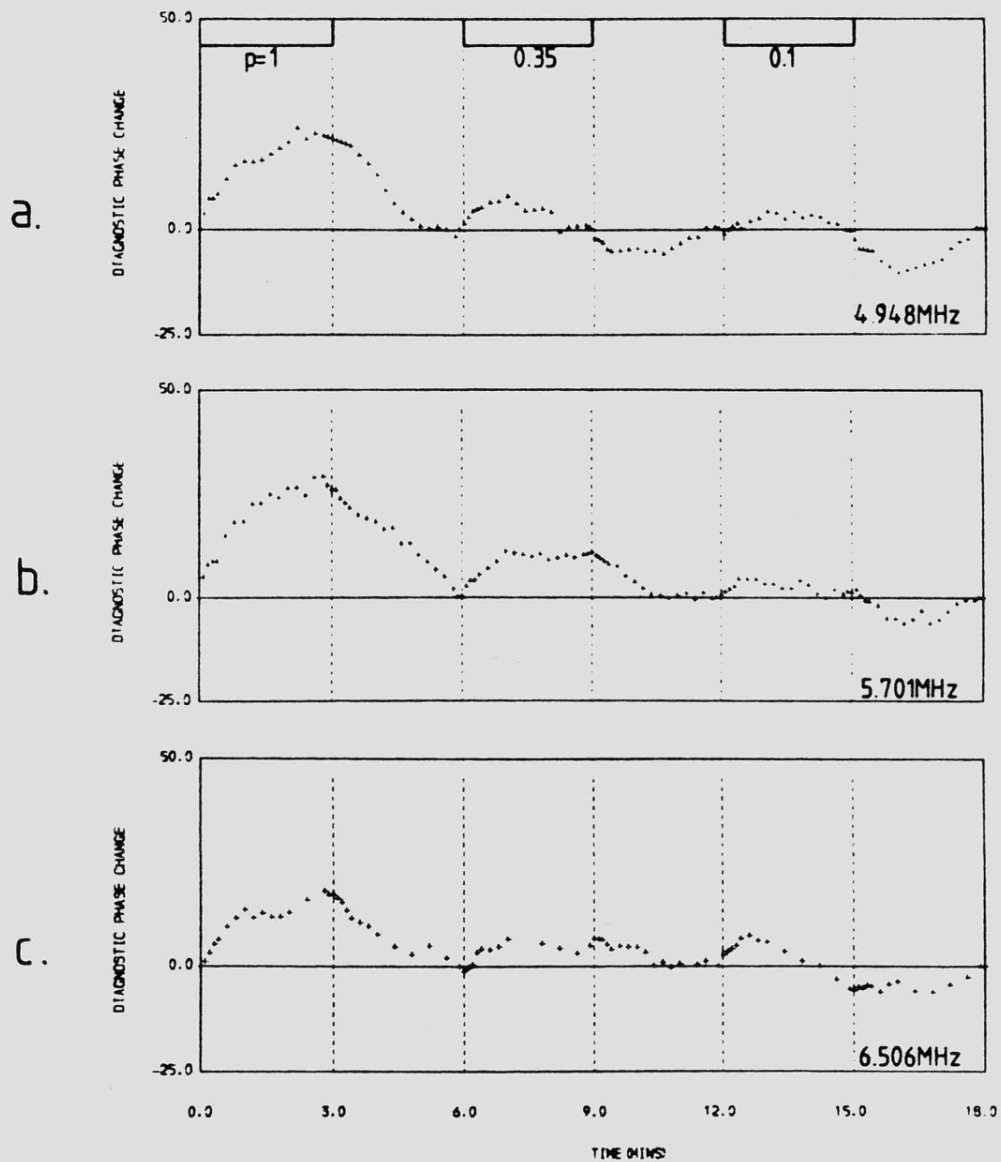


Fig. 6.3 a-c Simultaneous phase changes of (a) 4.948, (b) 5.701 and (c) 6.506 MHz diagnostics during periods of changing heater ERP, Sept. 8, 1981.

Oct. 23, 1982 1100-1112UT Heater 5.423MHz ERP=260MW

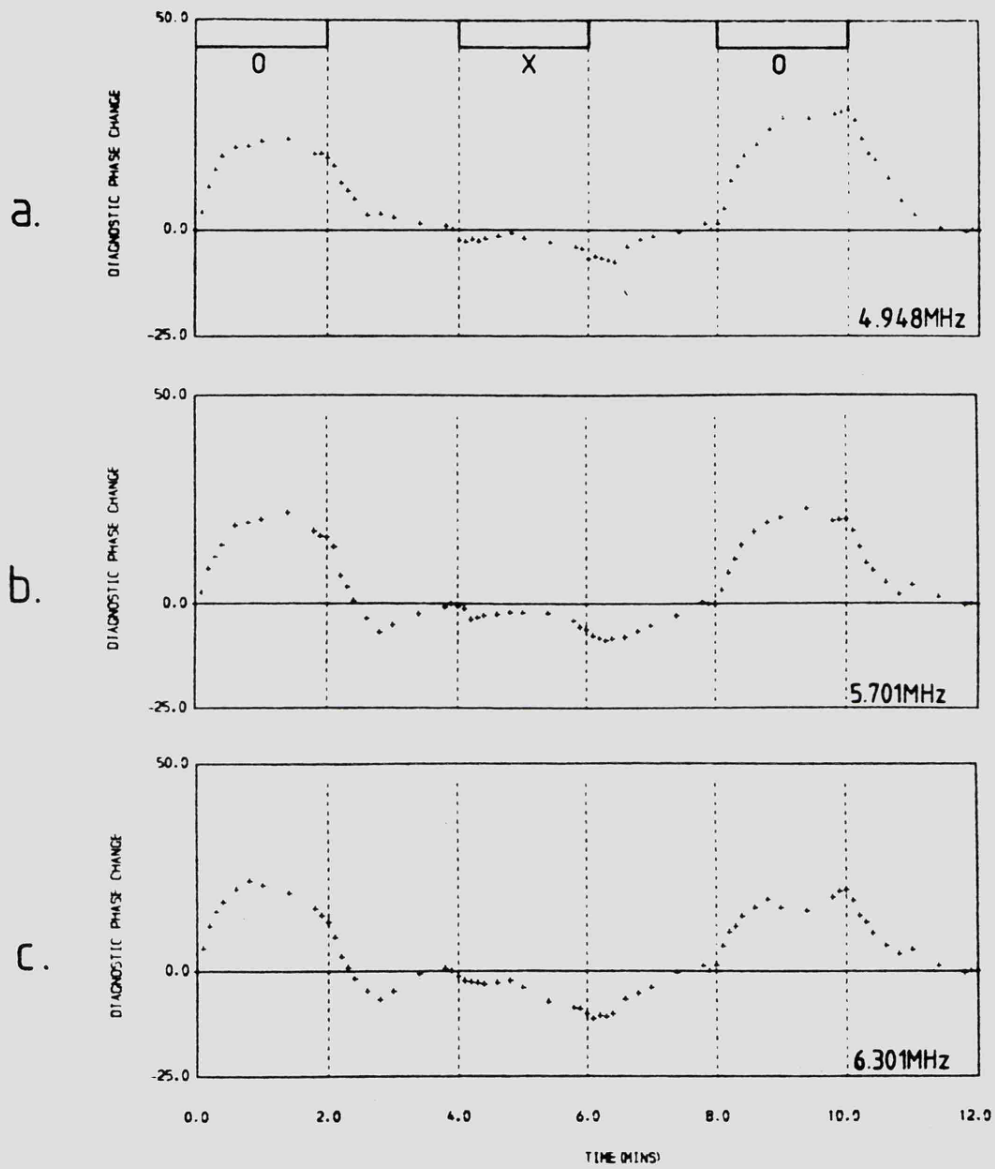


Fig. 6.4 a-c Simultaneous phase changes of (a) 4.948, (b) 5.701 and (c) 6.301 MHz diagnostics during periods of 0- and X-mode heating, Oct. 23, 1982.

polarization in alternate heater on periods. Strong phase changes are induced in all three diagnostics only during O-mode heating, confirming the result obtained with a single diagnostic in 1980 (fig. 6.1g).

It is clear from fig. 6.3 and 6.4 that the phase response of the diagnostic waves to heating exhibits no strong dependence on diagnostic frequency (unlike the amplitude response which was observed in chapter 5 to be highly frequency dependent).

Davies (1965) notes that when reflection height of a radio wave varies due to electron density changes, the resulting phase change is proportional to the wave frequency. However, if the electron density variations take place well below the radio wave reflection height, the phase changes are inversely proportional to wave frequency. The small range of diagnostic frequencies employed (~ 1.5 MHz) does not enable this frequency dependence to be evaluated.

The weak diagnostic phase response to X-mode heating indicates that the effects occur in the F-region due to anomalous absorption in the vicinity of the O-mode pump reflection height. The weak frequency dependence of the phase response strongly suggests that large scale plasma density perturbations occur over a height range large enough to include the reflection regions of all three diagnostics (~ 20 km).

It should be noted that the diagnostic phase response indicates large scale plasma enhancements in all the cases observed.

6.3 Interpretation of results

6.3.1 Outline of physical processes

The energy which causes changes in the electron plasma during

ionospheric heating by high power radio waves is transferred from the heater to the plasma by deviative absorption and anomalous absorption due to the excitation of various plasma instabilities (see chapter 7). Deviative absorption effects occur predominantly near the reflection level of the heater wave. Anomalous absorption takes place near the upper hybrid resonance point of the heater. However the upper hybrid resonance and reflection points are approximately 1 km apart. On the scales of the plasma density inhomogeneities involved in producing the diagnostic phase changes this is a negligibly small distance. The immediate effect of the energy input is an increase in the electron temperature, T_e . In the lower F-region heat transport processes are negligible on scales large enough to produce HF radio wave phase changes. The energy equation of the electron gas can then be written (see chapter 3, section 3.2),

$$\frac{3}{2} \frac{\partial T_e}{\partial t} = Q' - \frac{3}{2} R (T_e - T_0) \quad 6.1$$

where T_0 is the background ion and neutral temperature which changes insignificantly during the short periods of heating employed for these experiments. The first term on the right-hand side of equation 6.1 is the heat input rate per electron and the second is the heat loss rate per electron due to collisions with background particles. It is extremely difficult to calculate the time evolution of T_e from equation 6.1. The value of E_0 , the electric field strength of the heater wave on which Q' depends, is a complicated function of position and time. Anomalous absorption arises when the electromagnetic heater wave excites Langmuir waves which in a magnetoactive plasma cannot be excited at frequencies much below the upper-hybrid frequency. As pointed out in chapter 5, X-mode waves are reflected in the

ionosphere at an altitude where their frequency is below the upper-hybrid frequency; only O-mode heating can lead to anomalous absorption.

If electron temperature changes induced by heating are fairly small and Q' is constant during the period of heating, then $\Delta T_e(t)$, the change in electron temperature as a function of time, would be expected to have the form $\Delta T_{00}(1 - e^{-t/\tau_T})$ during heating and will decay as $\Delta T_{00} e^{-t/\tau_T}$. It is assumed that the period of heating is large compared with τ_T and that ΔT_{00} is a constant depending on Q' . τ_T is approximately equal to $1/R$. Such electron temperature changes have been found to occur at all altitudes in the ionosphere e.g. Meltz et al., (1974), Mantas et al., (1981).

Recently Showen and Behnke (1978) have demonstrated that Q' is not constant but depends on the excitation of plasma instabilities and their overshoot behaviour. Thus the simple exponential response is not an adequate description of the growth of T_e during heating. The relaxation of T_e after heating is well described in terms of a simple exponential decay as expected. Stubbe et al., (1982a) have shown that on the basis of the resonance instability theory of Das and Fejer (1979), ionospheric variability which may be both natural or induced, also plays an important role in the level of anomalous absorption of the heating wave which can further complicate the time dependence of Q' (see chapter 7).

The effect of a change in electron temperature on ionospheric electron number density, N_e depends very much on altitude. In the lower F-region diffusion processes can be neglected for large scale ($>1\text{km}$) changes in N_e . The change in N_e is then basically determined by the temperature dependence of the electron loss rate.

The differential equation which determines the rate of change of N_e is

$$\frac{\partial N_e}{\partial t} = q_p - q_L = q_p - \alpha N_e^2 \quad 6.2$$

where q_p and q_L are the total electron production and loss rates respectively, and α is the effective recombination coefficient. α is a decreasing function of electron temperature (Biondi, 1969; Gurevich, 1978), thus as T_e increases because of heating, α decreases and N_e increases. As indicated above, T_e varies in a rather complicated and not entirely predictable way, therefore it is not possible to use equation 6.2 to solve for $N_e(t)$. However, an approximate value for $N_e(t)$ can be found if the changes in T_e , and N_e due to heating are assumed to be small and if $\tau_T \ll 1/\alpha N_e$. For these conditions during heater 'on' periods, the variation in electron density as a function of time, $\Delta N_e(t)$ would have the form, $\Delta N_0 (1 - e^{-t/\tau_N})$, while during heater 'off' periods it should decay as $\Delta N_0 e^{-t/\tau_N}$. It is assumed that the heating period is fairly long compared with the electron density response time, τ_N , which from 6.2 is approximately given by

$$\tau_N = 1/(\partial q_L / \partial N_e) \approx 1/2 \alpha N_e \quad 6.3$$

In the lower F-region $\tau_N/\tau_T \approx 10$ (Gurevich, 1978) and the heating period was about three times τ_N so the approximation is valid. It is also clear that the larger the change in T_e due to heating, the larger the change in α and the larger ΔN_0 . Thus ΔN_0 should increase with increasing Q' .

An increase in N_e in the ionosphere causes a decrease in the plasma refractive index for radio waves (Ginzburg, 1970) which reduces the phase path of a diagnostic radiowave passing through the heated region causing a phase advance at the receiver. Since the observed phase changes, $\Delta\varphi$, in the diagnostic signal should respond instantaneously to changes in N_e , $\Delta\varphi(t)$ will have a form similar to $\Delta N_e(t)$ with rise and fall times of τ_N . Also, $\Delta\varphi_0$, as defined in Section 6.2, should increase with increasing Q' as does N_e .

6.3.2 Observed phase change response times

The analysis above suggests that the phase changes observed in the diagnostic wave during the experiments of 8, 12 and 13 October 1980 (figure 6.1) result from increases in plasma density during the 'on' period of the heater and plasma density decay during the time when the heater was turned off. The average value of τ_N estimated from the phase change response times τ_1 and τ_2 is approximately 38s which compares well with the expected value of τ_N , about 32s, in the lower F-region (Gurevich, 1978). As mentioned in section 6.2, the values of τ_1 and τ_2 did not exhibit any significant dependence on the maximum phase change $\Delta\varphi_0$ during each 2 minute period, a result to be expected if

$$\tau_1 \simeq \tau_2 \simeq \tau_N = \partial q_L / \partial N_e$$

which is independent of Q' . The fact that $\tau_1 \simeq \tau_2$

is itself an important result consistent with the analysis in section 6.3.1 and indicates that the characteristic fluctuation times for changes in Q' and T_e are small compared with τ_N .

6.3.3. X- and O-mode heating

Figure 6.1g and 6.3 indicate clearly that much smaller phase

changes are induced in the diagnostic signal by X-mode heating than by O-mode heating at the same heater carrier frequency. This is consistent with the conclusion noted in section 6.3.1 that the X-mode contributes heat to the electron plasma only by deviative absorption, whereas the O-mode contributes heat by both deviative and anomalous absorption. As a result the phase changes produced in the diagnostic wave are much smaller in the X-mode case. The apparent slight increase in diagnostic phase path in fig. 6.4 during X-mode heating is probably due to small natural plasma density changes in the background ionosphere. In the case of the heating sequence in fig. 6.1g, the reflection height of the 3.515MHz X-mode was in excess of 10 km below the 3.778 MHz diagnostic reflection height (see section 5.4b). It could be argued that the very small diagnostic response to X-mode heating is due to the large separation of their reflection points. However, in the case of the sequences in fig. 6.4 the 4.948 MHz reflection point was within 2 km of the X-mode pump reflection height. It can be concluded that the X-mode pump produces no appreciable F-region heating.

6.3.4 Effects of changing ERP

In section 6.3.1 it was established that the factor which determines the maximum diagnostic phase change $\Delta\varphi_o$ is Q'_d , the total amount of power absorbed from the heater. This is composed of a contribution due to deviative absorption, Q'_d and a contribution due to anomalous absorption, Q'_a .

As is well known, Q'_d is proportional to E_o^2 . The dependence of Q'_a on pump electric field is more complicated because of the existence of electric field thresholds and the nonlinear growth and stabilization of FAI which cause the anomalous absorption of

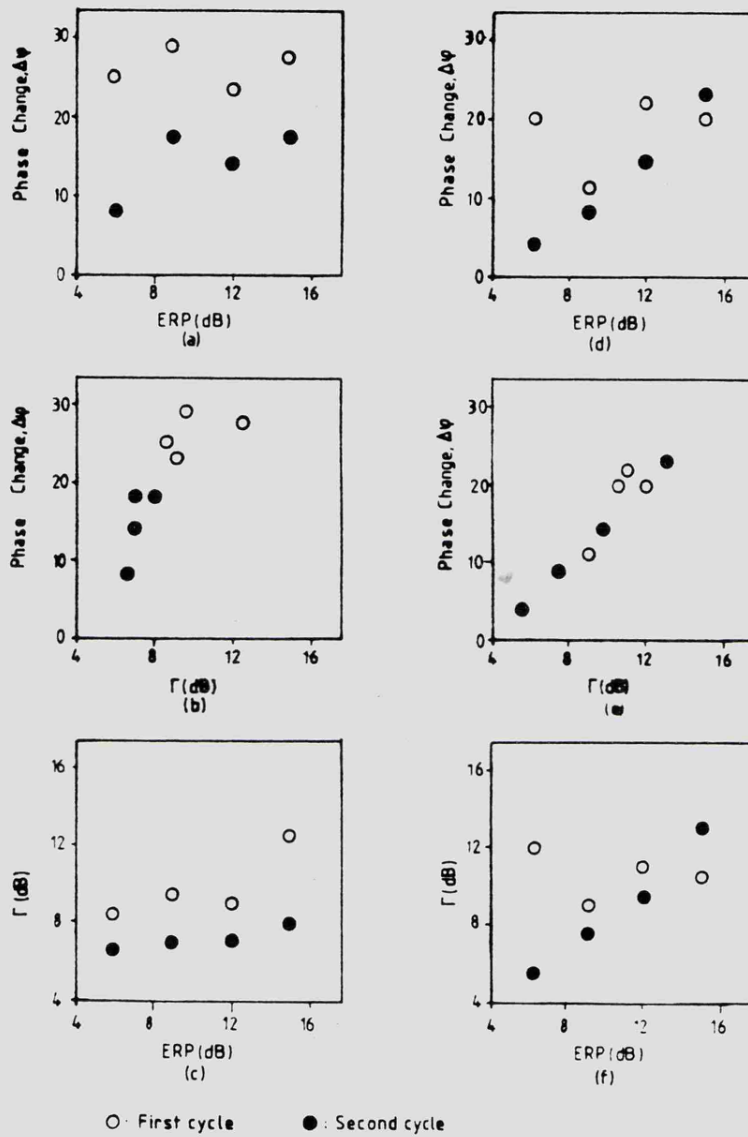


Fig. 6.5 Graphs illustrating the relationship between diagnostic phase changes, $\Delta\varphi$ diagnostic absorption Γ , and heater ERP. Four cycles of changing ERP are included. Each cycle (two on Oct. 8, 1980, a-c; two on Oct. 12, 1980, d-f) consists of four values of ERP = p. 160 MW, p = 1, 0.5, 0.25, 0.125.

the pump (see chapter 7). Stubbe et al., (1982a) have shown that ionospheric variability can be an extremely important factor in the level of anomalous absorption suffered by the heater wave. The value of E_o in the lower F-region depends on several factors, such as D- and E-region absorption, which reduce E_o , and on focussing and defocussing effects due to a spatially varying refractive index for the heater wave. The existence of a reflected heater wave can increase the value of E_o , though the reflected wave is much reduced when FAI are excited by the incident heater wave. The value of E_o^2 is, of course, proportional to the effective radiated power, (ERP).

Although the actual values of E_o and Q' are not known, the effect of changing E_o on $\Delta\phi_o$ and therefore on Q' can be deduced. In chapter 5 it was established that the anomalous absorption was proportional to field aligned irregularity amplitude squared but only weakly dependent on radiowave frequency. Thus, the anomalous absorption Γ suffered by the diagnostic wave provides a measure of the anomalous absorption of the heater wave.

During the two cycles of four periods of heating on 12 October in which the heater ERP was successively halved, the diagnostic amplitude during heater 'off' was constant (apart from the normal periodic fading due to small scale ionospheric variability) to within about 2 dB. Thus the value of E_o^2 was reduced by a factor of approximately a half for each successive heating period (i.e. 4 values of E_o^2 were available).

A graph of $\Delta\phi_o$ against ERP measured in dB above 5 MW for the two cycles from 12 October, 1980 (fig. 6.5d) indicates poor overall correlation between $\Delta\phi_o$ and ERP except for the second cycle.

However a graph of $\Delta\varphi_o$ against Γ for the same data set shows very good correlation for both cycles (fig. 6.5f). Graphs for the data from 8 October, 1980 reveal a similar result, although the background absorption was a little more variable (5 dB changes) making the estimated values of Γ less reliable. The correlation between $\Delta\varphi_o$ and ERP (figure 6.5a) is very poor while that between $\Delta\varphi_o$ and Γ is quite good. Graphs of Γ against ERP for the two data sets (figs. 6.5c and f) are revealing. On the 8 October 1980, there is little correlation between Γ and ERP, however on the 12 October (figure 6.5f) during the second cycle Γ and ERP are well correlated. The difference in the gradients of the plots of $\Delta\varphi_o$ against Γ for the 8 and 12 October 1980 data may be attributed to differences in the background ionospheric parameters on the two days (e.g. T_e and plasma density gradient differences).

The dependence of Γ on ERP has been investigated in chapter 5 and certain conclusions from that study are of relevance to the interpretation of the results presented here, namely that several different mechanisms may be responsible for determining the level of Γ , among them ionospheric variability. In many cases therefore, ERP is not necessarily the most important factor in determining the energy input to the electronic plasma. It is evident from the graphs, fig. 6.5, that if $\Delta\varphi_o$ is taken as a measure of the amount of heating power put into the ionosphere, then Q' is much more sensitive to changes in Γ than ERP. The only cycle which exhibited a correlation between Q' and ERP was the second cycle on the 12 October (fig. 6.5d) but this was also the only cycle during which Γ was found to be proportional to ERP. It was pointed out in chapter 5 that this can occur when the ionospheric variability increases to the point where changes on a scale of the order of

one radio wavelength occur in a time shorter than the resonance instability growth time. The second heating cycle on the 12 October did indeed occur during a period of increased ionospheric variability as indicated by the increased fading rate of diagnostic amplitude. If the background absorption is constant, the deviative absorption Q'_d is proportional to E_o^2 which in turn is proportional to the ERP. Assuming, as before, that E_o does not vary due to changes in ionospheric structure, it appears that changes in Q'_d do not significantly affect $\Delta\varphi_o$. However, changes in anomalous absorption Q'_a , as indicated by the variation of diagnostic anomalous absorption, produce marked changes in $\Delta\varphi_o$. It is evident that E_o^2 determines the power density incident on the F-region which in turn determines the upper limit of power that can be absorbed by the electron plasma. The amount of power which is actually absorbed is clearly sensitive to other factors. For example, one might argue that the threshold electric fields and FAI growth rates and saturation amplitudes may vary in an unpredictable way more than the controlled variation of E_o (see chapter 7). Ionospheric variability during a heating cycle might be the controlling factor in how much power is absorbed. The foregoing suggestions are somewhat speculative and further experiments will be necessary before a final conclusion can be drawn. Theory predicts that the anomalous absorption due to the resonance instability might be greater at high latitudes as a consequence of a more efficient excitation mechanism when the electric field is close to being perpendicular to the geomagnetic field. This prediction appears to be confirmed by the present experimental results.

6.4 Conclusions

In the high latitude heating experiments described, it has been possible to induce phase changes in a low power diagnostic wave reflected from the lower F-region near the heated volume. The phase changes in the diagnostic signal indicate that the plasma density of the lower F-region was increased during heating. This was due to the decrease in the effective electron loss rate caused by the induced increase in electron temperature.

The effect of heating on the plasma as indicated by the asymptotic limit of the induced diagnostic phase change, $\Delta\varphi_0$, after heater switch on was not well correlated with effective radiated power (ERP). It was however well correlated with the level of anomalous absorption Γ of the diagnostic wave which provided an estimate of the level of anomalous absorption of the heater wave. Assuming a fairly constant background ionosphere and that the deviative absorption is proportional to ERP, the low correlation between Γ and ERP indicates that deviative absorption did not contribute significantly to the plasma heating. In contrast, the level of anomalous absorption was well correlated with $\Delta\varphi_0$ therefore it is concluded that anomalous absorption contributes more significantly to plasma heating than deviative absorption.

During previous heating experiments carried out at low-latitudes (Arecibo) and at mid-latitudes (Platteville) the anomalous absorption was found to be similar to, but slightly greater than, deviative absorption. These results, together with the high latitude results described here, suggest that the relative contribution of anomalous and deviative absorption to ionospheric heating has a latitudinal dependence, the anomalous absorption becoming increasingly important at high latitudes.

7. SELF ABSORPTION EFFECTS

7.1 Introduction

It is currently accepted that thermal parametric instabilities are responsible for the generation of small scale field aligned irregularities (FAI) in the F-region by a high power EM pump wave (Grach et al., 1977; Das and Fejer, 1979; Inhester et al., 1981; Kuo and Lee, 1982; Stubbe et al., 1982b; Dysthe et al., 1983). The precise details of the mechanism remain uncertain. It is evident however that the anomalous absorption of the pump itself plays an important role in this process. An experimental investigation of the nonlinear reflectivity of the pump wave can therefore provide important information regarding the growth, stabilization and decay processes of FAI generated during heating. Recent measurements of the signal strength of an ionospherically reflected high power pump wave have revealed important new features of the nonlinear interaction between the pump and FAI which it generates. These observations constitute the first systematic investigation of the effects of transmitted pump power changes on the onset and growth of thermal parametric instabilities. During experiments in which the pump power was steadily increased from zero (MW) to full power, and then steadily decreased to zero, a hysteresis effects was observed in the pump anomalous absorption. This result has important consequences with regard to the nature of the mechanisms which cause the growth of FAI.

The growth mechanisms proposed in the literature can be classified broadly into two types. Type I processes have a power threshold for the high power radio wave (pump) but require no initial striations to be present (Grach et al., 1977; Das and Fejer, 1979; Dysthe et al., 1983). Type II have a threshold which depends on the product of pump power and the striation amplitude, producing explosive striation growth above the threshold (Vaskov and Gurevich, 1977; Inhester et al., 1981).

It has been suggested that the first mechanism may initially amplify the striations until the threshold of the second mechanism is reached, which then leads to further growth (Inhester et al., 1981; Stubbe et al., 1982a). This preliminary heating stage (type I instability) is necessary because the pump power required to exceed the threshold of the type II instability can be prohibitively high when the initial amplitude of the background irregularities is low (Inhester et al., 1981).

7.2 Pump wave measurements

During experiments on 10 September 1981 the effective radiated power (ERP) of a 5.423 MHz pump wave was changed from 0 to 260 MW (full power) by increasing the ERP in steps of 6.5MW at 9s intervals. Subsequently, the ERP was progressively reduced by 6.5 MW steps at 9s intervals from full power down to 0 MW. Thus one complete cycle of increasing and decreasing ERP was completed in 12 min. This heating sequence was repeated several times. The amplitudes of the pump wave reflected from the ionosphere was measured by a receiver at the South-site (fig.4.2). The data for a single heating cycle is illustrated in fig. 7.1. It includes both the reflected pump power data and a plot of ERP as a function of time. The amplitudes of two low power diagnostic signals of 5.701 and 6.505 MHz were also monitored at the same receiver site. The geometry of the diagnostic system was identical to that described in chapter 5.

In fig. 7.2 the received signal amplitudes for the 5.423 MHz pump are displayed for four consecutive cycles (including the cycle in fig. 7.1) of increasing and decreasing ERP. There is a gap of 24 min between the end of cycle b and the beginning of cycle c during which time the pump was off. During this time gap an ionogram was taken and electron density profile derived from this

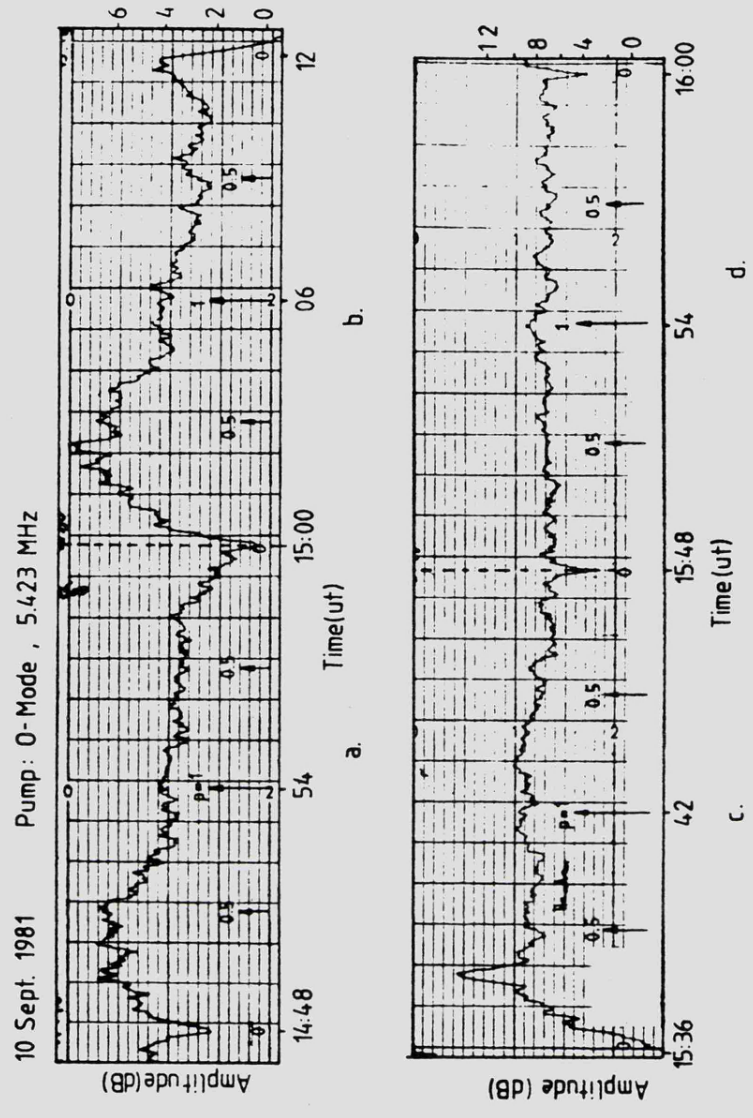


Fig.7.2. The reflected heater signal strength during four sequences of increasing and decreasing heater ERP (see fig.7.1).

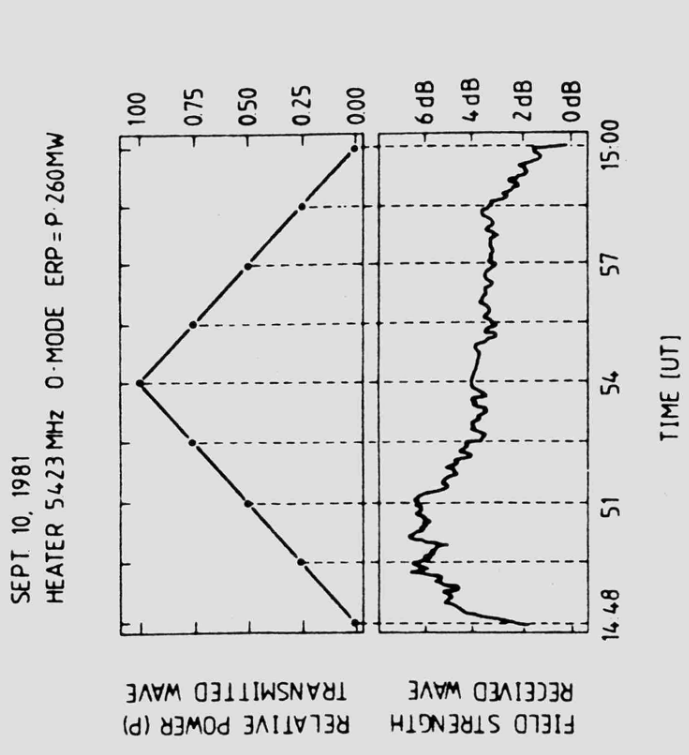


Fig.7.1 Signal strength data of the ionospherically reflected heater wave vs. time (lower panel) together with the corresponding transmitted power (upper panel).

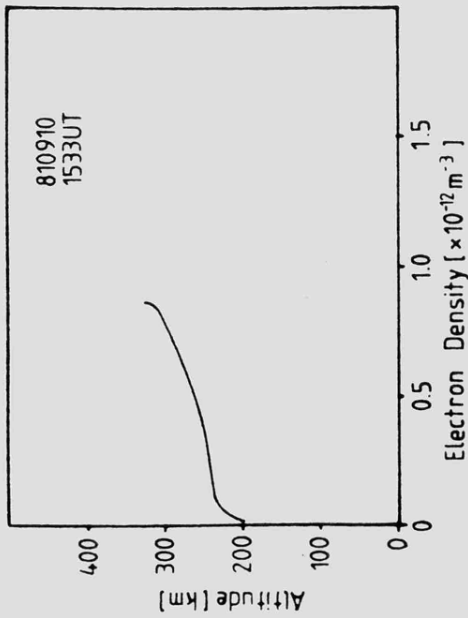
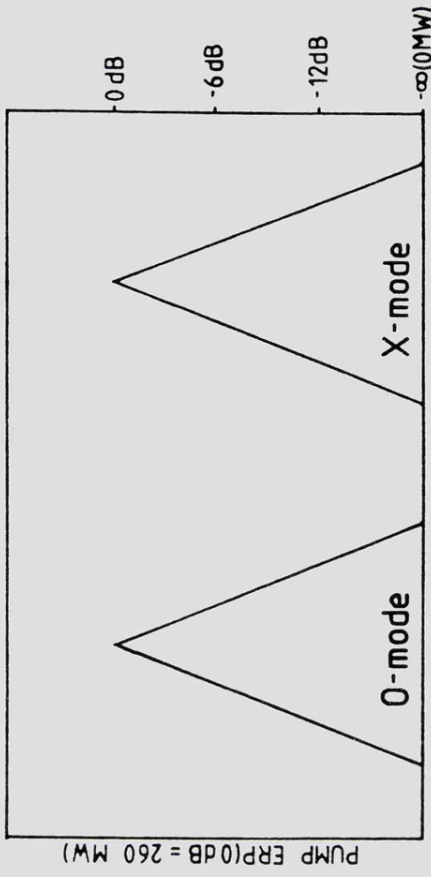
is illustrated in fig. 7.3. It is clear that cycles a to c are very similar. They exhibit the following common features.

- (i) a sudden rise in signal level during the first step from 0 to 6.5 MW ERP,
- (ii) a slower rise during the subsequent steps up to about 30-50% of full power,
- (iii) a fall in signal level during subsequent steps of increasing ERP
- (iv) a fairly constant level during the decrease from full power down to the last few steps before 0 MW is reached,
- (v) a final rapid fall from 6.5 MW to 0 MW.

Cycle d does not exhibit features (ii) and (iii). It consists of only (i) immediately followed by (iv) and then (v). All of the features above illustrate the nonlinear character of the ionospheric reflectivity of high power radio waves. Features (ii) and (iii) indicate an 'overshoot' effect. The asymmetry of the reflected pump signal between the stages of increasing and decreasing ERP constitute a hysteresis effect.

Similar experiments to those described above in which O-mode power stepping sequences were followed by X-mode power stepping sequences were performed on 23 October 1982. The results of these experiments indicate that while in each case the O-mode sequences exhibit hysteresis, the X-mode heating sequences did not. Data for an O-mode power stepping sequence and an X-mode sequence are illustrated in fig. 7.4. In the light of the evidence presented in chapter 5, this result strongly suggests that the hysteresis effect is associated with the generation of FAI since X-mode heating does not excite FAI.

OCT. 23, 1982 HEATER: 5.423 MHz



Radio Wave	Heater	Diagnostic 1	Diagnostic 2	Diagnostic 3
Frequency (MHz)	5.423	4.948	5.701	6.506
Reflection Height, h (km)	248.4	244.8	251.3	262.4
Scale Height H (km)	28.7	19.6	39.6	48.5

Fig. 7.3 Electron density profile deduced from an ionogram Sept 10, 1981, 1533UT. The table lists the reflection heights and local plasma scale height for the heater wave and diagnostic signals.

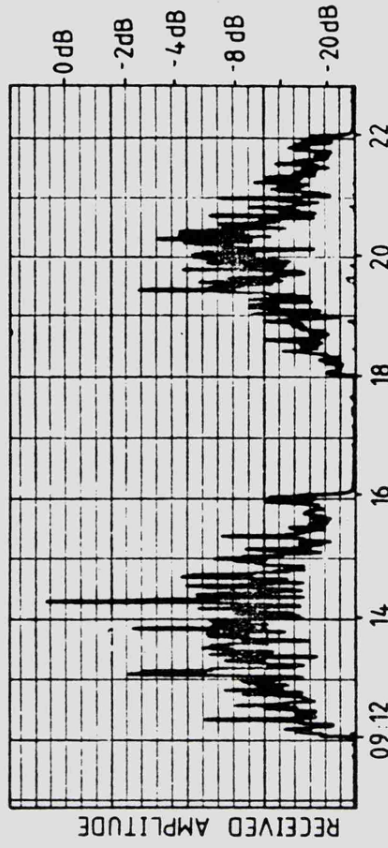


Fig. 7.4

As fig. 7.1 but with sequences of both O- and X-mode heating. Note in this case the heater transmitter power was changed in equal dB steps above 6.5 MW.

7.3 Pump Anomalous Absorption and Hysteresis Effect

If P_T and P_R are the ERP and received power levels of the pump, respectively, measured in dB above an arbitrary level, an absorption index, Γ , can be defined such that,

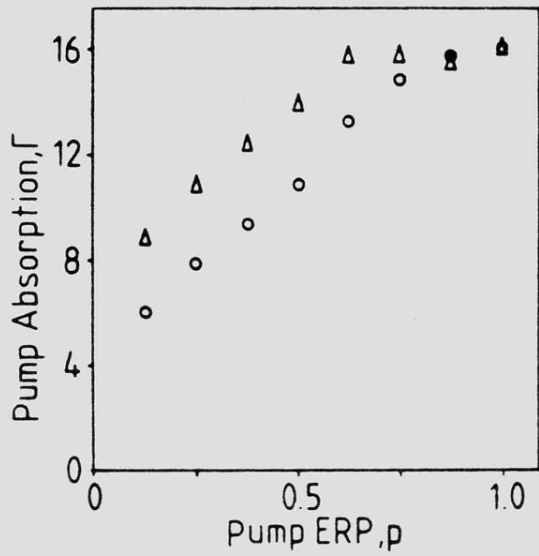
$$\Gamma = P_T - P_R \quad 7.1$$

In order to determine the effect of changing ERP on anomalous absorption due to field aligned irregularities, Γ was calculated for the data in fig. 7.2. For this purpose, P_T was defined in dB above 2.6 MW.

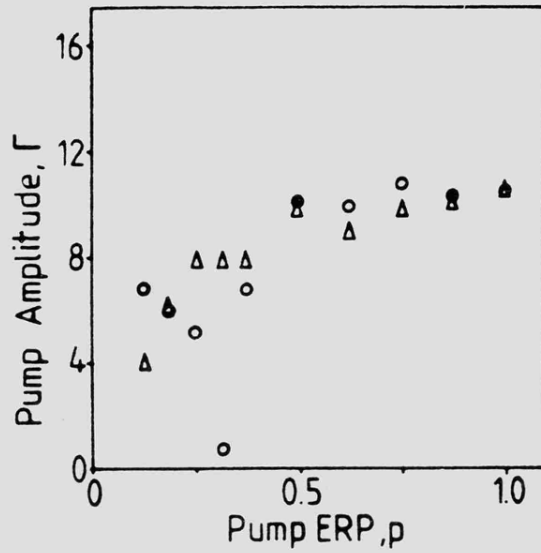
No significance can be attributed to the absolute value of received signal strength because this very much depends on the receiver antenna configuration and receiver characteristics, (see section 5.3).

Also the value of Γ does not represent the absolute absorption coefficient which must be defined in terms of the wave energy flux entering and leaving a given region of the ionosphere. However, changes in Γ with changing P_T do represent the changes in non-linear absorption. In the present case the 0 dB level in the received signal represents a detected voltage of about 0.3 mV.

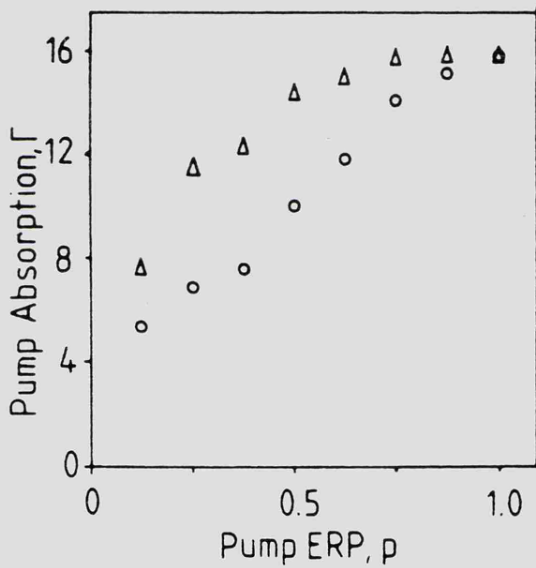
In fig. 7.5a-d graphs of Γ as a function of fractional ERP have been plotted for each of the four cycles. Fig. 7.6a-d illustrates the anomalous absorption of the 5.701 and 6.506 MHz diagnostics during cycles a-d. The diagnostic waves suffer anomalous absorption due to mode conversion into plasma waves in the heated F-region. Although a certain amount of non-linear D-region absorption of the pump can be expected, the similarity between variations in the absorption levels of the diagnostic signals which respond only to F-region heating and that of the pump is evidence for the assumption that the variations in Γ are due to anomalous absorptions of the pump itself in the F-region.



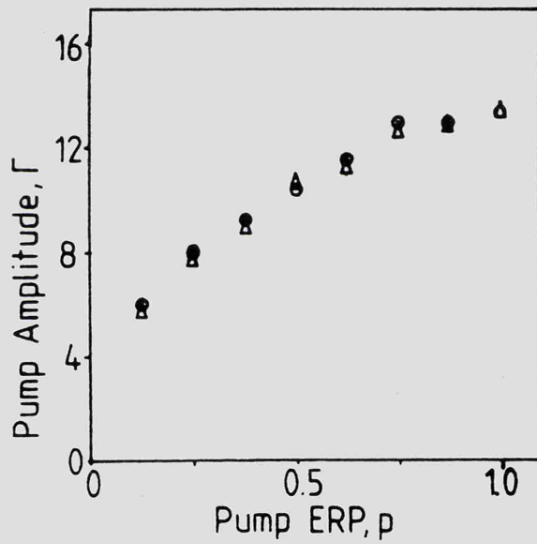
a. 1448-1500 UT



c. 1536-1548 UT



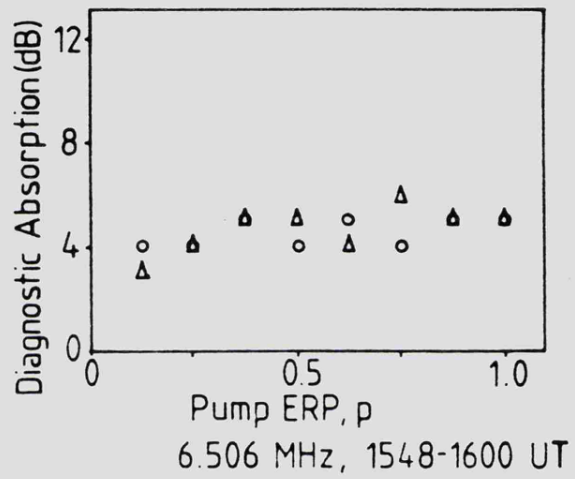
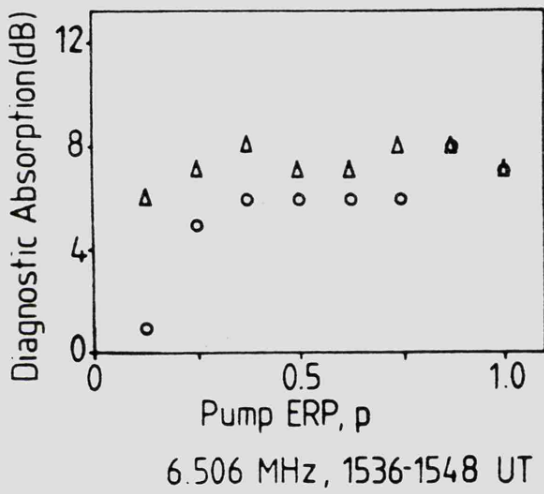
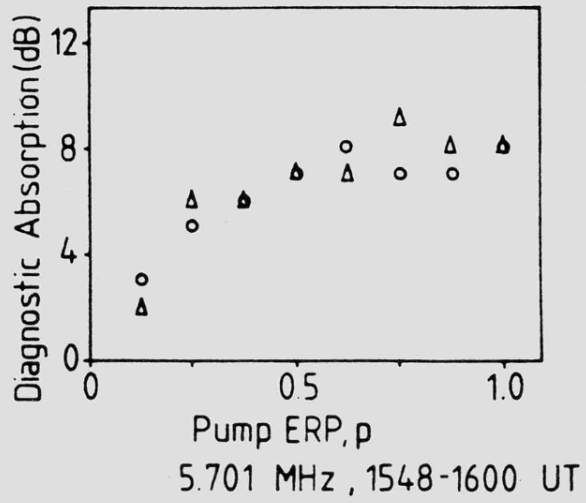
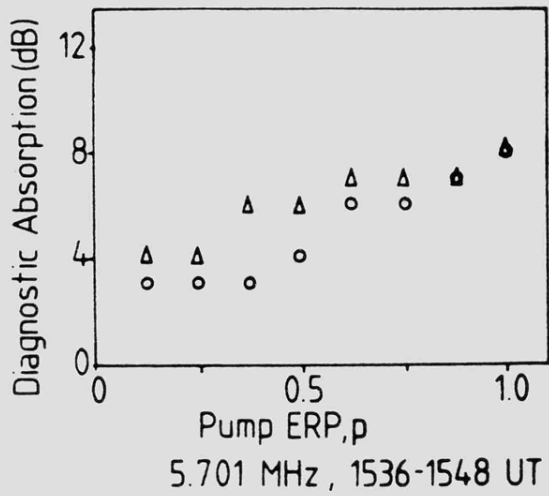
b. 1500-1512 UT



d. 1548-1600 UT

o : increasing ERP Δ : decreasing ERP

Fig.7.5 Graphs of pump self absorption vs pump ERP deduced from the data depicted in fig.7.2. Each of the four sequences (represented by a single panel) consists of data corresponding to increasing (o) and decreasing (Δ) ERP, Oct 10, 1981.



c.

d.

Fig.7.6 c,d as Fig.7.6 a,b except (c) 1536-1548 UT and (d) 1548-1600 UT.

Graphs a to c in fig. 7.5 illustrate clearly the existence of a hysteresis effect, although in the case of 7.5c it occurs only over small ERP range corresponding to the sharp peak in the received pump signal which occurs at about 1538 UT. At a given value of ERP, Γ has respectively values of Γ_i and Γ_d depending on whether the ERP is increasing or decreasing, such that,

$$\Gamma_d - \Gamma_i = \Delta\Gamma > 0 \quad 7.2$$

An anomalous absorption hysteresis effect is present in at least one of the diagnostic signals in each of cycles a and b. Hysteresis is almost entirely absent in the diagnostic amplitudes in cycles c and d. The electron density profile constructed from an ionogram taken at 1533 UT (see fig. 7.3) indicates that the reflection heights of the pump, the 5.701 MHz and the 6.506 MHz diagnostics were respectively 248.4, 251.3 and 262.4 km. The separation of the reflection heights are within one FAI scale length (see chapter 5). Consequently a similar (hysteresis) effect will be expected in the anomalous absorption of each of the above radio waves.

7.4 A model of FAI growth and stabilization

A complete theory of FAI requires an explanation of both the excitation and stabilization at an equilibrium amplitude. FAI excitation mechanisms have received considerable attention in the literature, (Perkins, 1974; Perkins et al. 1974; Vaskov and Gurevich, 1975, 1977; Lee and Fejer, 1978; Grach et al. 1977; Fejer, 1979; Das and Fejer, 1979; Inhester et al., 1981; Lee and Kuo, 1981; Dysthe et al, 1983). Stabilization on the other hand has been almost completely neglected. Inhester et al (1981) and Stubbe et al. (1982b) have suggested that pump extinction due to anomalous absorption could cause the

termination of unstable FAI growth. The latter authors have applied pump extinction to the theory of Das and Fejer (1979). They have also demonstrated that ionospheric variability can play an important role in determining the equilibrium FAI amplitudes. The Das and Fejer theory takes into account only primary scattering of the EM pump wave into Langmuir waves and the resulting differential heating in the 'beat' field of the two waves. Inhester et al. (1981) have proposed a type II mechanism complementary to the type I mechanism of Das and Fejer which takes into account higher order scattering of Langmuir waves. Das and Fejer (1979) and Inhester et al. (1981) have demonstrated only that FAI growth occurs when the pump power exceeds a certain threshold. These authors do not explicitly calculate FAI growth rates or saturation amplitudes. Dysthe et al. (1983) have evaluated the thresholds and growth rates for a thermal oscillating two stream instability which is similar to the mechanism proposed by Das and Fejer. Their method of calculating growth rates is applicable to both the Das and Fejer and (with some modification) Inhester et al. theories. In the following section the theories of Das and Fejer, Inhester et al., Dysthe et al and Stubbe et al. (1983) are developed into a unified theory of FAI growth and saturation which explains in a semi-quantitative way the observations presented in the previous section.

7.4.1 FAI excitation and growth

A mathematical model of FAI generation is now developed. This combines type I and type II growth stages with FAI amplitude stabilization of both stages by pump extinction due to anomalous self absorption. FAI decay is also modelled explicitly.

In the discussion which follows typical parameters for the lower F region are assumed and these are indicated in table 7.1.

Electron Density, N_e	$4.5 \cdot 10^{11} \text{ m}^{-3}$
Plasma Frequency, $\omega_e/2\pi$	6 MHz
Electron Temperature, T_e	1500 K
Ion Temperature, T_i	1000 K
Electron Collision Frequency, ν	600 s^{-1}
Debye Length, λ_D	$4 \cdot 10^{-3} \text{ m}$

Table 7.1 Some typical lower F-region parameters.

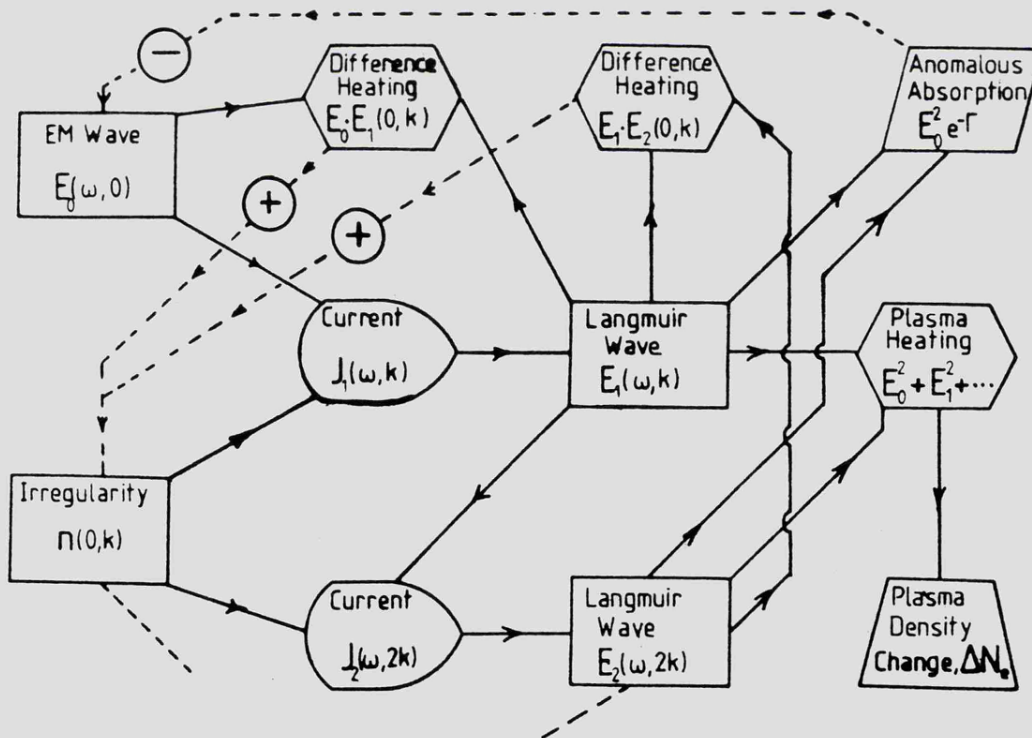


Fig.7.7 Schematic flow diagram of the excitation, growth and stabilization mechanism of FAI. Positive feedback paths which cause FAI growth are shown as dashed lines containing plus signs. Negative feedback paths which stabilized FAI growth are shown as dashed lines containing minus signs.

A schematic representation of the proposed model is reproduced in fig. 7.7. Primary Langmuir waves with electric fields $\underline{E}_1(\omega, \underline{k})$ are generated by the scattering of an EM pump field with a component $\underline{E}_0(\omega, 0)$ perpendicular to the magnetostatic field from FAI with perturbation plasma densities $n(0, \underline{k})$. ω is the pump angular frequency and \underline{k} the FAI wave vector (perpendicular to the magnetostatic field). Secondary Langmuir waves with electric fields $\underline{E}_2(\omega, 2\underline{k})$ are generated by the scattering of primary Langmuir waves from the FAI. Scattering higher than second order is neglected at this stage. Its effects on the results obtained with the present model are discussed in section 7.4.11. Following Inhester et al. (1981) a monochromatic FAI spectrum is assumed.

The type I mechanism involves differential heating due to interference between \underline{E}_0 and \underline{E}_1 . The total heat input due to differential heating by the beat field, Q_{10} is (Das and Fejer, 1979; see chapter 3, section 3.4),

$$Q_{10} = \nu \epsilon_0 \int_{-\infty}^{\infty} \overline{\underline{E}_1 \cdot \underline{E}_0} \sec \theta dh = p q_1 E_{00}^2 \left(\frac{n}{N_0} \right) \quad 7.3a$$

where

$$q_1 = - \frac{2\pi \epsilon_0 \nu H}{\cos \theta} \quad b$$

The symbols are those used in section 3.4.

\underline{E}_0 consists of contributions from the incident and reflected pump waves and in the absence of absorption the resulting standing wave is (Das and Fejer, 1979),

$$E_0^2(h) = \frac{E_{00}^2}{2} (1 + p \sin 2k_0 h) \quad 7.3c$$

7.3a differs from 3.44b in that the $e^{-2\nu H/c}$ factor is assumed to be unity.

Inhester et al. (1981) have derived an expression for Q_{21} , the height integrated differential heating caused by interference between \underline{E}_1 and \underline{E}_2 . Q_{21} is given by (eq.3.50)

$$Q_{21} = 2\nu\epsilon_0 \int_{-\infty}^{\infty} \overline{\underline{E}_1 \cdot \underline{E}_2} \sec\theta dh = q_2 E_{00}^2 \left(\frac{n}{N_0}\right)^3 \quad 7.4a$$

where $q_2 = -\pi\omega\epsilon_0 H F(\underline{k}) / \cos\theta$ b

$$F(\underline{k}) = \frac{q\lambda_D^2 k^2}{(q\lambda_D^2 k^2)^2 + 4(\nu/\omega)^2} \quad c$$

Eq. 7.4c differs from 3.50 in that the terms involving Ω_e have been dropped since they do not quantitatively affect the results which follow. The result 7.4c is derived using the dispersion relation 3.33 for Langmuir waves.

Unlike Q_{10} , Q_{21} is dependent on k and does not require the presence of the reflected pump wave to produce a net heating effect. Inhester et al. (1981) assume that E_0^2 is independent of height over the resonance region. When anomalous absorption of the pump is included (as in section 7.4.10) this assumption is not valid.

The integrands in 7.3 and 7.4 are essentially resonance type functions. Thus the total differential heat input occurs in a small height range (see section 7.4.8 and appendix B). The heat balance equation for temperature deviations, T , from background electron temperature, T_{e0} , can be written (Vaskov and Gurevich, 1977; Gurevich, 1978)

$$\frac{3}{2} \frac{\partial}{\partial t} \left(\frac{T}{T_{e0}} \right) - 4.5 D_{||} \frac{\partial^2}{\partial \zeta^2} \left(\frac{T}{T_{e0}} \right) - 2.7 D_{\perp} \frac{\partial^2}{\partial \zeta^2} \left(\frac{T}{T_{e0}} \right) = \frac{Q}{N_0 T_{e0}} \delta(\zeta) \quad 7.5a$$

where ζ and ξ are respectively coordinates parallel and perpendicular to the geomagnetic field. $\delta(\zeta)$ is the Dirac delta function. The coefficient on the LHS of 7.5a are (Braginskii, 1965)

$$D_{\parallel} = \frac{T_{e0}}{0.51 m_e \nu} \quad , \quad D_{\perp} = \frac{T_{e0} \nu}{m_e \Omega_e^2} \quad 7.5b$$

They have typical values of (Table 7.1) $0.69 \times 10^8 \text{ m}^2 \text{ s}^{-1}$ and 0.16 respectively. The relationship between T and the plasma density perturbation n is derived from the diffusion equation (Eq. 3.6b). This can be approximated to (Inhester et al., 1981)

$$\frac{T}{T_{e0} + T_{i0}} = - \frac{n}{N_0} \quad 7.6$$

where T_{i0} is the background ion temperature.

Substituting 7.6 into 7.5a produces

$$\frac{3}{2} \frac{\partial n}{\partial t} - 4.5 D_{\parallel} \frac{\partial^2 n}{\partial \zeta^2} - 2.7 D_{\perp} \frac{\partial^2 n}{\partial \xi^2} = - \frac{Q}{T_{e0} + T_{i0}} \delta(\zeta) \quad 7.7$$

In deriving 7.7 it is assumed that ion transport can be neglected (Gurevich, 1978; Das and Fejer, 1979). Equations similar to 7.7 have been solved by Dysthe et al. (1983) for the case when Q is proportional to n i.e. for type I instabilities. In their

calculation it was assumed n and T were proportional to

$e^{ik\xi - k_{\parallel}|\zeta| + \gamma t}$. The appearance of $|\zeta|$ instead of ζ in the exponent

above reflects the fact that the perturbations are assumed to decrease symmetrically with a decrement k_{\parallel} away from a plane

perpendicular to the ζ axis through $\zeta = 0$. The delta function

in 7.7 maintains a discontinuity in the gradients of n and T

at $\zeta = 0$ (see fig. 7.8).

Eq. 7.7 can be solved when Q is a nonlinear function of n in a manner similar to that employed by Dysthe et al. (1983) if it is assumed that in general,

$$n(\xi, \zeta, t) = n(\zeta, t) e^{ik\xi} \quad 7.8a$$

where $n(\zeta, t) = n(0, t) e^{-k_{||}|\zeta|}$ b

Then, integrating 7.7 over ζ gives

$$q D_{||} k_{||} n(0, t) = - \frac{Q(n(0, t))}{T_{e0} + T_{i0}} \quad 7.9$$

Substituting for $\frac{\partial}{\partial \zeta} = -k_{||}$ into 7.7 now produces, for $\zeta \neq 0$,

$$\frac{\partial n(0, t)}{\partial t} - \frac{Q^2}{D_1 n(0, t)} + D_2 n(0, t) = 0 \quad 7.10a$$

where $D_1 = 27 D_{||} (T_{e0} + T_{i0})^2$ b

$$D_2 = 1.8 D_{\perp} k^2 \quad c$$

This equation for $n(0, t)$ forms the basis for the calculation of pump thresholds and instability growth rates.

7.4.2 Threshold and growth rates for type I instabilities

When the primary scattered wave alone is taken into account only a type I instability is present and $Q = Q_{10}$ is substituted into 7.10. This produces a linear differential equation which has a solution

$$n(0, t) = n(0, 0) e^{\gamma_1 t} \quad 7.11a$$

where $\gamma_1 = (q_1^2 E_0^4 / N_0^2 D_1) - D_2$ b

and $n(0,0)$ is the initial amplitude of FAI at the pump resonance height ($\zeta=0$) just before switching on the pump.

The threshold electric field, E_{t1} is obtained by setting σ_1 to zero, with $E_{t1} = E_0$ in 7.10. Then,

$$E_{t1}^2 = N_0 (D_1 D_2)^{\frac{1}{2}} / q_1 \quad 7.12a$$

Hanuse (private communication, 1983) reports backscatter at 14 MHz from FAI produced by the heater at Ramfjordmoen operating at 5.423 MHz on 20 October 1982. The irregularities which scatter 14 MHz radar waves have wavenumbers perpendicular to the magnetic field of 0.6 m^{-1} . This determines the corresponding value of D_2 from 7.10c. The corresponding value of E_{t1} with typical F region parameters (Table 7.1) a plasma scale height of 40 km and plasma density of $4.5 \times 10^{11} \text{ m}^{-3}$ is 0.4 Vm^{-1} . The estimated pump electric field when the Ramfjordmoen heater operates at full power is 0.75 Vm^{-1} if absorption and focussing effects are neglected (see chapters 2 and 4).

E_{t1} in 7.12a is independent of $n(0,0)$. This is characteristic of a linear instability, and implies that the instability can grow from an infinitesimally low background amplitude. When the threshold is greatly exceeded then the growth rate becomes

$$\sigma_1 = D_2 (E_0 / E_{t1})^4 \quad 7.12b$$

Relation 7.12a is essentially the result obtained by Das and Fejer (1979). σ_1 in 7.12b is in agreement with Dysthe et al.'s (1983) conclusion which is derived from a more rigorous calculation in which

the full diffusion and heat balance equations are solved simultaneously.

7.4.3 Type II instability threshold and growth rate

After substituting $Q=Q_{21}$ in eq. 7.10 a nonlinear equation for $n(0,t)$ is obtained as follows,

$$\frac{\partial n(0,t)}{\partial t} - \frac{q_2^2 E_0^4 n^5(0,t)}{D_1 N_0^6} + D_2 n(0,t) = 0 \quad 7.13$$

This has a solution of the form

$$n(0,t) = \frac{a}{\left(1 - \left(1 - \left(\frac{a}{n(0,0)}\right)^4\right) e^{bt}\right)^{1/4}} \quad 7.14a$$

where $a = (q_2^2 E_0^4 / N_0^6 D_2 D_1)^{-1/4}$ b

$b = 4D_2$ c

$n(0,t)$ in 7.14 increases with time if

$$n(0,0) > a$$

This condition results in a threshold electric field E_{t2} which is determined by substituting

$$\partial n(0,t)/\partial t = 0, \quad E_0 = E_{t2}$$

into 7.10. E_{t2} is then given by

$$E_{t2}^2 \cdot \frac{n^2(0,0)}{N_0^2} = \frac{N_0 (D_1 D_2)^{1/2}}{q_2} \quad 7.15$$

Equation 7.15 is characteristic of an explosive growth in $n(0,t)$ (Weiland and Wilhelmsson, 1977). Clearly $n(0,t)$ becomes infinite as $t \rightarrow t_\infty$ (see Fig. 7.9) where

$$t_\infty = \frac{1}{b} \ln\left(\frac{1}{1 - (a/n(0,0))^4}\right) \simeq \frac{1}{4D_2} \left(\frac{E_{t2}}{E_0}\right)^4 \quad 7.16$$

Fig.7.8 Schematic representation of variation of plasma density, n , of FAI along the magnetic field direction (ζ).

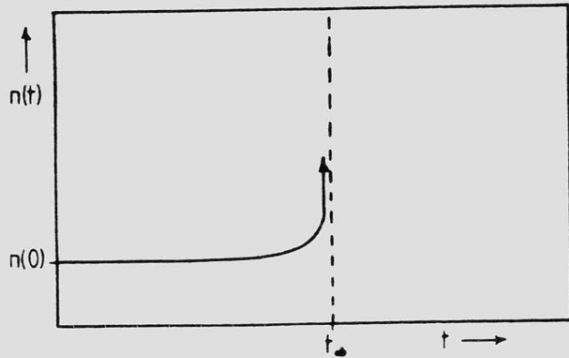
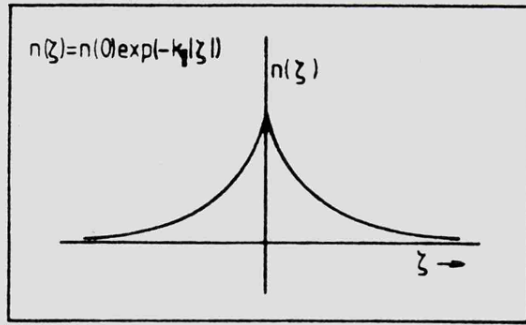


Fig.7.9 Schematic representation of explosive growth in n .

Fig.7.10 A graph of Z against X for different values of γ^2

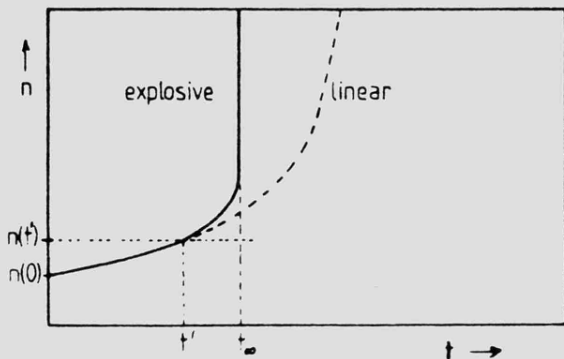
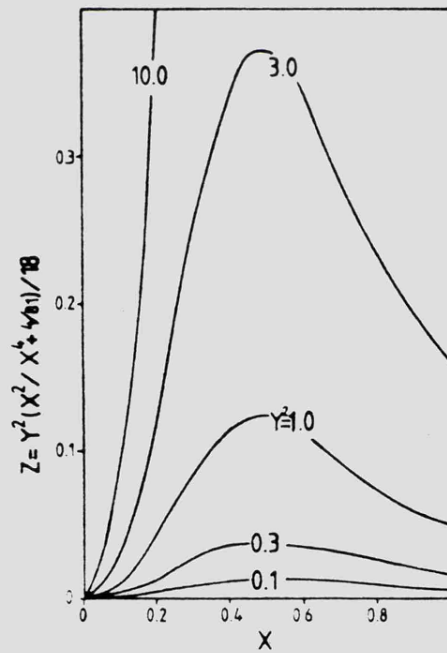


Fig.7.11 Schematic representation of growth in n under the influence of type I (linear) and type II (explosive) instabilities.

7.4.4 Comparison of type I and type II thresholds

The ratio of the threshold fields E_{t1}/E_{t2} of the two types of instabilities is (from 7.12a and 7.15)

$$(E_{t1}/E_{t2})^2 = \frac{1}{18p} \left(\frac{n(0,0)}{N_0} \right)^2 \cdot \frac{\omega}{\nu} \cdot \frac{\lambda_D^2 k^2}{(\lambda_D^2 k^2)^2 + (4/81)(\nu/\omega)^2} \quad 7.17$$

The ratio in 7.17 depends both on the initial FAI amplitude $n(0,0)$ and their wavenumber k perpendicular to the magnetic field.

Writing

$$(\lambda_D^2 k^2)/(\nu/\omega) = X^2 \quad , \quad (n/N_0)/(\nu/\omega) = Y \quad 7.18$$

7.17 becomes

$$(E_{t1}/E_{t2})^2 = \frac{1}{18p} Y^2 \frac{X^2}{X^4 + 4/81} = Z \quad 7.19$$

A graph of Z against X , with $p=1$, is plotted in fig. 7.10 for various values of Y^2 . It is clear from the graph that when

$$Y^2 < 1 \implies Z < 1$$

for all values of X . Thus, the type I instability is preferentially excited for all wavenumbers, under these circumstances. When

$Y^2 \gg 1$ i.e. when the initial FAI amplitudes are sufficiently large, Z can exceed 1 but only for a limited range of k values which satisfy

$$X \simeq 4/81$$

It is assumed in what follows that (unless otherwise stated) the threshold field for the type I instability is below that of the type II instability i.e.

$$E_{t1} < E_{t2}$$

When the condition above holds FAI grow in two stages,

Stage (1): When the pump threshold is exceeded a type I instability is excited and n grows from its initial value with the linear growth rate γ_1 (7.11).

Stage (2): When the FAI reaches an amplitude $n(0,t)$ such that

$$n(0,t) E_0 > n(0,0) E_{t2}$$

then a type II instability is excited and $n(0,t)$ continues to increase explosively until saturation occurs due to extinction of the pump. $n(0,t)$ as a function of time is illustrated in Fig. 7.11. FAI amplitude saturation constitutes a third stage in the evolution of the FAI and is dealt with in section 7.4.9.

It is possible that stage (2) will not occur if E_0 is only a little above E_{t1} so that $n(0,t)$ saturates at a value $n(0,\infty)$ such that

$$n(0,\infty) E_0 < n(0,0) E_{t2} .$$

When both types of instability are present the pump threshold field is somewhat below E_{t1} as will be demonstrated later.

7.4.5. Quasilinear growth rate of type II instability

The initial growth rate of the type II instability can be calculated from 7.14 and 7.15 with $E_0 \gg E_{t2}$.

In the limit $t \rightarrow 0$, then

$$\lim_{t \rightarrow 0} \frac{1}{n} \frac{\partial n(0,t)}{\partial t} = D_2 \left(\frac{E_0}{E_{t2}} \right)^4 = \gamma_{20} \quad 7.20$$

This quasi-linear growth rate, γ_{20} , is applicable to the initial growth of FAI for times which are short compared to t_{∞} in 7.16. Unstable growth over periods which are short compared with characteristic growth times will be discussed in more detail in the following chapter which is concerned with modulated heating.

When modulation frequencies are large compared with $\mathcal{T}_{i,2}$ in 7.11 and 7.20, the FAI growth and decay stages are quasi-linear. FAI decay has received little attention in the literature. It is therefore useful at this point to briefly outline how the decay rates can be calculated with the present model.

7.4.6 FAI decay rates

\mathcal{T}_- , the decay rate of FAI when the pump is switched off, can be defined

$$\mathcal{T}_- = \frac{1}{n(o,t)} \cdot \frac{\partial n(o,t)}{\partial t} \quad , \quad E_o = 0 \quad 7.21a$$

Setting E_o (and hence Q) to zero in equation 7.10 results in the following expression for \mathcal{T}_- ,

$$\mathcal{T}_- = -D_2 = -1.8 D_1 k^2 \quad 7.21b$$

This result is clearly independent of the instability which caused the FAI growth and is in agreement with the result stated by Gurevich (1978, p. 315).

Hedberg et al. (1982) have reported that time constants associated with the decay of radar backscatter cross-sections with heater switch-off depend on radar frequency. This is a consequence of the dependence of \mathcal{T}_- on k (in 7.21b). For $k = 0.6 \text{ m}^{-1}$ (14MHz radar), $\mathcal{T}_- \sim 0.1 \text{ s}^{-1}$ by 7.21b. This decay rate is consistent with the decay time of approximately 5 s reported by Hedberg et al. (1982) for 14MHz radar backscatter.

7.4.7. Saturation scale-lengths of FAI

When saturation occurs, $\partial n / \partial t$ is zero. This condition, substituted into 7.7 defines the value of $n(\zeta, t)$ at saturation, $n(\zeta, \infty)$.

Thus,

$$4.5 D_{\parallel} \frac{n(\zeta, \infty)}{L_{\parallel}^2} - 2.7 D_{\perp} \frac{(2\pi)^2}{L_{\perp}^2} n(\zeta, \infty) = 0 \quad 7.22$$

where $1/L_{\parallel} \equiv \partial/\partial \zeta$ and $2\pi/L_{\perp} = k$.

L_{\parallel} and L_{\perp} are respectively the parallel and perpendicular scale lengths of FAI. Then, from 7.22.

$$L_{\parallel} = \frac{1}{2\pi} \left(\frac{5}{3} \frac{D_{\parallel}}{D_{\perp}} \right)^{1/2} L_{\perp} = 0.29 \frac{\Omega_e}{\nu} L_{\perp} \quad 7.23$$

The relationship between L_{\parallel} and L_{\perp} at saturation is independent of both the growth mechanism and pump ERP. Typically, from 7.23 for $k \sim 0.6 \text{ m}^{-1}$, $L_{\parallel} \sim 43 \text{ km}$.

7.4.8 The effect of pump extinction on differential heating

When anomalous absorption of the pump wave is taken into account in the calculation of the differential heating then Q_{10} has the form, approximately (with $\cos \theta = 1, \zeta \equiv h$),

$$Q_{10} = 2\nu\epsilon_0 \int_{-\infty}^{\infty} (E_+ e^{-\int_{-\infty}^h f_{11} dh} + E_- e^{-\int_{-\infty}^h f_{11} dh})^2 f_{10} dh \quad 7.24a$$

E_+ and E_- are respectively the electric fields of the incident and reflected pump wave amplitudes related by

$$E_- = E_+ e^{-\int_{-\infty}^{\infty} f_{11} dh} = E_+ e^{-\tau/4} \quad 7.24b$$

$f_{11}(h)$ is the energy density profile of primary Langmuir waves generated by the EM pump by scattering from FAI and $f_{10}(h)$ is the energy density profile of the beat field of the pump and primary Langmuir waves (see appendix B for details). f_{10} and f_{11} have respectively the following form (Dysthe et al., 1983; Inhester et al., 1981)

$$f_{10}(h) \propto \frac{1}{D(\omega, k)} = \frac{h/H}{(h/H)^2 + (v/\omega)^2} \quad 7.25a$$

and

$$f_{11}(h) \propto \frac{1}{D^2(\omega, k)} = \frac{(h/H)^2}{[(h/H)^2 + (v/\omega)^2]^2} \quad 7.25b$$

where $D(\omega, k)$ is the Langmuir wave dispersion relation (eq. 3.33) in a linear electron density profile of the form,

$$\omega_e^2 = \omega^2 \left(1 + \frac{h}{H}\right) \quad 7.25c$$

Stubbe et al. (1982a) have estimated the effect of introducing the anomalous absorption of the pump itself into the calculation of the differential heating term Q_{10} in 7.3. These authors assume that the pump power is reduced by the factor $e^{-\Gamma}$ in twice traversing the region where FAI exist. The exponent Γ is assumed to be

$$\Gamma = 2\chi L \quad 7.26$$

where χ is a constant absorption coefficient and L is the thickness of the absorbing layer. This enables ρ in eq. 7.3 to be determined. With these assumptions, Stubbe et al. obtain the following for Q_{10} ,

$$Q_{10} = q_1 E_0^2 \frac{n}{N_0} \left(\sin \varphi e^{-\Gamma} - (1 - e^{-\Gamma})^2 / 2\pi \right) \quad 7.27$$

φ is the relative phase of the incident and reflected pump waves at the resonance height ($h = 0$). E_0 is now the pump electric field in the absence of anomalous absorption.

It is not easy to justify the assumption that the FAI excitation region (the width of f_{10}) is small compared with the pump anomalous absorption region (the width of f_{11}). The widths of the functions f_{10} and f_{11} in 7.24 are in fact comparable, that of f_{11} being somewhat smaller than that of f_{10} . Also, whereas the integral $\int_0^\infty f_{11}(h)dh$ converges, $\int_0^\infty f_{10}(h)dh$ does not.

The integral in 7.24 is difficult to evaluate exactly. An approximate analytical form can be obtained if it is assumed that the width of f_{11} is much smaller than that of f_{10} . Then, Q_{10} becomes (see appendix B)

$$Q_{10} = g_1 E_0^2 \frac{n}{N_0} C_1(\Gamma) \quad 7.28a$$

where
$$C_1(\Gamma) = e^{-\Gamma/2} \left(\sin \varphi - \left(\frac{\cosh(\Gamma/2) - 1}{\pi} \right) \ln a \right) \quad 7.28b$$

and
$$a = L_{\parallel} \omega / H\nu \quad 7.28c$$

L_{\parallel} is the scale length of FAI parallel to the magnetic field. It depends on Q_{10} when the FAI amplitudes are below their saturation value $n(\zeta, \omega)$. However, since $\ln a$ is an extremely weak function of L_{\parallel} and $C_1(\Gamma)$ is only important near $n(\zeta, t) \sim n(\zeta, \omega)$, the value of L_{\parallel} given by 7.23 may be employed in 7.28b.

A similar calculation can be performed to estimate the effect of pump extinction on the calculation to evaluate Q_{21} . Allowing for anomalous absorption of the pump, Q_{21} , is given by, approximately,

$$Q_{21} = 2\nu\epsilon_0 \int_{-\infty}^{\infty} \left(E_0 e^{-\int_0^h f_{11}(h)dh} \right)^2 f_{21}(h) dh \quad 7.29a$$

The function $f_{21}(h)$, which represents the energy density profile of the beat field between primary and secondary Langmuir waves, has the form (Inhester et al., 1981),

$$f_{21}(h) \propto \frac{1}{D^2(\omega, k) D(\omega, 2k)} = \frac{(h/H) + 12 \lambda_D^2 k^2}{((h/H) + 12 \lambda_D^2 k^2)^2 + (\nu/\omega)^2} \frac{1}{((h/H) + 3 \lambda_D^2 k^2)^2 + (\nu/\omega)^2} \quad 7.29b$$

The width of $f_{21}(h)$ is somewhat smaller than that of $f_{11}(h)$.

With the assumption that the width of $f_{21}(h)$ is very small compared with that of $f_{11}(h)$, 7.29a becomes (see Appendix B),

$$Q_{21} = q_2 E_0^2 \left(\frac{n}{N_0} \right)^3 C_2(\Gamma) \quad 7.30a$$

where $C_2(\Gamma) = e^{-\Gamma/4} \quad 7.30b$

7.4.9 Effect of pump extinction on FAI growth

In chapter 5, the anomalous absorption Γ of an EM wave due to scattering from FAI was evaluated in terms of the mean-square perturbation amplitude $\langle |n|^2 \rangle$ of the irregularities. Γ is given by (eq. 5.19),

$$\Gamma = \sigma \langle |n|^2 \rangle$$

where σ is a function of radio wave frequency and plasma density gradient.

This result takes into account only the scattering of the pump into primary Langmuir waves. When secondary scattering is taken into account, there is a further contribution to which is proportional to

$$\langle |n|^4 \rangle \quad . \quad \text{Inhester et al. (1981) have demonstrated that}$$

this contribution is smaller than that for primary scattering.

Consequently only the effect of primary scattering is included in the calculation of anomalous absorption at this stage. The effects of higher order scattering are discussed in section 7.4.11.

The negative feedback effect of anomalous pump wave absorption limits the growth of FAI and can eventually stabilize their amplitudes. In the present model, which assumes a monochromatic FAI spectrum, Γ can be written,

$$\Gamma(t) = \sigma n^2(0, t) \quad 7.31$$

In order to obtain a qualitative understanding of the effects of pump extinction each type of instability is initially investigated separately.

(i) Effect on type I instability:

Substituting 7.31 for Γ in 7.27 and then 7.27 in 7.10, the equation of FAI growth becomes

$$\frac{\partial n(0, t)}{\partial t} - \frac{q_1^2 E_0^4 n(0, t)}{N_0^2 D_1} C_1(n(0, t)) + D_2 n(0, t) = 0 \quad 7.32$$

Inspection of 7.32 reveals that n no longer increases without limit when E_0 exceeds the threshold field E_{t1} (eq. 7.12a). Rather, $n(0, t)$ approaches some asymptotic limit $n(0, \infty)$ when $\partial n(0, t)/\partial t$ approaches zero. 7.32 clearly must have at least two zeros when $\partial n(0, t)/\partial t = 0$. One corresponds to the threshold condition $E_0 = E_{t1}$ and the other to the saturation condition $n(0, t) = n(0, \infty)$. As $n(0, t)$ approaches $n(0, \infty)$ then $\Gamma(t)$ approaches a stable value, Γ_∞ . The saturation value of Γ is then given by

$$\left(\frac{E_0}{E_{t1}} \right)^2 C_1(\Gamma) - 1 = 0 \quad 7.33a$$

Since E_0^2 is proportional to the ERP (=PMW) of the transmitter, 7.33 can be transformed into a relationship for the pump and pump threshold powers, P and P_1 . Then,

$$\frac{P}{P_1} \cdot G_1(\Gamma) - 1 = 0 \quad 7.33b$$

A graph of Γ against P has the characteristics illustrated in fig. 7.12. For pump powers well above threshold, Γ becomes independent of P and has the value of approximately 7.3 dB when $\sin \varphi = 1$ and $a = L_{||} \omega / H\nu = 6.7 \cdot 10^4$ (typical values) Stubbe et al. (1982a) obtained an upper limit for Γ of 18dB from 7.27.

(ii) Effect on type II instabilities

When pump extinction effects are included in type II instabilities, the modified diffusion equation 7.10 becomes

$$\frac{1}{D_2} \frac{\partial n(0,t)}{\partial t} - \left(\frac{E_0}{E_{t2}}\right)^4 \frac{n^5(0,t)}{n^4(0,0)} + n(0,t) = 0 \quad 7.34$$

As in the previous case, $n(0,t)$ no longer increases without bound when $E_0 > E_{t2}$ but stabilizes at some finite value (see fig. 7.13). The saturation absorption level Γ in this case is given by

$$\left(\frac{E_0}{E_{t2}}\right)^4 e^{-(\Gamma - \Gamma_0)/2} \cdot \left(\frac{\Gamma}{\Gamma_0}\right)^2 = 1 \quad 7.35a$$

where

$$\Gamma_0 = \sigma n^2(0,0) \ll 1.$$

In terms of pump ERP, P , 7.35a becomes

$$\left(\frac{P \cdot \Gamma}{P_2 \cdot \Gamma_0}\right)^2 e^{-(\Gamma - \Gamma_0)/2} = 1 \quad 7.35b$$

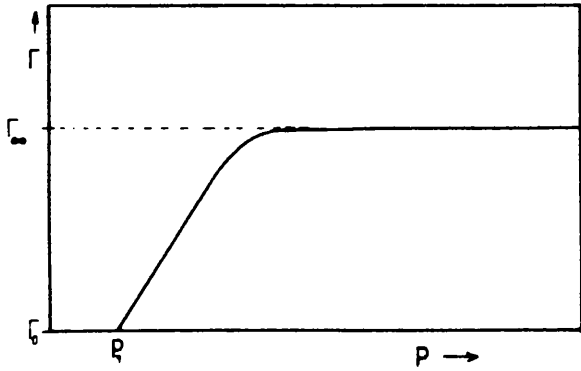


Fig.7.12 Schematic representation of anomalous absorption at Γ_0 for large pump powers for type I instabilities alone.

Fig.7.13 Time variation of n when a type II instability is stabilized by pump self absorption.

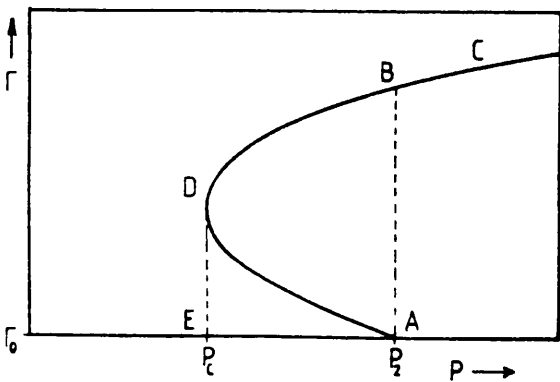
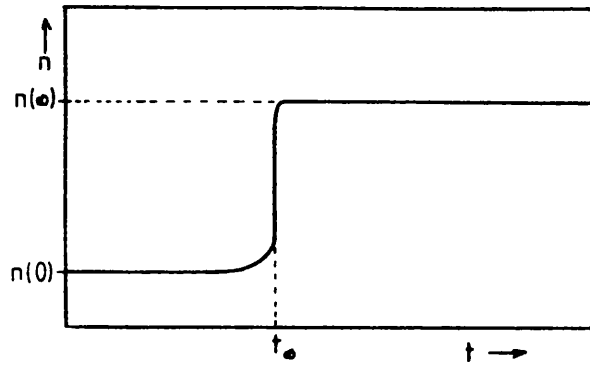


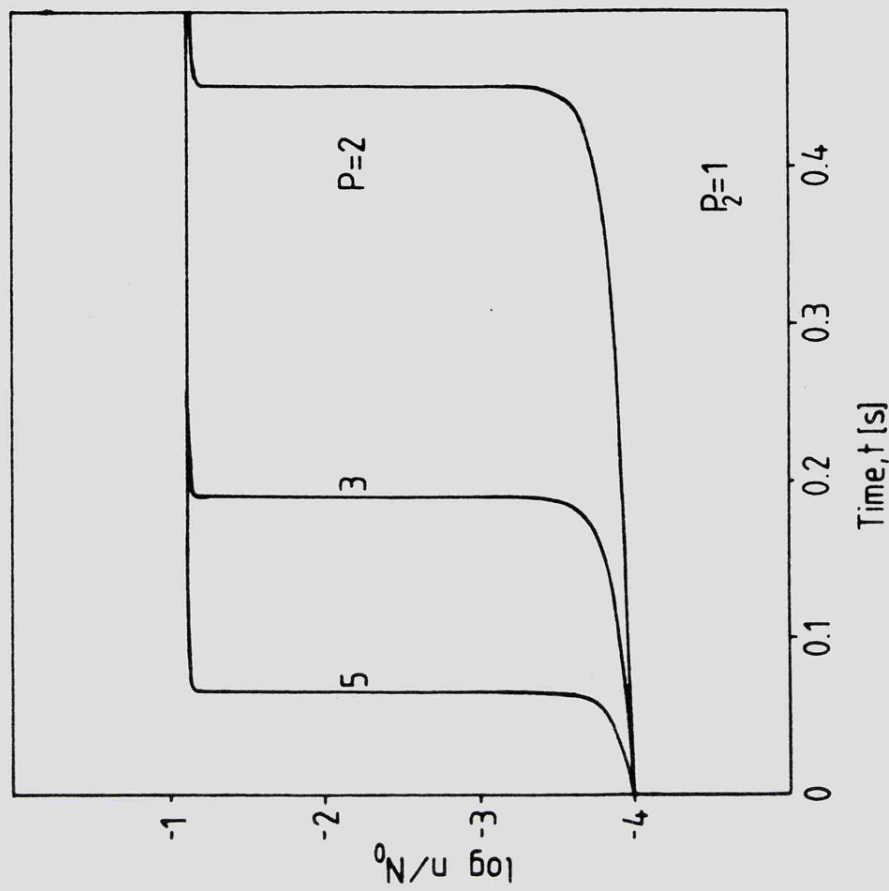
Fig.7.14 A schematic representation of the hysteresis effect in anomalous absorption. A sudden growth in Γ occurs when P exceeds P_2 . On lowering P , the value of Γ does not drop significantly until P reaches P_0 ($\ll P_2$).

where P_2 is the pump threshold power for the type II instability. The Γ vs P curve in Fig. 7.14 (solid line) is a double valued function between $P_c < P < P_2$. Such curves give rise to so called 'jump phenomena' commonly found in solutions to nonlinear differential equations such as the well known Duffing equation (Nayfeh and Mook, 1979). If P is gradually increased from 0, Γ is unaffected until $P = P_2$ (Point A). An increase in P beyond this point precipitates an explosive growth in n and Γ . The values of n and Γ then stabilize at point B. Further increases in P cause relatively small increases in n and Γ up to point C. On decreasing the pump power P the value of Γ follows the curve from C through B to D. Decreasing P below P_c causes the FAI to collapse to their original amplitudes (point E). The cycle ABCDE constitutes a hysteresis loop. P_c can be considerably below P_2 .

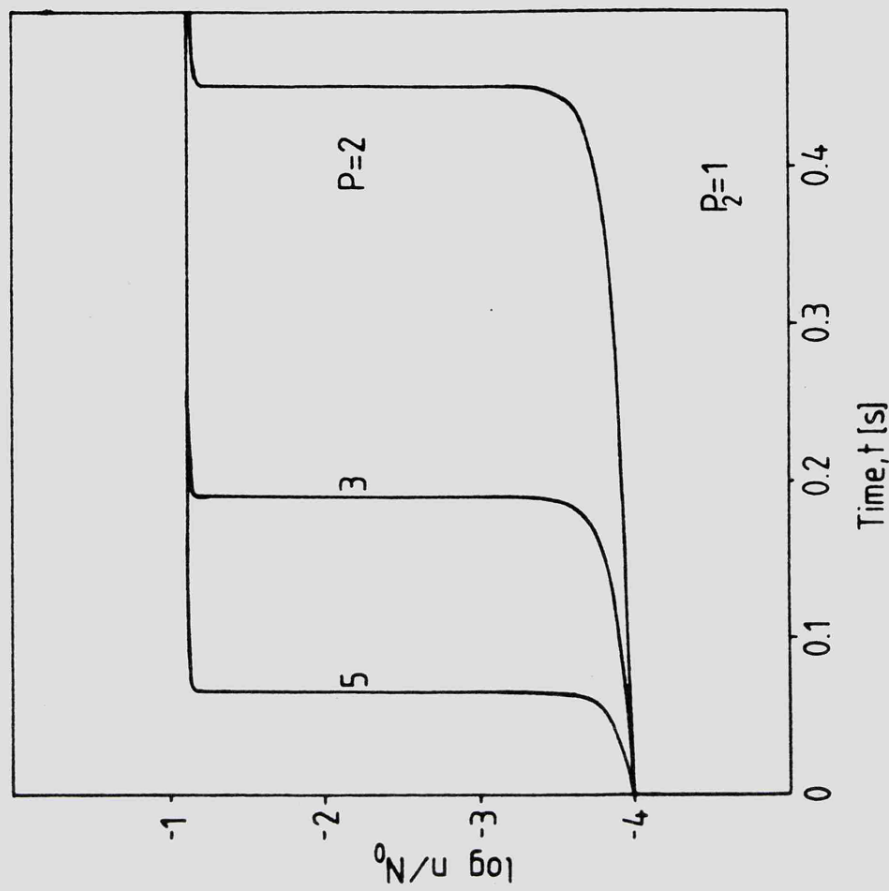
So far the two instability types have been treated separately in order to obtain a qualitative understanding of how pump extinction affects each growth mechanism. A semi-quantitative description of the excitation, growth and stabilization of FAI is obtained by solving the differential equation for the FAI amplitude, $n(0,t)$ with the expression 7.28a and 7.30a for the differential heating terms Q_{10} and Q_{21} substituted into 7.10. This equation then becomes

$$\frac{1}{D_2} \frac{\partial n(0,t)}{\partial t} + n(0,t) - n(0,t) P^2 \left(\frac{n(0,t)}{n(0,0)} \right)^2 \frac{e^{-\frac{\sigma}{4}(n^2(0,t) - n^2(0,0))}}{P_2} + e^{-\frac{\sigma}{2} n^2(0,t)} \left(\frac{1 - (\cosh(\Gamma/2) - 1) \ln a / \pi}{P_1} \right)^2 = 0 \quad 7.36$$

Equation 7.36 can be numerically integrated to obtain $n(0,t)$ as a function of time. This has been done for several values of $n(0,0)$, P and P_2 ; with $D_2 = 0.1$ and $a = 6.7 \cdot 10^4$. Fig. 7.15a-c illustrates solutions of 7.36 for $n(0,t)$, for type I

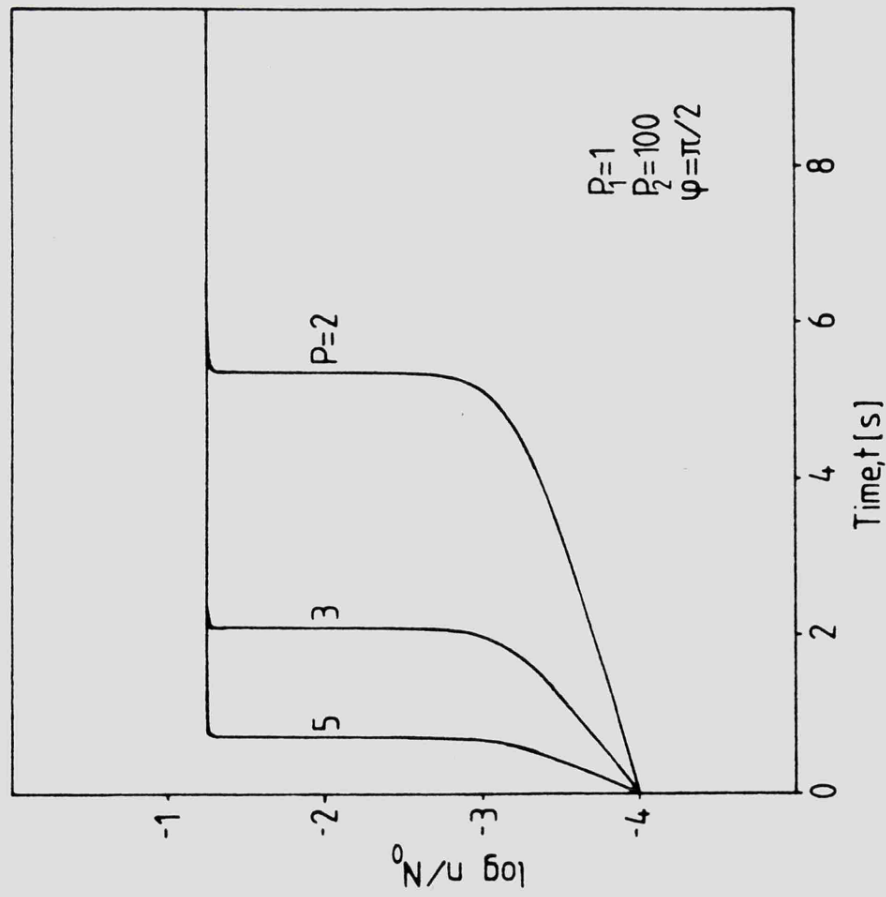


a.

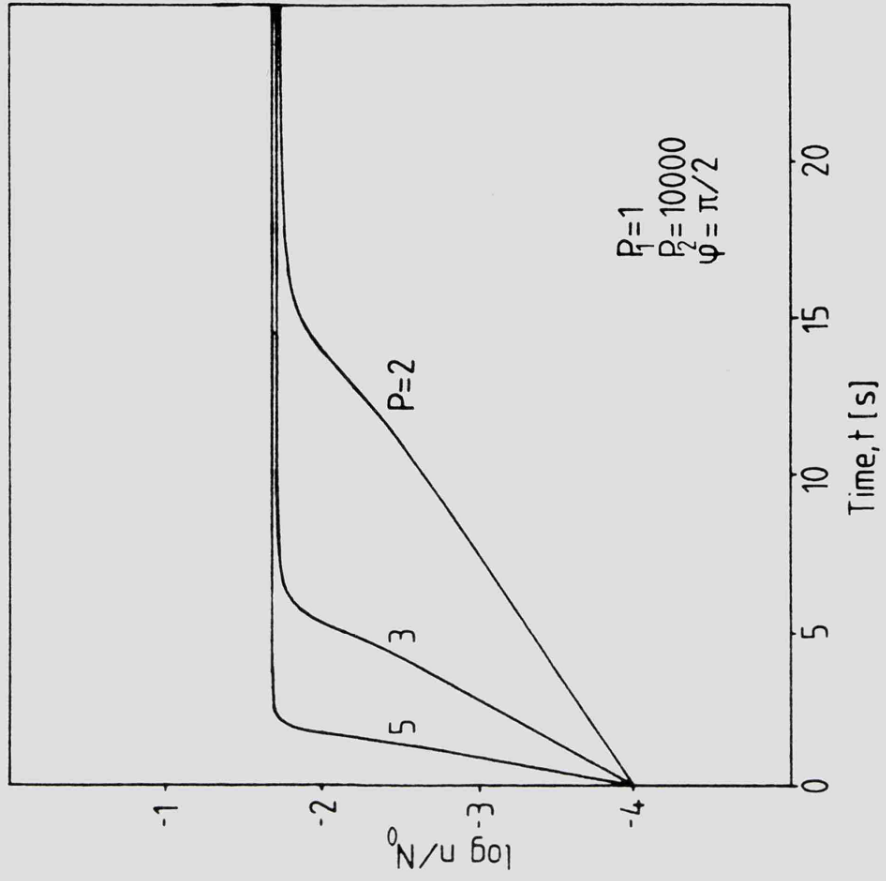


b.

Fig. 7.15 a, b Graphs of $\log n/N_0$ vs time. Each panel contains three curves corresponding to different values of pump power P . The curves are calculated by solving equation 7.36 numerically. (a) depicts a type I instability above ($P_2 = \infty$) and (b) depicts a type II instability above ($P_1 = \infty$).



c.



d.

Fig.7.15 c,d As fig.7.15 a,b but with both type I and type II instabilities present simultaneously. (c) depicts the case when the type II instability is strongly excited while in (d) and the type II instability is only weakly excited.

(7.15a), type II (7.15b) and type I and II combined (7.15c). These figures are typical examples of the behaviour obtained for a wide range of pump and threshold field parameters.

A typical solution of 7.36 for $n(0, t)$ consists of three stages, the first is quasilinear growth which is initially due to the type I instability but subsequently is dominated by the type II instability. During the second stage the growth rate becomes infinite (explosive growth) due to the presence of the type II instability. The final stage consists of stabilization of the value of $n(0, t)$ due to pump extinction. This latter effect occurs when $n(0, t)$ is very close to its saturation value, $n(0, \infty)$, as indicated by the sudden change from $\frac{\partial n}{\partial t} \rightarrow \infty$ to $\frac{\partial n}{\partial t} \rightarrow 0$ at a value of $n(0, t)$ just below $n(0, \infty)$. The type II instability dominates over the type I instability as soon as $n^2(0, 0) P_2 \simeq n^2(0, t) P_1$. Thus only when $P_2 \gg P_1$ does the type I instability dominate the growth stages of n . Then the explosive growth stage is absent. Such an example is indicated in fig. 7.15d when $P_2/P_1 = 10^4$. The graphs all illustrate the insensitivity of the saturation amplitude to pump power P . However the growth time does strongly depend on P ranging from ~ 100 s when P just exceeds P_1 to much less than 0.1s when P greatly exceeds P_2 . The effect of the presence of both type I and II differential heating Q_{10} and Q_{21} simultaneously on the saturation amplitude of the FAI is determined by applying the condition $\partial n/\partial t = 0$ to equation 7.36. The result is

$$P \left\{ \frac{\Gamma \cdot e^{(\Gamma_0 - \Gamma)/4}}{\Gamma_0 \cdot P_2} + e^{-\Gamma/2} \left(\frac{1 - (\cosh(\Gamma/2) - 1)(na)/\pi}{P_1} \right) \right\} = 1 \quad 7.37$$

Theoretical curves derived from 7.37 illustrating the variation of the

saturation level of anomalous absorption Γ with pump power P for various values of threshold powers P_1 and P_2 and initial values of Γ , $\Gamma_0 (= \sigma n^2(0,0))$ are illustrated in fig. 7.16 a-c. σ/N_0^2 determined theoretically in chapter 5 is approximately 10^4 m^6 . giving a value of $\Gamma = 1 \text{ Neper}$ ($\equiv 4.3 \text{ dB}$) when $(n/N_0) = 0.01$ (see fig. 5.13). A value of $(\ln a)/\pi = 3.5$ (implying $a = 6.7 \times 10^4$) has been assumed throughout. In the cases depicted in the graphs (fig. 7.16 a-c), P_1 is always less than P_2 . In cases where P_2 is less than P_1 the type I instability has no effect on the growth and saturation process.

In fig. 7.16a, three curves are plotted. Two (dashed) curves correspond to the cases when the two instabilities operate alone. The third (solid) curve depicts the case when both instabilities are operating together. The respective threshold powers P_1 and P_2 of the type I and type II instabilities are taken to be 0 dB and 10dB relative to some arbitrary power level. No hysteresis effect occurs when the type I instability operates alone even though FAI are excited when the pump power exceeds 0dB. When the pump power, P exceeds P_2 by more than 10dB anomalous absorption becomes independent of P and stabilizes at **1.7** Nepers ($\equiv 7.3 \text{ dB}$). The anomalous absorption level corresponds to a FAI amplitude n/N_0 of 0.013.

When the type II instability operates alone FAI are excited when the pump power exceeds 10dB. Γ increases from its initial value of 10^{-3} ($\equiv n/N_0 = 0.00035$) to a value of 44 Nepers ($n/N_0 = 0.066$). Increasing P to 10dB above threshold increases Γ to 53 Nepers ($n/N_0 = 0.073$). Γ continues to increase for increasing P . On reducing P , the hysteresis effect is apparent. The FAI do not collapse until P falls to approximately 32dB below the threshold power.

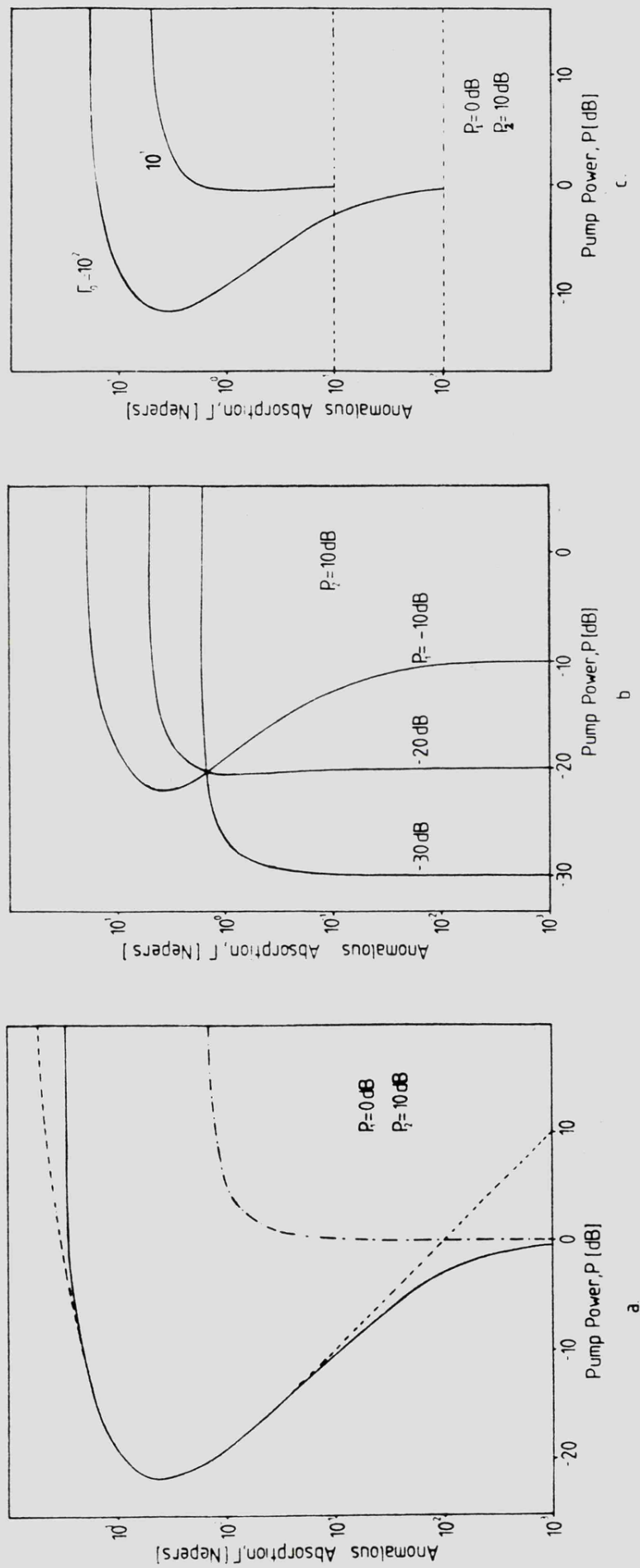


Fig. 7.16 Theoretical curves illustrating the variation of anomalous absorption, Γ , after FAI stabilization as a function of pump power, P . The effect of combining a type I instability (chain line) and a type II instability (dashed line) is illustrated in (a). (b) illustrates the effect of varying the difference in P_1 and P_2 ($P_2 > P_1$) and (c) illustrates the effect of altering the initial level of anomalous absorption, Γ_0 .

The effect of introducing a type I instability in combination with the type II instability has essentially three effects.

(a) The effective threshold power P_t is reduced to

$$P_t = \frac{P_1 \cdot P_2}{P_1 + P_2} \implies P_t < P_{1,2} \quad 7.38$$

(b) Once excited, the saturation amplitude of FAI is between the values which are found when each instability type operates alone. However Γ (and N/N_0) does not increase appreciably above its value at $P = P_t$ when P increases above P_t , and the FAI amplitude becomes effectively independent of P . Γ asymptotically approaches a value of 29 Nepers ($N/N_0 = 0.054$), as $P \rightarrow \infty$.

(c) Hysteresis occurs in the same manner as when the type II instability operates alone. However when the type I instability is also present the FAI collapse when P is reduced to 22dB below threshold. Thus the presence of the type I instability has the effect of reducing the range of values of P over which the hysteresis cycle is observed. Graphs 7.16 b and c illustrate the effects of changing respectively (i) the relative threshold powers of the two instabilities,

(ii) the initial FAI amplitude, with the following results:

As P_1 is reduced the range of pump power over which the hysteresis effect is observed is reduced. The actual pump power P_c at which the FAI collapse when pump power is being reduced is largely independent of P_1 . If P_1 is below P_c the hysteresis effect disappears (fig. 7.16b). The effect of increasing the initial FAI amplitude while maintaining P_1 and P_2 constant reduces both P_c and the saturation amplitude of the FAI (see Fig. 7.16c).

For given ionospheric conditions, the product $P_2 \cdot n^2(0,0)$ (or equivalently $P_2 \cdot f_o$) is constant since the threshold electric field

measured in the F-region, E_{t2} from (7.15) is given by

$$P_2 n^2(0,0) \propto E_{t2}^2 n^2(0,0) = N_0^3 (D_1 D_2)^{1/2} / q_2$$

where N_0 is the bulk plasma density, D_1 and D_2 are related to the plasma thermal conductivity (7.10) and q_2 is a constant of proportionality in the relationship between differential heat input to the FAI and the pump electric field squared (7.4b).

The values of $P_t - P_c$ and $\frac{n(0,\infty)}{N_0}$ derived from figs. 7.16 which characterise the hysteresis effect are listed in table 7.2 for different values of $(P_2 - P_1)$ and $n(0,0)/N_0$.

7.4.10 Effects of ionospheric variability on FAI growth and saturation

Stubbe et al. (1982a) have explained how the Das and Fejer (type I) mechanism of FAI excitation is affected by the variability of the F-region plasma. The high sensitivity of this mechanism to small changes in plasma density can be accounted for as follows:

If the electric field strength of the combined incident and reflected waves, at the upper hybrid resonance point, is an increasing function of altitude, FAI growth occurs (Das and Fejer, 1979). The electric field strength depends on the relative phase of the incident and reflected waves. Equations 7.27 and 7.28 indicate that φ need only change from $+\pi/2$ to $-\pi/2$ for strong FAI growth to become strong damping. This requires a change of only one quarter of a wavelength in the phase path between the upper hybrid resonance and the reflection point of the pump.

The time constant associated with changes in φ is τ_φ .

If

$$\tau_\varphi \cdot \gamma_1 \ll 1$$

7.39

where γ_1 , is the FAI growth rate due to the type I instability

n_0/N_0	$P_2 - P_1$ [dB]	P_t [dB]	$P_t - P_c$ [dB]	n_∞/N_0
$3.5 \cdot 10^{-4}$	10	-0.5	22	$5.4 \cdot 10^{-2}$
$3.5 \cdot 10^{-4}$	20	-10	12	$4.4 \cdot 10^{-2}$
$3.5 \cdot 10^{-4}$	30	-20	-	$2.3 \cdot 10^{-2}$
$3.5 \cdot 10^{-4}$	40	-30	-	$1.3 \cdot 10^{-2}$
$1.0 \cdot 10^{-4}$	10	-0.5	12	$4.4 \cdot 10^{-2}$
$3.5 \cdot 10^{-3}$	10	-0.5	2	$2.3 \cdot 10^{-2}$

Table 7.2 Summary of the main features of graphs 7.16 a-c. n_0/N_0 is the initial FAI amplitude (relative to background plasma density), $P_2 - P_1$ represents the difference (in dB) between the type II and type I thresholds, P_t is the effective threshold, $P_t - P_c$ represents the size of the hysteresis effect, being the difference (in dB) between the onset of high anomalous absorption (at P_t) when P is increasing and the cutoff (at P_c) when P is decreasing (see fig.7.14 for schematic representation). n_∞/N_0 is the FAI amplitude obtained when P greatly exceeds the threshold P_t .

(eq. 7.11), then the FAI do not grow to the saturation level derived in Section 7.4.9. Stubbe et al (1982a) assume that

$$\gamma_1 \propto \left(\frac{P}{P_1} - 1\right) \quad 7.40$$

However, it has been demonstrated that for the present model

$$\gamma_1 = D_2 \left(\frac{P^2}{P_1^2} - 1\right) \quad 7.41$$

which is in agreement with the result of Dysthe et al. (1983).

Under condition 7.39 the FAI amplitude, \bar{n} averaged over times which are long compared with τ_φ is given approximately by (Stubbe et al. 1982a).

$$\bar{n} = n_0 e^{D_2 (P^2/P_1^2 - 1) \tau_\varphi} \quad 7.42$$

and the corresponding anomalous absorption value $\bar{\Gamma}$ is

$$\bar{\Gamma} = \Gamma_0 e^{2D_2 (P^2/P_1^2 - 1) \tau_\varphi} \quad 7.43$$

γ_1 is an increasing function of P . As P is increased, a point is reached when

$$\tau_\varphi \gamma_1 > 1$$

is satisfied, then FAI growth is unaffected by ionospheric variability and FAI amplitudes are once more stabilized by pump self extinction. The dependence of the saturation level of anomalous absorption $\bar{\Gamma}$ on pump power P when ionospheric variability

is high (i.e. when condition 7.39 is satisfied) is illustrated schematically in fig. 7.17 for several values of τ_{φ} . When $\tau_{\varphi} \rightarrow \infty$ the Γ vs P curve is the same as that in fig. 7.12.

The type II instability of Inhester et al. (1981) produces a net differential heating effect without the presence of a reflected pump wave. The type of ionospheric variability which produces only small phase path changes therefore has no effect on the type II instability. In order for F region plasma density changes to affect the growth of striations by the type II mechanism, the upper hybrid resonance point would have to move vertically by a distance comparable with L , the vertical extent of the FAI, i.e. by several tens of kilometers. This is in strong contrast to the phase changes of a few metres required to change the phase of the reflected pump wave and so destroy the heating effect of the type I instability.

If however F-region plasma changes cause rapid variation in the pump electric field due to focussing and defocussing, then the type II instability growth could still be limited by the variable nature of ionosphere. When the type II threshold is only marginally exceeded, so that the type II growth rate τ_2 is small compared to the fluctuation rate $\frac{1}{\tau_E} \left(= \frac{1}{E_0} \frac{\partial E_0}{\partial t} \right)$ of the pump electric field E_0 , then FAI growth is quasi-linear for periods longer than τ_E . Under these circumstances the quasi-stationary value of the FAI amplitude would be, by analogy with 7.42,

$$\bar{n} = n_0 e^{D_2 (P^2/P_2^2 - 1) \tau_E} \quad 7.44$$

Large variations in D region absorption could cause the pump electric

Fig.7.17 Schematic representation of the effect of ionospheric variability time constants, τ_{φ} on the saturation of type I instabilities. The solid line represents a quiet ionosphere.

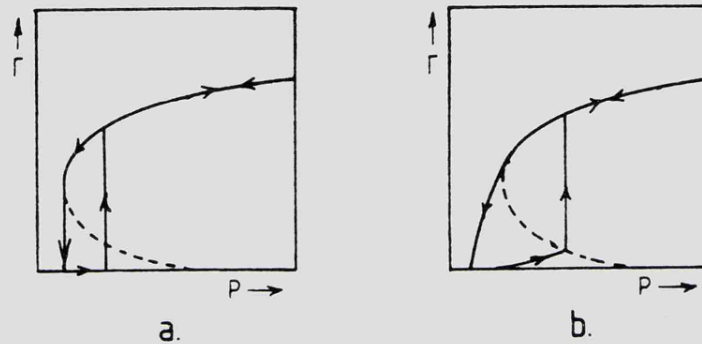
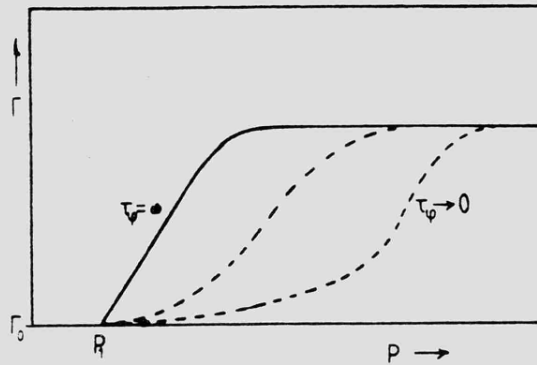


Fig.7.18 Schematic representation of the hysteresis effect in a quiet (a) and variable (b) ionosphere.

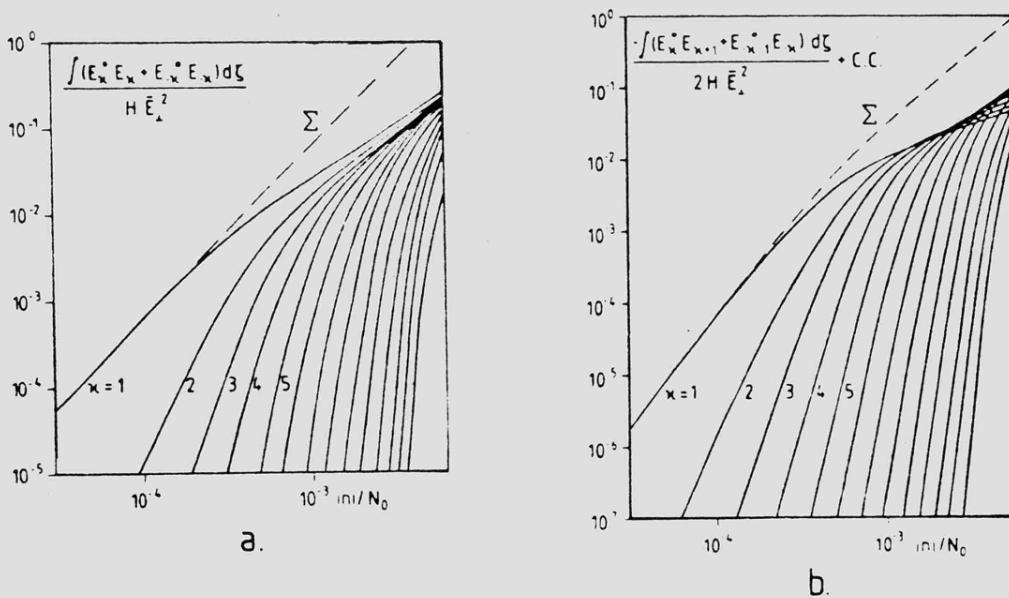


Fig.7.19 The effect of multiple scattering on anomalous absorption (a) and differential heating (b). Each curve represents the contributions of an order of scattering to the heating process. Σ represents the sum in each case (from Inhester et al., 1981).

field to vary and lead to a limitation of type II instability growth similar to that produced by rapid focussing and defocussing. However it is difficult to envisage a mechanism which could produce large fluctuations in D-region absorption on short time scales under the geomagnetically quiet conditions prevailing during the heating experiments. The pump wave itself could of course change the D-region characteristics during the period of heating, but this would have only a transient effect on the pump intensity immediately after pump switch-on and switch-off. The character of the hysteresis effect in anomalous absorption presented in the previous section is altered when ionospheric variability influences the growth of type I instabilities. Increased ionospheric variability has the effect of suppressing FAI growth and making FAI amplitudes highly dependent on pump power, P . Thus, the onset of the type II instability stage occurs at higher pump powers. This has the effect of increasing the range of values of P over which hysteresis occurs. The effect of ionospheric variability on hysteresis is difficult to assess quantitatively. A qualitative comparison of hysteresis curves under quiet and variable ionospheric conditions is depicted in fig. 7.18 a and b.

7.4.11 Effects of higher order scattering from FAI

In the present model scattering from FAI up to second order has been included. Inhester et al. (1981) have demonstrated that when the relative FAI amplitude n/N_o exceeds approximately 10^{-3} , the contribution of higher order scattering to differential heating is comparable with that of primary and secondary scattering. The higher order terms also contribute to anomalous absorption but never exceed the first order term (see Fig. 7.19).

Inhester et al. (1981) also noted that when multiple scattering occurs, and n/N_0 exceeds 10^{-3} , differential heating and anomalous absorption cannot be expressed as a linear superposition of the contribution of each order of scattering. By a numerical analysis these authors have demonstrated that the combined effect of the multiple scattering processes lead to differential heating and anomalous absorption which are both proportional to $(n/N_0)^2$. Thus, anomalous absorption during multiple scattering has the same dependence on n/N_0 , as first order scattering. However, the nonlinearity in the differential heating term which is third order when only the primary and secondary Langmuir waves are included is reduced by one order during multiple scattering. This reduces the efficiency of the explosive growth of FAI irregularities without reducing the effectiveness of pump self extinction. As a result, the saturation level of FAI amplitudes would be smaller than predicted by the present model.

7.4.12 Summary of FAI growth, saturation and decay model

Three mechanisms are involved in FAI growth and saturation:

- (I) Type I instability has a pump threshold P_1 , which is independent of initial FAI amplitudes and a linear growth rate. If the pump power exceeds P_1 FAI can grow from an infinitesimally small background level.
- (II) The FAI amplitude is increased by the type I instability to a level at which the type II instability threshold is exceeded. The type II then causes explosive growth of the FAI.
- (III) When the FAI amplitude reaches a certain value self-anomalous absorption of the pump reduces the effective

power of the pump. The heating due to the pump becomes equal to energy dissipation and growth of FAI is terminated.

The presence of a type II instability gives rise to a hysteresis effect in anomalous absorption when the pump power is steadily increased from zero to full power and then reduced to zero again. The presence of type I instability sets an upper limit to the FAI amplitude.

The effect of ionospheric variability is to increase the dependence of the amplitude of FAI which grow by type I instabilities on pump power.

7.5 Comparison of Model Results with Observations

7.5.1 The Hysteresis effect

The model of FAI excitation, saturation and decay outlined in the previous section qualitatively explains the nonlinear character of the reflectivity of the lower F-region in the presence of a high power E-M pump wave. The relationship between pump power P and anomalous absorption Γ is a double valued function for values of P given by

$$P_c < P < P_t$$

where P_c is some lower cutoff power and P_t is the initial threshold power for FAI growth. The theoretical Γ vs P curves exhibit the so called 'jump phenomenon' which constitutes the hysteresis effect (see fig. 7.14).

Depending on the initial FAI amplitude and relative threshold powers of the type I and type II instabilities, the model predicts saturation FAI amplitudes of between approximately 1-7% of the mean background plasma densities. Higher FAI saturation amplitudes correspond to lower initial FAI amplitudes. For typical values of

relative threshold powers of type I and type II instabilities, the power at which the FAI collapse, P_c predicted by the model is typically 10 to 30 dB below the pump threshold power P_t (see table 7.2).

The predicted values of saturation FAI amplitude are consistent with those determined experimentally from anomalous absorption measurements (chapter 5). The pump threshold power P_t and cutoff power P_c are difficult to observe experimentally. There certainly appear to be no sudden increases in anomalous absorption at pump powers which would correspond to explosive growth at the instability threshold. Similarly no sudden decreases in anomalous absorption are noted. In all the observed cases of hysteresis reported in section 7.2, the Γ vs P hysteresis curves have fairly uniform gradients over a wide range of pump powers. This may be due to the following causes:

- a) The pump electric field is not uniform in space. This is because the pump beam itself is not homogeneous and medium scale inhomogeneities in the F-region plasma can cause local focussing and defocussing of the pump beam. As a result, the instability threshold may only initially be satisfied at a number of points in the pump beam. As the pump power is increased, the instability threshold power is exceeded over an increasingly large volume of plasma. Thus, there is no sudden explosive growth of FAI throughout the region of ionospheric plasma illuminated by the beam.
- b) A possible factor which contributes to the ill defined position of pump threshold and cutoff is the effect of ionospheric variability. In principle it is possible that the onset of the two types of instability, although temporally separated, may occur at the same ERP. This would be likely if the striation growth due to the type I instability were to have a high saturation amplitude so that the type 2 instability threshold was immediately exceeded. This could

be the case in a quiet ionosphere. However, as was argued in section 7.4.10, in a time varying ionosphere, the saturation level of the striation amplitude is greatly reduced and is highly power dependent. In this case a further rise in ERP may be required before the threshold of the type 2 instability was exceeded. This effect of separating in power the two instability thresholds is illustrated in fig. 7.18 a, b.

The absence of any noticeable hysteresis effect during cycle d (fig. 7.2) suggests that the threshold of the type 2 instability was exceeded during the first step in ERP from 0-6.5 MW. The reduction in threshold power required could be a consequence of either changes in the variability of the ionosphere or of the influence of previous heating cycles in creating a residue of relatively large amplitude striations, amounting to a pre-conditioning of the ionosphere. Comparison of the ionogram taken during the experiment, with those taken before and after, indicate that the F-region critical frequency fell from 9.3 MHz at 1408 UT to 8.3 MHz at 1533 UT with a further drop to 6.5 MHz by 1636 UT. It is concluded therefore, that the changes observed in the variation of the received pump signal during the experiment were due to natural changes in the ionosphere.

7.5.2 Explanation of the 'overshoot' effect

During three of the four heating cycles presented in section 7.2 the reflected pump signal exhibited an overshoot effect during the stage when the effective radiation power (ERP) of the pump was increasing. The overshoot (features (ii) and (iii) in section 7.2) is characterized by a local maximum in received pump power at a value of ERP well below full power.

The overshoot effect is illustrated schematically in fig. 7.20

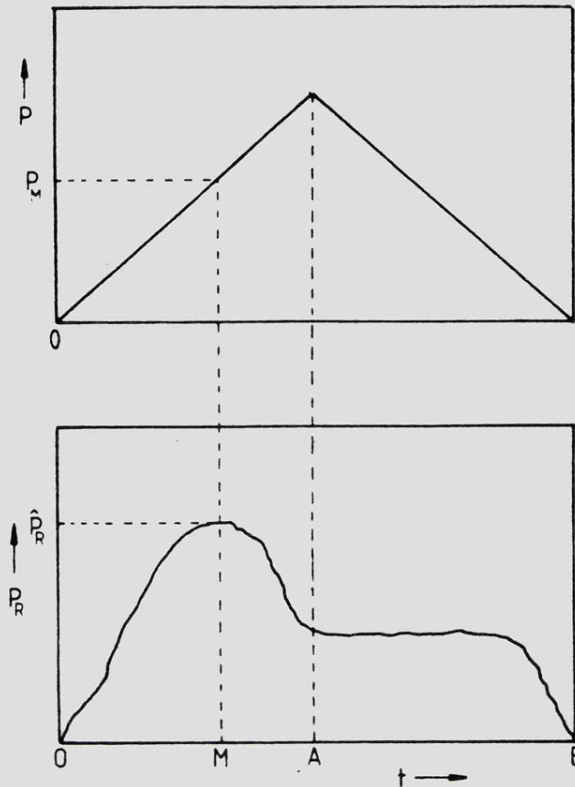


Fig.7.20 A schematic representation of the overshoot effect. A local maximum in the pump reflected power, P_R occurs at a transmitter power $P = P_M$ which is well below the maximum power available. As P is increased beyond P_M , P_R starts to decrease.

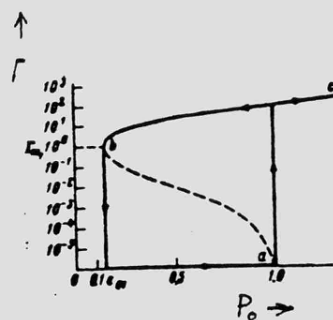


Fig.7.21 The hysteresis curve for absorption coefficient Γ vs. normalized pump power, P_0 calculated by Grach et al. (1979) from equation 7.49.

By analogy with fig. 7.1, time runs along the axis OB. Between O and A, pump transmitted power P in fractions of full power is proportional to time so OA can be regarded as the linear P axis. Between A and B, P decreases linearly from full power (at A) to zero (at B). P_R is the received pump power measured in dB above an arbitrary voltage. If V_R is the measured voltage of the received pump signal and V_0 some reference voltage then

$$P_R = 10 \log (V_R/V_0)^2 \quad 7.45a$$

and

$$P_T = 10 \log (P/P_0) \quad b$$

where P_0 is an arbitrary pump power level, and P_T is the pump power measured in dB above P_0 . Substituting 7.45b into 7.1 gives

$$\Gamma = 10 \log (P/P_0) - P_R \quad 7.46$$

Between points O and P_M on the P axis (fig. 7.20) P_R is an increasing function of P , i.e. $\partial P_R / \partial P > 0$. At $P = P_M$, $\partial P_R / \partial P$ becomes equal to zero. When $P > P_M$, $\partial P_R / \partial P$ becomes negative. Thus, a local maximum in P_R occurs below $P = \text{Full Power}$, if the condition

$$\partial P_R / \partial P < 0 \quad 7.47$$

can be satisfied in the range $0 \leq P \leq \text{Full Power}$. Differentiating 7.46 with respect to P and expressing 7.47 in terms of $\partial \Gamma / \partial P$ produces the condition

$$P \frac{\partial \Gamma}{\partial P} > 10 \log e \approx 4.3 \quad 7.48$$

This relationship demonstrates that the overshoot effect is a consequence

of Γ being an increasing function of P . As long as the gradient $\partial\Gamma/\partial P$ has a high enough value at a sufficiently large value of P , then P_R will begin to fall even though P is still increasing. In cycle b (Fig. 7.5b (lower curve)) there is an increase in $\partial\Gamma/\partial P$ at a pump power $P = 0.4$ where fig. 7.2b indicates that the local maximum in P_R occurs. This increase may be associated with the onset of the second stage of FAI growth due to a type II instability. At values of P below 0.4, $\partial\Gamma/\partial P$ is positive so it can be assumed that a type I instability is already causing FAI growth.

A brief version of the above analysis can be found in Kopka et al. (1982).

7.6 Comparison with Grach et al's theory

Grach et al. (1979) have developed a nonlinear theoretical model of FAI amplitude saturation based on pump extinction. For the reasons presented in section 3.4.6, Grach et al's (1979) calculation is difficult to compare with the model which was developed in section 7.4. The difficulty arises partly from the complicated manner in which Grach et al. calculate the amplitude of the scattered Langmuir waves (see Dysthe et al., 1983 for comments) and partly because of their application of a random phase approximation to multi-scattering of plasma waves. These authors do appear to take energy transport due to Langmuir wave refraction into account. Their final result is an approximate relationship between a normalized pump wave power P_0 and anomalous absorption coefficient, Γ , which can be written

$$\Gamma(1 - P_0 \alpha e^{-\Gamma})^2 = \beta (P_0(1 - e^{-\Gamma}))^2 \quad 7.49$$

where α and β are constant coefficients. A graph of Γ against P_0 employing 7.49 is plotted in fig. 7.21. The Γ vs P_0 curve in fig. 7.21 exhibits the jump phenomenon and consequent hysteresis effect already discussed with regard to the Γ vs P curve in fig. 7.16. The dependence of Γ on pump power in fig. 7.21 is clearly qualitatively similar to that derived from the theory developed in detail in this chapter, even though there are differences of detail. Equation 7.49 does not explicitly indicate the presence of two different growth processes (compare with eq. 7.37). However in the concluding section of Grach et al's (1979) paper reference is made to the nonlinear stage as corresponding to the theory of Vaskov and Gurevich (1975, 1977) (see chapter 3). Thus the present theory (presented in detail in this chapter) differs from that of Grach et al. (1979) primarily in the manner in which the nonlinear growth stage is treated.

7.7 Conclusions

Results of recent high latitude modification experiments have been presented in which the signal strength of an ionospherically reflected high power radio wave was measured while the ERP of the high power transmitter was steadily increased and decreased. A hysteresis effect in the reflected pump amplitude was observed, i.e. at a given pump ERP the reflected signal was greater during the period of increasing ERP than during the period of decreasing ERP.

A model of FAI excitation, saturation and decay has also been developed which accounts for the observations in a semi-quantitative way. The model is necessarily very simple in order to make the problem tractable.

The hysteresis effect is consistent with the excitation of field aligned irregularities by the pump wave. This process involves a two stage growth mechanism together with an amplitude stabilization stage due to pump self extinction. Changes in the effects observed during several repeated cycles of increasing and decreasing ERP can be attributed to natural changes in the background ionosphere as indicated by ionograms taken before, during and after the experiment. This illustrates the important influence of the background ionospheric condition on F-region modification.

8. F-REGION CROSS-MODULATION

8.1 Introduction

It was established in chapter 5 that high power radio waves strongly modify the radio wave absorption coefficient of the F-region. The effect is due to the generation of small scale field aligned irregularities during heating. A modulated heating wave should therefore give rise to a modulation of FAI amplitudes which in turn causes amplitude modulation of an initially unmodulated diagnostic wave passing through the heated region.

This F-region cross-modulation mechanism is very different from the well known "Luxembourg effect" which operates in the D-region, where collisional heating, with a short time constant, is responsible for the cross-modulation effects of strong radio waves (Tellegen, 1933; Bailey and Martyn, 1934). In the F-region collisional heating is rather weak with a long time constant and is thus unlikely to cause significant cross-modulation (Stubbe et al., 1982b).

Substantial HF absorption changes on time scales short enough to cause F-region cross-modulation arise because of the excitation of various parametric instabilities. The measurement of cross-modulation depth as a function of modulation frequency provides a method of determining the time constant associated with those instabilities.

The time response of diagnostic signal amplitude to F-region modification by a high power pump is a complicated process. It probably includes several stages which involve the excitation of more than one type of parametric instability together with saturation processes

(see chapter 7). However theoretical considerations together with the observations described in chapters 5 and 7 indicated that the diagnostic amplitude response time is likely to be in the range 0.1 to 10 sec. This has prompted a search for F-region cross-modulation effects in the modulation frequency range 1-10Hz.

8.2 Experimental arrangement

8.2.1 Pump modulation

Amplitude modulation of the pump wave is achieved most simply by on-off keying (Schwarz, 1970). On-off keying of a pump wave of carrier frequency, f_p produces a series of sidebands which are harmonics of the fundamental modulation frequency Ω . The power in these sidebands falls off as n^{-2} where the sideband frequency f_n is related to n by

$$f_n = f_p \mp n \Omega$$

and n is an integer. The occurrence of multiple pump sidebands limits the frequency of diagnostics which can be employed during modulated heating. If the received diagnostic carrier power is P_d and the received power from the n^{th} pump sideband is P_n , then P_n is much less than P_d as long as the difference in the pump and diagnostic frequencies is much greater than the pump carrier and pump sideband frequency separation. If the diagnostic carrier frequency is f_d , then

$$|f_p - f_d| \gg |f_p - f_n| \implies P_d \gg P_n$$

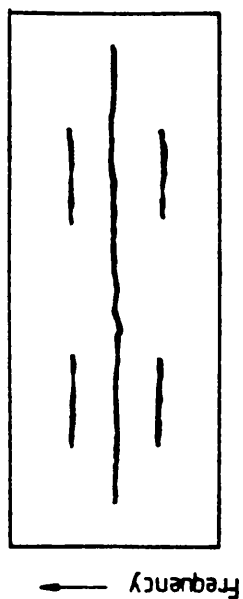
This condition ensures that the diagnostic receiver is not saturated by the pump sideband signal which lies within the receiver bandwidth. If the effective radiated powers of the pump and diagnostic are respectively 300MW and 30W, the frequency separation between the diagnostic and pump frequencies has to exceed 3000Ω to avoid sideband contamination of the diagnostic receiver.

When Ω greatly exceeds the bandwidth of the diagnostic receiver it is possible to use a smaller frequency difference if the entire bandwidth of the diagnostic receiver lies between two successive pump harmonics. Under these conditions however it would not be possible to measure the amplitude of the diagnostic carrier at f_d together with the sidebands at $f_d \mp \Omega$ with a single receiver.

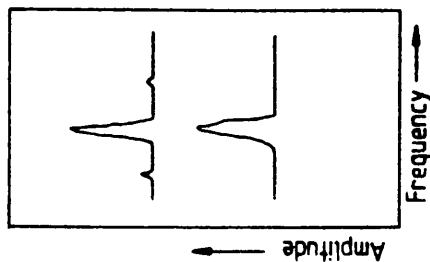
8.2.2 Diagnostics

The diagnostic transmitter-receiver configuration for cross-modulation observations is identical to that employed for phase and amplitude measurements (chapters 5 and 6). In order to detect cross-modulation of a diagnostic wave, the IF signal of a receiver mixed with a local oscillator is fed into the Ubiquitous spectrum analyser and the frequency spectrum displayed on an oscilloscope. It is possible to make a permanent record of spectra by connecting a Medelec UV plotter (see chapter 4 for details) to the output of the spectrum analyser. This arrangement is illustrated schematically in Fig. 8.1. Two forms of hard copy output are employed to record the spectra. The first type consists of a z-modulated time series (fig. 8.2a) and the second a 'waterfall' display of individual spectra which can be stored by the spectrum analyser before printing (Fig. 8.2b).

In order to maximise any cross-modulation effect the diagnostic frequency is set close to the pump frequency so that the pump and diagnostic reflection heights are separated by a distance less than the typical scale height of FAI (i.e. $\sim 10\text{km}$). Most of the heating experiments described in this thesis were carried out within a few hours of midday at frequencies well below f_oF_2 . Under these conditions ray tracing calculations (using the Jones 3D programme, Jones and Stephenson, 1975) indicate that the optimum diagnostic frequency is about 100kHz above that of the pump. Sideband



a.



b.

Fig. 8.2 Schematic representation of (a) z-mode and (b) 'waterfall' displays of spectra with the UV plotter.

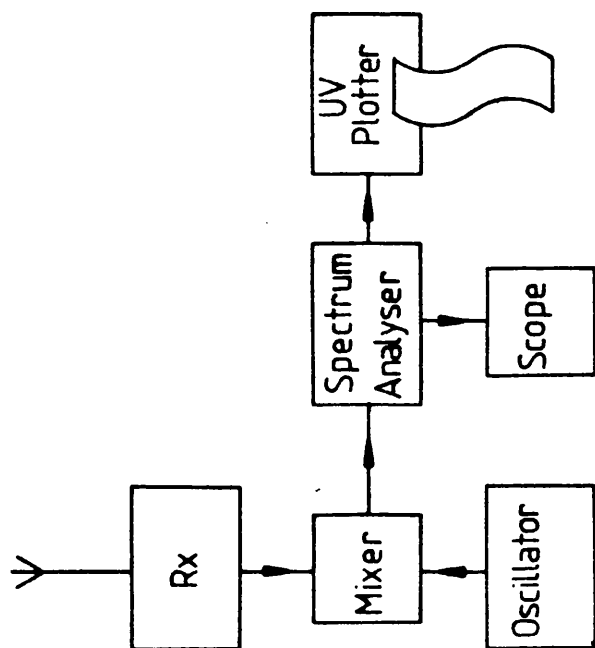


Fig. 8.1 Schematic diagram illustrating the diagnostic receiver, signal spectrum analyser and UV plotter employed in the cross-modulation experiment.

contamination of such a diagnostic is not a problem provided Ω does not exceed 20 Hz.

Ionograms from a KEL-IPS 42 ionosonde were routinely available between heating cycles.

8.2.3 Calibration of the system

In order to determine modulation depth (ratio of sideband to carrier power) of the diagnostic it was necessary to calibrate the output of the coupled receiver-spectrum analyser system described in 8.2.2. This was achieved by driving the system with a standard synthesizer signal (set to the required diagnostic carrier frequency) through a calibrated variable attenuator. Calibration at sideband frequencies was performed by offsetting the synthesizer to the required sideband frequency.

8.3 Experimental Results

8.3.1 First Evidence of an F-region Cross-Modulation effect

An F-region cross-modulation effect was first observed for a pump of 5.423 MHz, O-mode polarization and ERP of 260 MW, with a diagnostic wave of 5.701 MHz. Modulation frequencies of 1 and 2 Hz were employed. The UV plotter record reproduced in Fig. 8.3 clearly illustrates the appearance of two sidebands displaced by 2 Hz from the diagnostic carrier during two minute periods while the pump was being modulated at 2 Hz. During the pump 2 minute off periods, the diagnostic carrier is present without sidebands.

No attempt was made to systematically determine the relative amplitudes of the carrier and sidebands during these observations. They were intended primarily to test the feasibility of cross-modulation studies.

SEPT. 8, 1981 HEATER: 5.423 MHz 0-mode ERP=260 MW

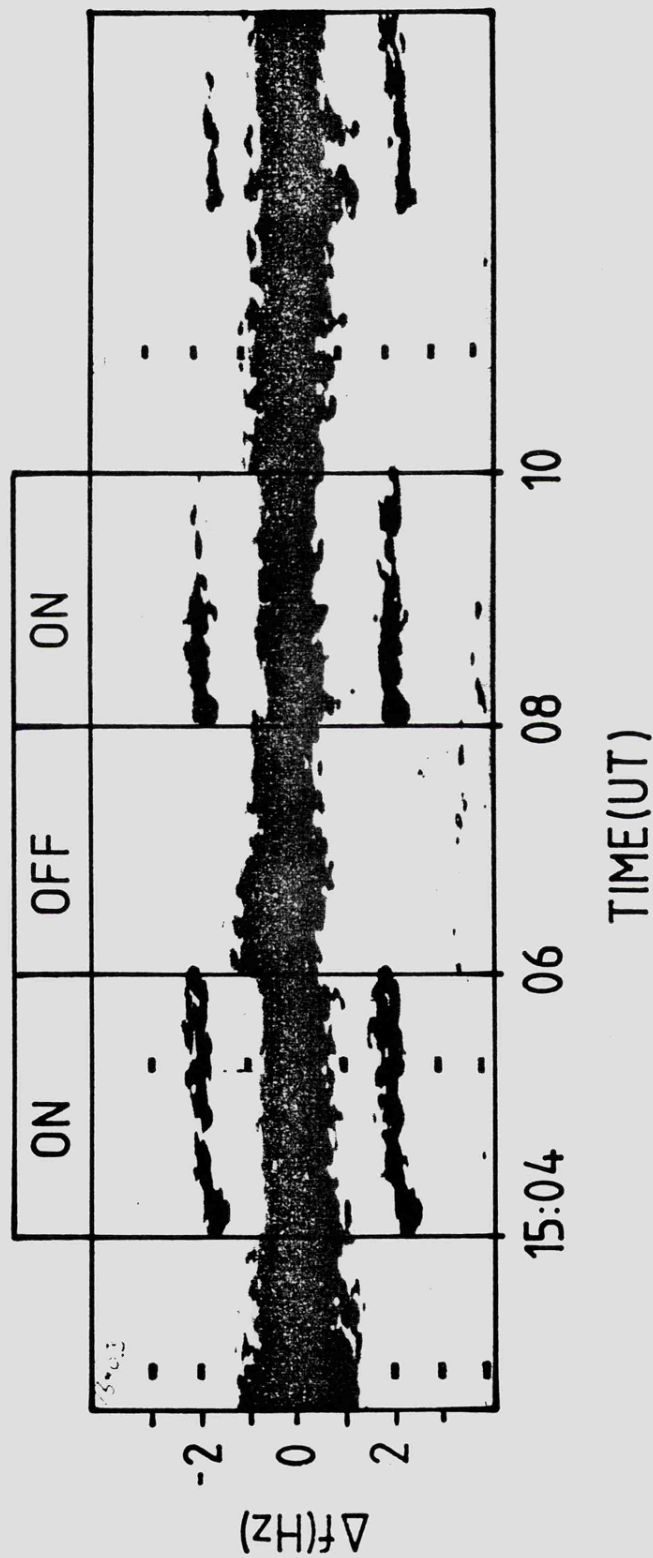


Fig. 8.3 An example of z-mode display of the spectrum of a 5.701 MHz diagnostic during modulated heating. The heater operated at full power (ERP = 260MW) 0-mode with 100% amplitude modulation at 2Hz, Sept. 8, 1981.

8.3.2 Systematic Cross-Modulation Measurements

During heating experiments performed on 23rd October 1982 a 5.423 MHz pump with ERP of 260 MW was modulated according to the sequence listed in table 8.1. The sequence was repeated several times and the spectrum of a 5.701 MHz diagnostic was displayed in the manner described in section 8.3.1. Fig. 8.4 illustrates a z-mode plot of the spectrum during part of a sequence. The 3 and 5 Hz sidebands generated by 0-mode heating can clearly be observed. The absence of a 3 Hz sideband during modulated X-mode heating is significant. No sidebands were observed at any time during modulated X-mode heating. During further sequences of modulated heating spectra were stored and subsequently printed on the UV plotter. It was possible to produce about 10 spectra during each 2 min stage of the sequence of modulated heating. Fig. 8.5a and b illustrate two spectra captured during 3Hz 0-mode heating. Note that these two spectra were recorded on two different output ranges of the spectrum analyser.

In addition to diagnostic spectra, the amplitudes of the pump, the 5.701 Hz diagnostic and two other diagnostics with frequencies of 4.948 and 6.301 MHz respectively were also monitored in the manner described in chapter 5.

The variation of these four signal amplitudes during a single modulation sequence is illustrated by the pen recorder output reproduced in fig. 8.6. It is important to note that 0-mode modulated heating has the effect of depressing the diagnostic amplitudes just as does unmodulated 0-mode heating (see chapter 5). During X-mode modulated heating the diagnostics recover their original amplitudes (i.e. X-mode heating produces the same response in the diagnostic signals as does switching off the pump).

OCT. 23, 1982 HEATER: 5.423 MHz ERP = 260 MW

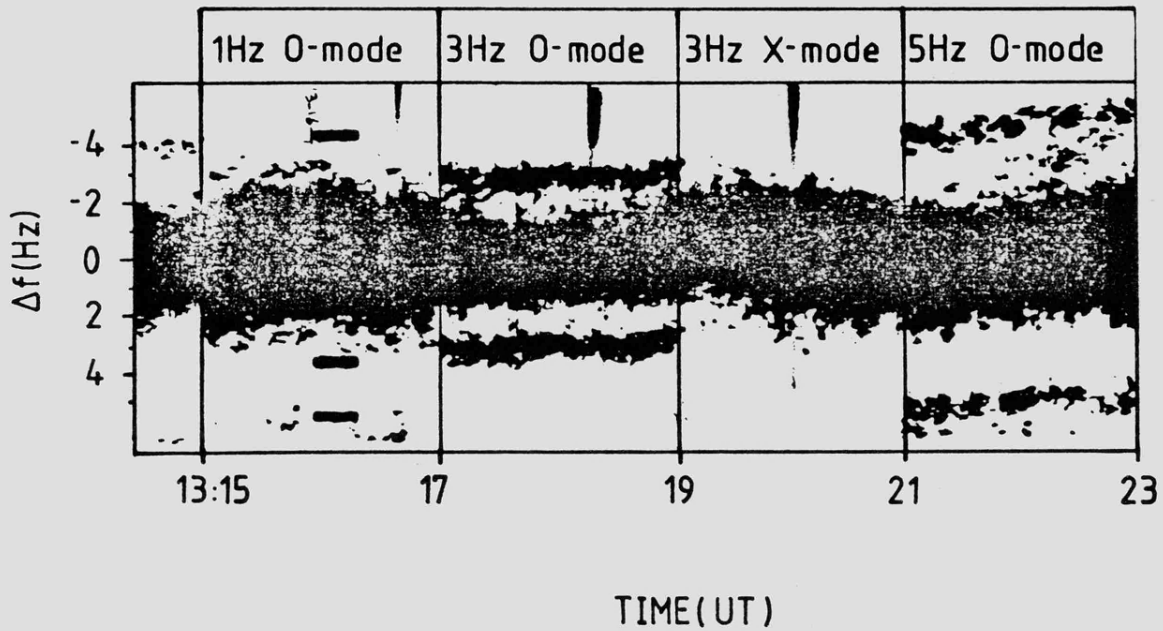


Fig. 8.4 As fig. 8.3 except that the heater was modulated according to the sequence in Table 8.1, Oct. 23, 1982.

Table 8.1 The sequence of modulated heating employed on Oct. 23, 1982.

Heating Period [min]	Modulation Frequency Ω [Hz]	Mode
2	1	O
2	3	O
2	3	X
2	5	O
2	9	O

Table 8.2 Carrier and sideband amplitudes measured during the modulated heating sequence in tables 8.1, Oct. 23, 1982.

Frequency [Hz]	Amplitude [dB]
0 [carrier]	-3.7 ± 6.8
1	-25.0 ± 5.7
3	-40.0 ± 2.8
5	-41.3 ± 2.4
9	-59.4 ± 2.8

OCT 23, 1982 HEATER 5.423 MHz ERP=260 MW
 MODULATION FREQUENCY= Ω [Hz]

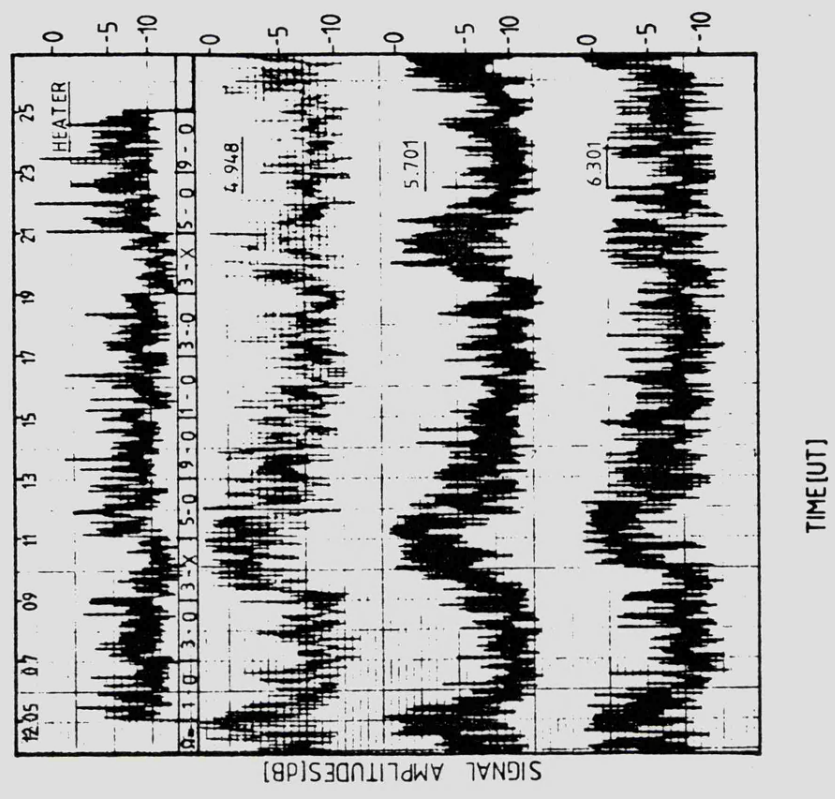


Fig. 8.6 Heater (5.423 MHz) and three diagnostic signal amplitudes (4.948, 5.701, 6.301 MHz) during modulated heating, Oct. 23, 1982, 1205-1225 UT.

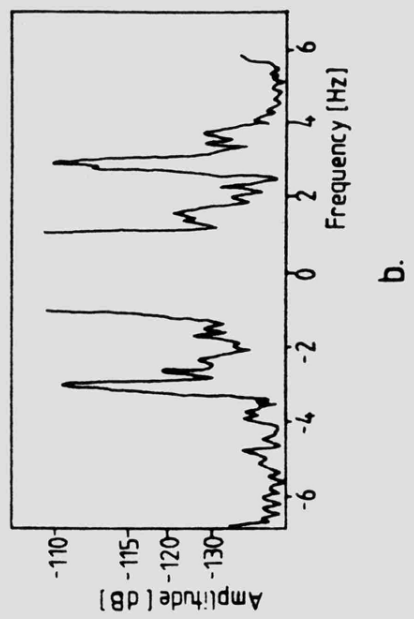
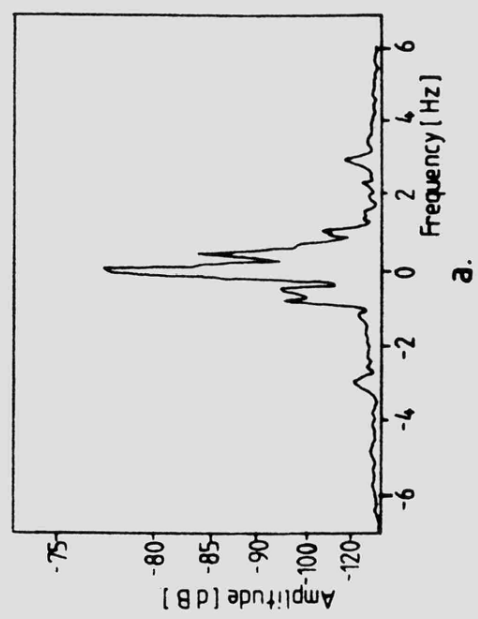


Fig. 8.5 Examples of diagnostic signal spectra recorded on the UV plotter during a period of modulated heating when the modulation frequency was 3Hz and the heater was operating in 0-mode. The two spectra correspond to two different gain settings of the spectrum analyser.

8.4 Carrier and sideband amplitude measurements.

Carrier and sideband amplitudes of a 5.701 MHz diagnostic signal in dB below the synthesizer signal were obtained from the hard copies of spectra recorded with the UV plotter. Calibration spectra were recorded immediately afterwards. The mean amplitude values together with standard deviations for data recorded during modulated heating on 23/10/82 between 1205 UT and 1225 UT are listed in table 8.2. The assumption of a single mean carrier level throughout the modulation sequence is justified by the fact that the deviation from the mean diagnostic signal level averaged over periods exceeding the amplitude fading period was less than 3dB. The larger mean deviation ($\bar{\pm}$ 6.8dB) of the diagnostic carrier amplitude determined from the spectrum analyser records results from amplitude values not forming a continuous time series so fading and transient response to pump on and off are not easily eliminated.

8.5 A model of the F-region Cross-Modulation Process

The results of the cross-modulation experiments are analogous to those of the diagnostic amplitude experiment reported in chapter 5. The absence of X-mode effects suggest that the observed cross-modulation of a diagnostic during modulated heating is due to the modulation of FAI amplitudes which lead to modulated anomalous absorption of the diagnostic waves.

The generally low modulation depth imposed on the diagnostic indicates that the modulation frequencies employed were much greater than the growth rate of FAI. If the modulation frequency were lower than the FAI growth rate, the FAI amplitudes would grow to full size during each 'on' stage of on-off keying resulting in comparable diagnostic carrier and sideband amplitudes.

8.5.1 A model of FAI amplitude modulation

The amplitude of FAI excited by a modulated pump must be considered on two time scales. t is the time measured from the start of an 'on' stage of on-off keying. The two time scales are then ,

(a) times longer than the modulation period, T , but less than the FAI time constant τ_n

$$\text{i.e. } T < t < \tau_n ,$$

(b) times shorter than the modulation period

$$\text{i.e. } 0 < t < T .$$

The time response of the FAI amplitude n is determined by equation 7.10. If this equation is averaged over times longer than T but shorter than τ_n then 7.10 becomes

$$\frac{\partial \bar{n}}{\partial t} - \frac{1}{D_1} \left(\overline{\frac{Q^2}{n}} \right) + D_2 \bar{n} = 0 \quad 8.1$$

where Q is the differential heat input due to interference between scattered highpower waves and D_1 and D_2 are constants related to the plasma thermal conductivity (see section 7.4).

The bar denotes time averaging. From 8.1 it can be concluded that \bar{n} responds as if the pump were unmodulated but has an effective pump power below the peak power. The FAI amplitude \bar{n} has a quasi-stationary value n_s when

$$\frac{1}{D_1} \left(\overline{\frac{Q^2}{n}} \right)_{\bar{n}=n_s} - D_2 n_s = 0 \quad 8.2$$

These conclusions are borne out by the diagnostic amplitude data in fig. 8.6. All three mean diagnostic amplitudes decay by approximately 5dB within 20s of pump switch on.

Once the mean FAI amplitude has reached a quasi-stationary value, the effect of cross-modulation is to cause a small perturbation in the amplitude, n' to be superimposed on top of the value n_s .

Thus,

$$n(t) = n_s + n'(t) .$$

During the on period of on-off keying, the pump power exceeds that required to maintain n_s and during the 'off' stage the pump power is zero and the FAI begin to decay. If $\tau_n \gg T$, then changes in n' are as the result of quasi-linear growth and decay of the FAI even if the instability is nonlinear (see section 7.4.3). The time response of n during a single on-off keying cycle beginning at $t = 0$ is thus,

$$n(t) = n_s e^{t/\tau_n} , \quad 0 < t \leq T/2 \quad 8.3a$$

$$\begin{aligned} n(t) &= (n_s e^{T/2\tau_n}) e^{-(t-T/2)/\tau_n} , \quad T/2 < t \leq T \quad b \\ &= n_s e^{-(t-T)/\tau_n} \end{aligned}$$

To a good approximation, n' has the following form when $t, T \ll \tau_n$

$$n' = n - n_s = n_s \cdot t / \tau_n , \quad 0 < t \leq T/2 \quad 8.4a$$

$$n' = n_s \cdot (T-t) / \tau_n , \quad T/2 < t \leq T \quad b$$

The resulting form of $n'(t)$ is a symmetrical sawtooth depicted in Fig. 8.7. Its peak to peak amplitude is $n_s \cdot T/\tau_n$. The assumption that τ_n has the same value (though opposite sign) while n' is increasing ($0 < t \leq T/2$) and decreasing ($T/2 < t \leq T$), is necessary in order to maintain the quasi-stationary nature of the FAI amplitudes.

This assumption can also be justified by noting that

$$n' \ll n_s \implies \overline{n^m} \equiv (\overline{n})^m \quad 8.5$$

where m is some arbitrary exponent. Then, to a good approximation,

$$n = n_s \quad 8.6a$$

$$\frac{\partial n}{\partial t} = \frac{\partial n'}{\partial t} = \mp \frac{n_s}{\tau_{n_{1,2}}} \quad b$$

where τ_{n_1} and τ_{n_2} are the respective time constants for the growth and decay stages during on-off keying. Substituting these expressions into 8.1 results in

$$\frac{n_s}{\tau_{n_1}} - \frac{\overline{Q^2}}{D_1 n_s} + D_2 n_s = 0 \quad , \quad 0 < t \leq T/2 \quad 8.7a$$

$$- \frac{n_s}{\tau_{n_2}} + D_2 n_s = 0 \quad , \quad T/2 < t \leq T \quad b$$

For square wave modulation, (fig. 8.8)

$$\overline{Q^2} = \frac{1}{T} \int_0^{T/2} Q^2 dt = \frac{Q^2}{2} \quad 8.8$$

Combining 8.2, 8.7 and 8.8. it is clear that

$$\tau_{n_1} = -\tau_{n_2} = \tau_n = D_2^{-1} \quad 8.9$$

The diagnostic response to modulated heating thus depends essentially on the FAI decay rate (section 7.4.6).

8.5.2. Diagnostic amplitude modulation

In chapter 5 an expression was derived for the anomalous absorption Γ of a diagnostic wave in terms of the mean square number density $\langle |n|^2 \rangle$ (amplitude) of FAI (Eq. 5.19).

$$\Gamma = \sigma \langle |n|^2 \rangle \quad 5.19$$

where σ is a constant given by (5.19b).

Thus fluctuations in n due to on-off keying the pump wave will cause fluctuations in a diagnostic signal V_d (Volts) recorded at a receiver. As explained in section 5.4.6 the signal strength measured during anomalous absorption V_d is related to that measured during heater off, V_{d0} by

$$V_d^2 = V_{d0}^2 e^{-\Gamma} \quad 8.10$$

where Γ is the anomalous absorption due to generation of FAI. Thus

$$\frac{1}{V_d} \frac{\partial V_d}{\partial t} = \frac{1}{\tau_d} = \frac{1}{2} \frac{\partial \Gamma}{\partial t} \quad 8.11$$

From 5.19a and 7.31

$$\Gamma = \sigma n_s^2$$

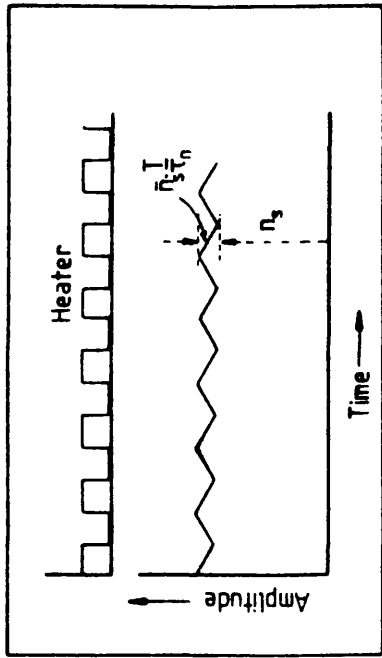


Fig. 8.7 The response of the diagnostic amplitude to modulated heating during the quasi-stationary stage.

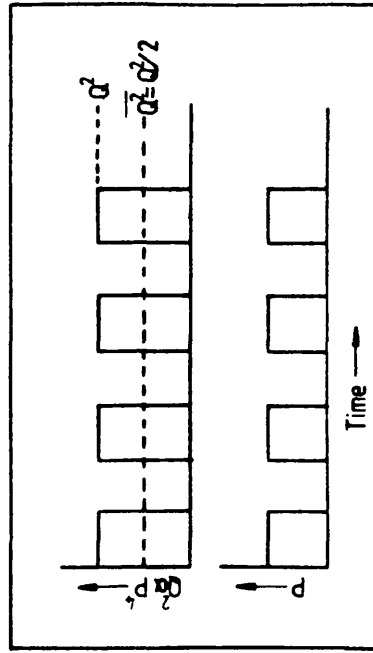


Fig. 8.8 Schematic illustration of the mean value of Q^2 during modulated heating.

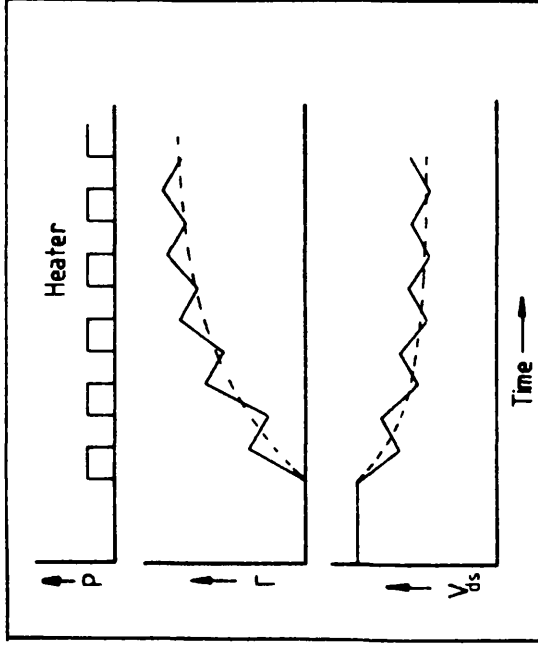


Fig. 8.9 The response of signal strength (Volts) to the switch-on of a modulated heater. The fluctuating signal strength steadily decays as the fluctuating anomalous absorption \bar{V} induced by the heater steadily increases.

where n_s^2 replaces $\langle |n|^2 \rangle$.

Under quasi-stationary conditions the FAI amplitude n_s gives rise to the anomalous absorption Γ_s and diagnostic amplitude V_{ds} . By analogy with 8.6b,

$$\frac{\partial \Gamma}{\partial t} = \frac{2\sigma n_s^2}{\tau_n} = \frac{2\Gamma_s}{\tau_n} \quad 8.12$$

Combining 8.10, 11 and 12 results in

$$\tau_d = -\tau_n / \Gamma_s \quad 8.13$$

When Γ_s is measured in dB, 8.13 becomes

$$\tau_n = -\Gamma_s \tau_d / 10 \log e \quad 8.14$$

The time response of the diagnostic amplitude (τ_d), by analogy with the FAI response time (τ_n) derived from the model in the previous section is a symmetrical sawtooth function with a peak to peak amplitude of $V_{ds} \cdot T / \tau_d$, superimposed on a quasi-stationary amplitude, V_{ds} . However, \bar{V}_d slowly decays to V_{ds} as $\bar{\Gamma}$ increases to Γ_s (Fig. 8.9).

8.5.3 Cross-modulation sidebands

The sawtooth amplitude depicted in fig. 8.9 when the quasi-stationary stage is reached can be represented by a Fourier series of the form (Champeney, 1973)

$$V_{ds} + V' = V_{ds} \left\{ 1 + \frac{T}{2\tau_d} + \frac{4T}{\pi^2\tau_d} (\cos(2\pi t/T) + \right. \\ \left. + \frac{\cos(6\pi t/T)}{3^2} + \dots) \right\} \quad 8.15$$

The power in the sidebands which correspond to the first harmonic of the modulation frequency, Ω , divided by the carrier power $(V'/V_{ds})^2$ is approximately

$$\left(\frac{V'}{V_{ds}}\right)^2 = \frac{4T^2}{\pi^4 \tau_d^2} = \frac{4}{\pi^4 \Omega^2 \tau_d^2} \quad 8.16$$

if

$$T \ll \tau_d .$$

When $(V'/V_{ds})^2$ is measured in dB, 8.16 can be written

$$\Delta P_{dB} = -10 \log (V'/V_{ds})^2 = 20 \log (\Omega \tau_d \pi^2 / 2) \quad 8.17$$

The power in the sideband corresponding to the second harmonic of Ω is approximately 19 dB below the power in the first harmonic and is unlikely to be detected in the present experiment.

8.6 Interpretation of Cross-modulation data

8.6.1 Diagnostic amplitude time constant

Equation 8.17 indicates that a graph of ΔP_{dB} against $\log_{10} \Omega$ should be a straight line of slope 20 and intercept on the ΔP_{dB} axis of $20 \log_{10} (\tau_d \pi^2 / 2)$. A graph of ΔP_{dB} against $\log \Omega$ is plotted in fig.8.10 from the data in table 8.2.

Straight lines fitted to the data by a least squares technique are also drawn in Fig.8.10. AB is derived without any constraint on its gradient. It is represented by the equation

$$\Delta P_{dB} = 31.9 \log_{10} \Omega + 18.9$$

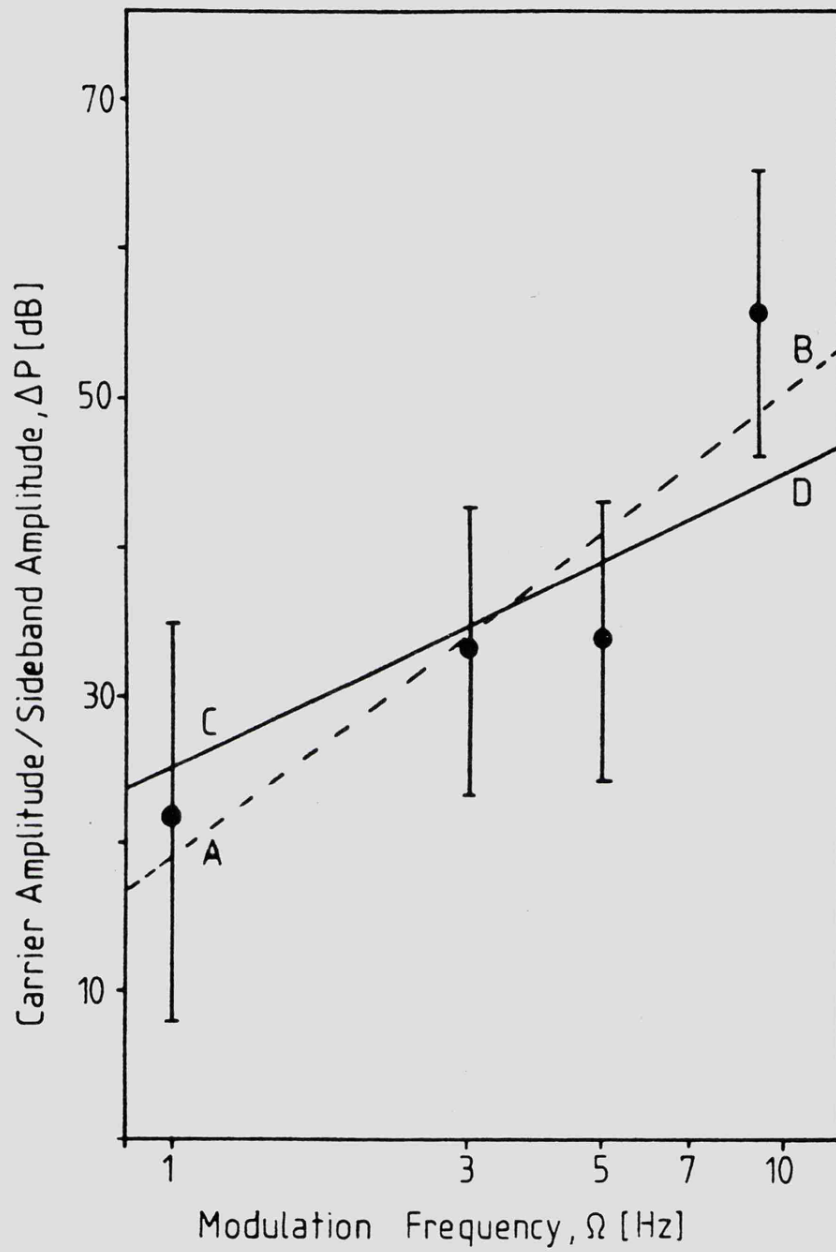


Fig. 8.10 A graph of the ratio of carrier to sideband amplitude in dB against modulation frequency. Two least squares fit lines are drawn. The dashed line, AB, is the best fit line. The solid line, CD, is the best fit line of slope 20.

Its gradient is 50% larger than required by equation 8.17. A second line CD deduced for the case when the line's gradient was constrained to a value of 20 is also drawn in Fig. 8.10. It has the equation

$$\Delta P_{\text{dB}} = 20 \log_{10} \Omega + 25.3$$

Because of the large error bars on the data points it is difficult to use a 'goodness of fit' to choose between these two lines. However the proposed model requires the slope to be 20 so the second line is more consistent with the model. The value of the diagnostic amplitude time constant deduced from the intercept of line CD on the ΔP_{dB} axis is $\tau_d = 3.73$ s.

8.6.2 FAI time constant

The mean value of the diagnostic anomalous absorption Γ_3 during the modulating heating sequence for which τ_d was derived in the previous section was 5dB (see Fig. 8.6). Substituting this value for into 8.14 together with $\tau_d = 3.73$ s produces a corresponding value of τ_n of 4.29 s. τ_n is far smaller than the time constant associated with phase changes of a diagnostic wave determined in chapter 6. This (latter) time constant, τ_N is that of bulk plasma changes and is determined not by plasma diffusion but by recombination. The difference in τ_n and τ_N justifies the arguments of chapter 5 that diagnostic amplitude changes are due to anomalous absorption due to scattering from small scale field aligned irregularities and not defocussing due to refractive index changes.

In section 8.5.1 it was demonstrated that $\tau_n = D_2^{-1}$ where D_2 (from 7.10) is given by

$$D_2 = 1.8 D_{\perp} k^2 \quad 8.18$$

D_{\perp} is the electron thermal conductivity perpendicular to the magnetic field and k is the FAI wavenumber perpendicular to the magnetic field.

In section 7.4.7 it was established that the condition of quasi-stationary FAI amplitude requires that

$$D_{\perp} k^2 = (5/3) \frac{D_{\parallel}}{L_{\parallel}^2} \quad 8.19$$

Combining 8.18 and 8.19 produces

$$D_{\parallel} = L_{\parallel}^2 / 3 \tau_n \quad 8.20$$

In order to test the consistency of the value of τ_n determined above it can be combined with the value L_{\parallel} determined in the anomalous absorption experiment described in chapter 5, to calculate D_{\parallel}

The diagnostic anomalous absorption experiments of 23 October 1982 (section 5.5) were performed immediately after the cross-modulation experiments described above. L_{\parallel} was found to be 52.4km. Substituting the values of L_{\parallel} and τ_n determined from anomalous absorption and cross-modulation experiments respectively, in 8.20, results in

$$D_{\parallel} = 2.13 \cdot 10^8 \text{ m}^2 \text{ s}^{-1}$$

This result is similar to the value of $6.9 \times 10^7 \text{ m}^2 \text{ s}^{-1}$ for D_{\parallel} obtained by substituting typical values of F-region parameters from table 7.1 into equ. 7.5b. It is consistent with a value of τ_e/ν approximately 3 times larger than the typical value from table 7.1.

8.7 Comments and Conclusions

The existence of an F-region cross-modulation effect associated with the amplitude modulation of FAI which give rise to anomalous absorption has been demonstrated. Measurements of the modulation depth as a function of modulation frequency enables time constants associated with FAI amplitude changes to be determined. Time

constants could, in principle, be evaluated by curve fitting to the diagnostic amplitude data presented as a time series (e.g. Fig. 8.6). However, curve fitting is extremely difficult when amplitude fading is present. The 'noisy' data cannot be time averaged over periods longer than the growth or decay times otherwise the changes that are being investigated will be smoothed out of the data.

There is an obvious advantage in being able to determine time constants from a quasi-stationary measurement. Cross-modulation carrier and sideband amplitudes are quasi-stationary. At least they can be averaged over periods much longer than the time constants themselves.

The disadvantages in determining time constants by the cross-modulation technique presented above is that only the FAI decay time constant can be derived. However the FAI growth is complicated because it consists of several stages so it is difficult to envisage how it may be determined accurately except perhaps by summing data from many on-off cycles.

The FAI decay time constant determined by the cross-modulation technique, together with the value of the FAI scale length determined in chapter 5, have been used to evaluate the thermal conductivity, $D_{||}$ of the F-region plasma parallel to the magnetic field. These measurements of the result is consistent with $D_{||}$ evaluated from typical F-region parameters. This result illustrates the way in which controlled experiments involving high power radio waves enable some of the important parameters of the natural F-region plasma to be determined in a relatively simple manner.

9. SUMMARY AND CONCLUSIONS

As a consequence of experimental and theoretical investigations presented in this thesis, the following important results have been established:

(a) The reflectivity of the F-region for HF radio waves whose frequencies differ from that of the modifying wave by less than approximately 1MHz is greatly decreased during heating.

This result is interpreted in terms of the excitation of small scale field aligned irregularities which cause electromagnetic waves to be converted into Langmuir waves. The resulting anomalous absorption of the electromagnetic waves is shown experimentally to exhibit a frequency dependence. A theory of anomalous absorption which takes full account of the presence of the geomagnetic field has been developed which has to be determined for the first time. The plasma density perturbations associated with the irregularities have also been evaluated from the theory.

(b) The plasma density of the lower F-region is enhanced on large spatial scales. The experimental evidence presented strongly suggests that anomalous absorption rather than direct deviative absorption of the high power modifying wave is responsible for the heating effect. This behaviour is in contrast to that reported during modification experiments at lower latitudes where anomalous absorption and deviative absorption were found to contribute almost equally to the large scale heating effects.

(c) The reflectivity of the high power radio wave itself has a highly non-linear behaviour and exhibits a hysteresis effect. The heater power reflected from the ionosphere as a function of transmitted power has been measured. The difference in reflected power noted during the increasing and

decreasing power sequences provide the first direct experimental demonstration of the existence of a hysteresis effect in ionospheric reflectivity. A simple theory has been developed which accounts for these observations in terms of a two stage excitation process for small scale field aligned irregularities whose amplitudes are stabilized by anomalous self absorption of the high-power wave.

(d) F-region cross-modulation of probing radio wave occurs when the modifying wave is amplitude modulated. This thesis contains the first detailed experimental investigation and theoretical analysis of this unexpected phenomenon.

F-region cross-modulation effects have been detected at modulation frequencies in the range 1-10 Hz and this suggests that the effect results from amplitude modulation of field aligned irregularities.

It is important to note that all of the above phenomena are strongly related through their dependence on the generation of small scale field aligned irregularities. The almost vertical magnetic fields at high latitudes ensures strong coupling between vertically propagating electromagnetic waves and Langmuir waves which results in highly efficient irregularity generation and anomalous radio wave absorption. The present work demonstrates the extremely important role played by small scale field aligned irregularity generation in F-region modification phenomenon at high-latitudes. These studies yielded important new information regarding the nonlinear plasma physics of the ionosphere. In addition they establish artificial modification as an immensely powerful technique for determining important geophysical parameters associated with the natural ionosphere. The chemical recombination rates in the lower F-region have been determined from the growth and decay times of large scale plasma density enhancements (result b). By combining the scale lengths of small scale irregularities along the magnetic field determined from multi-frequency anomalous

absorption measurements (result a) with irregularity time constants determined by F-region cross-modulation measurements (result d) plasma thermal conductivity along the magnetic field has been estimated. These measurements are rather crude, but they do establish the feasibility of such experiments.

Limitations of the present work

The accuracy of the quantitative results above (e.g. time constants, scale lengths, ionospheric parameters) is not limited so much by the diagnostic measuring equipment, but by the manner in which the data is logged. Thus far, only analogue data recording has been available to which only a limited amount of statistical analysis can be applied. This represents one of the most obvious limitations of the present work. The high latitude (auroral) ionosphere is a highly variable medium even under geomagnetically quiet conditions. Therefore information about its quiescent state can be extracted from diagnostic measurements only by employing data averaging techniques. The situation is further complicated when the transient response of the ionosphere is to be investigated. However this problem has, to some extent, been alleviated with regard to the measurement of time constants associated with small scale field aligned irregularities by employing the cross-modulation technique which resulted in a quasi-stationary measurement.

A second limitation of the present work is the reliance on natural D-region absorption to suppress the extra-ordinary mode relative to the ordinary mode of the low-power diagnostic radio signals. The X-mode is unwanted because only O-mode radio waves suffer anomalous absorption. This dependence on natural D-region absorption limits the experiment in two ways. First experiments can only be performed during daylight conditions and secondly, the diagnostic frequencies are restricted to those below about 5 times the electron gyrofrequency. Above this limiting

frequency, the difference between O- and X-mode absorption in the D-region becomes negligible.

In spite of the above limitations a remarkable amount of new information has been obtained regarding modification processes in the high-latitude ionosphere with extremely simple and inexpensive diagnostic equipment. Thus a firm basis for future experimentation has been established.

Future work

As a result of the success of the first three joint Leicester-M.P.I. heating campaigns, 1980-1982, further experiments employing the Ramfjordmoen heater are planned. The data logging limitations of the present experimental arrangement have been noted and developments are in progress to overcome these. The next series of experiments will be controlled by a microcomputer and data logging will be digital onto magnetic tape. The restriction imposed by lack of O- and X-mode discrimination will also be removed by employing active phased cross dipole antennas.

Four specific areas will benefit from digital data recording

1) Determination of ionospheric parameters

Clearly it is important to obtain reliable values of the time constants and scale lengths associated with the irregularities of various scales induced by heating in order that the theory of the processes associated with their generation be verified.

2) Cross-modulation theory

A very useful check on the F-region cross-modulation theory presented in Chapter 8 will be a determination of small scale irregularity decay times from transient diagnostic amplitude data. Averaging digital amplitude data over a number of heater on-off cycles should enable fast fading effects to be eliminated. Such a task is impossible when data is

in its present analogue form.

3) Artificial acoustic-gravity-wave generation

Further attempts should be made to detect heater induced neutral atmospheric waves. Fourier analysis of digital Doppler data will enable oscillations correlated with the heater on-off cycles to be picked out of the spectrum of natural oscillations.

4) Small scale field aligned irregularity structure

The importance of simultaneous anomalous absorption and backscatter radar measurements has been stressed in Chapter 5 with regard to investigating the properties of small scale field aligned irregularities. Preliminary experiments were conducted in October 1982 (the backscatter data from Upsala University is still being processed). Further experiments of this type will benefit greatly from the improved data handling capability of the HF diagnostic system.

A number of new areas for investigation are also suggested

(a) Upper F-region heating

There is a need to study response of the upper F-region near the layer peak. In contrast to the lower F-region, large scale plasma density depletions are expected in the upper F-region. Only nighttime conditions will enable radio waves in the frequency range 2.75 - 8 MHz to be reflected from ionospheric layers with altitudes in excess of 300 km.

(b) Artificial Spread-F

An attempt must be made to investigate thoroughly the conditions under which artificial spread-F can be generated at high-latitude. The (almost completely) negative results so far obtained with regard to this phenomenon is one of the most puzzling aspects of the experiments performed so far with the Ramfjordmoen heater. It needs to be established whether the absence of spread-F is due to (i) the conditions for its generation not

yet having been satisfied, or (ii) other phenomena, which are more efficiently excited tending to suppress it.

One difficulty encountered in observing artificial spread-F at high latitude is associated with the ubiquity of the occurrence of natural spread-F. A second difficulty arises from the predicted field aligned nature of the medium scale irregularities which cause it. This makes it less readily observable by vertical or near vertical soundings.

(c) Enhanced plasma line

Reports of enhanced plasma line observations at Ramfjordmoen utilizing the EISCAT UHF radar (Stubbe et al. 1982b) indicate that a strong enhancement is observed only for a short time (0.2 - 2s) after switch on. Although observations along the field line are not entirely satisfactory, these results are consistent with the hypothesis that anomalous absorption which arises within a few seconds of heater switch on does suppress the excitation of competing instability processes. Simultaneous plasma line and HF anomalous absorption studies will greatly improve understanding of the temporal development of field aligned irregularities.

(d) Medium scale irregularities

Fejer (1983) has suggested a method by which the medium scale plasma density irregularities which are generated in the heater standing wave below its reflection point can be detected. Fejer's technique is based on the theory of wave propagation in periodic structures (Brillouin, 1953). The theory predicts that a discontinuity occurs in the group propagation velocity versus frequency curve at a frequency which depends on the periodicity of the standing wave structure. Measurements with a multi-frequency pulse sounder with high frequency resolution should enable the standing wave structure to be detected.

A pulse sounder is under construction at Leicester and is expected to be deployed in the forthcoming heating campaign in Sept. 1983. Its main

purpose is to provide height information within the heated volume together with additional information concerning heater induced amplitude effects. An attempt will also be made to detect medium scale irregularities utilizing the technique suggested by Fejer.

(e) EISCAT studies

One of the main reasons for constructing a high power facility at Ramfjordmoen was to take advantage of the most powerful ground based ionospheric diagnostic probe currently available, namely the EISCAT radar system. Thus far surprisingly little use has been made of this sophisticated probe. It should provide an ideal tool for investigating large scale plasma temperature and density modification throughout the F-region. Such information is essential if accurate models of the physical processes involved in such changes are to be constructed. In this way, the potential of the high power facility as a means of studying the natural ionospheric plasma in a controlled manner can be fully realized.

(f) Theory

In addition to improving present experiments and developing new ones there is a great deal of scope for further theoretical work. Interest in field aligned irregularity growth and stabilization mechanisms is rapidly expanding. The theories which have been developed in this thesis have been deliberately simplified to enable analytic results to be obtained. In this way, the physical principles involved are highlighted at the expense, in certain cases, of fine detail. Whilst the formula for anomalous absorption derived in Chapter 5 is of sufficient accuracy to determine FAI structure, those associated with the hysteresis effect in Chapter 7 are only semiquantitative and require further development. Computer modelling, which has proved so successful in studies of laboratory plasmas (Potter, 1981) is an essential next step.

The development of the high-latitude heating facility has opened up a completely new branch of ionospheric physics. Already many new effects have been discovered and new theories developed to account for them. Much still remains to be done, however, and the next few years should see considerable development in this area of research.

APPENDIX ADIFFERENTIAL D-REGION ABSORPTION OF O- AND X-MODE RADIO WAVES

The nondeviative absorption, Γ_D , of an HF radio wave traversing the D-region is given by

$$\Gamma_D = 2 \cdot \int k_D'' dh \quad \text{A.1}$$

where k_D'' is the absorption coefficient (eq. 3.23). The factor of 2 in A.1 takes account of absorption of both the upgoing and reflected waves. George (1971) has summarized the wide range of data concerning Γ_D and its dependence of radio frequency, f (MHz) solar zenith angle, χ , season and solar activity, by employing a frequency independent parameter A , defined by

$$A = \Gamma_D \cdot (f \mp f_L)^2 \quad \text{A.2}$$

where f_L is the longitudinal component of the electron gyrofrequency and the plus and minus signs correspond to the O- and X-modes respectively. The dependence of A on χ is of the form,

$$A \propto \cos^n \chi \quad \text{A.3}$$

where n is a parameter which it is a function of latitude and season. The dependence of absorption on solar activity is taken into account by assuming that

$$A \propto (1 + 0.0067 R_Z) \quad \text{A.4}$$

where R_Z is the 13-month smoothed monthly mean Zurich sunspot number.

George (1971) defines a modified dip angle X as

$$X = \tan^{-1} (I \cos^{-1/2} \lambda) \quad \text{A.5}$$

where I is the actual dip angle and λ the geographic latitude.

Contours of constant A normalized to $\cos X = 1$ are reproduced in fig.

A.1. According to George (1971) the values of f_L and X appropriate for the Tromso region are 1.37 MHz and 66.5° respectively. The corresponding value of A during equinox (all of the experiments reported in this thesis were carried out in Sept. or Oct.) is 1100 dB MHz^2 .

George (1971) does not give values of η (in A.3) specifically for Tromso, however for normalization purposes this author employed $n = 0.8$, which reduces A to 472 dB MHz^2 at Midday for the geographical latitude of Tromso. Very low values of η , between 0.2 and 0.5, are reported by Davies (1960) for high latitudes. George (1971) reports $n = 0.28$ for Churchill ($X = 63.7$) during equinox. Low values of η indicate a low diurnal variation in A (during daylight hours).

George (1971) assumes a value of 200 for R_z in A.4. Thus the value of Γ_D appropriate at Tromso for a general R_z is (from A.2 and A.4)

$$\Gamma_D = 201.7 \cdot (1 + 0.0067 \cdot R_z) / (f - f_L)^2 \quad \text{dB} \quad \text{A.6}$$

Equation A.6 is employed to calculate the expected O- and X-mode absorption for different diagnostic waves under experimental conditions encountered at Tromso during 1980-82. Sunspot numbers are obtained from Solar Geophysical Data prompt report Vol. 460. The results of the calculation of Γ_D are listed in table A.1.

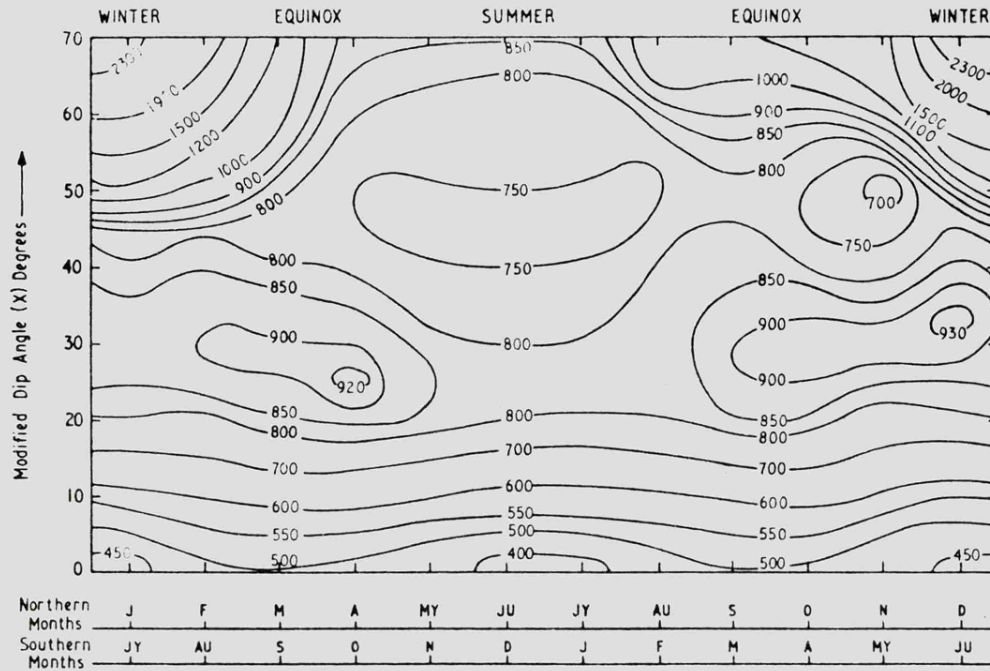


Fig. A.1 The seasonal and latitudinal variation of A (normalized to $\cos \chi = 1$ and $R_z = 200$) as a function of modified dip angle (from Geoge, 1971).

Date	Oct. 1980	Sept. 1981			Oct. 1982		
Sunspot no., R_z	150	143			93		
Diagnostic Frequency [MHz]	3.778	4.948	5.701	6.506	4.948	5.701	6.301
O-mode Absorption [dB]	15.1	9.2	7.8	6.3	8.1	6.5	5.5
X-mode Absorption [dB]	71.5	31.4	21.4	15.1	26.0	17.7	13.6

Table A.1 Results of the calculation of D region absorption of the O- and X-components of diagnostic signals with allowance made for sunspot number.

APPENDIX BAPPROXIMATE EVALUATION OF INTEGRALS IN CHAPTER 7

In order to determine the differential heating terms Q_{10} and Q_{21} in section 7.4.8, it is necessary to evaluate integrals of the form (equ. 7.24 and equ. 7.29)

$$I = \int_{-\infty}^{\infty} \overline{|E_0 \exp(-\int_{-\infty}^h p(h) dh)|^2} q(h) dh \quad \text{B.1}$$

where E is a constant electric field amplitude and $p(h)$ and $q(h)$ represent resonance functions which are only non-zero close to certain resonance points. The integral exponent in B.1 represents the effect of anomalous absorption, Γ , on the amplitude of the electric field.

Γ is given by

$$\Gamma = 4 \int_{-\infty}^{\infty} p(h) dh \quad \text{B.2}$$

I has a simple single integral form when either $p(h)$ or $q(h)$ are delta functions:

(i) if $p(h) = p_0 \delta(h-h_p)$, B.1 becomes

$$I = I_1 = I_1^- + I_1^+ \quad \text{B.3}$$

where

$$I_1^- = \int_{-\infty}^{h_p} \overline{E_0^2} q(h) dh$$

$$I_1^+ = \int_{h_p}^{\infty} \overline{(E_0 e^{-p_0})^2} q(h) dh$$

(ii) if $q(h) = q_0 \delta(h-h_q)$, B. 1 becomes

$$I = I_2 = q_0 \overline{E_0^2} \exp(-2 \int_{-\infty}^{h_0} p(h) dh) \quad \text{B.4}$$

In the integral in 7.24, $p(h)$ and $q(h)$ are of the

$$p(h) = \alpha_0 \frac{(h+a)^2 \cdot n^2(h)}{((h+a)^2 + c^2)^2}, \quad q(h) = \beta_0 \frac{(h+a) \cdot n(h)}{(h+a)^2 + c^2} \quad \text{B.5}$$

where α_0 , β_0 , a and c are constants and $n(h)$ is a slowly varying function of h . $n(h)$ represents the amplitude of field aligned irregularities discussed in chapter 7. The resonance point for both p and q is at $h = -a$. The width of $p(h)$ is smaller than $q(h)$, thus B.3 applies approximately. Integral 7.24 is complicated by the inclusion of both upgoing and downgoing wave fields. This is necessary because $q(h)$ is antisymmetrical about $h = -a$. The $\overline{E_0^2}$ factors in the integrands of B.3 have the form

$$\overline{E_0^2} = E_{00}^2 (A^2 + B^2 + 2AB \sin(2k_0 h - \varphi)) \quad \text{B.6}$$

where

$$A = 1, \quad B = e^{-2p_0} \quad h \leq -a$$

and

$$A = e^{-p_0}, \quad B = e^{-p_0} \quad h > -a$$

The sine term in B.6 in which φ represents the phase difference in the upward and downward waves, arises from the standing wave nature of the electric field. Substituting B.6 into B.3 produces

$$I_1 = E_{00}^2 e^{-2p_0} \left\{ 2 \int_{-\infty}^{\infty} (1 + \sin(2k_0 h - \varphi)) q(h) dh + \right. \\ \left. + 2 (\cosh 2p_0 - 1) \int_{-\infty}^0 q(h) dh \right\} \quad \text{B.7}$$

The first term in B.7 has the value (Das and Fejer, 1979)

$$2 \pi \beta_0 e^{-2k_0 c} E_{00}^2 e^{-2p_0} n(-a) \sin \varphi$$

The second term in B.6 can be evaluated approximately by assuming that $n(h)$ is constant between $a \pm L$ and zero elsewhere, where L is the vertical scale length of the FAI. The second term in B.7 is then,

$$2\beta_0 E_{o0}^2 e^{-2\rho_0} n(-a) (1 - \cosh 2\rho_0) \ln \sec(\tan^{-1}(L/c)) .$$

c is approximately Hv/ω (see section 7.4.8) which is much smaller than L and $1/k_0$, so I_1 can be written

$$I_1 = 2\pi\beta_0 E_{o0}^2 n(-a) \left\{ e^{-\Gamma/2} (\sin \varphi - \frac{(\cosh(\Gamma/2) - 1) \ln(L/c)}{\pi}) \right\} \quad \text{B.8}$$

where $\Gamma = 4\rho_0$ is the anomalous absorption from B.2. B.8 determines the form of 7.28.

In the integral in 7.29, $p(h)$ is the same as above, but $q(h)$ is of the form

$$q(h) = \gamma_0 \frac{(h+4a) \cdot n^3(h)}{((h+a)^2 + c^2)^2 \cdot ((h+4a)^2 + c^2)^2}$$

where γ_0 is a constant. The resonance point of $q(h)$ is again at $h=-a$, but the width of $q(h)$ is smaller than that of $p(h)$.

In this case, B.4 applies approximately, so I_2 , taking into account the symmetrical properties of $p(h)$ about $h=-a$, can be written

$$I_2 = \gamma_0 E_o^2 e^{-\Gamma/4} \quad \text{B.9}$$

which determines the form of eq. 7.30. In B.4 the downgoing wave plays no significant part in the instability and can be neglected.

References

- Akasofu S. - I., ed. (1980), 'Dynamics of the Magnetosphere',
D. Reidel Pub.Co., Dordrecht, Holland.
- Alfven H. and C.G. Fälthammer (1963), 'Cosmical Electrodynamics',
Clarendon Press, Oxford.
- Allen E.M., G.D.Thorne and P.B.Rao (1974), Radio Sci., 9, 905.
- Appleton E.V. (1932), J.Inst.Elect.Eng., 71, 642.
- Appleton E.V. and M.A.F. Barnett (1925a), Nature, 115, 333.
- Appleton E.V. and M.A.F. Barnett (1925b), Proc.Roy.Soc., A109, 621.
- Arnush D., B.D.Fried and D.F.Kennel (1974), J.Geophys.Res., 79, 1885.
- Bailey D.K. and D.F.Martyn (1934), Phil.Mag., 18 , 369.
- Basu S., S.Basu, A.L.Johnson, J.A.Klobucher and C.M.Rush (1980),
Geophys.Res.Lett., 7, 609.
- Beer, T. (1974), 'Atmospheric Waves' Adam Hilger, London.
- Bennett J.A. (1974), Proc.IEEE, 62 1577.
- Bennett J.A. (1976), J.Plasma Phys. 15, 151.
- Bernstein I.B. (1958), Phys.Rev. 109, 10.
- Biondi M.A. (1969), Can.J.Phys., 47, 1711.
- Booker H.G. (1935), Proc.Roy.Soc., A150, 267.
- Booker H.G. (1956), J.Atmos.Terr.Phys., 8, 204.
- Bowhill S.A. (1974), Radio Sci., 9, 975.
- Boyd T.J.M. and J.J.Sanderson (1969), 'Plasma Dynamics', Nelson, London.
- Braginskii S.I. (1965), 'Transport Phenomena in Plasma' in Reviews of
Plasma Physics, Vol.1, ed. M.A. Leontovich, Consultants Bureau, New York.
- Breit G. and M.A.Tuve (1925), Nature, 116, 357.
- Breit G. and M.A.Tuve (1926), Phys.Rev., 28, 554.
- Brillouin L. (1953), 'Wave Propagation in Periodic Structures', Dover
Publications, New York.

- Budden K.G. (1961), 'Radio Waves in the Ionosphere', Cambridge Univ. Press, London.
- Budden K.G. (1972), J.Atmos.Terr.Phys., 34, 1909.
- Budden K.G. and P.D.Terry (1971), Proc.Roy.Soc., A321, 275.
- Burinskaya T.M. and A.S.Volokitin (1979), Sov.J.Plasma Phys., 5, 755.
- Carlson H.C., W.E.Gordon and R.L.Showen (1972), J.Geophys.Res., 77, 1242.
- Carlson H.C. and L.M.Duncan (1977), Radio Sci., 12, 1001.
- Carlson H.C., V.B. Wickwar and G.P.Mantas (1982), J.Atmos.Terr.Phys., 44, 1082.
- Carpenter G.B. (1974), Radio Sci., 9, 965.
- Carroll J.C., E.J.Violette and W.F.Utlaut (1974), Radio Sci., 9, 895.
- Champeney D.C. (1973), 'Fourier Transforms and Their Physical Applications', Academic Press, London.
- Chapman S. and T.G.Cowling (1970), 'The Mathematical Theory of Nonuniform Gases', Cambridge Univ.Press, London.
- Chen F.F. (1974), 'Introductions to Plasma Physics', Plenum Press, New York.
- Chen H.C. and J.A.Fejer (1975a), Phys. Fluids, 18, 1809.
- Chen H.C. and J.A.Fejer (1975b), Radio Sci., 10, 167.
- Clemmow P.C. and J.P. Dougherty (1969), 'Electrodynamics of Particles and Plasmas', Addison-Wesley Pub.Co., Reading, Mass.
- Coco D. and S. Ganguly (1982), J.Geophys.Res., 87, 7551.
- Cohen R. and J.D.Whitehead (1970), J.Geophys.Res., 75, 6439.
- Cragin B.L. and J.A.Fejer (1974), Radio Sci., 9, 1071.
- Cragin B.L., J.A.Fejer and E.Leer (1977), Radio Sci., 12, 273.
- Das A.C. and J.A.Fejer (1979), J.Geophys.Res., 84, 6701.

- Davies K. (1960), J.Geophys.Res., 65, 2285.
- Davies K. (1965), 'Ionospheric Radio Propagation', Nat.Bur.Stand.
Monograph 80, U.S. Govn.Print., Washington, D.C.
- Davies K. (1969), 'Ionospheric Radio Waves', Blaisdell Pub.Co., Waltham
Mass.
- Davies K., J.M.Watts and D.H.Zacharisen (1962), J.Geophys.Res., 67, 601.
- Dawson J. and C.Oberman (1962), Phys.Fluids, 5, 517.
- Dawson J. and C. Oberman (1963), Phys.Fluids, 6, 394.
- Denisov N.G. (1957), Sov.Phys. JETP, 4, 544.
- Dolgoplov V.V. (1966), Sov.Phys.Tech.Phys., 11, 198.
- Dubois D.F. and M.V.Goldman (1972), Phys.Rev.Lett., 28, 218.
- Dysthe K.B., E.Mjølhus, H.L.Pécseli and K.Rydpal (1983), Phys.Fluids,
26, 146.
- Fejer J.A. (1975), Phil.Trans.Roy.Soc.Lond., A280, 151.
- Fejer J.A. (1979), Rev.Geophys.Space Phys., 17, 135.
- Fejer J.A. (1983), J.Geophys.Res., 88, 489.
- Fejer J.A. and W.Calvert (1964), J.Geophys.Res., 69, 5049.
- Fejer J.A. and E.Leer (1972), J.Geophys.Res., 77, 700.
- Fejer J.A. and Y.Y.Kuo (1973), Phys.Fluids, 16, 1490.
- Fialer P.A. (1974), Radio Sci., 9, 923.
- Frey A. and W.E.Gordon (1982), J.Atmos Terr.Phys., 44, 1101.
- Fuchs V., K.Ko and A.Bers (1981), Phys.Fluids, 24, 1251.
- George P.L. (1971), J.Atmos.Terr.Phys., 33, 1893.
- Georges T.M. (1967), 'Ionospheric Effects of Atmospheric Waves', ESSA
Tech.Rep. IER 57-ITSA 54, U.S. Govn.Print., Washington, D.C.
- Georges T.M. (1970), J.Geophys.Res., 75, 6436.
- Germantsev G.G., N.P.Komrakov, P.P.Korobkov, L.F.Mironenko, N.A.Mityakov,
V.O.Rapoport, V.Yu.Trachtengerts, V.L.Frolov and V.A.Cherepovitskii
(1973), JETP Lett., 18, 364.

- Ginzburg V.L. (1970), 'The Propagation of Electromagnetic Waves in Plasmas', Pergamon, Oxford.
- Golant V.E. and A.D.Piliya (1972), Sov.Phys.Uspekhi, 14, 413.
- Golant V.E., A.P.Zhilinsky and I.E. Sakharov (1980), 'Fundamentals of Plasma Physics', Wiley, New York.
- Gordeyev G.V. (1952), Sov.Phys, JETP, 6, 660.
- Gordon W.E., H.C. Carlson and R.L.Showen (1971), J.Geophys.Res., 76, 7808.
- Gordon W.E. and H.C.Carlson (1974), Radio Sci., 9, 1041.
- Gossard E.E. and W.H.Hooke (1975), 'Waves in the Atmosphere', Elsevier Sci.Pub.Co., Amsterdam.
- Grach S.M. and V.Yu.Trakhtengerts (1975), Izv.Vyssh.Ucheb.Zaved. Radiofiz., 18, 1288.
- Grach S.M., A.N.Karashtin, N.A.Mityakov, V.O.Rapoport and V.Yu Trakhtengerts (1977), Radio Phys.Quantum Electron., 20, 1254.
- Grach S.M., A.N.Karashtin, N.A.Mityakov, V.O.Rapoport and V.Yu Trakhtengerts (1979), Sov.J.Plasma Phys., 4, 742.
- Grad H. (1958), 'Principles of the Kinetic Theory of Gases' in Handbuch der Physik, Vol.XII, p.205, Springer Verlag, Berlin.
- Graham K.N. and J.A.Fejer (1976), Radio Sci., 11, 1057.
- Grigoryév G.I. (1975), Radio Phys. Quantum Electron., 18, 1335.
- Gurevich A.V. (1978), 'Nonlinear Phenomena in the Ionosphere', Springer Verlag, New York.
- Gurevich A.V. and V.V.Migulin (1982), J.Atmos.Terr.Phys., 44, 1019.
- Heading J. (1961), J.Res.Nat.Bur.Stand., 65D, 595
- Heading J. (1962), 'An Introduction to Phase-Integral Methods', Methuen, London.

- Hedberg A., H.Derblom, B.Thidé, H.Kopka and P.Stubbe (1982),
 'Observations of H.F. backscatter associated with the heating
 experiment in Tromso' - submitted to Radio Science.
- Hines C.O. (1960), Can.J.Phys., 38, 1441.
- Inhester B., A.C.Das and J.A.Fejer (1981), J.Geophys.Res., 86, 9101.
- Jackson J.E. (1971), 'The p'(f) to N(h) inversion problem in ionospheric
 soundings', GSFC Rep. X-625-71-186, Greenbelt, Maryland.
- Jones R.M., (1970), Radio Sci., 5, 793.
- Jones R.M. and J.J.Stephenson (1975), 'Versatile three-dimensional ray
 tracing computer program for radio waves in the ionosphere', OT
 Rep. 75-76, U.S.Gov.Print., Washington, D.C.
- Jones T.B. (1973), AGARD Conf.Proc., 138, 24-1.
- Jones T.B., T.Robinson, H.Kopka and P.Stubbe (1982), J.Geophys.Res.,
87, 1557.
- Kopka H., P.Stubbe, T.B.Jones and T.Robinson (1982), Nature, 295, 680.
- Krall N.A. and A.W.Trivelpiece (1974), 'Principles of Plasma Physics',
 McGraw-Hill, New York.
- Kuo S.P. and M.C.Lee (1982), Phys.Lett., 91A, 444.
- Kuo S.P., B.R.Cheo and M.C.Lee (1983), J.Geophys.Res., 88, 417.
- Landau L.D. and E.M.Lifshitz (1960), 'Electrodynamics of Continuous Media',
 Pergammon Press, Oxford.
- Lee M.-C. and J.A.Fejer (1978), Radio Sci., 13, 893.
- LeLevier R.E. (1970), J.Geophys.Res., 75, 6419.
- Lighthill M.J. (1965), J.Inst.Math.Applic., 1, 1.
- Livingston R.C. (1983), Radio Sci., 18, 253.

- Mantas G.P., H.C. Carlson and C.H. Lattoz (1981), *J. Geophys. Res.*, 86, 561.
- Meltz G., L.H. Holway and N.M. Tomljanovich (1974), *Radio Sci.*, 9, 1049.
- Minkoff J. (1974), *Radio Sci.*, 9, 997.
- Minkoff J., P. Kugelmann and I. Weissman (1974a), *Radio Sci.*, 9, 941.
- Minkoff J., M. Laviola, S. Abrams and D. Porter (1974b), *Radio Sci.*, 9, 957.
- Minkoff J. and R. Kreppel (1976), *J. Geophys. Res.*, 81, 2844.
- Muldrew D.B. (1978), *J. Geophys. Res.*, 83, 2552.
- Nayfeh A.H. and D.T. Mook (1979), 'Nonlinear Oscillations', Wiley, New York.
- Nishikawa K. (1968), *J. Phys. Soc. Jap.*, 24, 916, 1152.
- Perkins F.W. (1974), *Radio Sci.*, 9, 1065.
- Perkins F.W. and J. Flick (1971), *Phys. Fluids*, 14, 2012.
- Perkins F.W., C. Oberman and E.J. Valeo (1974), *J. Geophys. Res.*, 79, 1478.
- Perkins F.W. and E.J. Valeo (1974), *Phys. Rev. Lett.*, 32, 1234.
- Pitaevskii L.P. (1961), *Sov. Phys. JETP*, 12, 1008.
- Poeverlein H. (1962), *Phys. Rev.*, 128, 956.
- Potter D.E. (1981), 'Computational Plasma Physics' in 'Plasma Physics and Nuclear Fusion Research', ed. R.D. Gill, Academic Press, London.
- Rao P.B. and G.D. Thome (1974), *Radio Sci.*, 9, 987.
- Ratcliffe J.A. (1959), 'The Magneto-Ionic Theory and Its Applications to the Ionosphere', Cambridge Univ. Press, London.
- Ratcliffe J.A. ed. (1960), 'Physics of the Upper Atmosphere', Academic Press, New York.
- Ratcliffe J.A. (1977), *Contemp. Phys.*, 18, 165.

- Rawer K., S. Ramakrishnan and D.Bilitza (1975), 'Preliminary reference profiles for electron and ion density and temperatures proposed for the International Reference Ionosphere', Sci.Rep.W.B2, Inst.Phys. Weltraumforsch, Freiburg, FRG.
- Rishbeth H. and O.K.Garriott (1969), 'Introduction to Ionospheric Physics', Academic Press, New York.
- Rosenbluth M.N. (1972), Phys.Rev.Lett., 29, 565.
- Rufenach C.L. (1973), J.Geophys.Res., 78, 5611.
- Ryzhov Yu A. (1971), Sov.Phys. JETP, 32, 120.
- Ryzhov Yu A. (1972), Sov.Phys. JETP, 35, 490.
- Ryzhov Yu A. and V.V.Tamoikin (1970), Izv.Vyssh.Ucheb.Zaved.Radiofiz., 13, 356.
- Sanderson J.J. (1981), 'Kinetic Theory' in 'Plasma Physics and Nuclear Fusion Research', ed.R.D.Gill, Academic Press, London.
- Santoru J., A.Y.Wong and C.Darrow (1982), 'The HIPAS transmitting facility' presented at the URSI International Radio Symposium, Fairbanks, Alaska.
- Schunk R.W. (1977), Rev.Geophys.Space Phys., 15, 429.
- Schunk R.W. and A.F.Nagy (1978), Rev.Geophys. Space Phys., 16, 355.
- Schwarz M. (1970), 'Information Transmission, Modulation and Noise', McGraw-Hill, Tokyo.
- Showen R.L. and R.A.Behnke (1978), J.Geophys.Res., 83, 207.
- Showen R.L. and D.M.Kim (1978), J.Geophys.Res., 83, 623.
- Silin V.P. (1965), Sov.Phys.JETP, 21, 1127.
- Sitenko A.G. and K.N.Stepanov (1957), Sov.Phys.JETP, 4, 512.
- Sitenko A.G. and Yu.A.Kirochkin (1966), Sov.Phys.Uspekhi, 9, 430.

- Smith M.S. (1975), Proc. Roy. Soc., A346, 59.
- Stix T.H. (1962), 'The Theory of Plasma Waves', McGraw-Hill, New York.
- Stubbe P. (1968), J. Atmos. Terr. Phys., 30, 1965.
- Stubbe P. (1981), Radio Sci., 16, 417.
- Stubbe P. and H. Kopka (1980), 'Modification of the F-region by powerful radio waves' in 'Exploration of the Polar Upper Atmosphere', ed. C.S. Deehr and J.A. Holtet, D. Reidel Pub. Co., Dordrecht, Holland.
- Stubbe P., H. Kopka, T.B. Jones and T. Robinson (1982a), J. Geophys. Res., 87, 1551.
- Stubbe P., H. Kopka, H. Lauch, M.T. Rietveld, A. Brekke, O. Holt., T.B. Jones, T. Robinson, A. Hedberg, B. Thidé, M. Crochet and H.J. Lotz (1982b), J. Atmos. Terr. Phys., 44, 1025.
- Suchy K. (1974), Proc. IEEE, 62, 1571.
- Suchy K. (1981), Radio Sci., 16, 1179.
- Tellegen B.D.H. (1933), Nature, 131, 840.
- Thome G.D. and D.W. Blood (1974), Radio Sci., 9, 917.
- Thomson J.A. (1970), J. Geophys. Res., 75, 6446.
- Tomko A.A., A.J. Ferraro and H.S. Lee (1980), Radio Sci., 15, 675.
- Utlaut W.F. (1970), J. Geophys. Res., 75, 6402.
- Utlaut W.F. (1975), Proc. IEEE, 63, 1022.
- Utlaut W.F. and E.J. Violette (1972), J. Geophys. Res., 77, 6804.
- Utlaut W.F. and E.J. Violette (1974), Radio Sci., 9, 895.
- Vaskov V.V. (1979), Geomag. Aeron., 19, 159.
- Vashkov V.V. and A.V. Gurevich (1975), Sov. Phys. JETP, 42, 91.
- Vaskov V.V. and A.V. Gurevich (1976), Sov. J. Plasma Phys., 2, 62.
- Vaskov V.V. and A.V. Gurevich (1976a), Geomag. Aeron., 16, 28, 141.

- Vaskov V.V. and A.V.Gurevich (1977), Sov.Phys.JETP, 46, 487.
- Vaskov V.V. and A.V.Gurevich (1977a), Sov.J.Plasma Phys., 3, 185.
- Walker J.C.G. (1979), Rev. Geophys.Space Phys., 17, 534.
- Washimi H. and V.I.Karpman (1976), Sov.Phys.JETP, 44, 588.
- Weatherall J.C., J.P.Sheerin, D.R.Nicholson, G.L.Payne, M.V.Goldman
and P.J.Hansen (1982), J.Geophys.Res., 87, 823.
- Weiland J. and H.Wilhelmsson (1977), 'Coherent Non-linear Interaction
of Waves in Plasmas', Pergamon, Oxford.
- Weinberg S. (1962), Phys.Rev., 126, 1899.
- Weinstock J. (1974), Radio Sci., 9, 1085.
- White R.B. and F.F.Chen (1974), Plasma Phys., 16, 565.
- Whitehead J.D. (1956), J.Atmos.Terr.Phys., 9, 276.
- Wong A.Y., J.Santoru and G.G.Sivjee (1981a), J.Geophys.Res., 86, 7718.
- Wong A.Y., G.J.Morales, D.Eggleston, J.Santoru and R.Behnke (1981b),
Phys.Rev.Lett., 47, 1340.
- Yeh K.C. and C.H.Liu (1972), 'Theory of Ionospheric Waves', Academic
Press, New York.
- Yeh K.C. and C.H.Liu (1974), Rev.Geophys.Space Phys., 12, 193.

MODIFICATION OF THE HIGH LATITUDE IONOSPHERE
BY HIGH POWER RADIO WAVES

T.R.ROBINSON

ABSTRACT

The results of experiments to investigate the effects of high power radio waves on the high latitude ionosphere are presented. The experiments entailed probing the modified F-region with low power diagnostic radio waves. Measurements of the amplitude, phase and spectral content of the diagnostic signals yield information regarding the spatial and temporal structure of large-scale, predominantly isotropic irregularities and small-scale strongly field aligned irregularities induced in the ionospheric plasma by the high power radio waves.

By monitoring the signal from the ionospherically reflected high power radio wave itself it was also possible to study directly the nonlinear properties of ionospheric reflectivity.

The experimental observations indicate that anomalous absorption of electromagnetic waves, due to scattering from small-scale field-aligned irregularities, plays an important role in the ionospheric modification process at high latitudes. However, it is necessary to modify current theories of anomalous absorption to take full account of the effect of the geomagnetic field. As a result, the scale lengths of small scale irregularities have been determined for the first time. Other new results include, the first direct observations of a hysteresis effect in anomalous absorption and the first observations of F-region cross modulation. Both of these phenomena have also been treated theoretically.

It has been demonstrated that, in addition to providing new information concerning nonlinear plasma phenomena caused by high power radio waves, the ionospheric modifications technique also enables parameters such as the recombination rate and the thermal conductivity of the natural ionosphere to be deduced.